

Molecular mechanisms underlying PDE3A-caused hypertension with brachydactyly (HTNB)

DISSERTATION

Inaugural-Dissertation
to obtain the academic degree
Doctor rerum naturalium (Dr. rer. nat.)

submitted to the Department of Biology, Chemistry, Pharmacy
of Freie Universität Berlin

by

MARIA ERCU

from Constanta, Romania

Berlin, 2020

This work was conducted from January 2017 until June 2020 at Max Delbrück Center for Molecular Medicine in the Helmholtz Association (MDC) in Berlin under the supervision of Priv.-Doz. Dr. Enno Klussmann.

Dissertation submitted on: 17.06.2020

Date of Disputation: 30.10.2020

1. Reviewer: PD Dr. Enno Klussmann

2. Reviewer: Prof. Dr. Helge Ewers

I hereby declare that the following work was performed by me alone, only with the use of literature and materials listed. I further declare that to the best of my knowledge this work is novel and does not conflict with any earlier published dissertations.

Berlin, 17.06.2020

Maria Ercu

Table of Contents

Table of Contents	4
Abbreviations	8
List of Tables	13
List of Figures	15
1. Summary	18
2. Zusammenfassung	19
3. Introduction	21
3.1. Hypertension with brachydactyly type E (HTNB)	21
3.2. cAMP signaling	23
3.2.1. Protein kinase A (PKA)	26
3.2.2. A-kinase anchoring proteins (AKAPs)	26
3.2.3. Cyclic nucleotide phosphodiesterases (PDEs)	29
3.3. Cyclic guanosine monophosphate (cGMP)-inhibited cyclic adenosine monophosphate (cAMP) phosphodiesterase 3A (PDE3A)	33
3.4. PDE3A mutations cause HTNB	35
3.5. Cardiac hypertrophy	36
3.6. PDE3 as pharmacological target	37
3.6.1. Targeting PDE3A activity	37
3.6.2. PDE3A compartment-specific therapy	38
3.7. Aim of the thesis	40
4. Materials and Methods	41
4.1. Materials	41
4.1.1. Equipment and software	41
4.1.2. Antibodies	45
4.1.3. Buffers and chemicals	47
4.1.4. Plasmids	49
4.1.5. Oligonucleotides	50
4.1.6. Enzymes and cloning reagents	51

4.1.7.	Bacterial strains.....	52
4.1.8.	Bacterial growth medium.....	52
4.1.9.	Eukaryotic cells	52
4.2.	Methods.....	53
4.2.1.	Cell culture	53
4.2.2.	Transfection	53
4.2.3.	Fluorescence Resonance Energy Transfer (FRET) measurements	53
4.2.4.	Cell and tissue lysis.....	55
4.2.5.	Bradford assay and sample preparation	56
4.2.6.	Immunoprecipitation	56
4.2.7.	Immunoblotting.....	57
4.2.7.1.	Sodium dodecyl sulfate (SDS)-Polyacrylamide gel electrophoresis (PAGE).....	57
4.2.7.2.	Western blotting.....	57
4.2.7.3.	Immunodetection	57
4.2.7.4.	Coomassie staining	58
4.2.8.	Mass Spectrometry	58
4.2.9.	Immunofluorescence microscopy.....	58
4.2.10.	Confocal microscopy (Laser scanning microscope (LSM) 780).....	59
4.2.11.	Molecular cloning	59
4.2.11.1.	Polymerase Chain Reaction (PCR) with non-complementary primers.....	59
4.2.11.2.	Site-directed mutagenesis	60
4.2.11.3.	DNA cleavage with restriction endonucleases.....	61
4.2.11.4.	Agarose gel electrophoresis	61
4.2.11.5.	DNA purification from agarose gels	62
4.2.11.6.	Ligation	62
4.2.11.7.	Transformation	62
4.2.11.8.	Culture inoculation	62
4.2.11.9.	DNA isolation and purification.....	63
4.2.11.10.	DNA sequencing	63
4.3.	Statistical analysis	63
5.	Results.....	64

5.1. A deletion in the regulatory region of the <i>PDE3A</i> gene recapitulates HTNB in a rat model	64
5.2. Elucidating molecular mechanisms underlying HTNB using a rat model	69
5.2.1. PDE3A expression in the aorta of WT, Δ 3aa HET and functional DEL animals.....	69
5.2.2. PDE3A deletion in the enzyme's regulatory domain and proliferation .	70
5.3. New human mutations in <i>PDE3A</i>	73
5.3.1. A new mutation in the regulatory region of the <i>PDE3A</i> gene causes HTNB.....	73
5.3.2. A new mutation in the region encoding the catalytic domain of PDE3A.....	74
5.4. PDE3A mutations cause aberrant signaling both in the cytosol and at the plasma membrane (PM)	77
5.4.1. PDE3A1 and 2 are located mainly in the cytosol and the activity of mutant PDE3A is increased.....	78
5.5. Mutations in the regulatory region of the <i>PDE3A</i> gene altered protein-protein interactions	87
5.5.1. Characterizing PDE3A-14-3-3 θ interaction in H9C2 cells	96
5.5.2. PDE3A interacts with the catalytic subunit α of PKA in human heart and cardiomyocytes from non-affected and patient-derived induced pluripotent stem cells (iPSCs).....	97
5.6. Hypertension-causing PDE3A mutations protect against cardiac damage	99
5.6.1. PDE3A1 and PDE3A2 expression in the heart of WT, Δ 3aa HET and functional DEL animals	99
5.6.2. Cardiac parameters of Δ 3aa HET mutant rats are not significantly altered compared to those of WT animals.....	100
5.6.3. Expression of the excitation-contraction coupling components and 14-3-3 θ in rat heart of WT and mutant rats	102
5.6.4. Cardiac parameters of WT, Δ 3aa HET, functional DEL and R862C animals upon isoproterenol treatment	105

5.6.5. Protein expression in rat heart from WT, Δ 3aa HET and functional DEL animals upon isoproterenol treatment	108
6. Discussion	109
6.1. Mutations in the regulatory region of the <i>PDE3A</i> gene are causative for HTNB, while the <i>PDE3A</i> enzymatic pocket is required for a normal skeletal development	109
6.2. Mutations in the regulatory domain of the <i>PDE3A</i> gene induce aberrant signaling	113
6.3. Mutations in the regulatory region of the <i>PDE3A</i> gene lead to altered protein-protein interactions	117
6.4. <i>PDE3A</i> mutations that cause HTNB are cardioprotective	120
6.4.1. HTNB rat model is protected against hypertension-associated end-organ damage	120
6.4.2. Elucidating the molecular mechanism underlying the cardioprotective effects of the <i>PDE3A</i> mutations.....	121
6.4.3. The HTNB animal models are protected from cardiac damage upon cardiac stress induction	123
6.5. <i>PDE3A</i> mutations can both cause and prevent disease	124
7. Outlook	127
8. References	129
9. Publications	145
9.1. Articles	145
9.2. Oral presentations.....	145
9.3. Poster presentations.....	146
10. Acknowledgements	147
11. Appendix.....	149
11.1. Supplemental Results	149
11.2. Plasmid sequences of cloned constructs.....	155
11.3. Mass spectrometry results.....	173

Abbreviations

°C	degree Celsius
3D	three-dimensional
β-AR	β-adrenergic receptor
Δ3aa	3- amino acid deletion
μg	microgram
μL	microliter
μM	micromolar
A447T	alanine substituted by threonine at position 447
A447V	alanine substituted by valine at position 447
aa	amino acid
AC	adenylyl cyclase
ACRDYS2	acrodysostosis
AKAP	A-kinase anchoring protein
Ang II	angiotensin II
ANP	atrial natriuretic peptide
AT ₁ R	angiotensin type I receptors
Bcl-2	B-cell lymphoma 2
BIG1	Brefeldin A-inhibited guanine nucleotide-exchange protein 1
Bilginturan	brachydactyly-short stature-hypertension
BNP	B-type natriuretic peptide
bp	base pair
BP	blood pressure
BPM	beats per minute
BSA	bovine serum albumin
C subunit	catalytic subunit of PKA
Ca ²⁺	calcium
Ca _v 1.2	L-type Ca ²⁺ channel
CaMKII	Ca ²⁺ /calmodulin-dependent kinase type II
cAMP	cyclic adenosine-3',5'-monophosphate
Cav3	caveolin 3

CFP	cyan fluorescent protein
CFTR	cystic fibrosis transmembrane conductance regulator
cGMP	cyclic guanosine-3',5'-monophosphate
CNG	cyclic nucleotide-gated ion channel
CREB	cAMP response element-binding protein
DAPI	4', 6-diamidino-2'-phenylindole dihydrochloride
DBP	diastolic blood pressure
DEL	deletion
DMEM	Dulbecco's modified eagle medium
DPBS	Dulbecco's phosphate-buffered saline
EDTA	ethylenediaminetetraacetic acid
EF	ejection fraction
Epac	exchanged proteins activated by cAMP
ERK	extracellular signal-regulated kinase
FBS	fetal bovine serum
FMP	Leibniz-Institut für Molekulare Pharmakologie
FRET	fluorescence resonance energy transfer
F	forskolin
G449D	glycine substituted by aspartate at position 449
G449S	glycine substituted by serine at position 449
G449V	glycine substituted by valine at position 449
G _s	α-subunit of the stimulatory G protein
G _β	β-subunit of the G protein
G _γ	γ-subunit of the G protein
GAPDH	glyceraldehyde 3-phosphate dehydrogenase
GC	guanylyl cyclase
GDP	guanosine diphosphate
GTP	guanosine triphosphate
GPCR	G-protein coupled receptors
GSKIP	GSK3β-interacting protein
GWAS	genome-wide association studies
HCN	hyperpolarization-activated cyclic nucleotide-gated channel
HE staining	hematoxylin and eosin staining
HET	heterozygous

Abbreviations

HOM	homozygous
HRP	horseradish peroxidase
Hsp	heat shock protein
HTNB	autosomal dominant hypertension with brachydactyly
IBMX	3-isobutyl-1-methylxanthine
ICER	inducible cAMP early repressor
ICUE3	indicator of cAMP using Epac
IF	immunofluorescence
IgG	immunoglobulin G
IP	immunoprecipitation
IPSC	induced pluripotent stem cell
Iso	isoproterenol
IVSd	intraventricular septum diameter
k_{cat}	catalysis constant
K_m	Michaelis constant
KO	knock-out
LB medium	lysogeny broth medium
LFQ	label-free quantification
LP	long-pass
LV	left ventricle
LVID	left ventricular internal diameter
LVPWd	End-diastolic left ventricular posterior wall thickness
MAPK	mitogen-activated protein kinase
MDC	Max Delbrück Centre for Molecular Medicine
min	minute
mg	milligram
mL	milliliter
mm	millimeter
mm ³	cubic millimeter
mmHg	millimeter of mercury
MLB	mild lysis buffer
MLC	myosin light chain
MLCK	myosin light chain kinase
MLCP	myosin light chain phosphatase

MyBPC	myosin-binding protein C
NaCl	sodium chloride
NHR	N-terminal hydrophobic region
nm	nanometer
NO	nitric oxide
O/N	overnight
p	value used for statistics assessment
P/S	Penicillin/Streptomycin
PAD	peripheral artery disease
PAGE	SDS-polyacrylamide gel electrophoresis
PBS	phosphate-buffered saline
PCR	polymerase chain reaction
PDE	cyclic nucleotide phosphodiesterase
PDE3A	cGMP-inhibited cAMP phosphodiesterase 3A
PICA	posterior inferior cerebellar artery
PK	protein kinase
PKA	protein kinase A
PKC	protein kinase C
PKG	protein kinase G
PLN	phospholamban
PM	plasma membrane
PMA	phorbol 12-myristate-13-acetate
POPDC	Popeye domain containing protein
PP	protein phosphatase
PP1	protein phosphatase 1
PP2A	protein phosphatase 2A
PPP2CB	protein phosphatase 2 catalytic subunit
PPP2R1A	protein phosphatase 2 scaffold subunit c
PPP2R2A	protein phosphatase 2 regulatory subunit B α
POD	peroxidase
PVDF	polyvinylidene fluoride
R subunit	regulatory subunit of PKA
R862C	arginine substituted by cysteine at position 862
RAAS	renin-angiotensin-aldosterone system

Abbreviations

RhoA	Ras homology family member A
RT	room-temperature
RyR	ryanodine receptor
RyR2	ryanodine receptor 2
S446P	serine substituted by proline at position 446
SBP	systolic blood pressure
SDS	sodium dodecyl sulfate
sec	seconds
Ser	serine
SD	standard deviation
SEM	standard error mean
sGC	soluble guanylyl cyclase
SLB	standard lysis buffer
SERCA2	sarcoplasmic reticulum Ca ²⁺ ATPase
SKIP	sphingosine kinase-interacting protein
SR	sarcoplasmic reticulum
SV	end-systolic volume
STUB1	STIP1 homology and U box-containing protein 1
T445A	threonine substituted by alanine at position 445
T445del	deletion of threonine at position 445
T445N	threonine substituted by asparagine at position 445
T445S	threonine substituted by serine at position 445
TAE	Tris-acetate EDTA
TBS	Tris-buffered saline
TBS-T	Tris-buffered saline-Tween
Thr	threonine
Tyr	tyrosine
UCR	upstream conserved region
VASP	vasodilator-stimulated phosphoprotein
VSMC	vascular smooth muscle cell
WT	wild-type
YFP	yellow fluorescent protein

List of Tables

Table 1: Overview of AKAPs expressed in the cardiovascular system and of the processes they regulate	28
Table 2: Overview of PDE families expressed in the heart and vasculature and of the cardiovascular processes regulated by them	32
Table 3: Equipment.....	41
Table 4: Disposable material	43
Table 5: Commercial kits	44
Table 6: Software.....	44
Table 7: Primary antibodies used for Western blotting or Immunofluorescence	45
Table 8: Secondary antibodies used for Western blotting or Immunofluorescence...	46
Table 9: Buffers and solutions	47
Table 10: Media, chemicals and fluorescent dyes	48
Table 11: Plasmids	49
Table 12: DNA oligonucleotides used for cloning, site-directed mutagenesis and sequencing.	50
Table 13: Enzymes and PCR reagents	51
Table 14: Bacterial strains	52
Table 15: Growth media for bacteria	52
Table 16: Eukaryotic cell lines	52
Table 17: Composition of PCR mix.....	59
Table 18: PCR protocol	60
Table 19: Composition of mutagenesis PCR mix	60
Table 20: Mutagenesis PCR protocol.....	60
Table 21: Composition of plasmid and insert digestion	61
Table 22: Composition of plasmid and insert ligation	62
Table 23: Radio-telemetric blood pressure measurements	66
Table 24: Radio-telemetric blood pressure measurements	76
Table 25: Potential interaction partners identified in the PDE3A IP from human heart detected by mass spectrometry based on the intensity values	89
Table 26: Potential interaction partners identified in the PDE3A IP from human heart detected by mass spectrometry based on the label-free quantification (LFQ) intensity values.....	91

Supplemental Table S1: Statistical analysis for the SBP, DBP and heart rate measured for WT, Δ 3aa HET, Δ 3aa HOM and functional DEL rat models	149
Supplemental Table S2: All proteins identified to co-precipitate with PDE3A in the human heart via mass spectrometry	173

List of Figures

Figure 1: Key features of the HTNB syndrome.....	22
Figure 2: Schematic representation of the cAMP signaling cascade.....	24
Figure 3: Schematic representation of an AKAP signalosome	27
Figure 4: Classification of the PDE families based on their substrate specificities	30
Figure 5: Schematic representation of the PDE3A gene and protein isoforms and the mutations identified to cause HTNB	35
Figure 6: Schematic representation of the hyperphosphorylation and hyperactivity of mutant PDE3A.....	36
Figure 7: PDE3A-dependent control of Sarcoplasmic Reticulum Ca ²⁺ ATPase 2 (SERCA2) activity.....	39
Figure 8: Principle of FRET illustrated using the cytosolic sensor ICUE3	54
Figure 9: HTNB rat model.....	65
Figure 10: HTNB is recapitulated by a rat model expressing mutant (Δ 3aa) PDE3A	69
Figure 11: PDE3A1 and PDE3A2 expression in the aorta of WT, Δ 3aa HET and functional DEL rats	70
Figure 12: Similar thoracic aorta media thickness between WT and mutant rats.....	71
Figure 13: Cell proliferation markers were similarly expressed in aorta of WT and HTNB mutant rats.....	73
Figure 14: A G449S substitution in PDE3A causes HTNB	74
Figure 15: Missense mutation identified in the region encoding the catalytic domain of PDE3A.....	76
Figure 16: Schematic representation of mCherry-tagged PDE3A1 and PDE3A2 WT and mutant (Δ 3aa, G449S, T445N and R862C) variants	77
Figure 17: mCherry-tagged PDE3A1 and PDE3A2 are localized mainly in the cytosol in HEK293 cells	79
Figure 18: Controls for FRET experiments	81
Figure 19: Mutations in the regulatory region of the PDE3A gene increase the activity of the enzyme in the cytosol.....	83
Figure 20: BAY 41-8543 caused greater inhibition of mutant PDE3A2 than WT.....	85
Figure 21: PDE3A-T445N mutation increases the activity of the enzyme at the PM.	87
Figure 22: Potential PDE3A interaction partners identified via mass spectrometry analysis	93

List of Figures

Figure 23: Endogenous PDE3A immunoprecipitation from human heart and detection of 14-3-3 θ	94
Figure 24: Increased interaction between mutant PDE3A and 14-3-3 θ	95
Figure 25: PDE3A and 14-3-3 θ expression in H9C2 cells	97
Figure 26: Endogenous PDE3A immunoprecipitations from human heart and cardiomyocytes from non-affected and patient-derived IPS cells and detection of the catalytic subunit α of PKA	98
Figure 27: PDE3A1 and PDE3A2 expression in the left ventricle of WT, Δ 3aa HET and functional DEL rats	100
Figure 28: Cardiac parameters of Δ 3aa HET and Δ 3aa HOM rats were comparable to those of WT controls	101
Figure 29: Expression of excitation-contraction coupling system components and 14-3-3 θ in the heart of WT and mutant animals	104
Figure 30: The cardiac response in WT, Δ 3aa HET, functional DEL and R862C rats upon stress induced by isoproterenol treatment differs between the genotypes	108
Figure 31: Schematic representation of the proposed mechanism for PDE3A mutation-induced hypertension and cardioprotection.....	126
Supplemental Figure S1: Expression of hypertrophy markers, ANP and BNP, in the heart of WT and mutant animals.....	150
Supplemental Figure S2: Expression of cell proliferation markers in the heart of WT and mutant animals	151
Supplemental Figure S3: Expression of excitation-contraction coupling system components in the heart of WT and mutant animals	152
Supplemental Figure S4: Expression of other PDEs, phosphorylated PKC substrate proteins and 14-3-3 θ in the left ventricle of WT and mutant animals.....	154
Supplemental Figure S5: Vector map of PDE3A1- Δ 3aa-mCherry.....	157
Supplemental Figure S6: Vector map of PDE3A1-G449S-mCherry.....	159
Supplemental Figure S7: Vector map of PDE3A1-R862C-mCherry.....	161
Supplemental Figure S8: Vector map of PDE3A1-T445N-mCherry	163
Supplemental Figure S9: Vector map of PDE3A1-WT-mCherry	165
Supplemental Figure S10: Vector map of PDE3A2- Δ 3aa-mCherry.....	166
Supplemental Figure S11: Vector map of PDE3A2-G449S-mCherry.....	168

Supplemental Figure S12: Vector map of PDE3A2-R862C-mCherry..... 169
Supplemental Figure S13: Vector map of PDE3A2-T445N-mCherry 171
Supplemental Figure S14: Vector map of PDE3A2-WT-mCherry 172

1. Summary

Hypertension represents the main risk factor for cardiovascular death worldwide. Autosomal dominant hypertension with brachydactyly (HTNB) is a salt-resistant Mendelian syndrome characterized by progressive hypertension, brachydactyly type E and blood vessel hyperplasia. It resembles essential hypertension. If untreated, patients die from stroke before age 50 years.

This study provides strong evidence that mutations affecting a 15 bp regulatory region of the phosphodiesterase 3A (*PDE3A*) gene cause HTNB. A new human mutation that affects the 15 bp region of the *PDE3A* gene was identified. A CRISPR/Cas9 rat model was generated carrying a 9 bp deletion in the same regulatory region, which is analogous to a human 3 bp deletion and which recapitulates HTNB. The mutated *PDE3A* gene drives mechanisms that increase vascular smooth muscle cell (VSMC) proliferation and peripheral vascular resistance causing hypertension; heart function, however, appears normal. PDE3A hydrolyses cyclic adenosine-3',5'-monophosphate (cAMP) and is inhibited by cyclic guanosine-3',5'-monophosphate (cGMP). Treatment of the mutant rats with the soluble guanylyl cyclase (sGC) activator, BAY 41-8543, a derivative of riociguat, reduced the blood pressure to wild-type levels, suggesting that activation of sGC could be a treatment option for patients with HTNB. The mutant PDE3A enzymes show increased enzyme activity, aberrant phosphorylation and an increased interaction with the adaptor protein 14-3-3 θ . Furthermore, a new mutation affecting the region encoding the catalytic domain of PDE3A was identified. All patients carrying this mutation suffer from brachydactyly type E but not all of them have hypertension. This mutant enzyme does not increase PDE3A activity, further confirming that only mutations affecting the regulatory region of the *PDE3A* gene increase the hydrolytic activity of the enzyme. Lastly, mutations located in the regulatory region of the *PDE3A* gene protect the heart against cardiac remodeling, hypertrophy and heart failure.

In conclusion, these findings could lead to the identification of novel therapeutic strategies targeting PDE3A signaling compartments for the treatment of HTNB and essential hypertension, as well as heart failure.

2. Zusammenfassung

Hypertonie stellt den Hauptrisikofaktor für kardiovaskulär bedingte Todesfälle weltweit dar. Autosomal-dominante Hypertonie mit Brachydaktylie (HTNB) ist ein salz-resistentes Syndrom, das nach dem Mendelschen Erbgang vererbt wird. Es zeichnet sich durch fortschreitende Hypertonie, Brachydaktylie Typ E und Hyperplasie der Blutgefäße aus und ähnelt der essentiellen Hypertonie. Unbehandelt versterben Patienten noch vor Vollendung ihres 50. Lebensjahres an den Folgen eines Schlaganfalls.

Diese Studie liefert aussagekräftige Belege, dass Mutationen in der 15 Basenpaar (bp) langen regulatorischen Region des Phosphodiesterase 3A (*PDE3A*)-Gens HTNB verursachen. Eine neue humane Mutation der 15 bp Region des *PDE3A*-Gens wurde identifiziert. Repräsentativ für diese Mutation wurde mit Hilfe von CRISPR/Cas9 ein Rattenmodell generiert, welches eine Deletion von 9 bp in eben dieser regulatorischen Region aufweist. Diese ist somit zu der humanen Deletion von 3 bp analog und rekapituliert HTNB. Das mutierte *PDE3A*-Gen fördert Mechanismen, die die Proliferation von glatten Gefäßmuskelzellen (VSMC) und den peripheren Gefäßwiderstand erhöhen und somit Hypertonie verursachen; die Herzfunktion erscheint dagegen normal. *PDE3A* hydrolysiert zyklisches Adenosinmonophosphat (cAMP) und wird durch zyklisches Guanosinmonophosphat (cGMP) inhibiert. Die Behandlung der mutierten Ratten mit dem löslichen Guanylyl-Zyklase (sGC)-Aktivator BAY 41-8543, einem Derivat von Riociguat, führte zu einer Reduktion des Blutdrucks auf Wildtyp-Level. Dies suggeriert, dass die Aktivierung von sGC eine Behandlungsoption für Patienten mit HTNB darstellen könnte. Die mutierten *PDE3A*-Enzyme zeigen erhöhte Enzymaktivität, aberrante Phosphorylierung und eine vermehrte Interaktion mit dem Adapterprotein 14-3-3 θ . Des Weiteren wurde eine neue Mutation in der für die katalytische Domäne von *PDE3A* kodierenden Region identifiziert. Alle Träger dieser Mutation leiden unter Brachydaktylie Typ E, aber nicht alle weisen Hypertonie auf. Das mutierte Enzym erhöht nicht die *PDE3A*-Aktivität, was weiterhin bestätigt, dass nur die regulatorische Region des *PDE3A*-Gens betreffende Mutationen die hydrolytische Aktivität des Enzyms steigern. Zuletzt schützen Mutationen in der regulatorischen Region des *PDE3A*-Gens das Herz gegen Remodellierung, Hypertrophy und Herzversagen.

Zusammenfassend könnten diese Erkenntnisse zur Identifizierung neuer therapeutischer Strategien führen, welche PDE3A-Signalkompartimente als Ziel haben und zur Behandlung von HTNB und essentieller Hypertonie, sowie Herzversagen eingesetzt werden könnten.

3. Introduction

3.1. Hypertension with brachydactyly type E (HTNB)

Hypertension is the major risk factor for cardiovascular disease. Autosomal dominant hypertension with brachydactyly (HTNB) clinically resembles essential hypertension, i.e. high blood pressure due to unknown cause (Schuster et al. 1996, Bähring et al. 2004, Toka et al. 2015, Bolívar 2013). Blood pressure is the pressure with which the blood acts on the walls of blood vessels. Blood pressure regulation is a complex mechanism that involves the heart, blood vessels, kidneys, adrenal glands and autonomic nervous system, especially the sympathetic nervous system (Cowley 2006). Treatments with anti-hypertensive drugs reduce target organ damage and hypertensive-dependent complications i.e. stroke, heart attack and heart failure (Schmieder 2010). However, treatments targeting the causes of essential hypertension have not yet been developed (Bolívar 2013). New genes and mechanisms that influence blood pressure have been identified by studying congenital conditions; however, all of the identified mechanisms involve increased sodium reabsorption in the distal nephron (Lifton 2004, Toka, Koshy and Hariri 2013). Half of the patients with essential hypertension are salt-resistant, meaning that high salt intake does not induce a change in blood pressure larger than 5 mmHg (Lopez et al. 1995). Therefore, there is a need to understand the blood-pressure-elevating mechanisms in this hypertensive population and to define novel therapeutic approaches (Lopez et al. 1995). HTNB-affected individuals are salt-resistant (Schuster et al. 1996, Bähring et al. 2004, Toka et al. 2015). Thus, this disease can serve as an appropriate model to study salt-resistant hypertension and to potentially identify novel molecular targets for pharmacological intervention.

HTNB, also known as brachydactyly-short stature-hypertension (Bilginturan) syndrome, is characterized by age-dependent progressive hypertension and blood vessel hyperplasia. The second trait is brachydactyly type E, defined by short metacarpals, metatarsals and short stature (Figure 1) (Schuster et al. 1996, Luft et al. 2003, Bähring et al. 2008). If untreated, blood pressure increases by 50 mmHg and patients die from stroke before age 50 years (Schuster et al. 1998). Surprisingly, hypertension-associated end organ damage such as cardiac hypertrophy, kidney damage or hypertensive retinopathy is absent (Hattenbach et al. 1998, Toka et al. 2015).

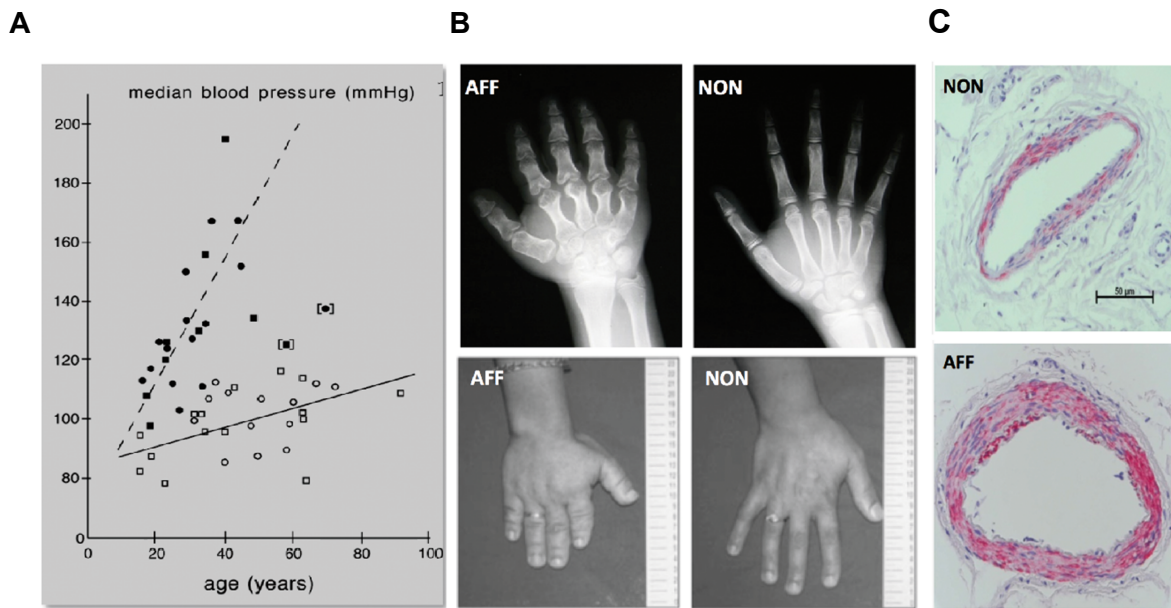


Figure 1: Key features of the HTNB syndrome (Schuster et al. 1996, Luft et al. 2003, Bähring et al. 2008). **(A)** Increase in median blood pressure with increasing age. The solid black symbols represent affected family members, where the increase in blood pressure is dramatic and if untreated leads to death by age 50. The two exceptions (solid black symbols with brackets) were patients being treated for hypertension. The open symbols show the non-affected family members with blood pressure increases similar to those observed in most societies. **(B)** Hands from non-affected (NON) and brachydactyly type E-affected individuals (AFF). **(C)** Giemsa stain of buttocks biopsies-derived artery sections from a 25-year old affected (upper panel) and non-affected (lower panel) sibling of similar age.

HTNB is caused by mutations in the gene encoding for cyclic guanosine monophosphate (cGMP)-inhibited cyclic adenosine monophosphate (cAMP) phosphodiesterase 3A (PDE3A). PDE3A belongs to the superfamily of cyclic nucleotide phosphodiesterases (PDEs), enzymes responsible for the termination of cyclic nucleotide-dependent signaling (Maurice et al. 2014). Therefore, PDE3A is an essential component in one of the most important signaling pathways in the cardiovascular system, cAMP signaling, which controls a variety of processes including excitation-contraction coupling, relaxation and basal pacemaking activity. Impaired cAMP signaling leads to severe cardiovascular diseases (Fischmeister et al. 2006, Perera and Nikolaev 2013, Zaccolo 2009).

3.2. cAMP signaling

Signal transduction systems permit cells to generate suitable responses to changes in the extracellular environment and aberrant intracellular signaling can have detrimental effects and cause severe pathological conditions (Wheeler-Jones 2005). Cyclic AMP is a ubiquitous second messenger that functions as a signal transducer of many extracellular cues (Beavo and Brunton 2002). It predominantly integrates input received from G-protein coupled receptors (GPCRs) and further activates multiple signaling pathways that will give rise to specific cellular responses (Wright, Schobesberger and Gorelik 2015, Pierce, Premont and Lefkowitz 2002). To exert its effects, cAMP binds with high affinity and activates one or more of its downstream effector proteins. To date, four types of cAMP effector proteins have been identified, i.e. cAMP-dependent protein kinase (protein kinase A, PKA), exchange proteins activated by cAMP (Epac), cyclic nucleotide-regulated channels (comprising two structurally related groups, namely the cyclic nucleotide-gated ion channels (CNG) and the hyperpolarization-activated cyclic nucleotide-gated channels (HCN)) and the Popeye domain containing (POPDC) proteins (Figure 2) (Lorenz, Bertinetti and Herberg 2017, Lezoualc'h et al. 2016, DiFrancesco and Tortora 1991, Brand and Schindler 2017, Kaupp and Seifert 2002).

Introduction

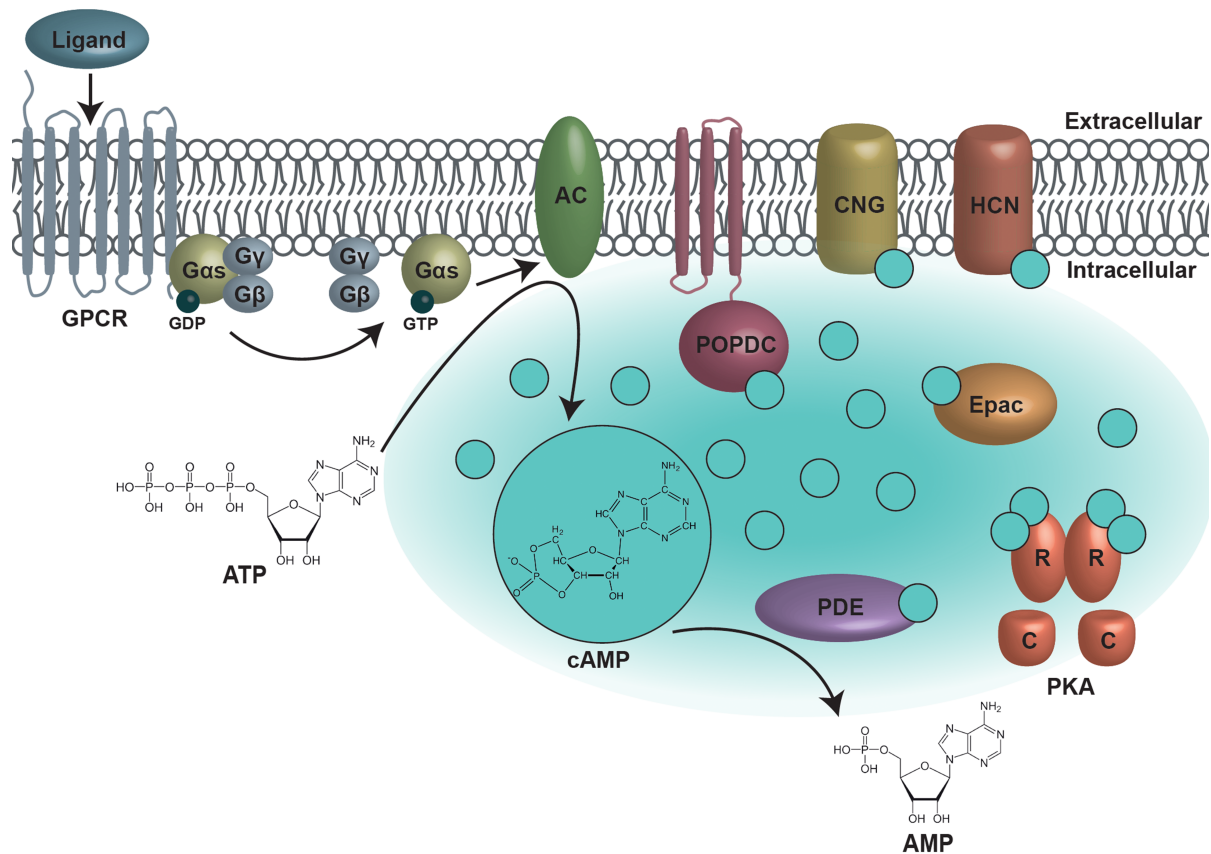


Figure 2: Schematic representation of the cAMP signaling cascade. Upon ligand binding to a GPCR the receptor undergoes a conformational change. G α s subunit dissociates from the GPCR and the G β -G γ complex and exchanges the bound guanosine diphosphate (GDP) for a guanosine triphosphate (GTP). The active GTP-bound G α s subunit activates AC, which in turn catalyzes the formation of the second messenger cAMP from adenosine triphosphate (ATP). cAMP binds to and activates its effector proteins: PKA, Epac, CNG, HCN and the POPDC proteins. Termination of cAMP signaling is mainly achieved by PDEs, enzymes that hydrolyze cAMP to AMP. GPCR G-protein coupled receptor; AC adenylyl cyclase; PKA protein kinase A; Epac exchange proteins activated by cAMP; CNG cyclic nucleotide-gated ion channels; HCN hyperpolarization-activated cyclic nucleotide-gated channels; POPDC Popeye domain containing proteins; PDE cyclic nucleotide phosphodiesterase. Adapted from (Nikolaev and Zaccolo 2017).

Tight control of the intracellular signaling is required in order for a limited number of cAMP effectors to link a multitude of extracellular cues to specific biological responses. This is achieved through the compartmentation of cyclic nucleotide signaling. The cellular processes that ensure this are the following: the cAMP synthesis and diffusion, formation of multi-protein signaling complexes and cAMP degradation.

cAMP is generated from ATP by enzymes termed adenylyl cyclases (ACs) that are stimulated by the α -subunits of stimulatory G proteins (G_s), which in turn are activated upon stimulation of β -adrenoceptors (β -ARs) (Figure 2) (Pierce et al. 2002, Cooper 2003, Cooper and Tabbasum 2014, Efendiev and Dessauer 2011). All AC isoforms are directly or indirectly regulated by calcium (Ca^{2+}) influx (Mons et al. 1998, Jaiswal and Conti 2003, Halls and Cooper 2011), suggesting that crosstalk between signaling pathways is essential for regulation of cellular activity and to further increase the range of cellular responses. The multi-protein signaling complexes are created with the aid of the family of A-kinase anchoring proteins (AKAPs). These proteins act as scaffolds and engage in direct interaction with a variety of proteins, including PKA. They form multi-protein signaling complexes targeting them to specific subcellular compartments (Figure 3) (Szaszák et al. 2008, Skroblin et al. 2010, Dema et al. 2015, Pidoux and Taskén 2010, Scott, Dessauer and Taskén 2013, Nikolaev and Zaccolo 2017). The proteins responsible for termination of cAMP signaling and therefore essential in assuring the spatio-temporal control of cAMP signaling, are termed cyclic nucleotide phosphodiesterases (PDEs). They locally catalyze the hydrolysis of the phosphodiester bond within the second messenger, converting cAMP to AMP (Figure 2) (Maurice et al. 2014, Baillie, Tejada and Kelly 2019, Ercu and Klusmann 2018).

Dysregulation in local cAMP signaling is detrimental. In the cardiovascular system, it leads to severe pathological conditions such as abnormal cardiac remodeling and heart failure (Lohse, Engelhardt and Eschenhagen 2003, Gold, Gonen and Scott 2013, Zoccarato et al. 2015). Local cAMP signaling components and real-time cAMP level changes can be visualized with high spatial and temporal resolution by fluorescence resonance energy transfer (FRET)-based imaging with the aid of genetically encoded sensors (e.g. cAMP-binding and PKA activity sensors) (Berisha and Nikolaev 2017, Froese and Nikolaev 2015, Pavlaki and Nikolaev 2018, Musheshe, Schmidt and Zaccolo 2017, Greenwald, Mehta and Zhang 2018, Ross et al. 2018). These sensors can be targeted to specific locations within the cell, including at the sarcolemma, and therefore close to the ion channels or at the sarcoplasmic reticulum (SR), in the vicinity of proteins that regulate Ca^{2+} cycling, i.e. the sarcoplasmic reticulum Ca^{2+} ATPase 2 (SERCA2) and ryanodine receptor 2 (RyR2) (Thestrup et al. 2014, Sprenger and Nikolaev 2013, Perera et al. 2015, Sprenger et al. 2015). FRET measurements can also be used to monitor cAMP levels

in *ex vivo* and *in vivo* hearts as well as intact cardiac tissue (Jungen et al. 2017). Understanding cAMP dynamics at the subcellular microdomain level and changes in cyclic nucleotide signaling during disease could lead to the identification of novel and more specific therapeutic targets for the treatment of cardiovascular diseases. Therefore, FRET-based imaging is a suitable approach to investigate and understand the pathology underlying HTNB.

3.2.1. Protein kinase A (PKA)

PKA is the major downstream effector of cAMP. It is a serine/threonine (Ser/Thr) protein kinase that controls a variety of processes, including cardiomyocyte contraction, metabolism and cell growth and division (Francis and Corbin 1994). The PKA holoenzyme is a heterotetramer consisting of two regulatory (R) subunits, each bound to one catalytic (C) subunit. The R subunits subtypes comprise type I (RI α or RI β) and type II (RII α or RII β), while there are three types of catalytic subunit isoforms, namely C α , C β and C γ (Taylor et al. 2012). Upon cAMP binding to the R subunits, the C subunits are released and activated and therefore able to phosphorylate substrate found in the close vicinity (Francis and Corbin 1994). This theory was recently confirmed by a light-activated cross-linking mass spectrometry approach (Walker-Gray, Stengel and Gold 2017). In contrast, early biochemical experiments showed that the PKA holoenzyme can also be active (Yang, Fletcher and Johnson 1995, Kopperud et al. 2002). Recent FRET-based measurements revealed that minimal dissociation of the C subunits from the holoenzyme is caused by physiological cAMP levels, thus limiting PKA to act only on the substrates found in its close vicinity and therefore supporting the notion of an active PKA holoenzyme. (Smith et al. 2017).

3.2.2. A-kinase anchoring proteins (AKAPs)

AKAPs are a family of anchoring proteins consisting of more than 40 members. They are key players in coordinating cAMP-dependent signaling responses by targeting PKA and additional signaling proteins, including PDEs, ACs, other protein kinases (PKs) and phosphatases (PPs) to specific locations within the cell (Figure 3) (Skroblin et al. 2010, Rababa'h et al. 2014, Welch, Jones and Scott 2010, Langeberg and Scott 2015).

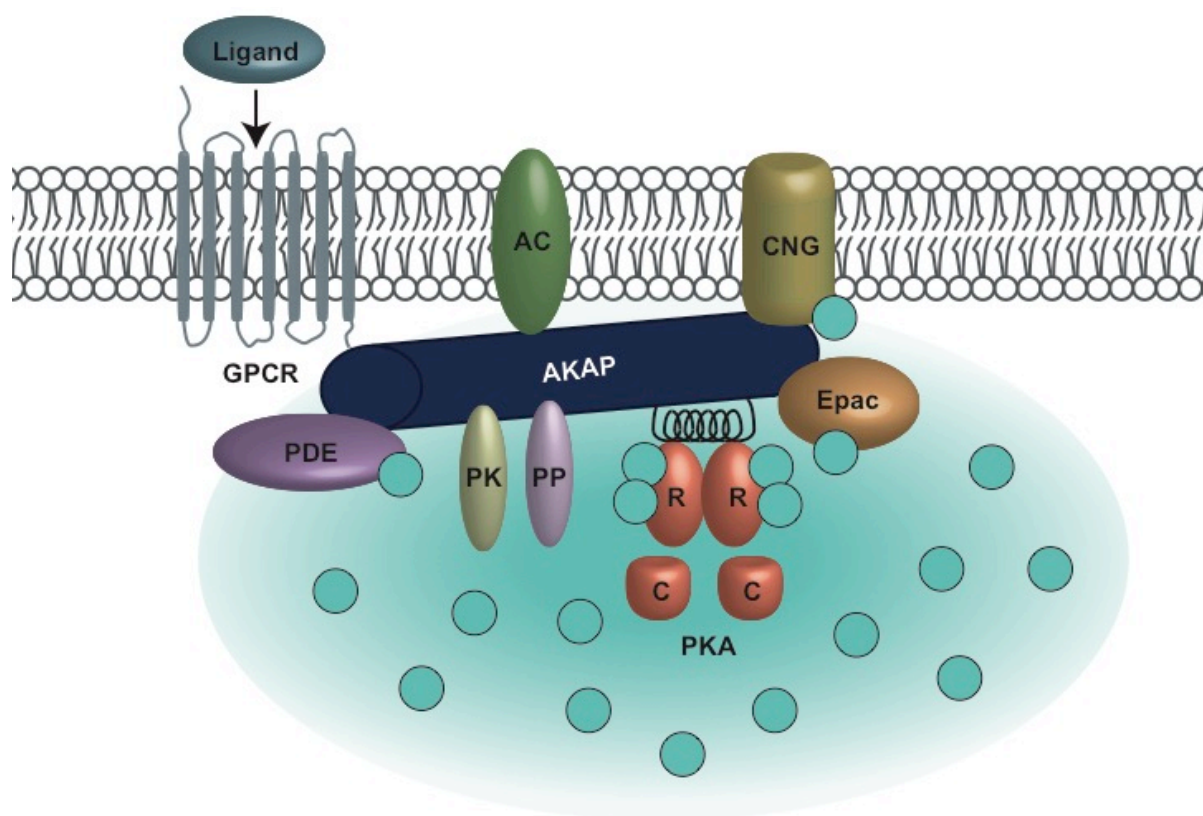


Figure 3: Schematic representation of an AKAP signalosome. AKAPs orchestrate local cAMP signaling by tethering PKA and other cAMP effector proteins, such as PDEs, AC, and other protein kinases and phosphatases and substrates to specific subcellular compartments. AKAP A-kinase anchoring proteins; PK protein kinases; PP protein phosphatases. Adapted from (Nikolaev and Zaccolo 2017).

Various AKAPs can be found at distinct subcellular compartments, including the plasma membrane (PM, e.g. AKAP18 α , AKAP18 β and AKAP79 (Fraser et al. 1998, Trotter et al. 1999, Dell'Acqua et al. 1998)), the cytosol (e.g. sphingosine kinase-interacting protein (SKIP), GSK3 β -interacting protein (GSKIP) (Kovanich et al. 2010, Hundsrucker et al. 2010, Deák et al. 2016, Dema et al. 2016, Scholten et al. 2006)), the sarcoplasmic reticulum (SR, e.g. AKAP18 δ (Lygren et al. 2007)), intracellular vesicles (STIP1 homology and U box-containing protein 1 (STUB1) (Dema et al. 2020)), the cytoskeleton (e.g. gravin, ezrin (Taskén and Aandahl 2004)), the mitochondria (e.g. D-AKAP1 (Huang et al. 1999)) and the nucleus (e.g. pericentrin and AKAP350 (Diviani et al. 2000, Gillingham and Munro 2000)).

AKAPs are essential players in a variety of processes that are required for the proper functioning of the heart and vasculature. More specifically, they are required

Introduction

for proper excitation-contraction coupling (Gray et al. 1998, Marx et al. 2000, Lygren et al. 2007, Ahmad et al. 2015b), for maintaining the endothelial barrier function and thus the vascular integrity (Radeva et al. 2014, Kwon et al. 2012) and vascular tone (Navedo and Santana 2013) and for regulating action potential duration (Marx et al. 2002, Frey et al. 2004), cardiac repolarization (Marx et al. 2002) and β -AR desensitization and resensitization (Fan et al. 2001, Gardner et al. 2006). In the cardiovascular system, AKAPs are also involved in several pathophysiological conditions. For instance, some of these proteins modulate stress signal-induced pathways, leading to cardiac hypertrophy and ultimately to heart failure (Deák and Klussmann 2016, Diviani et al. 2016). A summary of the AKAPs expressed in the heart and vasculature and of the cardiovascular processes that they regulate is presented in Table 1.

Table 1: Overview of AKAPs expressed in the cardiovascular system and of the processes they regulate (Ercu and Klussmann 2018, Gray et al. 1998, Marx et al. 2000, Lygren et al. 2007, Ahmad et al. 2015b, Radeva et al. 2014, Kwon et al. 2012, Navedo and Santana 2013, Marx et al. 2002, Frey et al. 2004, Fan et al. 2001, Gardner et al. 2006, Deák and Klussmann 2016, Diviani et al. 2016).

Common name	Gene name	Alternative name	Regulated cardiovascular process
D-AKAP1	<i>AKAP1</i>	AKAP121/ AKAP149/ AKAP84	Cardiac stress response
D-AKAP2	<i>AKAP10</i>	-	Cardiac repolarization
AKAP9 (long isoform)	<i>AKAP9</i>	-	Endothelial barrier function
AKAP18 α AKAP18 γ AKAP18 δ	<i>AKAP7</i>	-	Excitation-contraction coupling
AKAP79	<i>AKAP5</i>	AKAP75/ AKAP150	Vascular tone Excitation-contraction coupling β -ARs desensitization/ resensitization cycle
AKAP220	<i>AKAP11</i>	-	Endothelial barrier function

AKAP-Lbc	<i>AKAP13</i>	Brx-1/ Proto-Lbc/ Ht31	Cardiac stress response
mAKAP β	<i>AKAP6</i>	AKAP100	Excitation-contraction coupling Cardiac stress response
AKAP Yotiao	<i>AKAP9</i>	GC-NAP	Cardiac repolarization
Gravin	<i>AKAP12</i>	AKAP250	Endothelial barrier function β -ARs desensitization/ resensitization cycle
SKIP	<i>SPHKAP</i>	-	Cardiac stress response

3.2.3. Cyclic nucleotide phosphodiesterases (PDEs)

PDE hydrolysis represents the main route for lowering the intracellular levels of cyclic nucleotides and therefore for terminating cyclic nucleotide-dependent signaling (Maurice et al. 2014). The most well documented cyclic nucleotides are cAMP and cGMP, both being important regulators of cardiac function. cGMP is generated by the enzyme guanylyl cyclase (GC), upon stimulation by either nitric oxide (NO) or natriuretic peptides and it exerts its effect by activating its effector proteins, namely protein kinase G (PKG) and cyclic nucleotide-gated channels (Shah and MacCarthy 2000). To increase the cell's ability to process multiple inputs and generate complex cellular responses, there is molecular crosstalk between cAMP and cGMP signaling pathways. One example where this becomes evident is regulation of PDE activity. In the heart, cGMP intracellular concentration indirectly influences the intracellular concentration of cAMP by regulating the activity of PDEs that hydrolyze cAMP. For instance, cGMP inhibits PDE3A since it competes with cAMP for binding in the active site of the enzyme (Zaccolo and Movsesian 2007).

The PDE superfamily consists of more than 100 members generated from 21 genes via differential transcription initiation sites and alternative splicing. There are 11 families of PDEs (PDE1-PDE11) some of which can selectively hydrolyze either cAMP (PDE4, 7 and 8) or cGMP (PDE5, 6, 9), while others can catalyze the hydrolysis of both second messengers and are called dual-specificity PDEs (PDE1, 2, 3, 10 and 11) (Maurice et al. 2003) (Figure 4). They do not only differ in their substrate specificities but also in their primary structure, kinetics and modes of regulation (Conti and Beavo 2007).

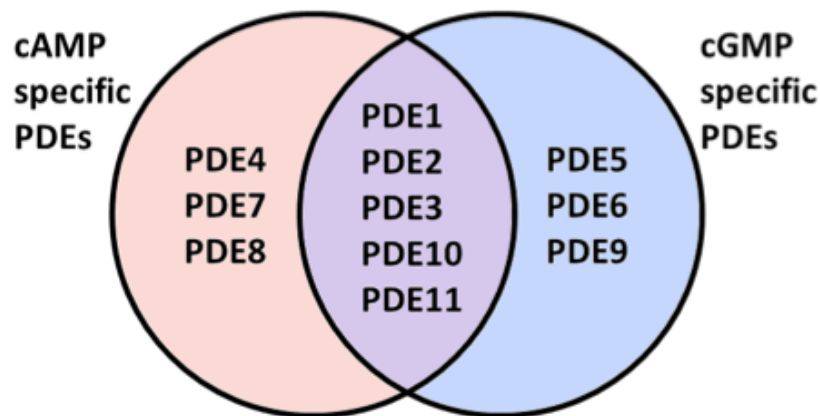


Figure 4: Classification of the PDE families based on their substrate specificities. PDE families 4, 7 and 8 hydrolyze cAMP only, whereas PDE5, 6 and 9 are cGMP-specific. The remaining five families, namely PDE1, 2, 3, 10 and 11, are the so-called dual-specific PDEs catalyzing the hydrolysis of both cAMP and cGMP (Ercu and Klussmann 2018).

All PDEs share a similar structure consisting of an N-terminal regulatory domain, a conserved catalytic domain and a C-terminal domain (Conti and Beavo 2007, Keravis and Lugnier 2010, Anant et al. 1992, Baillie et al. 2000). The N terminus is family-specific and can be post-translationally modified (e.g. phosphorylated). It also contains domains essential for binding of regulatory molecules (e.g. calmodulin), dimerization (e.g. GAF domains) and localization (targeting domains and motifs essential for protein-protein interactions) (Conti and Beavo 2007, Omori and Kotera 2007, Francis, Blount and Corbin 2011). The conserved catalytic domain displays 25 % to 52 % homology between all PDEs and has binding sites for divalent metals: a Zn^{2+} binding motif in the active site and another binding site occupied either by Mg^{2+} (predominant case), Mn^{2+} or Co^{2+} (Ke and Wang 2007). The C-terminal domain can also be modified: it can be phosphorylated by the mitogen-activated protein kinase (MAPK) (PDE4) or prenylated (PDE6) (Anant et al. 1992, Baillie et al. 2000).

The intracellular localization of PDEs is essential for achieving a coordinated cAMP-dependent signaling response (Omori and Kotera 2007). PDEs can be found at various subcellular locations, including the PM (e.g. PDE2A, PDE3A1, PDE6 α and PDE6 β (Wechsler et al. 2002, Rosman et al. 1997, Zhang et al. 2004)), the cytosol (e.g. PDE3A3, PDE5 (Wechsler et al. 2002, Senzaki et al. 2001)), the Golgi

apparatus and centrosomes (e.g. PDE7A1 (Han et al. 2006)) and the nucleus (e.g. PDE9A1 (Wang et al. 2003)). PDE tethering to subcellular compartments is achieved *via* structural motifs within the N-terminal regulatory domain, which either target the enzyme to specific locations or promote specific protein-protein interactions leading to the enzyme's incorporation in a number of signaling complexes (Stangherlin and Zaccolo 2012, Azevedo et al. 2014). Hydrophobic motifs target PDEs to the membrane e.g. the NH₂-terminal domain TAPAS-1 of PDE4A1 leads to membrane insertion by interaction with phosphatidic acid (Baillie et al. 2002), upstream conserved region 2 (UCR2) promotes membrane insertion of PDE4A5 (Beard et al. 2002), PDE2A1 N-terminus is more hydrophilic and leads to cytosolic distribution (Acin-Perez et al. 2011, Russwurm et al. 2009) and PDE3 has two N-terminal hydrophobic regions that target the enzyme to the membrane (Kenan et al. 2000, Shakur et al. 2000). PDEs are integrated into specific macromolecular complexes upon their interaction with various AKAPs: PDE4D3 interacts with mAKAP (Dodge-Kafka et al. 2005), AKAP Yotiao (Marx et al. 2002) and AKAP450 (Taskén et al. 2001), PDE4D was shown to interact with gravin and AKAP18 (Willoughby et al. 2006, Lygren et al. 2007) and PDE3A1 is recruited in a complex coordinated by AKAP18 (Ahmad et al. 2015b). PDEs have been shown to interact with other non-scaffolding proteins, including the cystic fibrosis transmembrane conductance regulator (CFTR) (PDE3A) (Penmatsa et al. 2010), small heat shock protein 20 (Hsp20) (members of the PDE4 family) (Sin et al. 2011) and β -arrestin (PDE4D5) (Baillie et al. 2007, Perry et al. 2002).

Various PDEs regulate different aspects of cardiac and vascular physiology (Kim and Kass 2017), such as cardiac contractility (PDE families 2, 3, 4, 5 and 8) (Yan, Miller and Abe 2007), basal pacemaking activity (PDE families 3 and 4) (Galindo-Tovar, Vargas and Kaumann 2009), endothelial barrier function and therefore vascular integrity (PDE families 2, 3, 4 and 5) (Surapisitchat et al. 2007, Chen et al. 2016). In addition, various PDEs are involved in pathological processes, for instance they are implicated in cardiac remodeling, which ultimately leads to cardiac dysfunction (PDE family members PDE1A, PDE3A, PDE4B, PDE4D, PDE5 and PDE9A) (Fischmeister et al. 2006, Ding et al. 2005, Abi-Gerges et al. 2009, Miller et al. 2009, Bobin et al. 2016) (Table 2).

Table 2: Overview of PDE families expressed in the heart and vasculature and of the cardiovascular processes regulated by them (Ercu and Klussmann 2018, Kim and Kass 2017, Yan et al. 2007, Galindo-Tovar et al. 2009, Surapisitchat et al. 2007, Chen et al. 2016, Fischmeister et al. 2006, Ding et al. 2005, Abi-Gerges et al. 2009, Miller et al. 2009, Bobin et al. 2016).

PDE family	PDE Gene	Substrate specificity	Regulated cardiovascular process
PDE1	<i>PDE1A</i>	cAMP, cGMP	Cardiac stress response
	<i>PDE1B</i>		
	<i>PDE1C</i>		
PDE2	<i>PDE2A</i>	cAMP, cGMP	Endothelial barrier function
			Excitation-contraction coupling
PDE3	<i>PDE3A</i>	cAMP, cGMP	Endothelial barrier function
	<i>PDE3B</i>		Excitation-contraction coupling
			Basal pacemaking activity of the SA node
PDE4	<i>PDE4A</i>	cAMP	Cardiac stress response
	<i>PDE4B</i>		Endothelial barrier function
	<i>PDE4C</i>		Excitation-contraction coupling
	<i>PDE4D</i>		Basal pacemaking activity of the SA node
PDE5	<i>PDE5A</i>	cGMP	Cardiac stress response
			Endothelial barrier function
			Excitation-contraction coupling
PDE8	<i>PDE8A</i>	cAMP	Cardiac stress response
	<i>PDE8B</i>		Excitation-contraction coupling
PDE9	<i>PDE9A</i>	cGMP	Cardiac stress response

3.3. Cyclic guanosine monophosphate (cGMP)-inhibited cyclic adenosine monophosphate (cAMP) phosphodiesterase 3A (PDE3A)

PDE3A, along with PDE3B, belongs to the PDE3 subfamily that hydrolyzes both cAMP and cGMP (Figure 4) in a competitive manner. PDE3A is highly expressed and plays important roles in vascular smooth muscle cells (VSMCs), cardiac myocytes, platelets and oocytes, whereas PDE3B is mainly expressed in adipose and soft tissue. Upon alternative splicing, three PDE3A isoforms are generated, namely PDE3A1 (136 kDa), PDE3A2 (118 kDa) and PDE3A3 (94 kDa) (Figure 5). They are located in different cellular compartments. PDE3A1 is the main isoform found in human cardiomyocytes and is predominantly localized at membranes. It contains two N-terminal hydrophobic regions (NHR), of which the first one consists of four transmembrane domains, while the second one consists of a cluster of hydrophobic amino acids and presents no transmembrane region. PDE3A2, which lacks the first but contains the second NHR can be both membrane-associated and cytosolic and is the main variant found in VSMCs. PDE3A3 is found only in the cytosol, since it lacks both previously mentioned hydrophobic regions. All three isoforms possess the same catalytic region and present high similarities regarding their catalytic activity and inhibitor sensitivity (Figure 5). More specifically, the three PDE3A isoforms show no significant differences with respect to the Michaelis constant (K_m) and to the catalysis constant for the conversion of substrate into product (k_{cat}) values for cAMP. Moreover, the sensitivity of cAMP hydrolytic activity to competitive inhibitors, i.e. cGMP and cilostazol, was comparable between the three isoforms (Wechsler et al. 2002, Hambleton et al. 2005, Ahmad et al. 2015a). A three-dimensional (3D) crystal structure of PDE3A is not available, however it has 69 % of the sequence identical to PDE3B, for which a X-ray structure exists (Scapin et al. 2004). Therefore, using PDE3B crystal structure, a 3D molecular model of PDE3A catalytic domain was constructed (Muñoz-Gutiérrez et al. 2017).

The activity and interaction partners of a protein could potentially be influenced by dimerization of the protein. There is no published evidence that PDE3A dimerizes, however other PDEs are known to form dimers. For instance, PDE4D3 has been shown to oligomerize *via* its upstream conserved regions 1 and 2 (UCR1 and 2) (Richter and Conti 2002) and further results indicate that dimerization is a conserved

Introduction

property for all long PDE4 isoforms, mediated by the UCR domains (Xie et al. 2014). Furthermore, recent evidence showed that PDE4 dimerization regulates the enzyme's activity through the interaction of UCR2 and the catalytic domain (Cedervall et al. 2015). A similar mechanism could also induce PDE3A dimerization and regulate its activity.

Phosphorylation alters protein-protein interactions and the compartmentalization of proteins. PDE3A interacts with and modulates the activity of CFTR in a pig trachea submucosal gland secretion model. The interaction increases upon PKA-dependent phosphorylation of PDE3A (Penmatsa et al. 2010). PKA activation also increases the PDE3A interaction with Brefeldin A-inhibited guanine nucleotide-exchange protein 1 (BIG1) in HeLa cells (Puxeddu et al. 2009). PDE3A interaction with 14-3-3 proteins in response to phorbol 12-myristate-13-acetate (PMA)-induced phosphorylation of the enzyme has also been reported in HeLa cells (Pozuelo Rubio et al. 2005, Corradini et al. 2015). Also in HeLa cells, PDE3A was shown to associate with a protein phosphatase 2A (PP2A) complex, a heterotrimeric, conserved serine/threonine phosphatase complex, composed of protein phosphatase 2 catalytic subunit (PPP2CB), protein phosphatase 2 scaffold subunit α (PPP2R1A) and protein phosphatase 2 regulatory subunit B α (PPP2R2A) (Corradini et al. 2015). In the human heart, PKA-mediated phosphorylation of PDE3A1 at serine residues 292/293 induces its recruitment to an AKAP18-based signalosome composed of SERCA2, phospholamban (PLN), PKA-RII and PKA-C α subunit (Ahmad et al. 2015b). Furthermore, PDE3A interactions with caveolin 3 (Cav3), protein phosphatase 1 (PP1) in the human myocardium (Ahmad et al. 2015b) as well as with plectin in HeLa cells (Pozuelo Rubio et al. 2005) have been observed.

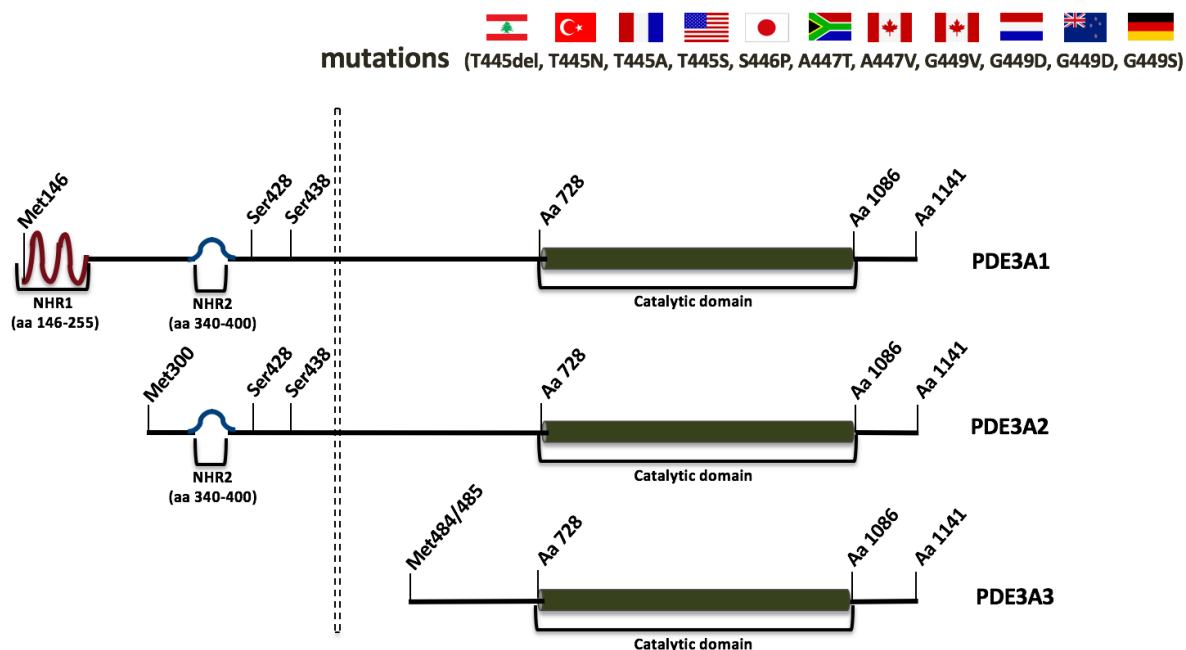


Figure 5: Schematic representation of the PDE3A gene and protein isoforms and the mutations identified to cause HTNB. The PDE3A family consists of three isoforms, namely PDE3A1, PDE3A2 and PDE3A3, which have the same conserved catalytic domain and C-terminal domain but differ in their N-terminal regulatory domain. PDE3A1, which contains two N-terminal hydrophobic regions, NHR1 comprising four transmembrane domains and NHR2, a cluster of hydrophobic amino acids, is a transmembrane protein. PDE3A2 lacks the transmembrane region but encompasses NHR2 and therefore can be found both in the cytosol as well as associated to membranes. PDE3A3 lacks both hydrophobic regions and can be found only in the cytosol. Ten PDE3A mutations have been found in families affected by HTNB coming from the countries indicated by the flags. The mutations are clustered between amino acids 445 and 449, within the regulatory domain of PDE3A and affect only the first two isoforms, PDE3A1 and PDE3A2 respectively, since the altered region is not present in PDE3A3. The mutations cause hyperphosphorylation of two adjacent serine residues, namely Ser428 and Ser438 (Ercu and Klussmann 2018).

3.4. PDE3A mutations cause HTNB

Ten mutations in *PDE3A* have been discovered in eleven unrelated families from Lebanon, Turkey, France, the United States, Japan, South Africa, Canada, Netherlands, New Zealand and Germany that were affected with HTNB (Maass et al. 2015, Toka et al. 2015, Ercu and Klussmann 2018, Renkema et al. 2018, Boda et al. 2016, Ercu et al. 2020). Nine of these mutations are missense mutations, whereas one of them is a 3-base pair deletion. All mutations are clustered in a hotspot region in the N-terminal regulatory domain of the *PDE3A* gene encoding amino acids 445-

Introduction

449. This region is not present in PDE3A3 (Figure 5). Six of these mutations (T445N, T445A, T445S, A447T, A447V and G449V) have been shown to cause increased phosphorylation of serine residues 428 and 438 (Ser428 and Ser438) of PDE3A1 and PDE3A2, as well as increased cAMP affinity and hydrolytic activity of the enzymes (Figure 6). The underlying molecular mechanism is unclear (Maass et al. 2015). The G449S substitution identified in a German family was recently discovered and characterized in this study (see below, Figure 14).

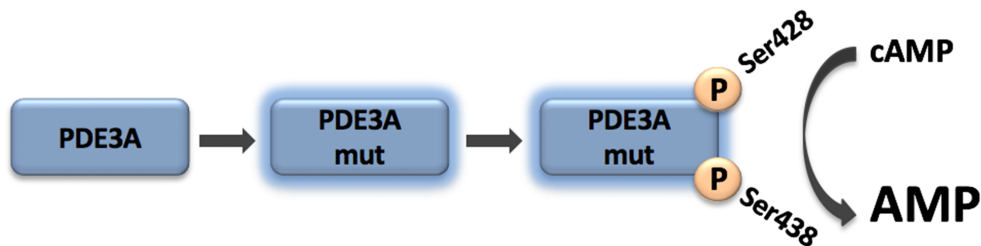


Figure 6: Schematic representation of the hyperphosphorylation and hyperactivity of mutant PDE3A. The mutations induce an increase in the phosphorylation of Ser428 and Ser438 as well as an increase in cAMP hydrolysis, causing low cAMP levels (Ercu and Klussmann 2018).

3.5. Cardiac hypertrophy

Heart failure is a major public health issue since it represents the most common cause of hospitalization in the Western world. At the moment, about 30 million patients worldwide are suffering from heart failure and it is predicted that the incidence will further increase (Savarese and Lund 2017). On the molecular level, cardiac remodeling is found at the basis of heart failure development and is characterized by cardiomyocyte hypertrophy, apoptosis and myocardial fibrosis (Schirone et al. 2017).

HTNB-affected individuals, despite their decades-long blood pressure elevations, hardly display any signs of cardiac damage. Affected family members showed comparable left ventricular mass and cardiac output values to non-affected individuals (Toka et al. 2015). Furthermore, the distensibility of the ascending aorta as well as the aortic pulse wave velocity, two parameters used to characterize the stiffness of the aorta, were measured and found unchanged in affected and non-affected family members. However, the effective arterial elastance, defined as the ratio between the left ventricular end-systolic pressure and stroke volume, was higher

in affected family members (Toka et al. 2015). Arterial stiffness is a hypertension-associated risk factor that significantly predicts cardiovascular mortality (Dogui et al. 2011, Redheuil et al. 2014).

Normal platelet function is essential for the maintenance of the cardiovascular homeostasis (Willoughby, Holmes and Loscalzo 2002). The platelet function is also not different between affected and non-affected relatives (Toka et al. 2015). Thus, HTNB patients showed normal cardiac function and morphology, similar arterial system properties as well as similar platelet aggregation response to healthy individuals (Toka et al. 2015).

3.6. PDE3 as pharmacological target

3.6.1. Targeting PDE3A activity

Most PDE families are expressed in the cardiovascular system and play essential roles in maintaining the proper functioning of the heart and vasculature (Table 2). Therefore, they are considered pharmacological targets for a variety of cardiovascular diseases including hypertension, heart failure, atherosclerosis and intermittent claudication (Maurice et al. 2014, Francis, Conti and Houslay 2011, Knight and Yan 2013, Liu, Shakur and Kambayashi 2011, Baillie et al. 2019). Several inhibitors of PDE3, 4 and 5 families are approved as drugs and some of them are used for the treatment of various cardiovascular diseases (Hiatt, Money and Brass 2008, Cone et al. 1999, Faxon et al. 2004, Gresele, Momi and Falcinelli 2011, Takigawa et al. 2010, Tariq and Aronow 2015).

Cilostazol and milrinone are two PDE3 inhibitors that have been approved as drugs for the treatment of specific cardiovascular diseases. Cilostazol is an antiplatelet agent that also possesses antiproliferative and vasodilatory properties. It has been on the market for almost three decades (Rogers, Oliphant and Finks 2015). Cilostazol is approved for the treatment of peripheral artery disease (PAD). It increases the walking distance of patients suffering from PAD (Hiatt et al. 2008), as well as it alleviates the intermittent claudication-induced symptoms, the major symptomatic manifestation of PAD (Cone et al. 1999, Faxon et al. 2004, Gresele et al. 2011). It also reduces the risk of restenosis in patients that underwent carotid artery stenting due to its inhibitory effect on smooth muscle cell proliferation (Takigawa et al. 2010). Despite the fact that cilostazol appears to be a promising

Introduction

agent in treating various diseases i.e. coronary artery, peripheral artery and cerebrovascular diseases, its use is limited due to side-effects, including increased heart rate, headache, dizziness and diarrhea, which cannot be tolerated by some patient (Rogers et al. 2015).

Milrinone, another PDE3 inhibitor that has been commercially available for over two decades has positive inotropic and vasodilatory properties. Therefore, it is used in end-stage heart failure patients in order to improve cardiac contractility and decrease vascular resistance. In addition, it appears that the vasodilatory properties might be particularly helpful in reducing the pulmonary artery pressure and hence improving the right ventricular function (Tariq and Aronow 2015). The long-term administration of milrinone is associated with severe side-effects, including sustained hypotension, atrial arrhythmias, cardiomyocyte apoptosis and an overall increase in cardiovascular mortality, and therefore it is only used in a selected group of patients (Cone et al. 1999, Overgaard and Dzavík 2008, Tariq and Aronow 2015, Movsesian 2015).

The available PDE3-related therapeutic approaches target the catalytic activity of the enzyme. Due to the fact that the catalytic site of PDE3B is highly similar to PDE3A and that the catalytic domains of PDE3A1, PDE3A2 and PDE3A3 are identical, agents that address the enzyme's activity inhibit all these variants (Hambleton et al. 2005). This lack in selectivity is a plausible explanation for the frequent and dramatic side effects caused by long-term administration of PDE3 inhibitor therapy (Ahmad et al. 2015a). Nevertheless, PDE3 isoforms are still attractive targets due to their high expression and the important roles they play in the cardiovascular system. In particular for hypertension, this was underlined by genome-wide linkage in a large subset of Chinese kindred where a locus for essential hypertension coincided with the *PDE3A* locus (Gong et al. 2003). In addition, four independent genome-wide association studies (GWAS) further identified the *PDE3A* locus as influencing blood pressure and a fifth one discussed its relevance (Ehret et al. 2016, Kato et al. 2015, Simino et al. 2013, Warren et al. 2017, Evangelou et al. 2018).

3.6.2. PDE3A compartment-specific therapy

Novel therapeutic approaches that address local PDE3A-driven signaling events but not its activity could pave the way to new PDE3A-dependent

antihypertensive treatments, while avoiding the adverse effects. Mutant PDE3A is erroneously localized in cells in response to forskolin/ PMA stimulation, activators of PKA and protein kinase C (PKC) respectively (Toka et al. 2015). In the human heart, PKA-mediated phosphorylation of wild-type PDE3A1 at serine residues 292/293 induces a change in its localization. It leads to its recruitment to an AKAP18-based signalosome that controls the Ca^{2+} re-uptake into the SR and thereby participates in the control of cardiac relaxation (Ahmad et al. 2015b). These findings indicate that the enzyme hyperphosphorylation induced by the mutations could affect both its protein-protein interactions as well as its cellular localization (Figure 7). Therefore, altered phosphorylation-dependent protein-protein interactions of PDE3A mutants could induce an abnormal localization of the enzyme and aberrant local cAMP levels that cause hypertension. Modulating the downstream signaling coordinated by PDE3A, especially identifying and targeting relevant interaction partners of the mutant enzyme in specific microdomains, could represent a promising new approach to reduce blood pressure in the general population.

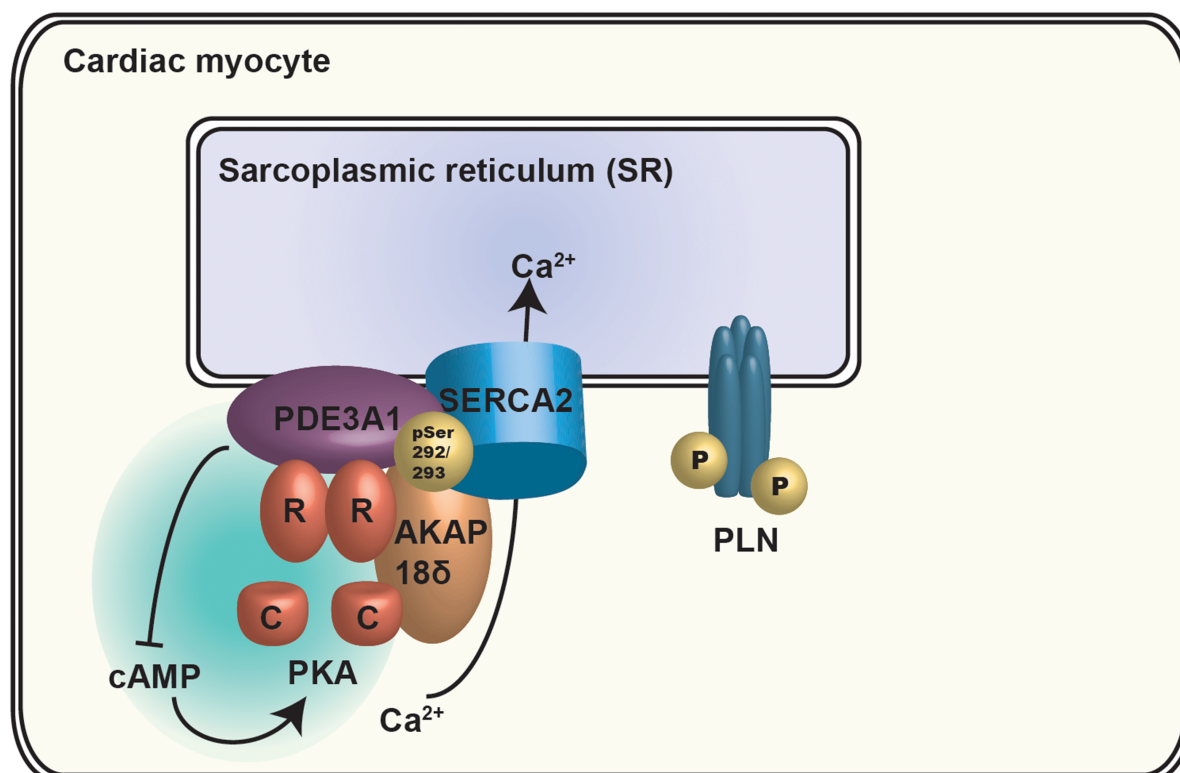


Figure 7: PDE3A-dependent control of Sarcoplasmic Reticulum Ca^{2+} ATPase 2 (SERCA2) activity. Intracellular Ca^{2+} cycling between the cytosol and the SR is the promoter of cardiac contraction and relaxation. A crucial role in Ca^{2+} homeostasis is played by SERCA2, which controls

Introduction

the Ca^{2+} re-uptake into the SR, therefore promoting cardiac relaxation. Activation of SERCA2 is mediated by dissociation of phospholamban (PLN), a SR phosphoprotein, upon its PKA-dependent phosphorylation. Simultaneously, PKA-phosphorylated PDE3A1 at Ser292/Ser293 is recruited to the AKAP18 δ -based signalosome that contains SERCA2 and PKA. PDE3A1 hydrolyzes cAMP and therefore limits PKA-induced PLN phosphorylation. Non-phosphorylated PLN interacts and subsequently inhibits SERCA2, SERCA2-mediated Ca^{2+} re-uptake into the SR is inhibited, which in turn terminates relaxation. SERCA2 Sarcoplasmic Reticulum Ca^{2+} ATPase 2; PLN phospholamban. Adapted from (Ahmad et al. 2015b).

3.7. Aim of the thesis

The aims of the thesis are to use animal models to confirm the causative role of PDE3A mutations in HTNB and to elucidate molecular mechanisms underlying PDE3A-associated HTNB and cardioprotective effect. Major objectives were investigating whether PDE3A mutations induce aberrant signaling or lead to altered protein-protein interactions. Furthermore, to gain insight into the molecular mechanism underlying the cardioprotective effect of PDE3A mutations, the cardiac function of the HTNB rat model upon cardiac stress induction, as well as the expression of various components of the excitation-contraction coupling machinery were investigated.

Prospectively, understanding the molecular mechanisms underlying the abnormal PDE3A signaling in HTNB could lead to the identification of new therapeutic strategies, which target PDE3A signaling compartments with high specificity, as opposed to the broadly effected PDE catalytic domain targets of existing pharmacologically active molecules. These approaches would not only be effective for patients with HTNB but could be extended to treatments of essential hypertension in the general population, as well as to novel therapeutic strategies for the treatment of heart failure.

4. Materials and Methods

4.1. Materials

4.1.1. Equipment and software

Table 3: Equipment

Equipment	Description	Supplier
Basic equipment		
Beckmann Coulter Large Scale Centrifuge	Large scale centrifuge	Beckmann Coulter GmbH (Krefeld, DE)
Centrifuge Universal 320 R	Centrifuge	Hettich (Tuttlingen, DE)
Duomax 1030	Shaking device	Heidolph Instruments (Schwaabach, DE)
ED124S	Analytical balance	Sartorius AG (Göttingen, DE)
Enspire® 2300	Microplate reader	PerkinElmer (Rodgau, DE)
Eppendorf Research pro	Multichannel pipette	Eppendorf AG (Wesseling-Berzdorf, DE)
Gel Doc 2000	Gel documentation system	Bio-Rad Laboratories (California, US)
IKA® MS 3 basic	Small shaker	IKA (Wilmington, US)
IKA® RCT Standard	Heating plate	IKA (Wilmington, US)
Infors HT Multitron Standard	Bacterial incubator and shaker	Infors AG (Bottmingen, CH)
Micra D-4	Tissue homogenizer	ART Prozess- & Labortechnik GmbH (Müllheim, DE)
MicroCentrifuge 2	Microscale centrifuge	NeoLab (Heidelberg, DE)
Micromat Duo	Microwave	AEG (Nürnberg, DE)
PipetBoy acu IBS	Pipettor	Integra Biosciences/ Ibs (Fernwald, DE)
Pipettes 2.5/ 10/ 20/ 200/ 1000/ 5000	Pipettes	Eppendorf (Hamburg, DE)
PTR 35	Eppi rotator	Gran Instruments Ltd (Cambridgeshire, UK)
RCT standard	Magnetic stirrer	IKA®-Werke GmbH & Co.KG (Staufen, DE)
RS-TR05	Falcon rotor	Phoenix Instruments (Garbsen, DE)
SBC 52	Electronic balance	Scaltec Instruments GmbH

Materials and Methods

		(Göttingen, DE)
Seven Easy™	pH meter	Mettler Toledo (Gießen, DE)
Thermomixer Compact	Shaking heater	Eppendorf (Hamburg, DE)
Titramax 100	Plate shaking device	Heidolph Instruments (Schwabach, DE)

Equipment for cell culture

Cryo-container 5100-0001	Freezing container	Thermo Fisher Scientific/ NALGENE (Bonn, DE)
GFL 1072	Waterbath	Gesellschaft für Labortechnik GmbH (Burgwedel, DE)
Incubator CB210	Cell incubator	Binder (Tuttlingen, DE)
Neubauer chamber	Cell counting	Paul Marienfeld GmbH & Co. KG (Lauda – Königshofen, DE)
Safe 2020	Sterile bench	Thermo Electron LED GmbH (Langenselbold, DE)
Scepter™ 2.0	Cell counting	Merck Millipore (Schwalbach, DE)
Tempcontrol 37-2 digital	Temperature regulator plate	PeCon GmbH (Erbach, DE)

Equipment for biochemical methods

MiniProtean®	Polyacrylamide gel electrophoresis cell	Bio-Rad laboratories GmbH (München, DE)
NanoDrop ND-1000	Spectrophotometer	PeqLab Biotechnologie GmbH (Erlangen, DE)
Odyssey Imager	Western blot detection system	LI-COR Biosciences (Bad Homburg, DE)
PerfectBlue mini L	Agarose gel electrophoresis chamber	PeqLab Biotechnologie GmbH (Erlangen, DE)
Power Pac 1000/ 3000	Power supply	Bio-Rad Laboratories GmbH (München, DE)
TProfessional TRIO	Thermocycler	Biometra (Göttingen, DE)
TransBlot Turbo	Western blot transfer system	Bio-Rad Laboratories GmbH (München, DE)

Equipment for microscopy

Zeiss Axioskop HBO 50	Fluorescence microscope	Carl Zeiss MicroImaging GmbH (Jena, DE)
Zeiss LSM 780	Confocal microscope	Carl Zeiss MicroImaging GmbH

		(Jena, DE)
Zeiss LSM510-META-NLO	Confocal microscope	Carl Zeiss MicroImaging GmbH (Jena, DE)

Table 4: Disposable material

Material/ number (no.) (#)	Article (Art.)	Description	Supplier
-------------------------------	----------------	-------------	----------

Basic material

Greiner centrifuge tubes, 15 and 50 mL		Falcon tubes	Sigma-Aldrich Chemie GmbH (München, DE)
Pipette tips		Laboratory essential	StarLab (Hamburg, DE)
Reaction tubes		Laboratory essential	Sarstedt (Nümbrecht, DE)

Cell culture material

6 well plate		6 well cell culture plate	TPP (Trasadingen, CH)
96 well microplate		96 well microplate	Greiner bio-one (Solingen, DE)
Cell culture dish 35 mm		Cell culture dish	TPP (Trasadingen, CH)
Cell culture dish 60 mm		Cell culture dish	TPP (Trasadingen, CH)
Cell culture dish 100 mm		Cell culture dish	TPP (Trasadingen, CH)
Cell scraper		Scrapping of cells	TPP (Trasadingen, CH)
Cryo-vials		Cryoconservation of cells	Carl Roth GmbH & Co KG (Karlsruhe, DE)
Filter tips		Pipette tips	StarLab (Hamburg, DE)
Filtertop		Filtertop 500 mL	TPP (Trasadingen, CH)
Scepter™ Sensors 60 µM		Cell counting	Merck Millipore (Schwalbach, DE)
T75 cell culture flask		Cell culture flask	TPP (Trasadingen, CH)

Material for biochemical methods

4 – 20 % Mini-Protean® TGX™ Precast Gel		Comerciant gradient gels for SDS-PAGE	Bio-Rad Laboratories GmbH (München, DE)
Hypodermic needles		Sterile hypodermic needles	B. Braun Melsungen AG (Hessen, DE)
PCR tubes, coloured		Tubes for PCR applications	Biozym Scientific (Olendorf, DE)
PVDF membranes		Western blotting membranes	Carl Roth GmbH & Co KG

Materials and Methods

			(Karlsruhe, DE)
Syringes	Sterile 1mL syringes	B. Braun Melsungen AG	(Hessen, DE)
Thermo Scientific™ Coverslips	Coverslips immunofluorescence	for Thermo Fisher Scientific	Gerhard Menzel B.V. & Co. KG (Braunschweig, DE)
Thermo Scientific™ SuperFrost® Adhesion slides	Microscope slides immunofluorescence	for Thermo Fisher Scientific	Gerhard Menzel B.V. & Co. KG (Braunschweig, DE)

Table 5: Commercial kits

Kit/ Art. no. (#)	Description	Supplier
NucleoSpin® Extract II kit	DNA purification of agarose gels and PCR mix	Macherey-Nagel (Düren, DE)
NucleoSpin® Plasmid QuickPure	Mini DNA preparation	Macherey-Nagel (Düren, DE)
NucleoBond® Xtra Midi/ Maxi	Midi DNA preparation	Macherey-Nagel (Düren, DE)

Table 6: Software

Software	Description	Supplier/URL
Adobe Illustrator CC 2017	Graphics editor	Adobe Systems, Inc. (San Jose, US)
Adobe Photoshop CS4	Image processing	Adobe Systems, Inc. (San Jose, US)
ApE A plasmid editor Ver 2.0.47	Cloning strategies	biologylabs.utah.edu/jorgensen/wayned/ape/
EndNote X7	Reference management	Thomson Reuters (Toronto, CA)
GraphPad Prism 7	Statistical analysis and graphics	GraphPad Software, Inc. (La Jolla, US)
Image J 1.48v	Image processing	https://imagej.nih.gov/ij/
Image Studio Lite	Western blot analysis	LI-COR Biosciences (Bad Homburg, DE)
Microsoft Excel 2011	Spreadsheet	Microsoft (Redmond, US)
Microsoft Power Point 2011	Presentation	Microsoft (Redmond, US)
Microsoft Word 2011	Word processing	Microsoft (Redmond, US)
SnapGene Viewer	Sequence analysis	GSL Biotech LLC (Chicago, US)
ZEN 2011	Confocal microscopy, image acquisition and analysis	Carl Zeiss MicroImaging GmbH (Jena, DE)

4.1.2. Antibodies

Table 7: Primary antibodies used for Western blotting or Immunofluorescence

Antibody	Application	Species	Supplier/ Art. no. (#)
14-3-3 θ	WB, IF	Mouse	Santa Cruz Biotechnology, #sc-69720
14-3-3 PAN	WB	Mouse	Santa Cruz Biotechnology, #sc-133233
ANP	WB	Rabbit	GeneTex, #GTX109255
BNP	WB	Rabbit	GeneTex, #GTX100538
CREB	WB	Mouse	Cell Signaling Technology, #9104
CREB (pSer133)	WB	Rabbit	Cell Signaling Technology, #9198
ERK	WB	Rabbit	Cell Signaling Technology, #9102
ERK (pThr202/ Tyr204)	WB	Rabbit	Cell Signaling Technology, #9101
GAPDH	WB	Rabbit	Cell Signaling Technology, #2118
Hsp60	WB	Rabbit	Cell Signaling Technology, #4870
Hsp90	WB	Mouse	Enzo Life Sciences, #SPA-830
MyBPC	WB	Rabbit	Santa Cruz Biotechnology, #sc-67353
MyBPC (pSer282)	WB	Rabbit	Enzo Life Sciences, # ALX-215-057-R050
PDE3A	WB, IP	Rabbit	Bethyl Laboratories, A302-740A
PDE3A	IP, IF	Rat	Custom-made, Eurogentec
PDE4A	WB	Rabbit	Abcam, #ab14607
PDE5A	WB	Rabbit	Abcam, #ab14672
PKA α cat	WB	Mouse	BD Biosciences #610980
pSer/ Thr PKA Substrate	WB	Rabbit	Cell Signaling Technology, #9621
PKA RII α	WB	Mouse	BD Biosciences #612243
PKA RII α (pSer96)	WB	Rabbit	Epitomics, #1151-1
pSer PKC Substrate	WB	Rabbit	Cell Signaling Technology,

Materials and Methods

			#2261
PLN	WB	Mouse	Thermo Fisher Scientific, #MA3-922
PLN (pSer16)	WB	Rabbit	Upstate Biotechnology, #P26678
RhoA	WB	Mouse	Santa Cruz Biotechnology, #sc-418
RhoA (pSer188)	WB	Rabbit	Abcam, #ab41435
RyR2	WB	Mouse	Thermo Fisher Scientific, #MA3-916
RyR2 (pSer2808)	WB	Rabbit	Abcam, #ab59225
Troponin I	WB	Rabbit	Cell Signaling Technology, #4002
Troponin I (pSer23/24)	WB	Rabbit	Cell Signaling Technology, #4004

Table 8: Secondary antibodies used for Western blotting or Immunofluorescence

Antibody	Application	Species	Supplier/ Art. no. (#)
Cy3-anti-Rabbit IgG	IF	Mouse	Jackson ImmunoResearch Laboratories; #211-165- 109
Cy5-anti-Mouse IgG	IF	Goat	Jackson ImmunoResearch Laboratories; #115-165- 003
Peroxidase (POD)-anti- goat IgG	WB	Donkey	Jackson ImmunoResearch Laboratories; #705-035- 147
POD-anti-mouse IgG	WB	Donkey	Jackson ImmunoResearch Laboratories; #705-035- 151
POD-anti-rabbit IgG	WB	Donkey	Jackson ImmunoResearch Laboratories; #705-035- 152
POD-anti-rat IgG	WB	Donkey	Jackson ImmunoResearch Laboratories; #705-035- 153
POD-anti-sheep IgG	WB	Donkey	Jackson ImmunoResearch Laboratories; #713-035- 147

4.1.3. Buffers and chemicals

Table 9: Buffers and solutions

Buffer/ solution	Composition/ Supplier/ Art. no. (#)
Bio Quenching buffer	50 mM NH ₄ Cl in 1X PBS
Blocking buffer (IF)	0.27 % fish skin gelatin in 1x PBS
Blocking buffer (Western blot)	5 % bovine serum albumine (BSA) or 5 % skim milk in 1x TBS-T
Coomassie fixation solution	40 % acetic acid, 10 % ethanol
Coomassie staining solution	0.025 % Coomassie brilliant blue; 10 % acetic acid
Coomassie destaining solution	10 % acetic acid
Lämmli sample buffer	40 % glycerol; 8 % SDS; 0.4 % bromophenol blue; 312.5 mM Tris-HCl; 200 mM DTT; pH 6.8
Lysis buffer	MLB: PhosSTOP EASY; Complete mini EDTA-free SLB: PhosSTOP EASY; Complete mini EDTA-free RIPA: PhosSTOP EASY; Complete mini EDTA-free
Mild lysis buffer (MLB)	0.2% Triton X-100, 2 mM EDTA, 2 mM EGTA in 1x DPBS
Phosphate-buffered saline (PBS)	137 mM NaCl; 2.7 mM KCl; 1.5 mM KH ₂ PO ₄ ; 8.1 mM Na ₂ HPO ₄ ; pH 7.4
RIPA buffer	50 mM Tris-HCl, pH 7.4; 150 mM NaCl; 1 % Triton X-100; 1 % sodium deoxycholate; 0.1 % SDS; 1 mM EDTA
SDS-polyacrylamide gel electrophoresis (PAGE) running buffer	25 mM Tris; 192 mM glycine; 0.1 % SDS
Semi-dry transfer buffer	48 mM Tris; 39 mM glycine; 20 % methanol, 1.3 mM SDS
Separating gel buffer	0.625 M Tris-HCl; pH 6.8
Standard lysis buffer (SLB)	10 mM K ₂ HPO ₄ ; 150 mM NaCl; 5 mM EDTA; 5 mM EGTA; 0.5 % Triton X-100; pH 7.4; 0.2 % sodium deoxycholate
Stacking gel buffer	0.75 M Tris-HCl; pH 8.8
Tank blot transfer buffer	20 mM Tris; 150 mM glycine; 10 % methanol, 0.02 % SDS
TBS + Tween (TBS-T)	1x TBS; 0.05 % Tween-20
TransBlot Turbo transfer buffer (1X)	20% (v/v) Trans blot transfer buffer (5X); 20% (v/v) 100% ethanol
Tris-acetate-EDTA (TAE) buffer	40 mM Tris; 1 mM EDTA; 1.14 % (v/v) glacial acetic acid
Tris-buffered saline (TBS)	10 mM Tris-HCl, pH 7.4; 150 mM NaCl
Trypsin-EDTA	Biohrom AG (Berlin, DE); #L2153

Materials and Methods

Table 10: Media, chemicals and fluorescent dyes

Substance	Supplier/ Art. no. (#)
30% Acrylamide / Bis Solution	Bio-Rad Laboratories GmbH (München, DE); #1610156
4', 6-Diamidine-2'-phenylindole dihydrochloride (DAPI)	Roche Diagnostics GmbH (Mannheim, DE); #10236276001
6X DNA loading buffer blue	New England BioLabs (Ipswich, US); #B7025S
Anti-FLAG® M2 Magnetic Beads	Sigma-Aldrich, #M8823
BAY 41-8543	Cayman Chemical (Michigan, US)
Bovine Serum Albumin (BSA)	SERVA Electrophoresis GmbH (Heidelberg, DE); #11926.04
Cilostamide	Sigma-Aldrich, #C7971
Complete mini EDTA-free	Roche Diagnostics (Mannheim, DE); #REF0693159001
Coomassie Plus™ Protein Assay Reagent	Thermo Fisher Scientific (Bonn, DE); #1856210
DMEM, GlutaMAX™	Life Technologies GmbH (Darmstadt, DE); #21885108
DPBS (1X) with Ca ²⁺ Mg ²⁺	GE Healthcare, #H15-001
DPBS (10X)	Life Technologies GmbH (Darmstadt, DE); #14200067
Fetal bovine serum (FBS) superior	Biochrom AG (Berlin, DE), #S0613
Forskolin	Biaffin GmbH & Co KG Life Sciences Institute (Kassel, DE); #PKE-FORS-050
HyperLadder I (HyperLadder™ 1kp)	BioLine GmbH (Luckenwalde, DE); #BIO33053
HyperLadder II (HyperLadder™ 50bp)	BioLine GmbH (Luckenwalde, DE); #BIO33054
IBMX	Sigma-Aldrich, #I5879
Immobilon™ Western Chemiluminescent HRP substrate	Merck Millipore (Schwalbach, DE); #WBKLS0500
Immu-Mount™	Thermo Fisher Scientific (Bonn, DE); #99-904-12
(+)-Isoproterenol hydrochloride	Sigma-Aldrich, #I5627
Lipofectamine™ 2000	Invitrogen (Carlsbad, US)
Milrinone	Sigma-Aldrich, #M4659
OptiMEM	Life Technologies GmbH (Darmstadt, DE), #31985
Penicillin/Streptomycin (P/S)	Biochrom/ Merck Millipore (Schwalbach, DE); #A2213
Phorbol-12-myristate-13-acetate (PMA)	Sigma-Aldrich, #P1585
PhosSTOP EASY pack	Roche Diagnostics (Mannheim, DE); #REF04906837001

Precision Plus Protein Standard Dual Color	Bio-Rad Laboratories GmbH (München, DE); #1610374
ProteinA-sepharose	Sigma-Aldrich, #P3391
Redsafe	Intron Biotechnology (Seongnam, KR); #21141
Skim milk powder	Fluka Analytical/ Sigma (Taufkirchen, DE); #70166
TransBlot Turbo transfer buffer (5X)	Bio-Rad Laboratories GmbH (München, DE); #1610156
Trypsin-EDTA (0.5%)	Biochrom/ Merck Millipore (Schwalbach, DE); #L2153

4.1.4. Plasmids

Table 11: Plasmids

Plasmid name	Vector	Resistance	Supplier/ Art. no. (#)
CFP	pcDNA3	Ampicilin	Addgene (Cambridge, US); #13030
CFP-YFP	pcDNA3	Ampicilin	Kindly provided by Dr. Claudia Rutz, Leibniz-Forschungsinstitut für Molekulare Pharmakologie (FMP) (Berlin, Germany)
ICUE3	pcDNA3	Ampicilin	Addgene (Cambridge, US); #61622
LynICUE3	pcDNA3	Ampicilin	Addgene (Cambridge, US); #61623
PDE3A1-Δ3aa-mCherry	pcDNA3.1	Kanamycin	Self-generated
PDE3A1-G449S-mCherry	pcDNA3.1	Kanamycin	Self-generated
PDE3A1-R862C-mCherry	pcDNA3.1	Kanamycin	Self-generated
PDE3A1-T445N-mCherry	pcDNA3.1	Kanamycin	Self-generated
PDE3A1-WT-mCherry	pcDNA3.1	Kanamycin	Self-generated
PDE3A2-Δ3aa-mCherry	pcDNA3.1	Kanamycin	Self-generated
PDE3A2-G449S-mCherry	pcDNA3.1	Kanamycin	Self-generated
PDE3A2-R862C-mCherry	pcDNA3.1	Kanamycin	Self-generated
PDE3A2-T445N-mCherry	pcDNA3.1	Kanamycin	Self-generated
PDE3A2-WT-mCherry	pcDNA3.1	Kanamycin	Self-generated
PDE3A2-Δ3aa -Flag	pcDNA3.1	Ampicilin	Cloned by Dr. Carolin Schächterle

Materials and Methods

PDE3A2-T445N-Flag	pcDNA3.1	Ampicilin	Cloned by Dr. Carolin Schächerle
PDE3A2-WT-Flag	pcDNA3.1	Ampicilin	Cloned by Dr. Carolin Schächerle
Venus	mVenus-C1	Kanamycin	Addgene (Cambridge, US); #27794

4.1.5. Oligonucleotides

Table 12: DNA oligonucleotides used for cloning, site-directed mutagenesis and sequencing.

Name	Use	DNA Sequence 5' → 3'
ICUE3 – 1 Fw	Sequencing	TGCCCGACAACCACTACCTG
ICUE3 – 2 Fw	Sequencing	GAGCTTCTGTTGGAGGCCATG
ICUE3 – 3 Fw	Sequencing	ATGAGCTGATCCCACACCCTG
ICUE3 – 4 Fw	Sequencing	CCAGCACCTGGGCTTATGTC
pCMV Fw	Sequencing	GAGCTCGTTTAGTGAACCGTC
PDE3A catalytic domain Fw	Sequencing	ATCCCTGCCTTGGAGTTGATG
PDE3A end Fw	Sequencing	AGTCGCACTCTTCAGAACAGA
PDE3A exon 4 Fw	Sequencing	CTCCTGGCAGACCCTTCTCTT
PDE3A start Fw	Sequencing	CAAGGGAATCCTGCTGATGAG
PDE3A-Δ3aa Fw	Site-directed mutagenesis	GGT AGA CCT GTG GCG GTG GTC CAA GTG G
PDE3A-Δ3aa Rv	Site-directed mutagenesis	CCA CTT GGA CCA CCG CCA CAG GTC TAC C
PDE3A-G449S Fw	Site-directed mutagenesis	ACC TCG GCC ACA AGT CTA CCC ACC T
PDE3A-G449S Rv	Site-directed mutagenesis	AGG TGG GTA GAC TTG TGG CCG AGG T
PDE3A-R862C Fw	Site-directed mutagenesis	GGCGGTGCTATATAACGATTGTTCAGTTTTGGAGA ATCA
PDE3A-R862C Rv	Site-directed mutagenesis	TGATTCTCCAAAACCTGAACAATCGTTATATAGCAC CGCC
PDE3A-T445N Fw	Site-directed mutagenesis	GGACCACCACCAACTCGGCCACAGG
PDE3A-T445N Rv	Site-directed mutagenesis	CCTGTGGCCGAGTTGGTGGTGGTCC
PDE3A2WT-ICUE3 Fw	Cloning	TATCAGGCTAGCATGTCCGGCTGCAGCAGCAAG
PDE3A2WT-ICUE3 Rv	Cloning	CAATGGATCCTTCTGGTCTGGCTTTTGGTTGG

T7 promoter Fw	Sequencing	TAATACGACTCACTATAGGG
----------------	------------	----------------------

4.1.6. Enzymes and cloning reagents

Table 13: Enzymes and PCR reagents

Enzyme/ Reagent	Concentration	Supplier/ Art. No. (#)
Agel-HF	20.000 U/mL	New England BioLabs (Ipswich, US); #R3552S
BamHI-HF	20.000 U/mL	New England BioLabs (Ipswich, US); #R3136S
CutSmart buffer	10x	New England BioLabs (Ipswich, US); #B7204S
dNTP mix	5 mM	Robklon GmbH (Berlin, DE), #E2800-04
DpnI	20.000 U/mL	New England BioLabs (Ipswich, US); #R0176S
MgCl ₂	25 mM	Robklon GmbH (Berlin, DE), #E2500-01
NheI-HF	20.000 U/mL	New England BioLabs (Ipswich, US); #R3131S
NotI-HF	20.000 U/mL	New England BioLabs (Ipswich, US); #R3189S
PfuUltra II Fusion HotStart DNA Polymerase	2500 U/ml	Agilent technologies (Santa Clara, US), #600670
PfuUltra II reaction buffer	10x	Agilent technologies (Santa Clara, US), #600670
T4 ligase	400.000 U/ml	New England BioLabs (Ipswich, US); #M0202S
T4 ligase reaction buffer	10x	New England BioLabs (Ipswich, US); #M0202S
XhoI	20.000 U/mL	New England BioLabs (Ipswich, US), #R0146S

4.1.7. Bacterial strains

Table 14: Bacterial strains

Bacterial strain	Genotype	Supplier
<i>E.coli</i> DH5- α	F-endA1 glnV44 thi-1 recA1 relA1 gyrA96 deoR nupG purB20 ϕ 80dlacZ Δ M15 Δ (lacZYA-argF) U169, hsdR17(rK–mK+), λ –	New England BioLabs (Ipswich, US)

4.1.8. Bacterial growth medium

Table 15: Growth media for bacteria

Bacterial growth medium	Composition
Lysogeny broth (LB) medium	10 g/l peptone; 5 g/l yeast extract; 5 g/l NaCl, pH 7.5

For LB agar plates, the LB medium was supplemented with 15 g/L agar and 100 ug/mL ampicillin or kanamycin.

4.1.9. Eukaryotic cells

Table 16: Eukaryotic cell lines

Cell lines	Description	Culture medium	Supplier/ Art. No. (#)
HEK293	Human embryonic kidney cell line	DMEM-GlutaMAX™ (Life Technologies GmbH, Darmstadt, DE; #21885108); 10 % fetal calf serum (FCS); 1 % penicillin/streptomycin (P/S) (100 U/ml)	Deutsche Sammlung von Mikroorganismen und Zellkulturen GmbH (DSMZ; Braunschweig, DE); #ACC305
HeLa-S3	Human cervical adenocarcinoma	DMEM-GlutaMAX™ (Life Technologies GmbH, Darmstadt, DE; #21885108); 10 % FCS; 1 % P/S (100 U/ml)	DSMZ (Braunschweig DE);
H9C2	Rat embryonic myoblast cell line	DMEM-GlutaMAX™ (Life Technologies GmbH, Darmstadt, DE; #21885108); 10 % FCS; 1 % P/S (100 U/ml)	ATCC, LGC Standards GmbH (Wesel, DE); # CRL-1446

4.2. Methods

4.2.1. Cell culture

HEK293, HeLa and H9C2 cells were grown in DMEM-GlutaMAX™ medium (Table 16). The cells were washed with 5 mL pre-heated PBS and detached using 3 mL 1X Trypsin-EDTA for 1-5 min at 37 °C. Trypsinization was stopped by adding 7 mL of serum-containing medium. A defined volume of cell suspension (e.g. 1 mL for 1:10 dilution) was then transferred into a new cell culture flask and fresh serum and Penicillin/Streptomycin (P/S)-containing DMEM-GlutaMAX™ medium was added.

4.2.2. Transfection

HEK293 cells were transfected with the above-mentioned plasmids (Table 11) using Lipofectamine 2000. Plasmids (1 µg/µL) and Lipofectamine (2 µL per 1 µg/µL DNA) were resuspended in OptiMEM and incubated for 5 min at room-temperature (RT). The Lipofectamine mixture was added to the DNA mixture (1:1) and incubated for 25 min at RT. During this time, the serum and P/S-containing DMEM-GlutaMAX™ medium was replaced with P/S-free DMEM-GlutaMAX™. Next, the Lipofectamine/DNA mixture was added onto the cells and incubated for 5 hours at 37 °C. The P/S-free medium was replaced by medium containing P/S and the cells were used for imaging or harvested 24 hours post transfection.

4.2.3. Fluorescence Resonance Energy Transfer (FRET) measurements

HEK293 cells (3×10^5 cells per well) were seeded onto poly-L-lysine hydrobromide pre-coated glass coverslips in 6-well plates. Transfections for transient expression were performed 24 hours post seeding using 1 µg/µL plasmid DNA and 2 µL Lipofectamine 2000 per 1 µg/µL DNA. The cells were transfected either with the indicator of cAMP using Epac (ICUE3) sensor alone or co-transfected with the sensor and the WT or mutant (T445N, Δ3aa and G449S) PDE3A2-mCherry constructs. The cells were also transfected with negative controls, namely cyan fluorescent protein (CFP), either alone or together with Venus, a variant of yellow fluorescent protein

Materials and Methods

(YFP), or with a CFP-YFP tandem construct representing the positive control to determine the maximum FRET signal.

The cytosolic Epac-based sensor, ICUE3 (Figure 8), consists of the cAMP binding domain of the Epac protein, which is flanked N-terminally by CFP and C-terminally by Venus. Under low cAMP levels, for example upon cAMP degradation by PDEs, the sensor is predominantly in a closed conformation and the distance between CFP and Venus is 10 nm or smaller. Therefore, upon excitation of CFP at 435 nm, the emission of Venus at 532 nm is predominantly observed, indicating high FRET. Upon cAMP binding to the Epac moiety, the sensor undergoes a conformational change and the distance between the two fluorophores increases to greater than 10 nm. In this state, little or no energy transfer will occur between CFP and Venus upon donor excitation resulting in low FRET, as indicated by comparatively higher measurements of 468 nm emissions from CFP than in the unbound state (Figure 8).

Low cAMP - High FRET

High cAMP - Low FRET

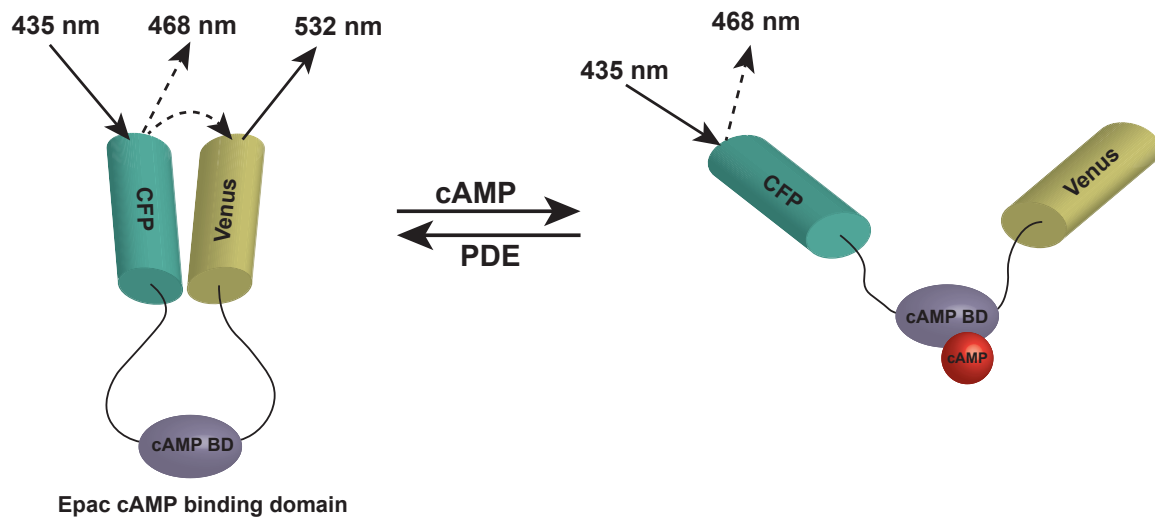


Figure 8: Principle of FRET illustrated using the cytosolic sensor ICUE3. The cytosolic FRET sensor, ICUE3, consists of a truncated version of the exchange factor activated by cAMP (Epac) containing the cAMP binding domain, flanked by the two fluorophores CFP and Venus. If cAMP levels are low, the sensor is predominantly found in a closed conformation, CFP and Venus are found in close proximity to each other (< 10 nm) allowing FRET to occur. Elevation of cAMP levels leads to cAMP binding to the Epac moiety, which induces a conformational change that separates the two fluorophores (> 10 nm), therefore preventing FRET (DiPilato and Zhang 2009).

FRET measurements were carried out 24 hours after transfection using an inverted confocal laser scanning microscope (CLSM510-META-NLO; Carl Zeiss) equipped with a Plan-Neofluar 40X/1,3 (Oil) in order to determine PDE3A activity. The excitation and emission intensities as well as the corresponding lasers are the following: CFP, excitation at 810 nm (ChameleonTM diode-pumped laser; Coherent) and emission between 430 to 505 nm; Venus or YFP, excitation at 514 nm (argon laser) and emission 520 to 560 nm; mCherry, excitation at 543 nm and a long-pass (LP) 560 nm emission filter for fluorescence detection; FRET, excitation at 810 nm and emission between 430 and 655 nm. A λ -stack (images of the same specimen are acquired at different wavelengths) with a linear spectral unmixing mode was employed to correct any CFP fluorescence cross-talk into the FRET channel (523-532 nm) and to calculate the FRET-based fluorescence. The λ -stack is an integral part of the confocal laser system software. In order to correct for direct excitation of the acceptor during donor excitation YFP correction was carried out.

FRET measurements for the ICUE3 sensor alone or when co-expressed with the various PDE3A-mCherry constructs were performed either in the absence of any treatment or in the presence of forskolin with or without milrinone, cilostamide or BAY 41-8543. The effect of treatments with the above-mentioned pharmacological agents on the cAMP levels is expressed as the FRET ratio, which is calculated by dividing the acceptor emission (Venus) at 532 nm by the donor emission (CFP) at 468 nm. The increase in cAMP levels compared to the basal is indicated by the percentage change in the FRET signal (Δ FRET (%)). This was calculated by subtracting the FRET ratio obtained upon stimulation from the corresponding FRET ratio of the control condition, which was then normalized to the FRET ratio of the control condition and finally multiplied by 100 to yield the percentage. The Δ FRET positively correlates with the cAMP concentration, meaning high Δ FRET shows high cAMP levels.

4.2.4. Cell and tissue lysis

Eukaryotic cells were washed once with ice-cold PBS. The cells were scraped in ice-cold lysis buffer and transferred into a 1.5 mL or 2 mL reaction tube and lysed by passing them through a syringe fitted with a 20 G x 1.5" hypodermic needle 5 times. Isolated left ventricles or aortas from rats were homogenized with a disperser

Materials and Methods

homogenizer (Table 3) in lysis buffer. Cell debris was removed by centrifugation at 4 °C for 10 min at 14,000 rpm and the supernatant was used in order to determine the protein concentration.

4.2.5. Bradford assay and sample preparation

The protein concentration of the cell or tissue lysates was determined using the Coomassie Plus Bradford protein assay (Table 10) according to the manufacturer's protocol. The assay is a colorimetric method in which the proteins bind to the Coomassie in an acidic environment, leading to a color change from brown to blue, which is then measured as an absorption maximum shift from 465 nm to 595 nm (the higher the absorption at 595 nm within a sample, the more protein the sample contains). In a 96-well plate, triplicates of 5 µL from each sample as well as of protein standards of defined concentration of 0.125-2 mg/mL were mixed with 250 µL of the Coomassie reagent, per well. An Enspire® microplate reader was used to measure the absorbance at 595 nm. Using the absorbance of the standards as a reference, the protein concentration of the samples was determined. The lysates were used to prepare samples of specific concentrations by adding appropriate volumes of Lysis buffer and/or Laemmli sample buffer (Table 9).

4.2.6. Immunoprecipitation

Cell lysates were incubated overnight (O/N) at 4 °C with Protein A sepharose beads (Table 10) and a specific antibody (Table 7), while rotating and shaking. An aliquot of the lysate (total protein, input) was collected and following Laemmli sample buffer (Table 9) addition, boiled for 10 min at 95 °C. The following day, the beads were sedimented by centrifugation for 2 min at 210 x g and 4 °C and the supernatant samples were collected, mixed with Laemmli sample buffer and boiled at 95 °C for 10 min. The beads were then washed four times with the lysis buffer (Table 9) supplemented with protease and phosphatase inhibitors. After the last washing step, the proteins were eluted from the beads with Laemmli sample buffer addition and incubation for 10 min at 95 °C, while vortexing.

4.2.7. Immunoblotting

4.2.7.1. Sodium dodecyl sulfate (SDS)-Polyacrylamide gel electrophoresis (PAGE)

SDS-PAGE is a technique employed to separate charged molecules according to their molecular weights in an electric field. SDS is used to unfold and mask the intrinsic charges of proteins, resulting in proteins having very similar charge-to-mass ratios. In this way, upon application of an electric field, the proteins migrate through the gel matrix towards the anode with a different velocity according to their mass, with the low molecular weight proteins moving at a faster rate than the high molecular weight ones. Proteins were denatured in Laemmli sample buffer (Table 9) for 5 min at 95 °C and were separated at 25 mA per gel either on 8 %, 10 % or 12 % SDS-PAGE gels or on 4-20 % precast protein gels (Table 4). Standardized protein molecular weight markers (Table 10) were used as a reference to determine the molecular weights of the proteins during separation.

4.2.7.2. Western blotting

Proteins separated by SDS-PAGE were transferred onto polyvinylidene fluoride (PVDF) membranes (Table 3), which had been activated with 99 % ethanol (Table 4). The transfer was achieved either using a wet transfer system/tank blot and tank blot transfer buffer (Table 9) (110 V, 2 hours and 4 °C) or by TransBlot Turbo transfer system (Table 3) (1.3 A/stack, 25 V, 10 min, RT) using the TransBlot Turbo transfer buffer (1X) (Tables 9 and 10).

4.2.7.3. Immunodetection

Following the Western blot procedure, to prevent non-specific binding of antibodies, the membranes were incubated in blocking buffer (either in 5 % skim milk or 5 % BSA in TBS-T (Table 9)) for 1 hour at RT under constant agitation. Next, the membranes were incubated O/N with primary antibody (Table 7) diluted in blocking buffer (Table 9) at 4 °C. The following day, the membranes were washed 3 x 10 min with TBS-T and then incubated for 1 hour with secondary antibody (Table 8) coupled to horseradish peroxidase (HRP) diluted in blocking buffer. Membranes were washed

Materials and Methods

3x 10 min in TBS-T and proteins were detected by enhanced chemiluminescence using an HRP substrate (Table 10).

4.2.7.4. Coomassie staining

Proteins separated by SDS-PAGE were fixed in gel using Coomassie fixation solution (Table 9) for 1 min at RT. Protein staining was performed with Coomassie staining solution (Table 9) for 1 hour at RT, followed by the destaining procedure done O/N at RT using the Coomassie destaining solution (Table 9).

4.2.8. Mass Spectrometry

After Coomassie Brilliant Blue staining, the lanes of interest were excised from the gel and minced to approximately 2 mm³ pieces. The gel pieces were digested with trypsin. Reduction of disulfide bonds and alkylation was not carried out. Samples were measured using the Thermo Orbitrap Elite, coupled to UltiMate 3000 RSLC nano LC system at the Leibniz-Forschungsinstitut für Molekulare Pharmakologie (FMP; Berlin, Germany). The MaxQuant software package version 1.5.5.1 was used for the analysis (FMP; Berlin, Germany).

4.2.9. Immunofluorescence microscopy

H9C2 cells were seeded onto 12 mm coverslips placed into 35 mm cell culture dishes. The cells were treated either with forskolin, or PMA or the combination of both compounds for 30 min. Next, the medium was aspirated, the cells were washed once with 1X PBS and then fixed with 10 % trichloroacetic acid for 10 min at RT. Upon removal of the fixing solution, the cells were washed three times with 1X PBS and then permeabilized with 0.1 % Triton-X for 5 min at RT, followed by three other washing steps with 1X PBS. The cells were blocked with blocking buffer (Table 9) for 1 hour at 37 °C in order to decrease the unspecific binding. The primary antibody (Table 7) was diluted in blocking buffer (Table 9) and 35 µL antibody dilution was added onto each coverslip. The incubation was performed in a wet chamber for 1.5 hours at 37 °C and was followed by three washings with 1X PBS. The coverslips were incubated simultaneously in a wet chamber for 1 hour at 37 °C with a fluorophore-coupled secondary antibody (Table 8) diluted in blocking buffer (Table 9) and DAPI (Table 10) for staining cell nuclei. The coverslips were washed three times

with 1X PBS and finally mounted on microscope slides using Immu-Mount™ (Table 10). The samples were stored O/N at 4 °C.

4.2.10. Confocal microscopy (Laser scanning microscope (LSM) 780)

The coverslips were analyzed *via* confocal microscopy using a laser scanning microscope (LSM) 780 at the Leibniz-Forschungsinstitut für Molekulare Pharmakologie (FMP; Berlin, Germany). The images were captured at 40X magnification and three channels were recorded: DAPI (laser: 405 nm and filter: 415-495 nm), Cy3 (laser: 561 nm and filter: 566-631 nm) and Cy5 (laser: 633 nm and filter: 638-740 nm).

4.2.11. Molecular cloning

4.2.11.1. Polymerase Chain Reaction (PCR) with non-complementary primers

PCR reactions with non-complementary primers were used in order to amplify specific regions or delete specific nucleotides from certain DNA constructs. For this purpose, specific forward and reverse DNA primers were utilized. The composition of the PCR reaction is described in Table 17, while the PCR reaction protocol is detailed in Table 18.

Table 17: Composition of PCR mix

Component	Volume [μ L]	Final amount
DNA template [5 ng/ μ L]	2.5	12.5 ng
Fw primer (10 μ M)	2	0.4 μ M
Rv primer (10 μ M)	2	0.4 μ M
PfuUltra II polymerase (2.5 U/ μ L)	1 μ L	2.5 U
PfuUltra II reaction buffer (10X)	5	1x
dNTP mix (5 mM)	5	0.5 mM
MgCl ₂ (25 mM)	2	1 mM
ddH ₂ O (RNase free)	ad 50 μ L	

Table 18: PCR protocol

Step	Temperature [°C]	Time [min]	Cycles
1. Preheating	92	2	
2. Denaturation	92	0.5	
3. Annealing	60	1	
4. Elongation	68	0.5	Repeat with step 2, 30x
5. Precooling	68	1	
6. Cooling	4	∞	

4.2.11.2. Site-directed mutagenesis

PCR was used to introduce specific point mutations into plasmid DNA. For this, primer pairs carrying the specific mutations were used (Table 12). The mutagenesis PCR mixture and reaction protocol are described in Tables 19 and 20. Next, the plasmid DNA was incubated with DpnI restriction enzyme for 1 hour at 37 °C in order to degrade the methylated, non-mutated, parental DNA. The enzyme was inactivated by incubation at 80 °C for 10 min.

Table 19: Composition of mutagenesis PCR mix

Component	Volume [μL]	Final amount
DNA template [1 ng/μL]	20	10 - 25 ng
Fw primer (10 μM)	2	0.4 μM
Rv primer (10 μM)	2	0.4 μM
PfuUltra II polymerase (2.5 U/μL)	1 μL	2.5 U
PfuUltra II reaction buffer (10X)	5	1x
dNTP mix (5 mM)	5	0.5 mM
MgCl ₂ (25 mM)	2	1 mM
ddH ₂ O (RNase free)	ad 50 μL	

Table 20: Mutagenesis PCR protocol

Step	Temperature [°C]	Time [min]	Cycles
1. Preheating	92	2	

2. Denaturation	92	0.5	
3. Annealing	55	1	
4. Elongation	68	1/ Kb of template	Repeat with step 2, 30x
5. Precooling	68	Double as step 4	
6. Cooling	4	∞	

4.2.11.3. DNA cleavage with restriction endonucleases

Digestion of DNA fragments was carried out for 1 hour at 37 °C. Depending on the pair of enzymes used (Table 13), the reactions were heated for additional 10 min to either 65 °C or 80 °C in order to inactivate the enzymes. The components and amounts used in the reaction mixture are described in Table 21.

Table 21: Composition of plasmid and insert digestion

Component	Volume [μ L]	Final amount
Plasmid [1 μ g/ μ L]	5	5 μ g
Restriction enzyme I	1	20 U
Restriction enzyme II	1	20 U
Cut Smart buffer (10X)	5 μ L	1x
ddH ₂ O (RNase free)	ad 50 μ L	

4.2.11.4. Agarose gel electrophoresis

The DNA fragments were visualized by agarose gel electrophoresis. Agarose (1 % (w/v)) was dissolved in TAE buffer (Table 9) and boiled in a microwave oven until the solution became clear. Afterwards, the agarose solution was left to cool down to approximately 50 °C, after which, the DNA stain Redsafe (Table 10; 1:20,000) was added and the gels were cast. After the gels polymerized, 5 μ L of the PCR reaction or the entire digestion reaction were mixed with DNA loading buffer and loaded onto the gel. The DNA molecular weight standard HyperLadder I or II was run alongside the samples in order to be able to determine the size of the DNA fragments. The gels were run for 60 min in 1X TAE buffer at 130 V and the DNA was visualized using a GelDoc 2000 imaging system with a 520 nm filter (Table 3).

4.2.11.5. DNA purification from agarose gels

The DNA band of interest was excised from the agarose gel and purified using a NucleoSpin® Extract II kit (Table 5) according to the manufacturer's instructions.

4.2.11.6. Ligation

The insert and vector fragments were mixed in a molar ratio of 3:1 and incubated together with the DNA Ligase and T4 ligase reaction buffer O/N at 16 °C, as described below (Table 22):

Table 22: Composition of plasmid and insert ligation

Component	Volume [μL]	Final amount
Plasmid	1	100 ng
Insert	x	Insert: plasmid molar ratio of 3: 1
T4 ligase	1	400 U
T4 ligase buffer (10X)	2 μL	1x
ddH ₂ O (RNase free)	ad 20 μL	

4.2.11.7. Transformation

In order to introduce DNA into the bacteria, plasmid DNA was added to *E.coli* DH5 α chemically competent cells, which were then incubated on ice for 10 min. A heat shock of 90 sec at 42 °C was used to promote bacterial uptake of the foreign DNA, which was followed by 5 min incubation on ice. Next, the transformed bacteria were incubated for 1 hour at 37 °C in normal LB medium under continuous agitation. Lastly, the bacteria were plated onto ampicillin or kanamycin containing agar plates and incubated O/N at 37 °C.

4.2.11.8. Culture inoculation

Single bacterial colonies were picked and grown O/N at 37 °C in 4 mL LB medium supplemented with 100 $\mu\text{g/ mL}$ ampicillin or kanamycin. In order to grow larger cultures, 1 mL of the bacterial preculture was transferred to 200 mL LB medium containing 100 $\mu\text{g/mL}$ ampicillin or kanamycin and were grown O/N at 37 °C.

4.2.11.9. DNA isolation and purification

The grown bacteria was harvested and the DNA was isolated using either the NucleoSpin® Plasmid QuickPure kit (for minipreparation of plasmid DNA) or the NucleoBond® Xtra Midi/ Maxi (for the midi or maxi preparation of plasmid DNA) according to the manufacturer's instructions (Table 5).

4.2.11.10. DNA sequencing

The purified DNA was sequenced by LGC Genomics (Berlin, DE) using standard and custom-made primers (Table 12) specific for the DNA of interest.

4.3. Statistical analysis

Statistically significant differences were determined with GraphPad Prism 7.0 software using one-way and two-way ANOVA and Bonferroni multi-comparison. Significant differences are indicated as * $p \leq 0.05$; ** $p \leq 0.01$; *** $p \leq 0.001$; **** $p \leq 0.0001$.

5. Results

5.1. A deletion in the regulatory region of the *PDE3A* gene recapitulates HTNB in a rat model

All HTNB-affected individuals have mutations within a 15-base pair (bp) region of the *PDE3A* gene. The HTNB mutations cause amino acid substitutions and deletions in a hotspot region of the N-terminal regulatory domain of PDE3A1 and PDE3A2; however, direct evidence showing that the mutations cause the disease was lacking. To validate that the mutations found in the regulatory region of the *PDE3A* gene cause HTNB we generated in a collaborative approach a rat model carrying an aberration in this region using CRISPR/Cas9. The animal model was generated by deleting 9 bps from the *Pde3a* gene using CRISPR/Cas9 (Laboratory of M. Bader, MDC). This deletion corresponds to the absence of three amino acids ($\Delta 3aa$) in the hotspot region of PDE3A regulatory domain. Analogous to a human deletion (Renkema et al. 2018), amino acids 441-443 are absent in the rat enzyme and they are analogous to amino acids 444-446 (Thr-Thr-Ser) in the human protein. HTNB is an autosomal dominant disease and therefore the patients carry the PDE3A mutations on one allele. Thus, the heterozygous animals match the patient situation. A rat model carrying a 20 bp deletion was also generated. The deletion causes a frameshift mutation that introduces a stop codon, creating a short, truncated protein that lacks the catalytic domain. This rat strain, when homozygous, represents a functional deletion (DEL), since it lacks catalytically active PDE3A (Figure 9) (Ercu et al. 2020).

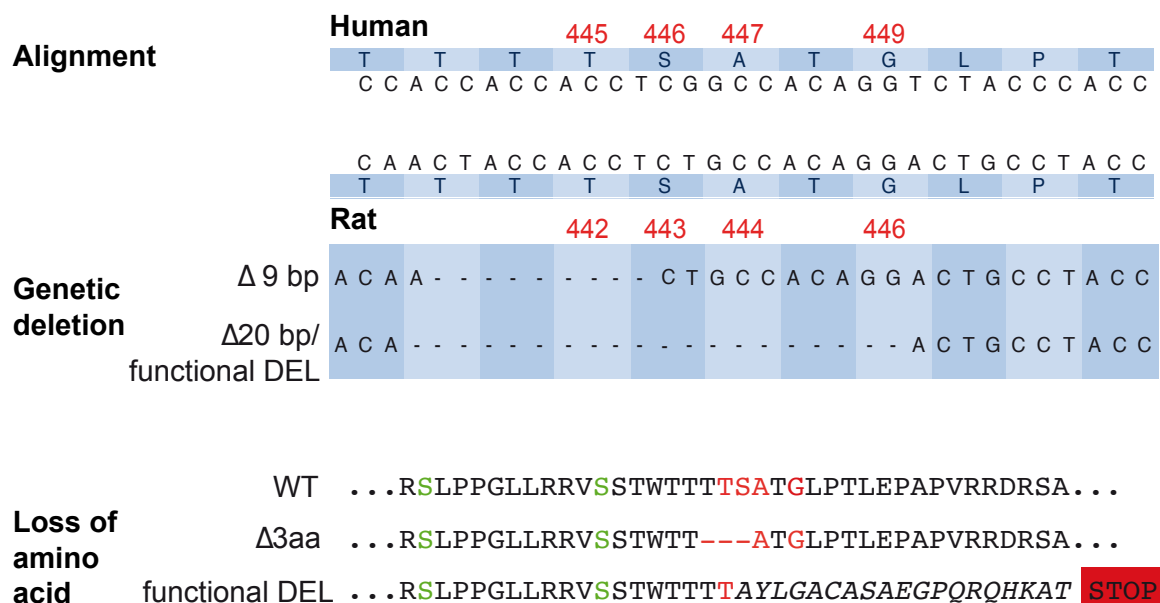


Figure 9: HTNB rat model. A 9 bp deletion in the *Pde3a* gene corresponding to a 3-amino acid deletion (Δ 3aa) in the protein recapitulates HTNB in a rat model. Another rat model harbors a 20 bp deletion in the PDE3A gene, thus resulting in a frameshift mutation and truncated, catalytically inactive protein (functional DEL). Shown is the alignment between human and rat gene and protein sequences (Ercu et al. 2020).

The heterozygous rats carrying the three amino acid deletion in PDE3A (Δ 3aa HET) had shorter digits as compared to wild-type (WT) and functional DEL animals, resembling the HTNB phenotype observed in patients. This was confirmed by MicroCT of the left forepaws with which the length of the metacarpal bone III was measured and quantified (Figure 10A; Preclinical Research Center, MDC).

Radio-telemetry measurements were performed in WT, Δ 3aa HET, homozygous Δ 3aa (Δ 3aa HOM), and functional DEL animals at age >9 months (Laboratory of M. Bader, MDC). The systolic (SBP) and diastolic (DBP) blood pressure values (mmHg) as well as the heart rate (beats per minute (BPM)) were recorded and are summarized in Table 23.

Results

Table 23: Radio-telemetric blood pressure measurements. Systolic (SBP) and diastolic (DBP) blood pressure (mmHg) as well as heart rate (BPM) values for WT (n = 6), Δ 3aa HET (n = 4), Δ 3aa HOM (n = 4) and functional DEL (n = 5) rats.

Genotype	SBP/DBP (mmHg)	BPM
WT	125/88	297
Δ 3aa HET	148/105	293
Δ 3aa HOM	155/120	294
Functional DEL	115/84	330

The Δ 3aa HOM (155/120 mmHg) followed by the Δ 3aa HET (148/105 mmHg) rats had the highest mean blood pressure values respectively, followed by the WT (125/88 mmHg) animals and lastly by the functional DEL (115/84 mmHg) group. The systolic blood pressure differs significantly between all groups except between Δ 3aa HET and HOM rats (Supplemental Table S1). The diastolic blood pressure is significantly different between all tested groups (Supplemental Table S1). With respect to heart rates, the WT and Δ 3aa animals had similar values (WT: 297 BPM; Δ 3aa HET 293 BPM and Δ 3aa HOM 294 BPM), whereas the functional DEL rats had the highest values (330 BPM) (Figure 10B). Significantly different heart rates were found between functional DEL rats and Δ 3aa HET and HOM animals respectively (Supplemental Table S1).

It was previously shown that VSMCs derived from patient mesenchymal stem cells proliferated faster than those derived from unaffected individuals (Maass et al. 2015). To verify that the HTNB rats show signs of increased cellular proliferation, morphological analysis of second-order mesenteric arteries from WT, Δ 3aa HET and functional DEL animals was employed (Laboratory of M. Bader, MDC). For this, hematoxylin and eosin (HE) staining was performed and the media-to-lumen ratio was calculated and quantified. The Δ 3aa HET rats displayed increased media-to-lumen ratio as compared to the WT animals, whereas the ratio of the functional DEL animals was decreased compared to the WT controls (Figure 10C) (Ercu et al. 2020).

PDE3A is inhibited by cGMP (Movsesian 2016). The small molecule BAY 41-8543 is a stimulator of soluble guanylyl cyclase (sGC), thereby promoting cGMP production. WT and Δ 3aa HET animals were treated with BAY 41-8543 and their mean arterial pressure was measured (Laboratory of M. Bader, MDC). The compound reduced the mean arterial pressure for both sets of animals, though more

efficiently for the mutant rats, from 114 to 92 mmHg compared to 91 from 99 mmHg for the WT animals (Figure 10D). Subsequent FRET experiments revealed that BAY 41-8543 caused inhibition of PDE3A (see below, Figure 20B). These data suggest that activation of sGC and therefore inhibition of PDE3A could be a potential treatment option for HTNB patients (Ercu et al. 2020).

HTNB patients present looping of their left-side posterior inferior cerebellar artery (PICA) or of vertebral artery (Naraghi et al. 1997). MicroCT imaging of brain vessels derived from WT and $\Delta 3aa$ HET rats showed that the mutant animals also have PICA loops, whereas no such loops were observed in the WT ones (Figure 10E; Preclinical Research Center, MDC) (Ercu et al. 2020).

Results

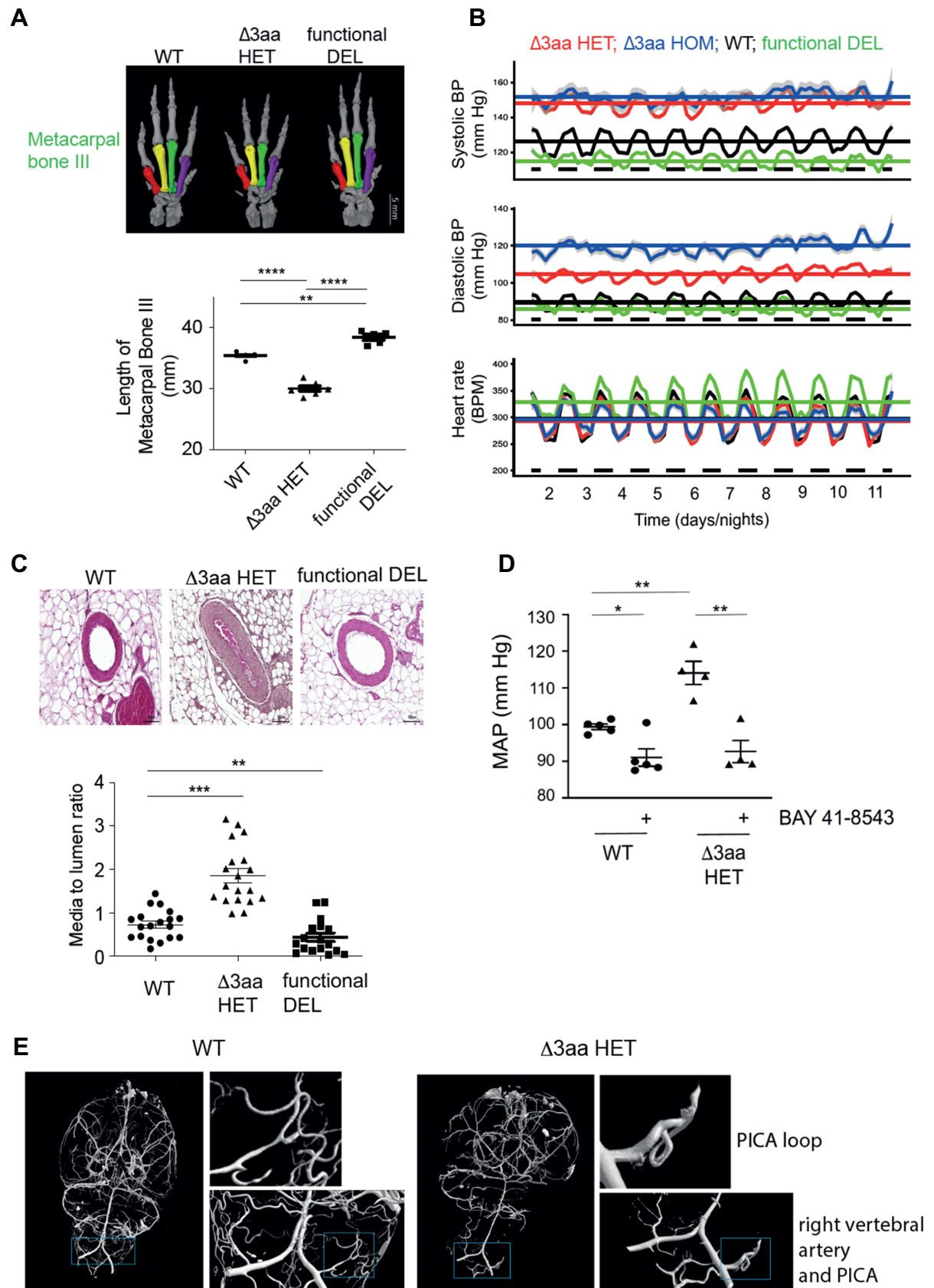


Figure 10: HTNB is recapitulated by a rat model expressing mutant ($\Delta 3aa$) PDE3A. (A) Upper panel: MicroCT images of the left front paws. Lower panel: Quantification of the forepaw metacarpal bone III. Statistical analysis was carried out using one-way ANOVA and Bonferroni multi-comparison (WT: n = 4; $\Delta 3aa$ HET: n = 7; functional DEL: n = 5). Mean \pm SEM is plotted, **p < 0.01, ****p < 0.0001. **(B)** Radio-telemetry measurements for WT (black; n = 6), $\Delta 3aa$ HET (red; n = 4), $\Delta 3aa$ HOM (blue; n = 4) and functional DEL (green; n = 5) rats. Blood pressure (systolic and diastolic, mmHg) and heart rate (BPM) over time (> 10 days) are plotted. Curves depict loess fits with gray intervals reflecting 95 % confidence intervals for loess parameters. Model expectation values for WT and mutant rats are depicted by the horizontal lines and the lower black bars represent night periods. All p values are listed in Supplemental Table S1. Significance (nested model likelihood ratio test p value) and effect size (model fit parameter, same unit as vertical axis) is noted. **(C)** Media-to-lumen ratio is increased in $\Delta 3aa$ HET rats and decreased in functional DEL animals compared to the WT ones. Upper panel: Representative images of mesenteric arteries from each rat genotype. Lower panel: Quantifications of 3-5 mesenteric arteries per rat are shown. Statistical analysis was carried out using one-way ANOVA and Bonferroni multi-comparison; n = 3 for WT, n = 3 for $\Delta 3aa$ and n = 2 for functional DEL. Mean \pm SEM is plotted, **p < 0.01, ***p < 0.001. **(D)** Mean arterial pressure measurements for WT and $\Delta 3aa$ HET animals upon treatment with the sGC stimulator BAY 41-8543. Statistical analysis was carried out using one-way ANOVA and Bonferroni multi-comparison; n = 5 for WT and n = 4 for $\Delta 3aa$ HET rats. Mean \pm SEM is plotted, *p < 0.1, **p < 0.01 **(E)** MicroCT images of rat brain vessels showing that $\Delta 3aa$ HET but not WT rats exhibit PICA loops. Microfil was used to perfuse brain vessels. Representative images for n = 5 for WT and n = 2 for $\Delta 3aa$ HET rats are shown (Ercu et al. 2020).

5.2. Elucidating molecular mechanisms underlying HTNB using a rat model

5.2.1. PDE3A expression in the aorta of WT, $\Delta 3aa$ HET and functional DEL animals

To elucidate molecular mechanisms involved in the HTNB animal model, we initially investigated the expression of PDE3A in the vessels of our model rats. For this, aorta was chosen as a representative vessel and the expression of PDE3A in WT, $\Delta 3aa$ HET and functional DEL rats was assessed. Two PDE3A isoforms, corresponding to PDE3A1 and PDE3A2, were detected in the aorta of WT and $\Delta 3aa$ HET rats and, as expected, were absent in the functional DEL animals. Lower levels of both isoforms were detected in the $\Delta 3aa$ HET animals as compared to the WT ones (Figure 11) (Ercu et al. 2020). This could either be caused by impaired

Results

detection of the protein by the PDE3A-specific antibody or due to protein degradation.

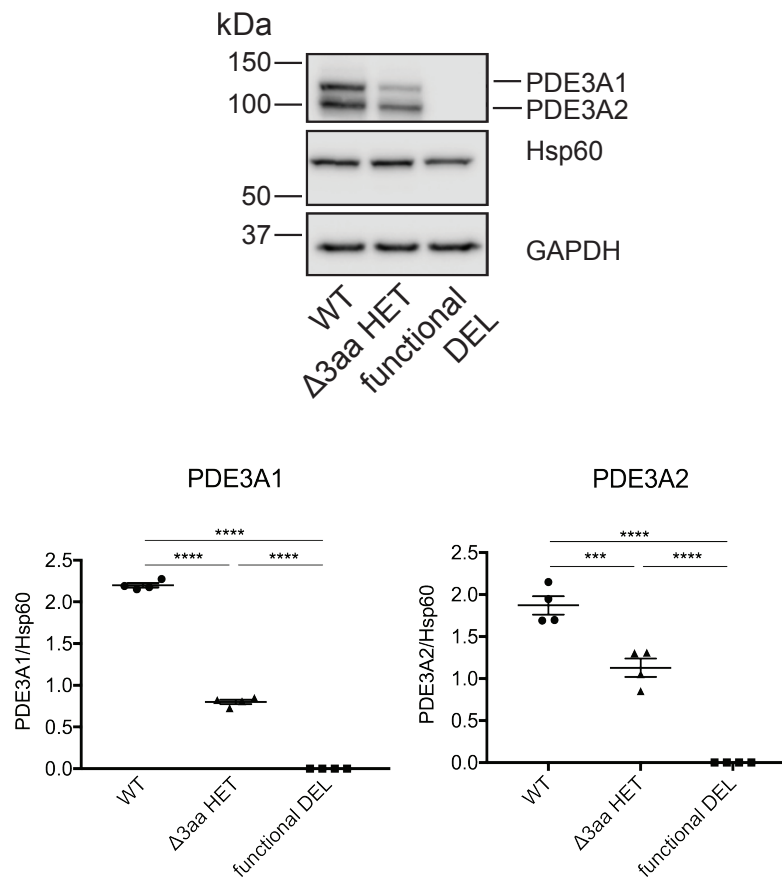


Figure 11: PDE3A1 and PDE3A2 expression in the aorta of WT, Δ3aa HET and functional DEL rats. Upper panel: PDE3A1 and PDE3A2 isoforms were detected by Western blotting in the aorta of WT, Δ3aa HET and functional DEL rats. PDE3A was not detectable in functional DEL animals. Hsp60 and GAPDH were detected as loading controls. Lower panel: Semi-quantitative analysis of PDE3A1 and PDE3A2 variants by densitometric analysis. The expression levels of PDE3A1 and PDE3A2 isoforms normalized to the loading control, Hsp60, are plotted. Statistical analysis was carried out using one-way ANOVA and Bonferroni multi-comparison; n = 4 independent experiments. Mean ± SEM is plotted, ***p < 0.001, ****p < 0.0001 (Ercu et al. 2020).

5.2.2. PDE3A deletion in the enzyme's regulatory domain and proliferation

We have shown that the HTNB rat model exhibits hyperplasia of second-order mesenteric arteries (Figure 10C). To assess whether the same happens in the aorta, HE staining was used to measure and compare the thickness of the aorta of WT,

$\Delta 3aa$ HET and functional DEL animals (Laboratory of M. Bader, MDC). More specifically, the thickness of the aortic media layer, the wide middle layer consisting of VSMCs, elastic tissue and collagen, was measured. No significant differences in the thoracic aorta media thickness were observed between the three genotypes (Figure 12) (Ercu et al. 2020).

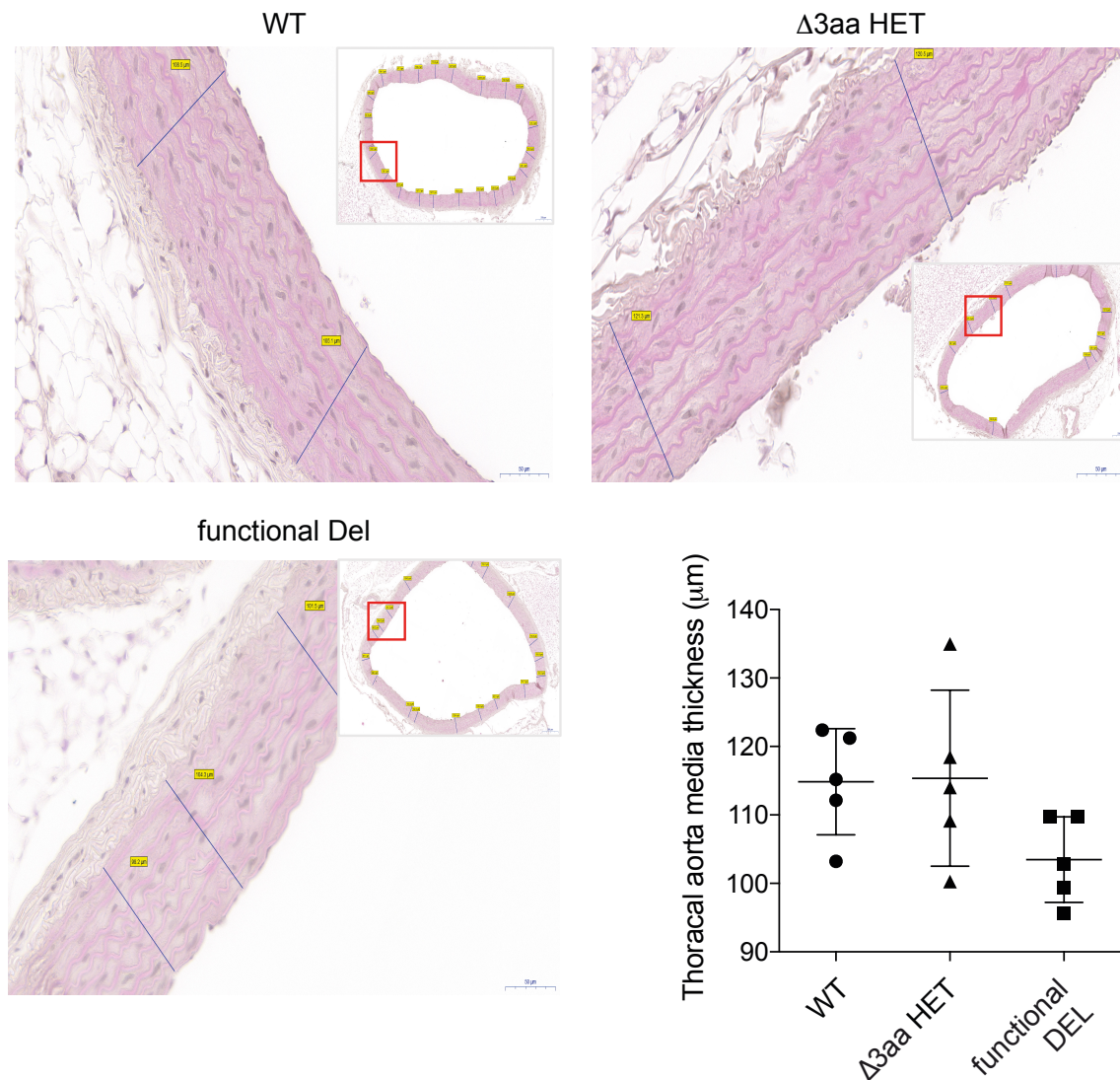


Figure 12: Similar thoracic aorta media thickness between WT and mutant rats. Hematoxylin and eosin (HE) staining images of the aorta of WT, $\Delta 3aa$ HET and functional DEL animals and the corresponding quantification of media thickness are shown. Statistical analysis was carried out using one-way ANOVA and Bonferroni multi-comparison; $n = 5$ animals per group. Mean \pm SD is plotted (Ercu et al. 2020).

Results

To validate the finding that the aorta is not affected by smooth muscle cell hyperproliferation, the level of proteins essential for cellular proliferation was investigated in aorta from WT, $\Delta 3aa$ HET and functional DEL rats. Cell proliferation is promoted *via* activation of extracellular signal-regulated kinase (ERK) 1 (44 kDa) and ERK2 (42 kDa) by phosphorylation at threonine and tyrosine residues 202 and 204 respectively (pThr202/Tyr204) (Chen, Sarnecki and Blenis 1992, Brunet et al. 1999, Kraus et al. 2015, Schevzov et al. 2015, Mebratu and Tesfaigzi 2009) and *via* activation of cAMP response element-binding protein (CREB) mediated by phosphorylation at serine residue 133 (pSer133) (Hudson et al. 2018, Long et al. 2001, Struthers et al. 1991). Moreover, inhibition of Ras homology family member A (RhoA) *via* phosphorylation at serine residue 188 (pSer188) has been shown to inhibit cellular proliferation (Lang et al. 1996, Sawada et al. 2009, Liu et al. 2017). No difference was observed in the expression levels of active ERK1/2 (pERK1/2) and active CREB (pCREB) in aorta of the three genotypes. While the amount of inactive RhoA (pRhoA) was significantly decreased in the aorta of functional DEL animals as compared to the WT controls, there was no significant difference in the amount of pRhoA expressed between aorta of WT and $\Delta 3aa$ HET rats (Figure 13). These data confirm the findings obtained by HE staining of thoracic aorta (Figure 12) and show that media hyperplasia occurs only in second-order mesenteric arteries.

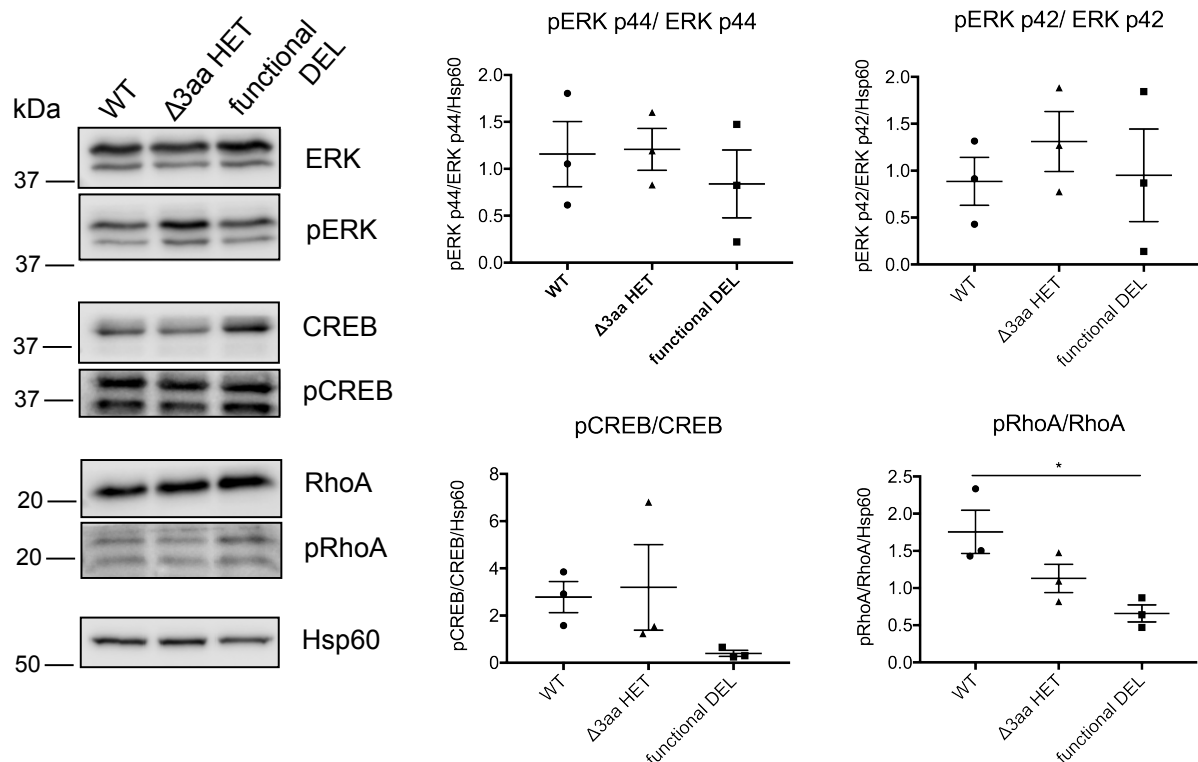


Figure 13: Cell proliferation markers were similarly expressed in aorta of WT and HTNB mutant rats. (A) Detection of phosphorylated and non-phosphorylated forms of cell proliferation markers pERK and ERK, pCREB and CREB, pRhoA and RhoA by Western blotting in aorta of WT, $\Delta 3aa$ and functional DEL rats. Hsp60 was detected as a loading control. (B) Semi-quantitative analysis of Western blots by densitometric analysis. The expression levels of the phosphorylated proteins normalized to the expression levels of the non-phosphorylated proteins and then to the loading control are plotted. Statistical analysis was carried out using one-way ANOVA and Bonferroni multi-comparison; $n = 3$ independent experiments. Mean \pm SEM is plotted, * $p < 0.1$.

5.3. New human mutations in *PDE3A*

5.3.1. A new mutation in the regulatory region of the *PDE3A* gene causes HTNB

The above-described data showed that the HTNB rat model resembles the HTNB phenotype in patients and thus that the mutations in the hotspot region of *PDE3A* regulatory domain are causative for HTNB. This conclusion was further confirmed by yet another mutation that was discovered in the hotspot region. This mutation causes a G449S substitution in *PDE3A*. A woman aged 54 years from Germany having a history of hypertension of 17 years as well as cerebral seizures and mild hypercholesterolemia was admitted to hospital due to severe hypertension (190/100 mmHg). She was also diagnosed with brachydactyly type E, confirming the diagnosis of HTNB (Figure 14). She did not show any symptoms of end organ damage (e.g. left ventricular hypertrophy, macrovascular damage, renal failure) that may have been caused by the severe hypertension. Her 23-year old daughter, who suffers from moderate age-related hypertension and brachydactyly type E, was also diagnosed with HTNB, having the same missense mutation in *PDE3A* (Figure 14) (Ercu et al. 2020).

Results

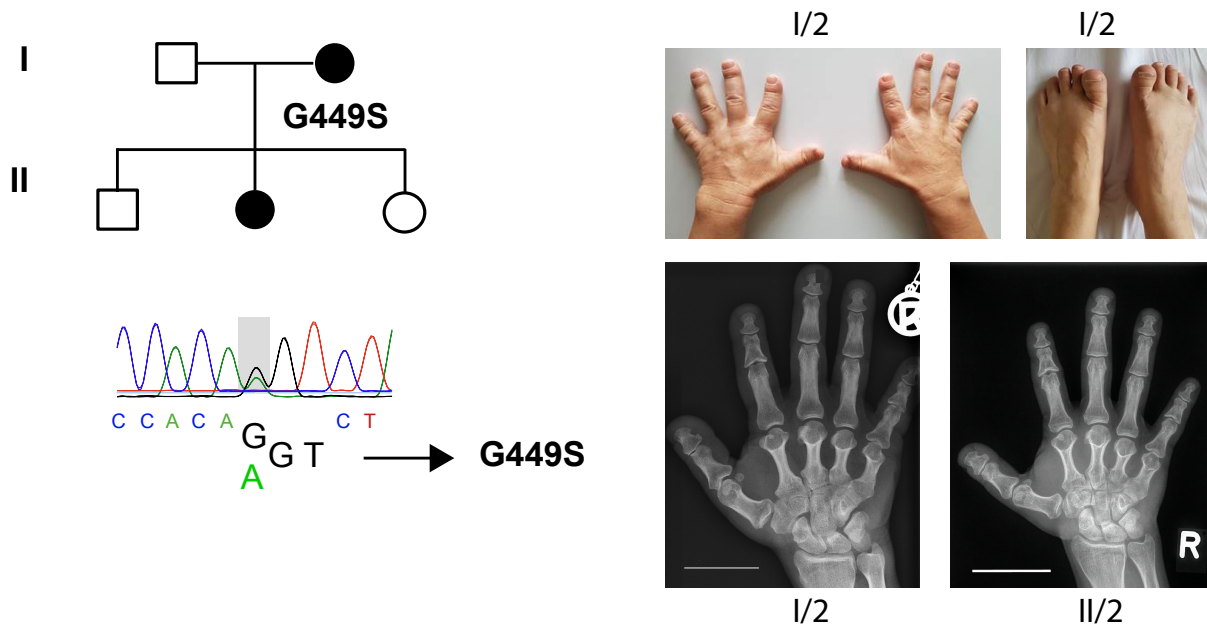
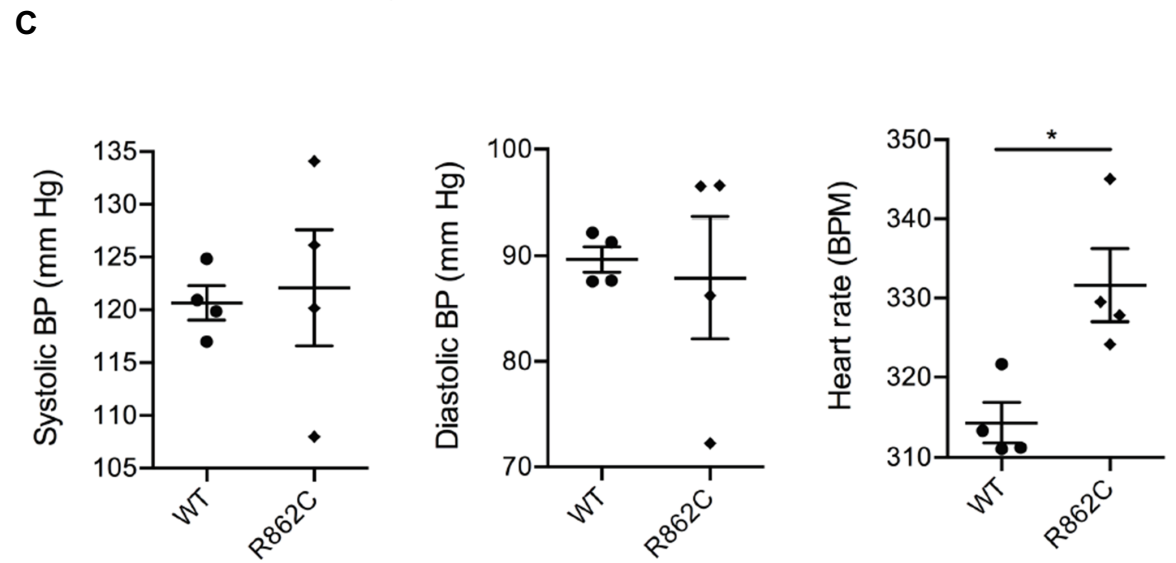
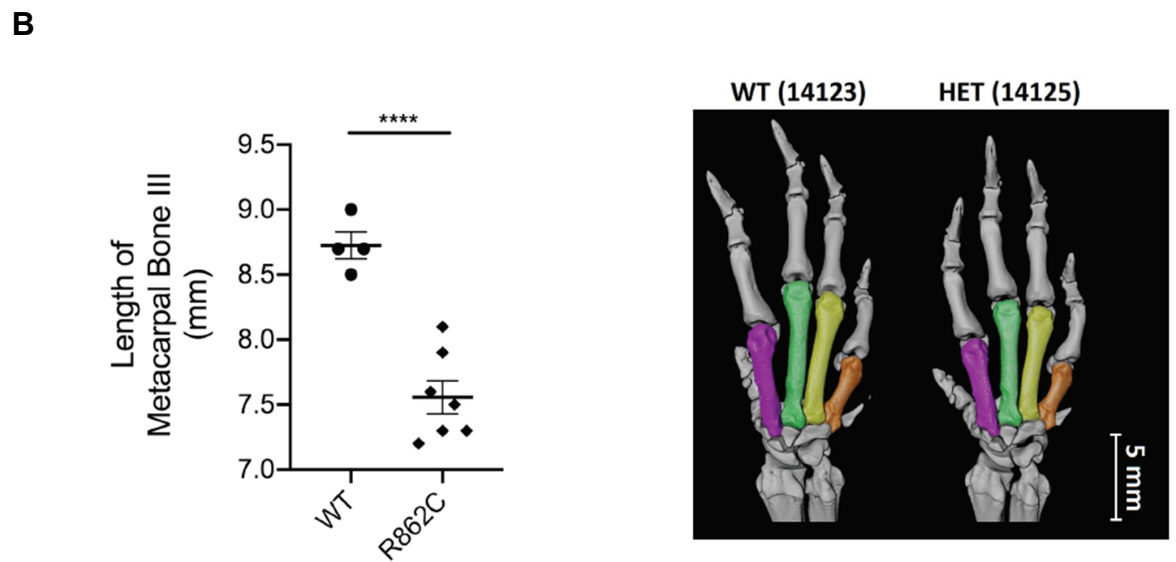
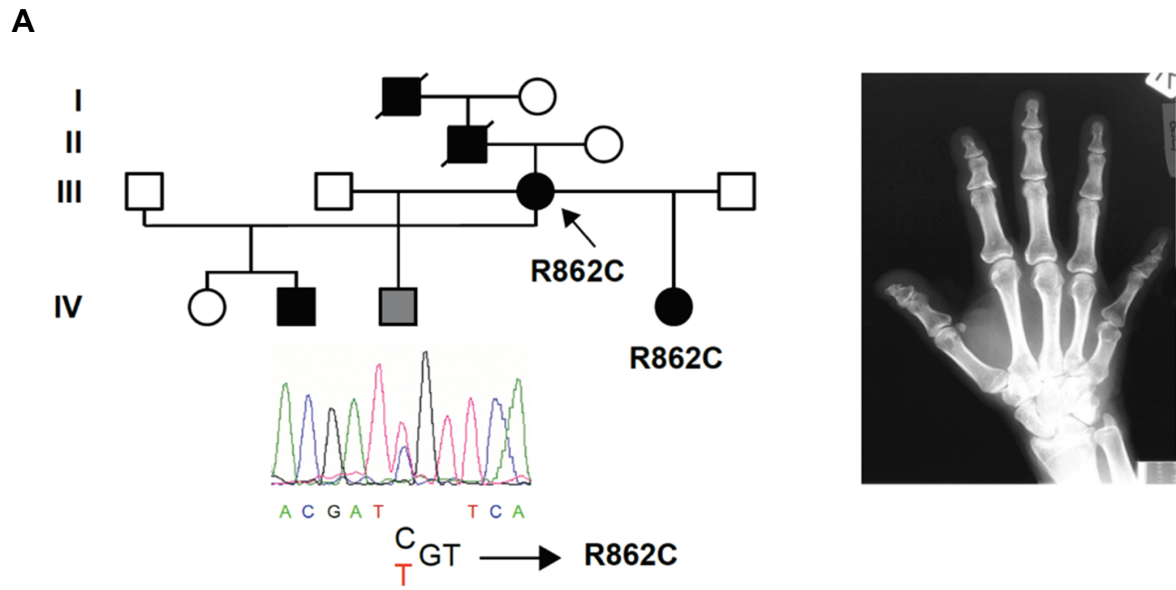


Figure 14: A G449S substitution in PDE3A causes HTNB. A novel G449S substitution in the N-terminal regulatory domain of PDE3A was found in a 54-year old woman and her 23-year old daughter. A pedigree showing the affected individuals (black) is presented. Photographs and roentgenograms displaying the hands and feet of the mother (I/2) are shown (Ercu et al. 2020).

5.3.2.A new mutation in the region encoding the catalytic domain of PDE3A

A new missense mutation in exon 13 of *PDE3A* was discovered in a New Zealand family. The mutation causes an R862C substitution within the enzyme's catalytic domain. All affected members suffer from brachydactyly type E. Members where hypertension was documented are shown in black in the pedigree. The gray proband did not display signs of hypertension since recordings of 122/84 mmHg were obtained at the age of 23 (Figure 15A). These data indicate that the HTNB phenotype is not 100 % penetrant when PDE3A mutations affect the region encoding for the catalytic domain of PDE3A.



Results

Figure 15: Missense mutation identified in the region encoding the catalytic domain of PDE3A.

(A) A novel R862C substitution in the catalytic domain of PDE3A was found in a New Zealand kindred. A pedigree showing the individuals carrying the mutations and affected (black) or not affected (gray) by hypertension is presented. Roentgenograms displaying the right hand of patient III/3 is shown. (B) MicroCT images of the right front paws and quantification of the forepaw metacarpal bone III. Statistical analysis was carried out using one-way ANOVA and Bonferroni multi-comparison (WT: n = 4; R862C: n = 7). Mean \pm SEM is plotted, ****p < 0.0001. (C) Radio-telemetry measurements for WT and R862C rats. The average blood pressure (systolic and diastolic, mmHg) and heart rate (BPM) for 10 days are plotted. Statistical analysis was carried out using unpaired t-test (WT: n = 4; R862C: n = 4). Mean \pm SEM is plotted, *p < 0.1.

As a model, rats carrying this mutation were generated using CRISPR/Cas9 (Laboratory of M. Bader, MDC). Similar to what was observed for the Δ 3aa HET animals (Figure 10A), the heterozygous rats carrying the R862C substitution had shorter digits as compared to the WT animals, therefore resembling the patient skeletal phenotype. This was shown by MicroCT imaging of the right forepaws in which the length of the metacarpal bone III was measured and quantified (Figure 15B; Preclinical Research Center, MDC).

Radio-telemetry measurements were performed in WT and R862C animals (Laboratory of M. Bader, MDC) (Figure 15C). The systolic (SBP) and diastolic (DBP) blood pressure values (mmHg) as well as the heart rate (beats per minute (BPM)) were recorded and are summarized in Table 24.

Table 24: Radio-telemetric blood pressure measurements. Systolic (SBP) and diastolic (DBP) blood pressure (mmHg) as well as heart rate (BPM) values for WT (n = 4) and R862C (n = 4) rats.

Genotype	SBP/DBP (mmHg)	BPM
WT	121/90	314
R862C	122/88	332

The systolic and diastolic blood pressure (BP) (mmHg) measurements showed no significant difference between the two groups of animals (Figure 15C and Table 24), unlike the Δ 3aa HET animals that had significantly higher systolic and diastolic BP than WT (Figure 10B). The heart rate (BPM) was significantly increased in the R862C rats compared to the WT (Figure 15C and Table 24), again in contradiction to the Δ 3aa HET animals, which exhibited similar heart rates to the WT (Figure 10B).

These data confirm that the mutations found in the region encoding the catalytic domain of PDE3A lead to a non-fully penetrant HTNB syndrome. More specifically, the skeletal phenotype, but not the blood pressure phenotype, is fully penetrant; i.e. mutations in the hot spot region in the N-terminal regulatory domain cause the manifestation of the whole phenotype, whereas the catalytic domain is required for normal skeleton development.

5.4. PDE3A mutations cause aberrant signaling both in the cytosol and at the plasma membrane (PM)

To gain insight into the molecular mechanisms underlying HTNB, the location and activity of WT and mutant PDE3A was measured using FRET. For this, a HEK293 cell system was used in which the cAMP-based sensor ICUE3 was co-expressed with either WT or mutant ($\Delta 3aa$, G449S, T445N and R862C) PDE3A. To be able to identify the cells expressing PDE3A, the WT and mutant PDE3A1 (membrane-bound) and PDE3A2 (cytosolic) variants were genetically fused with the fluorescent protein mCherry (Figure 16).

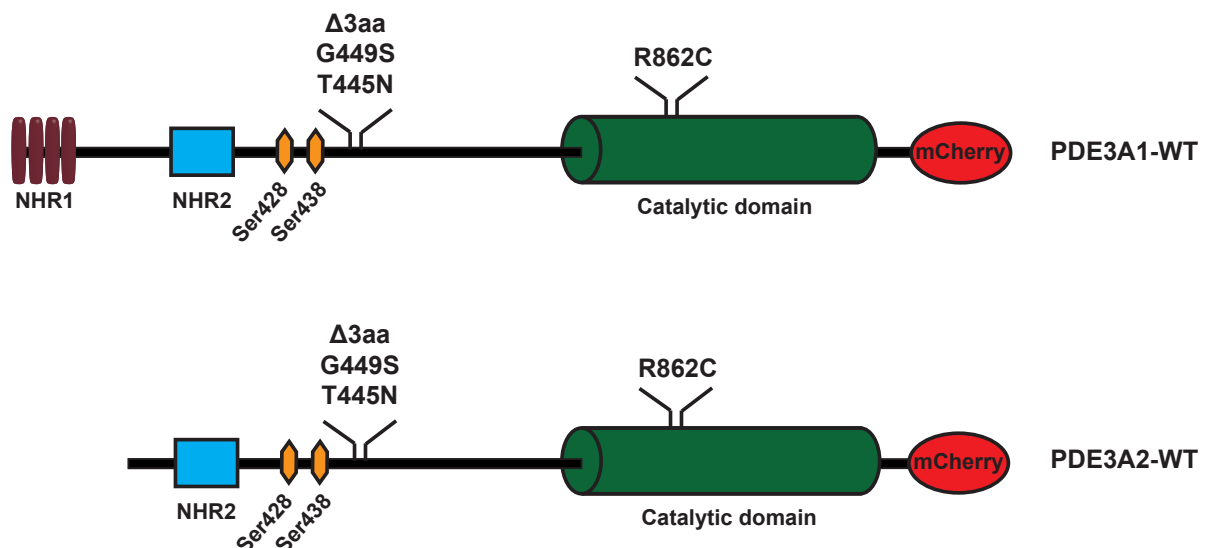


Figure 16: Schematic representation of mCherry-tagged PDE3A1 and PDE3A2 WT and mutant ($\Delta 3aa$, G449S, T445N and R862C) variants. The two N-terminal hydrophobic regions, NHR1 and NHR2, as well as the two serine residues (Ser428 and Ser438) that have been shown to be hyperphosphorylated in HTNB are also shown.

5.4.1. PDE3A1 and 2 are located mainly in the cytosol and the activity of mutant PDE3A is increased

PDE3A1 is predominantly localized to membranes, whereas PDE3A2 is primarily a cytosolic protein, although it can be membrane-associated as well (Figure 5 and Figure 16) (Wechsler et al. 2002).

To confirm expression of the mCherry-tagged PDE3A1 and PDE3A2 constructs, fluorescence microscopy imaging was conducted. WT, T445N and R862C PDE3A1 and PDE3A2 tagged with mCherry (red) were expressed in HEK293 cells and DAPI (blue) was used for nuclear staining. The T445N mutation was chosen as representative for the mutations affecting the hotspot region within the regulatory domain of the enzyme. Both PDE3A isoforms appeared to predominantly localize in the cytosol and no clear difference was visible between the WT and the mutant proteins. (Figure 17). Therefore, it was decided to initially measure FRET in the cytosol in order to investigate the activity of WT and mutant PDE3A.

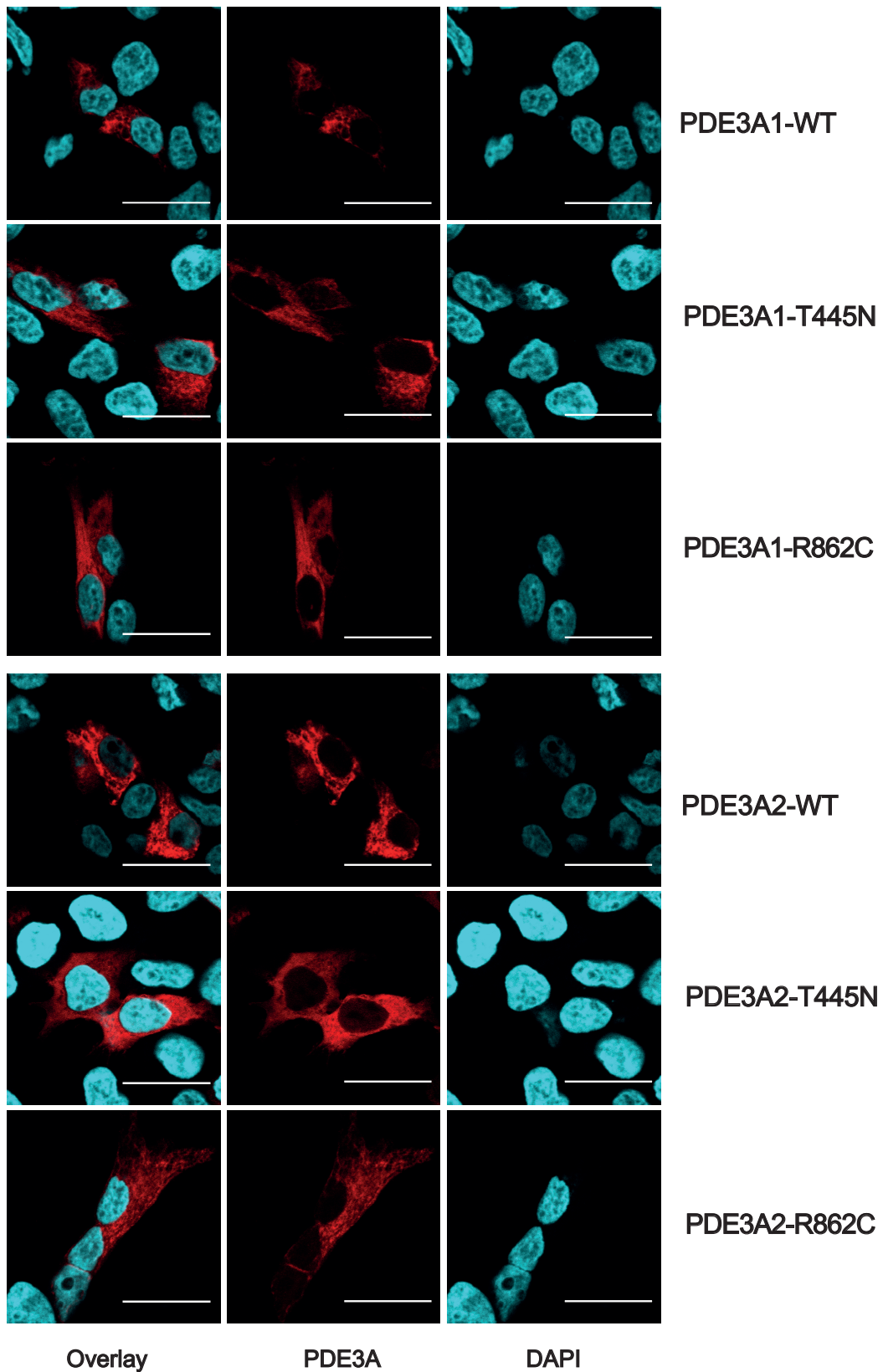


Figure 17: mCherry-tagged PDE3A1 and PDE3A2 are localized mainly in the cytosol in HEK293 cells. Microscopy images of HEK293 cells expressing WT, T445N or R862C PDE3A1 (upper panel) or PDE3A2 (lower panel) fused to mCherry (red). Nuclei were stained with DAPI. Scale bar: 20 μ M.

Results

The activity of WT and mutant (Δ 3aa, G449S, T445N and R862C) PDE3A was measured in HEK293 cells by FRET using the cytosolic cAMP-based sensor ICUE3 and the cytosolic PDE3A2 isoform. Only the cells expressing both the ICUE3 sensor (green signal) and PDE3A-mCherry (red signal) were selected for measurements. To test the system, HEK293 cells were transfected with the negative controls, namely CFP and Venus, either alone or together, or with a CFP-YFP tandem construct, which was used as a positive control to set 100 % FRET signal (Figure 18A). Further controls include the spectra showing the emission of ICUE3 sensor under resting conditions and upon the treatments used in the subsequent FRET experiments, i.e. the AC activator forskolin (F) (30 μ M, 2 min) and forskolin together with the PDE3 inhibitors milrinone (F+M) (30 μ M, 30 min) or cilostamide (F+C) (10 μ M, 20 min) or the sGC activator BAY 41-8543 (F+B) (15 μ M, 15 min) (Figure 18B) (Ercu et al. 2020).

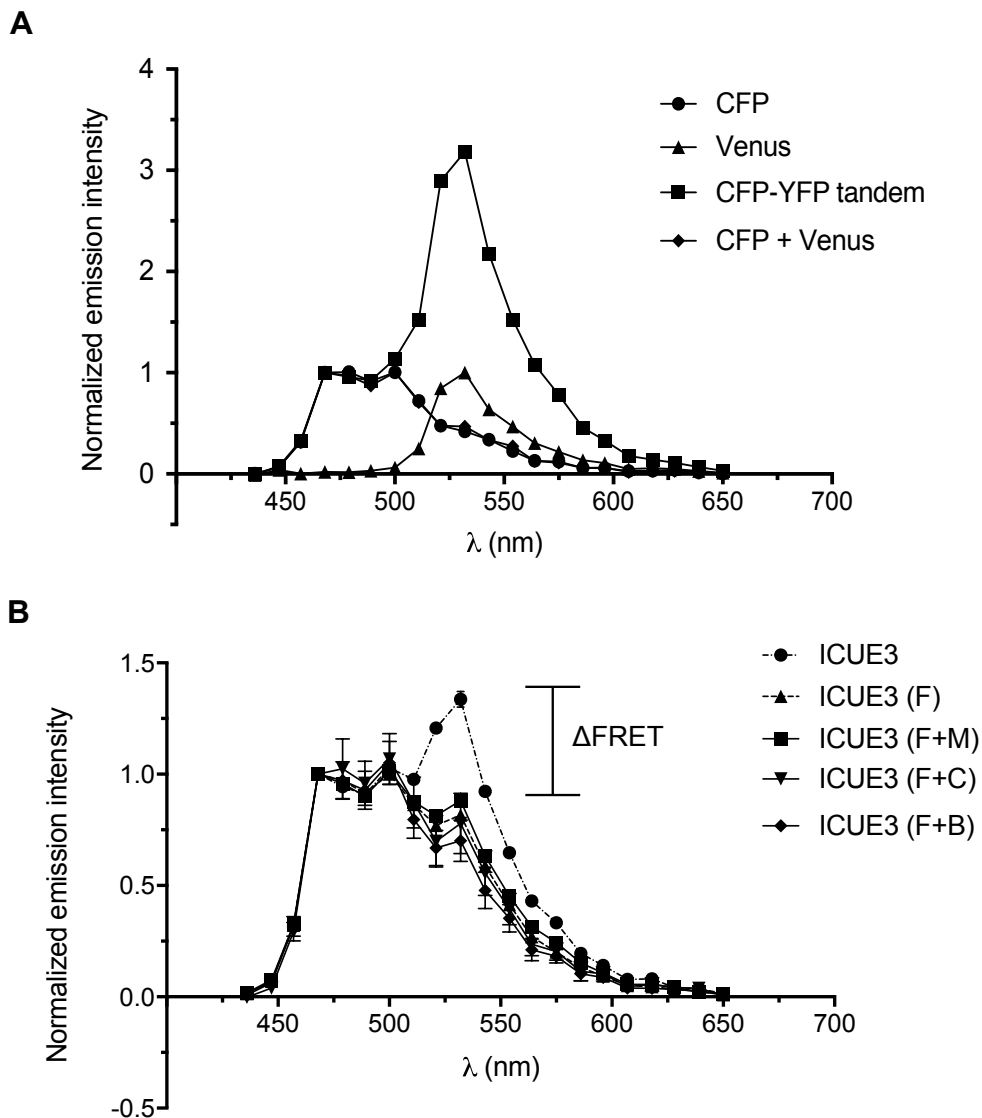


Figure 18: Controls for FRET experiments. (A) Emission spectra for CFP and Venus alone or co-transfected, as well as for a CFP-YFP fusion construct; $n = 37-74$ cells per condition. **(B)** Emission spectra of ICUE3 sensor under resting conditions and upon treatment with forskolin (F) ($30 \mu\text{M}$, 2 min) or with combination of forskolin with milrinone (F+M) ($30 \mu\text{M}$, 30 min), cilostamide (F+C) ($30 \mu\text{M}$, 20 min) and BAY 41-8543 (F+B) ($15 \mu\text{M}$, 15 min); $n = 25-65$ cells per condition. Δ FRET, which reflects the increase or decrease in cAMP levels compared to basal levels, is also illustrated (Ercu et al. 2020).

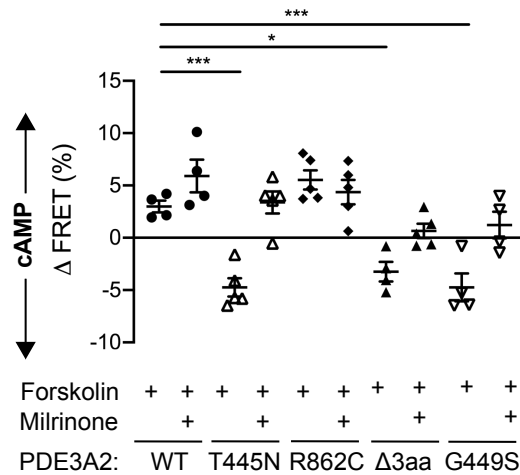
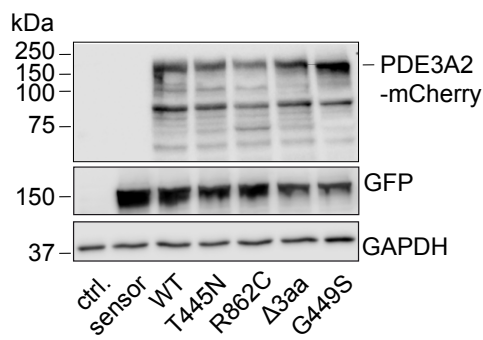
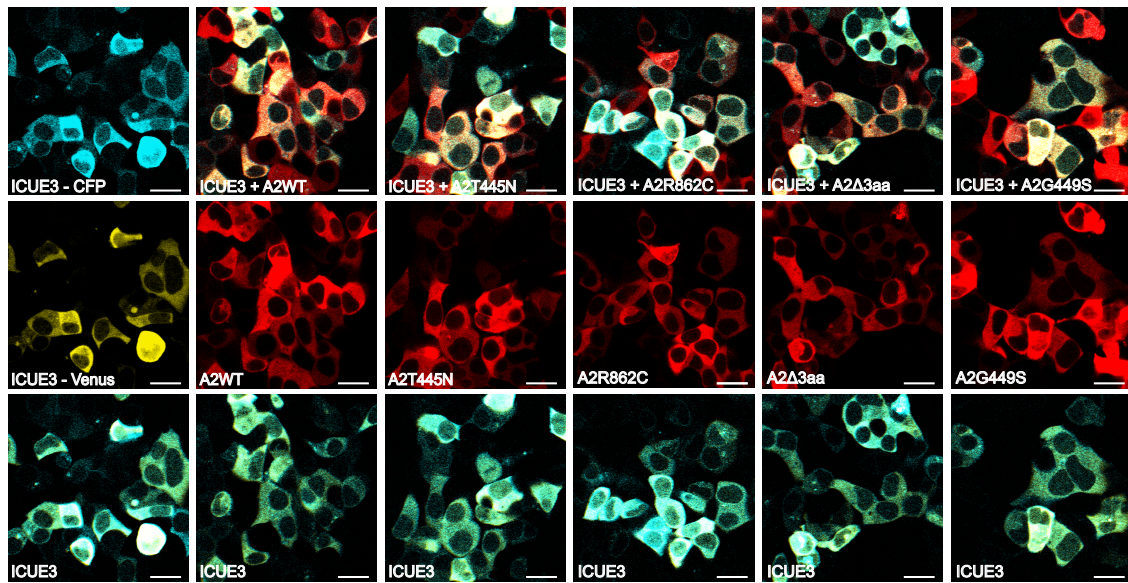
All PDE3A2 variants were expressed at similar levels and were localized mainly in the cytosol (Figure 19A). FRET measurements were performed in the absence (Figure 19C) or presence of forskolin ($30 \mu\text{M}$, 2 min) with or without the PDE3-specific inhibitor milrinone ($30 \mu\text{M}$, 30 min) (Figure 19A). The percentage

Results

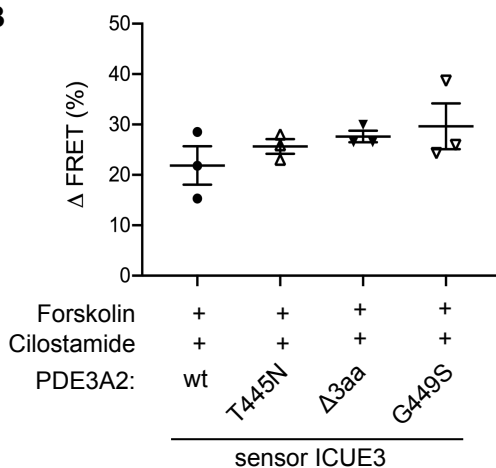
change in FRET, described by Δ FRET (%), shows the increase or decrease in cAMP levels compared to basal levels (Figure 18B). Δ FRET positively correlates with the cAMP concentration (high Δ FRET indicates high cAMP levels) and thus inversely correlates with PDE3A2 activity (high Δ FRET shows low PDE3A activity). Upon forskolin treatment, the cAMP level in cells expressing PDE3A2 mutants (Δ 3aa, G449S and T445N) was lower than in those expressing the WT, reflected by the smaller Δ FRET value. To further confirm this finding, the same FRET experiment was carried out using the enzyme with the catalytic domain substitution (R862C). No reduction in the Δ FRET was observed for the PDE3A2 variant incorporating the R862C substitution compared to the WT, suggesting similar cAMP levels in both conditions (Figure 19A). The data indicate that mutations in the regulatory region of the *PDE3A* gene increase the protein's enzymatic activity in the cytosol compared to the WT or to mutations located in the region encoding the catalytic domain of the enzyme. Under resting conditions, no difference was observed in the FRET signal of WT and mutant PDE3A2 (Δ 3aa, G449S, T445N and R862C), suggesting similar enzyme activities (Figure 19C). The PDE3-specific inhibitor milrinone led to an enzyme variant-specific increase in cAMP levels for WT, Δ 3aa, G449S and T445N PDE3A2 variants, reflected by an increase in the Δ FRET values, implying a partial inhibition of PDE3A enzyme activity. The cAMP hydrolytic activity of the PDE3A2 variant carrying the R862C substitution appeared to not be influenced by milrinone treatment (Figure 19A).

Another PDE3-specific inhibitor, cilostamide (10 μ M, 20 min), abolished the differences in Δ FRET between the WT and mutant PDE3A2 (Δ 3aa, G449S, T445N). This indicates that the WT and mutant proteins have similar sensitivity for this agent. Furthermore, cilostamide appeared to be more efficient in inhibiting PDE3A than milrinone, since it led to a higher increase in cAMP levels as compared to the later (Figure 19B) (Ercu et al. 2020).

A



B



C

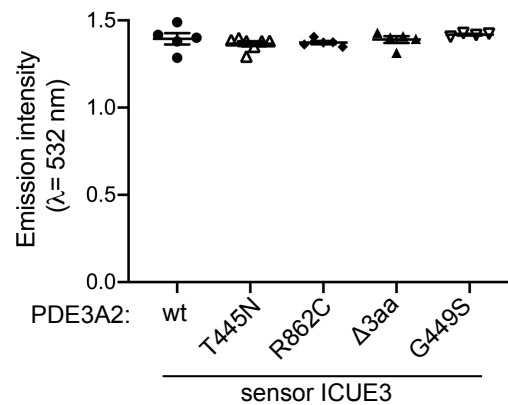


Figure 19: Mutations in the regulatory region of the *PDE3A* gene increase the activity of the enzyme in the cytosol. (A) Upper panel: Microscopy images of HEK293 cells transfected either with the ICUE3 sensor alone (cyan and yellow, green colocalization) or co-expressed with the specific

Results

PDE3A2 variant (WT, T445N, R862C, Δ 3aa and G449S) fused to mCherry (red and orange when colocalizing with the sensor). Scale bar: 20 μ M. Lower panel, left: Detection of mCherry-tagged PDE3A with a PDE3A specific antibody and of ICUE3 sensor with an antibody targeted against GFP by Western blotting. GAPDH was used as a loading control. Lower panel, right: Shown is the Δ FRET (%) for WT PDE3A2 and the various mutations (T445N, R862C, Δ 3aa and G449S) calculated either upon treatment with forskolin (30 μ M, 2 min) alone or together with milrinone (30 μ M, 30 min). “0 % Δ FRET” reflects the basal cAMP levels. Increases in cAMP levels correspond to increased Δ FRET and decreased PDE3A activity. Statistical analysis was carried out using two-way ANOVA and Bonferroni multi-comparison; $n > 4$ independent experiments with an analysis of 25-65 individual cells per experiment for each PDE3A variant and condition. Mean \pm SEM is plotted, * $p < 0.1$, *** $p < 0.001$. **(B)** Shown is the Δ FRET (%) for WT, T445N, Δ 3aa and G449S PDE3A2 upon treatment with forskolin (30 μ M, 2 min) and cilostamide (10 μ M, 20 min). Statistical analysis was carried out using two-way ANOVA and Bonferroni multi-comparison; $n = 3$ independent experiments with an analysis of 32-68 individual cells per experiment for each PDE3A variant and condition. Mean \pm SEM is plotted. **(C)** Shown is the emission intensity at 532 nm for WT, T445N, R862C, Δ 3aa and G449S PDE3A2 under resting conditions. Statistical analysis was carried out using one-way ANOVA and Bonferroni multi-comparison; $n > 4$ independent experiments with an analysis of 25-65 individual cells per experiment for each PDE3A variant and condition. Mean \pm SEM is plotted (Ercu et al. 2020).

WT and Δ 3aa HET animals were treated with BAY 41-8543 and the compound reduced their mean arterial pressure, though more efficiently for the mutant animals (Figure 10D). To verify whether the compound affects PDE3A activity, FRET measurements were used. HEK293 cells endogenously express sGC (Figure 20A). Cyclic GMP-mediated inhibition of PDE3A induced by BAY 41-8543 treatment (15 μ M, 15 min) increased the cAMP levels of cells expressing the T445N, Δ 3aa and G449S variants, as reflected by the increased Δ FRET values. The differences in Δ FRET and thus in cAMP levels are however not significant between the WT and the mutant PDE3A variants upon treatment with forskolin and BAY 41-8543 (Figure 20B) (Ercu et al. 2020).

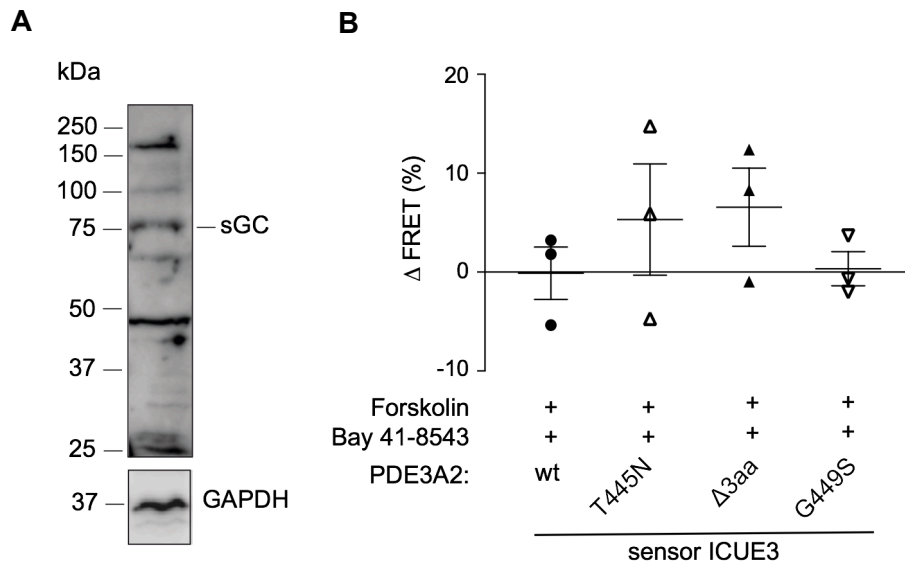


Figure 20: BAY 41-8543 caused greater inhibition of mutant PDE3A2 than WT. (A) Expression of soluble guanylyl cyclase (sGC) in HEK293 cells is shown by Western blotting. GAPDH was used as a loading control. (B) Shown is the Δ FRET (%) for WT, T445N, Δ 3aa and G449S PDE3A2 variants upon treatment with forskolin (30 μ M, 2 min) and BAY 41-8543 (15 μ M, 15 min). “0 % Δ FRET” reflects the basal cAMP levels. Statistical analysis was carried out using two-way ANOVA and Bonferroni multi-comparison; n = 3 independent experiments with an analysis of 32-68 individual cells per experiment for each PDE3A variant and condition. Mean \pm SEM is plotted (Ercu et al. 2020).

To elucidate whether there are differences in PDE3A activity between cytosol and PM, the activity of WT and the T445N mutant PDE3A was also measured at the PM of HEK293 cells. This was also done by FRET using the cAMP-based sensor LynICUE3, targeted to the PM *via* a myristoylation and palmitoylation sequence from Lyn kinase (DiPilato and Zhang 2009), and the membrane-localized PDE3A1 isoform tagged with mCherry (Table 24 and Figure 16). Both PDE3A1 variants were expressed at similar levels (Figure 21A). FRET measurements were performed in the presence (Figure 21A) or absence (Figure 21B) of forskolin (30 μ M, 2 min). In cells expressing PDE3A1-T445N, forskolin caused a reduction in Δ FRET as compared to the WT expressing cells, reflecting decreased cAMP levels in the mutant expressing cells (Figure 21A). These data suggest that the T445N mutation increases the hydrolytic activity of PDE3A at the PM. Under resting conditions, PDE3A1 WT and T445N enzyme activities were similar as no difference was observed in the emission intensity at 532 nm (Figure 21B). As a control, the spectra depicting the emission of

Results

LynICUE3 sensor under resting conditions and upon treatment with forskolin (F) (30 μ M, 2 min) are shown (Figure 21C).

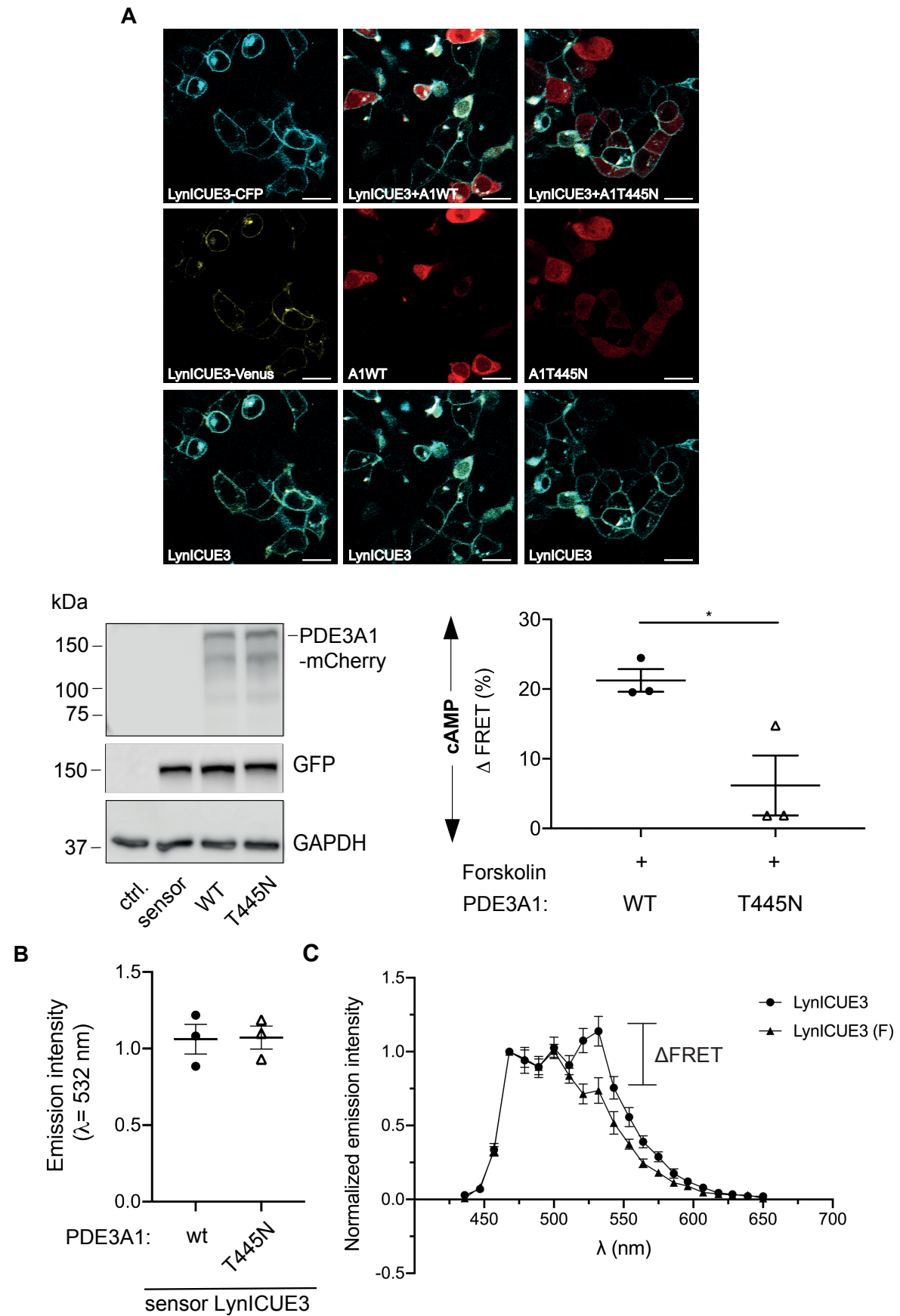


Figure 21: PDE3A-T445N mutation increases the activity of the enzyme at the PM. (A) Upper panel: Microscopy images of HEK293 cells transfected either with the LynICUE3 sensor alone (cyan and yellow, green colocalization) or co-expressed with the specific PDE3A1 variant (WT and T445N) fused to mCherry (red). Scale bar: 20 μ M. Lower panel, left: Detection of mCherry-tagged PDE3A1 with a PDE3A specific antibody and of ICUE3 sensor with an antibody targeted against GFP by Western blotting. GAPDH was used as a loading control. Lower panel, right: Shown is the Δ FRET (%) for WT PDE3A1 and the T445N mutation calculated upon treatment with forskolin (30 μ M, 2 min). “0 % Δ FRET” reflects the basal cAMP levels. Increases in cAMP levels correspond to increased Δ FRET and decreased PDE3A activity. Statistical analysis was carried out using two-way ANOVA and Bonferroni multi-comparison; n = 3 independent experiments with an analysis of 23-62 individual cells per experiment for each PDE3A variant and condition. Mean \pm SEM is plotted, *p < 0.1. **(B)** Shown is the emission intensity at 532 nm for WT and T445N PDE3A1 under resting conditions. Statistical analysis was carried out using one-way ANOVA and Bonferroni multi-comparison; n = 4 independent experiments with an analysis of 23-62 individual cells per experiment for each PDE3A variant and condition. Mean \pm SEM is plotted. **(C)** Emission spectra of LynICUE3 sensor under resting conditions and upon treatment with forskolin (F) (30 μ M, 2 min); n = 23-62 cells per condition. Δ FRET is also illustrated.

5.5. Mutations in the regulatory region of the *PDE3A* gene altered protein-protein interactions

PKA-induced phosphorylation of WT PDE3A1 leads to its recruitment into a SERCA2/AKAP18 signalosome located at the SR of cardiac myocytes. SERCA2 mediates Ca^{2+} re-uptake into the SR and therefore participates in the control of cardiac relaxation. The integration of PDE3A1 into the AKAP18-based signalosome is dependent on the PKA-dependent phosphorylation of the enzyme at serine residues 292/293 and involves direct interaction with both SERCA2 and AKAP18 (Ahmad et al. 2015b). Furthermore, PKA-mediated phosphorylation of PDE3A upon PMA and forskolin treatment was increased in the enzyme carrying mutations in the regulatory region of the *PDE3A* gene compared to the WT protein (Maass et al. 2015). Taking into account that PDE3A phosphorylation promotes its interaction with SERCA2 and AKAP18 (Ahmad et al. 2015b) and that PDE3A mutations causing HTNB induce increased enzyme phosphorylation (Maass et al. 2015), we aimed at identifying physiological PDE3A interactions and testing whether the mutations alter those protein-protein interactions.

Results

PDE3A is highly expressed in the heart. Therefore, to determine the PDE3A interactome and to identify interaction partners, endogenous PDE3A was immunoprecipitated from human heart lysate. Sample incubated with non-immune immunoglobulin G (IgG) was used as a negative control (Figure 22). The immunoprecipitates were separated on SDS gels stained using Coomassie Brilliant Blue and then the corresponding immunoprecipitation (IP) lanes were excised and analyzed by mass spectrometry analysis. Proteins that were enriched in PDE3A IP sample compared to the IgG IP, were considered as potential interactors of PDE3A. The intensity scores and the normalized label-free quantification (LFQ) intensity scores are summarized in Table 25 and 26, respectively. LFQ is a quantification method based on the raw intensities that aims to determine the relative amount of proteins in biological samples without making use of stable isotopes to label the protein. When using LFQ, normalization occurs on multiple levels to exclude outliers and to make sure that the intensities obtained reflect the amount of proteins within the sample (Asara et al. 2008). A summary of all proteins found to co-precipitate with PDE3A is presented in Supplemental Table S2.

Table 25: Potential interaction partners identified in the PDE3A IP from human heart detected by mass spectrometry based on the intensity values

Protein names	Gene names	Intensity IgG IP	Intensity PDE3A IP	LFQ intensity IgG IP	LFQ intensity PDE3A IP	Intensity PDE3A IP/ IgG IP	LFQ intensity PDE3A IP/ IgG IP
cGMP-inhibited 3,5-cyclic phosphodiesterase A	<i>PDE3A</i>	1571400	1248500000	0	2226900000	794,5144457	#DIV/0!
UHRF1-binding protein 1	<i>UHRF1BP1</i>	371780	57215000	0	57388000	153,8947765	#DIV/0!
Protein disulfide-isomerase A4	<i>PDIA4</i>	177550	17140000	0	0	96,53618699	#DIV/0!
Adenylyl cyclase-associated protein 1; Adenylyl cyclase-associated protein	<i>CAP1</i>	162340	7763800	0	0	47,82431933	#DIV/0!
Myozenin-2	<i>MYOZ2</i>	238430	7044200	0	3269400	29,54410099	#DIV/0!
14-3-3 protein theta	<i>YWHAQ</i>	2718300	61927000	0	22603000	22,78151786	#DIV/0!
Phosphoglycerate mutase 1; Probable phosphoglycerate mutase 4	<i>PGAM1;</i> <i>PGAM4</i>	658880	14684000	0	0	22,28630403	#DIV/0!
Tropomyosin alpha-4 chain	<i>TPM4</i>	229150	5068900	0	0	22,12044512	#DIV/0!
FYN-binding protein	<i>FYB</i>	905780	18605000	0	12138000	20,5403078	#DIV/0!
WD repeat-containing protein 47	<i>WDR47</i>	143430	2868500	0	5115000	19,9993028	#DIV/0!
Stathmin	<i>STMN1</i>	17770	309780	0	0	17,43275183	#DIV/0!
Alpha-actinin-2	<i>ACTN2</i>	3822500	60922000	8277400	96312000	15,93773708	11,6355377
cAMP-dependent protein kinase catalytic subunit alpha and subunit beta	<i>PRKACA;</i> <i>PRKACB</i>	270020	3879600	0	2492000	14,36782461	#DIV/0!
Titin	<i>TTN</i>	5168400	70197000	4936000	100400000	13,5819596	20,3403566
Glutamine synthetase	<i>GLUL</i>	282980	3729200	0	2395300	13,17831649	#DIV/0!
Glutathione synthetase	<i>GSS</i>	705560	8505400	0	0	12,0548217	#DIV/0!
Serpin B3	<i>SERPINB3</i>	14037000	152360000	9954100	120750000	10,85417112	12,1306798
T-complex protein 1 subunit delta	<i>CCT4</i>	178390	1698100	0	0	9,519031336	#DIV/0!
Troponin T, cardiac muscle	<i>HNTN1;</i> <i>TNNT2</i>	7996600	75380000	10831000	41371000	9,426506265	3,81968424
Protein S100-A7	<i>S100A7</i>	10578000	99446000	0	84095000	9,401210059	#DIV/0!
F-actin-capping protein subunit beta	<i>CAPZB</i>	404930	3620800	0	2190100	8,941792409	#DIV/0!
Alpha-aminoadipic semialdehyde dehydrogenase	<i>ALDH7A1</i>	1723800	14288000	0	3888800	8,288664578	#DIV/0!

Results

Plasminogen activator inhibitor 1 RNA-binding protein	<i>SERBP1</i>	229330	1865100	0	1756000	8,132821698	#DIV/0!
Protein S100-A8	<i>S100A8</i>	7889700	57470000	0	36332000	7,284180641	#DIV/0!
Myoferlin	<i>MYOF</i>	957540	6546200	0	0	6,836476805	#DIV/0!
F-actin-capping protein subunit alpha-2	<i>CAPZA2</i>	320170	2049000	0	0	6,399725146	#DIV/0!
Involucrin	<i>IVL</i>	2657200	16636000	0	10686000	6,260725576	#DIV/0!
Myosin-9	<i>MYH9</i>	1435800	8278500	1752700	5683400	5,765775178	3,24265419
Adenylate kinase 2, mitochondrial	<i>AK2</i>	553760	2995900	0	0	5,410105461	#DIV/0!
Protein ADP-ribosylarginine hydrolase-like protein 1	<i>ADPRHL1</i>	2690600	14322000	0	9199500	5,322976288	#DIV/0!
Myomesin-2	<i>MYOM2</i>	1269600	6548900	0	9774200	5,158238815	#DIV/0!
Tropomyosin alpha-1 chain	<i>TPM1</i>	56280000	282880000	73196000	116640000	5,026297086	1,5935297

Table 26: Potential interaction partners identified in the PDE3A IP from human heart detected by mass spectrometry based on the label-free quantification (LFQ) intensity values

Protein names	Gene names	Intensity IgG IP	Intensity PDE3A IP	LFQ intensity IgG IP	LFQ intensity PDE3A IP	Intensity PDE3A IP/ IgG IP	LFQ intensity PDE3A IP/ IgG IP
Titin	TTN	5168400	70197000	4936000	100400000	13,5819596	20,34035656
Serpin B3	SERPINB3	14037000	152360000	9954100	120750000	10,85417112	12,13067982
Alpha-actinin-2	ACTN2	3822500	60922000	8277400	96312000	15,93773708	11,63553773
Desmin	DES	19940000	82937000	3185700	22132000	4,159327984	6,947295728
Myosin-7; Myosin-6	MYH7; MYH6	264870000	1125600000	315320000	1806700000	4,249631895	5,729734873
Creatine kinase S-type, mitochondrial	CKMT2	177670000	257050000	49983000	212250000	1,446783362	4,246443791
Creatine kinase M-type	CKM	245490000	288380000	78308000	331010000	1,174711801	4,227026613
Fatty acid-binding protein, epidermal	FABP5	37191000	57468000	25586000	107340000	1,545212551	4,195263034
Annexin A5; Annexin	ANXA5	8530700	25738000	3838800	15809000	3,017102934	4,118214025
2,4-dienoyl-CoA reductase, mitochondrial	DECR1	79213000	198610000	23647000	95929000	2,50729047	4,056709096
Troponin T, cardiac muscle	HNTN1; TNNT2	7996600	75380000	10831000	41371000	9,426506265	3,81968424
Poly [ADP-ribose] polymerase 1	PARP1	7597600	14016000	6607800	23006000	1,844793093	3,481642907
Myosin light chain 3	MYL3	77500000	249890000	18223000	61347000	3,224387097	3,366459968
Myosin-9	MYH9	1435800	8278500	1752700	5683400	5,765775178	3,242654191
Medium-chain specific acyl-CoA dehydrogenase, mitochondrial	ACADM	65959000	117510000	26796000	85867000	1,781561273	3,204470817
Glycogenin-1	GYG1	12186000	17331000	8747900	26402000	1,42220581	3,018095772
Ig kappa chain C region	IGKC	17017000000	13795000000	2242800000	6738100000	0,810659928	3,004324951
Cytochrome c oxidase subunit 5A, mitochondrial	COX5A	17976000	16833000	12548000	36418000	0,93641522	2,902295186
14-3-3 protein gamma	YWHAG	16057000	43966000	3526100	9838100	2,738120446	2,790079691
Leukocyte elastase inhibitor	SERPINB1	3261700	7429600	1860000	5152400	2,277830579	2,770107527

Results

Prohibitin-2	PHB2	6232200	22917000	4043300	10721000	3,677192645	2,651547004
Voltage-dependent anion-selective channel protein 2	VDAC2	19326000	28448000	7236100	18849000	1,472006623	2,604856207
Decorin	DCN	2552300	3611500	2644900	6654100	1,414998237	2,515822904
14-3-3 protein beta/alpha	YWHAB	3880200	9326400	2482600	6038800	2,403587444	2,432449851
Calmodulin-like protein 3	CALML3	6054200	21102000	5950400	14169000	3,485514188	2,381184458
Myosin-binding protein C, cardiac-type	MYBPC3	25619000	81882000	51445000	122420000	3,196143487	2,37962873
Ryanodine receptor 2	RYR2	4998500	5669500	3594200	8538100	1,134240272	2,375521674
14-3-3 protein epsilon	YWHAE	51446000	158990000	10161000	23206000	3,090424912	2,283830332
Collagen alpha-2(VI) chain	COL6A2	4325200	5887600	4745900	10595000	1,361231851	2,232453275
L-lactate dehydrogenase A chain	LDHA	4937500	15821000	5754400	12526000	3,204253165	2,176769081
Galectin-3-binding protein	LGALS3BP	4777400	14340000	4549700	9780900	3,001632687	2,149790096
Isocitrate dehydrogenase [NAD] subunit, mitochondrial	IDH3B	8707300	21985000	6549700	13892000	2,524892906	2,121013176
Troponin I, cardiac muscle	TNNI3	46561000	96985000	17954000	37812000	2,082966431	2,106048791

The most abundant proteins identified to potentially co-precipitate with PDE3A, as well as PDE3A itself, summarized in Tables 25 and 26, are illustrated in Figure 22.

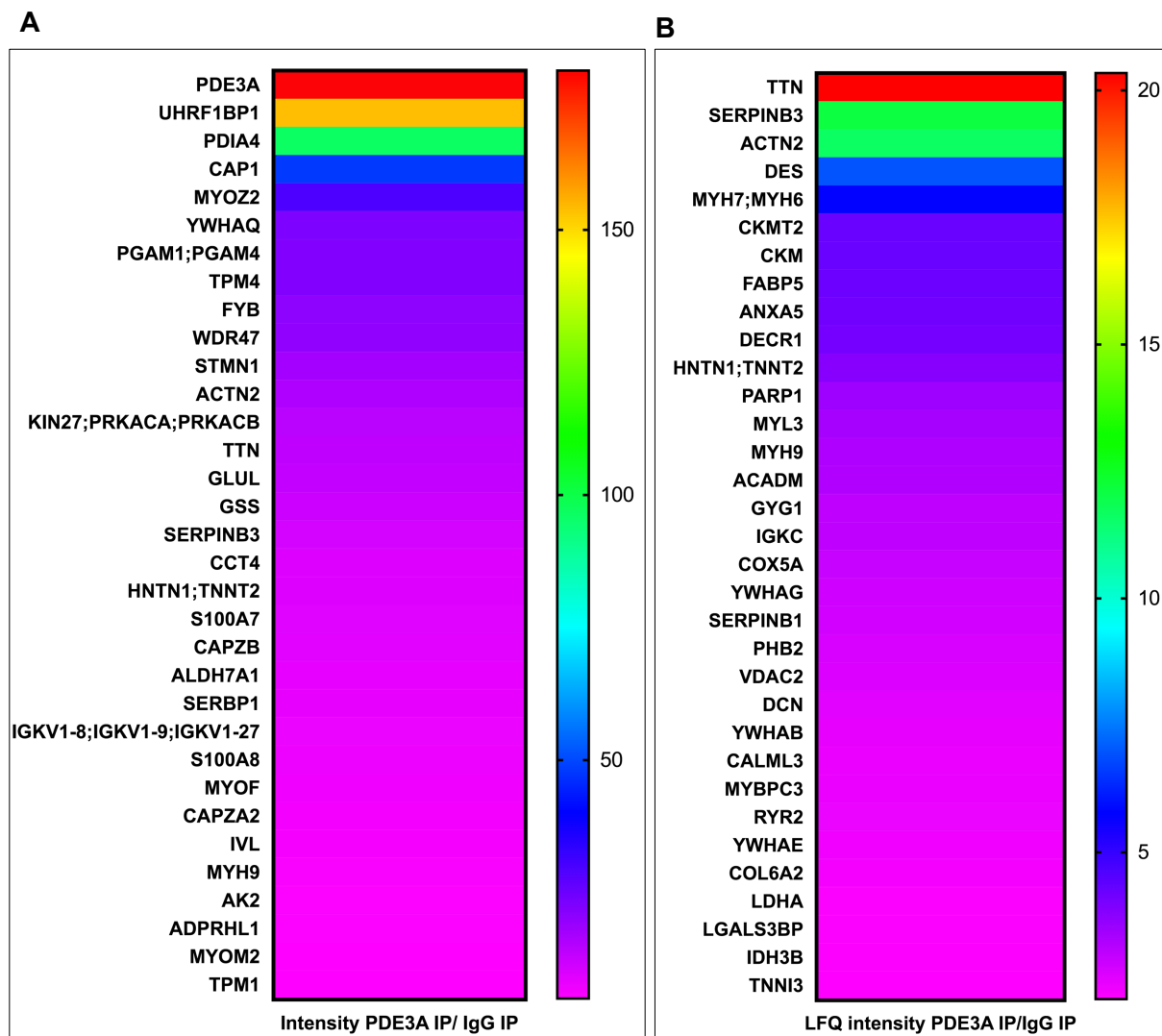


Figure 22: Potential PDE3A interaction partners identified via mass spectrometry analysis. (A) Heatmap illustrating the most abundant proteins calculated based on their intensity values in the IgG and PDE3A IP samples. PDE3A was identified as the strongest hit. Proteins and their respective intensity values are summarized in Table 25. **(B)** Heatmap illustrating the most expressed proteins calculated based on their LFQ intensity values in the IgG and PDE3A IP samples. Proteins and their respective LFQ intensity values are summarized in Table 26. The color-coded measures of intensity correspond to the scale on the right of each panel.

Results

One of the proteins identified *via* mass spectrometry was 14-3-3 θ (Table 25 and Figure 22A: *YWHAQ*). It belongs to the 14-3-3 family of adaptor proteins, that bind phosphorylated serine residues of a variety of signaling proteins (e.g. kinases and phosphatases). 14-3-3 proteins have already been shown to interact with PDE3A in HeLa cells (Pozuelo Rubio et al. 2005, Corradini et al. 2015). Five out of the seven isoforms of 14-3-3 family were associated with PDE3A and 14-3-3 θ showed the highest intensity. To validate the mass spectrometry analysis result, endogenous PDE3A was immunoprecipitated from human heart lysates and was showed that 14-3-3 θ co-immunoprecipitated with the enzyme (Figure 23).

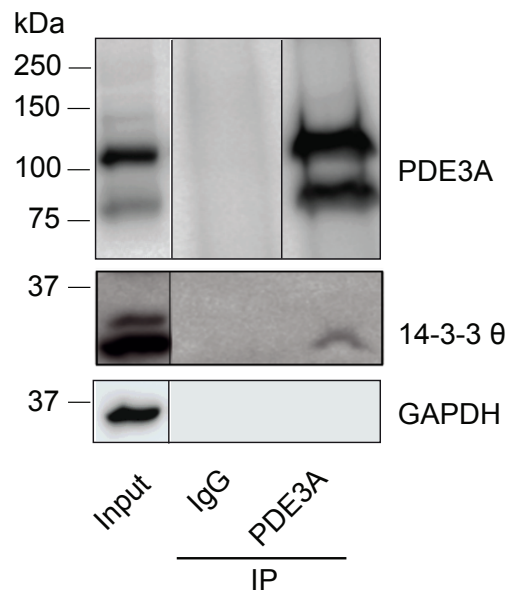


Figure 23: Endogenous PDE3A immunoprecipitation from human heart and detection of 14-3-3 θ . PDE3A was immunoprecipitated from human heart lysate (1 mg protein, 1mL) and 14-3-3 θ was found to co-precipitate with PDE3A. Detection of PDE3A and 14-3-3 θ was done by Western blotting. Sample incubated with non-immune IgG was used as control. Input sample (30 μ g) was also loaded on the gel as positive control. GAPDH was used as a loading control.

To examine whether PDE3A mutations that cause HTNB alter the interaction of the two proteins, FLAG-tagged WT and mutant (Δ 3aa and T445N) PDE3A2 variants were expressed in HEK293 cells and co-immunoprecipitated with 14-3-3 θ (cooperation with Dr. Carolin Schächterle). Since it was previously described that PDE3A interaction with 14-3-3 θ is dependent on PMA-induced phosphorylation of the enzyme at Ser428 (Pozuelo Rubio et al. 2005), HEK293 cells were treated with

PMA (16 μ M, 30 min). Also, 14-3-3 proteins bind to phosphorylated serine residues on their target proteins. Since forskolin is known to induce PKA-dependent PDE3A phosphorylation at various serine residues, including Ser312 and Ser438 (Wechsler et al. 2002), it was also used to stimulate the cells (30 μ M, 30 min). An increased interaction between both mutant PDE3A2 variants and 14-3-3 θ was observed upon PMA stimulation as compared to the WT protein, while treatment with forskolin did not affect the interaction (Figure 24). These data suggest that HTNB-causing mutations found in the regulatory region of the *PDE3A* gene induce an increased interaction of the enzyme with 14-3-3 θ compared to the WT protein, interaction that is dependent on the phosphorylation of PDE3A at Ser428 (Ercu et al. 2020).

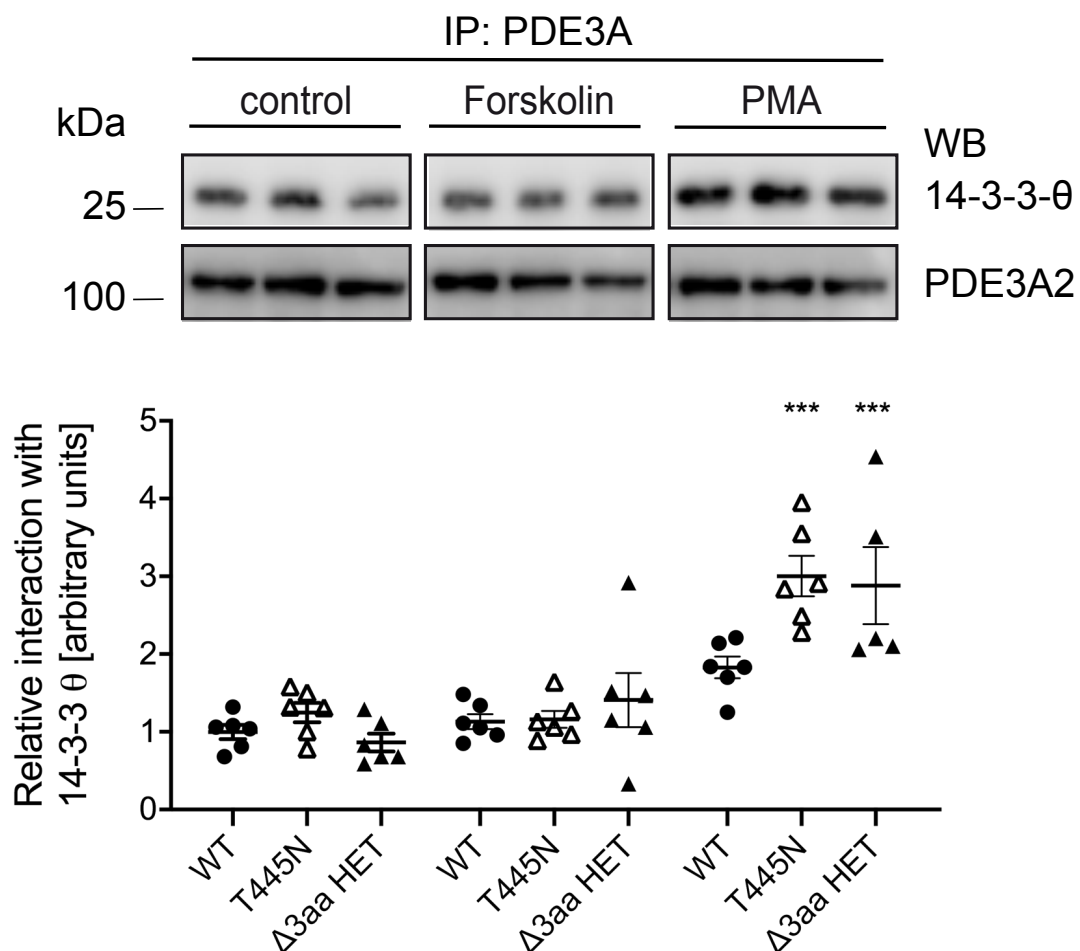


Figure 24: Increased interaction between mutant PDE3A and 14-3-3 θ . Upper panel: FLAG-tagged PDE3A2 WT and mutants (T445N and Δ 3aa) were transiently expressed in HEK293 cells and PDE3A2 variants were immunoprecipitated via their FLAG tag (1 mg protein, 1mL) upon treatment with either forskolin (30 μ M, 30 min) or PMA (16 μ M, 30 min). 14-3-3 θ co-immunoprecipitated with

Results

PDE3A2, more in the mutant conditions. Detection of PDE3A2 (WT, T445N and Δ 3aa) and 14-3-3 θ was done by Western blotting. Lower panel: Semi-quantitative analysis of the Western blots by densitometric analysis. Plotted are the expression levels of 14-3-3 θ normalized to the immunoprecipitated PDE3A2. Statistical analysis was carried out using one-way ANOVA and Bonferroni multi-comparison; n = 6 independent experiments. Mean \pm SEM is plotted, ***p < 0.001 (Ercu et al. 2020).

5.5.1. Characterizing PDE3A-14-3-3 θ interaction in H9C2 cells

To investigate whether the increased interaction between 14-3-3 θ and mutant PDE3A induces a change in the localization of the enzyme, immunofluorescence microscopy measurements in H9C2 cells were conducted (Figure 25). H9C2 cells are embryonic rat cardiomyocytes that express both PDE3A and 14-3-3 θ . The cells were treated with PMA (16 μ M, 30 min), forskolin (30 μ M, 30 min) or the combination of the two compounds to increase PDE3A phosphorylation at Ser428 and Ser438, while unstimulated cells served as control. PDE3A (red) and 14-3-3 θ (green) co-stainings were carried out and revealed that both proteins are distributed throughout the cell and therefore appeared to colocalize. No difference in PDE3A location within the cell and with respect to 14-3-3 θ was visible under this set-up in any of the treatment conditions compared to the control one (Figure 25).

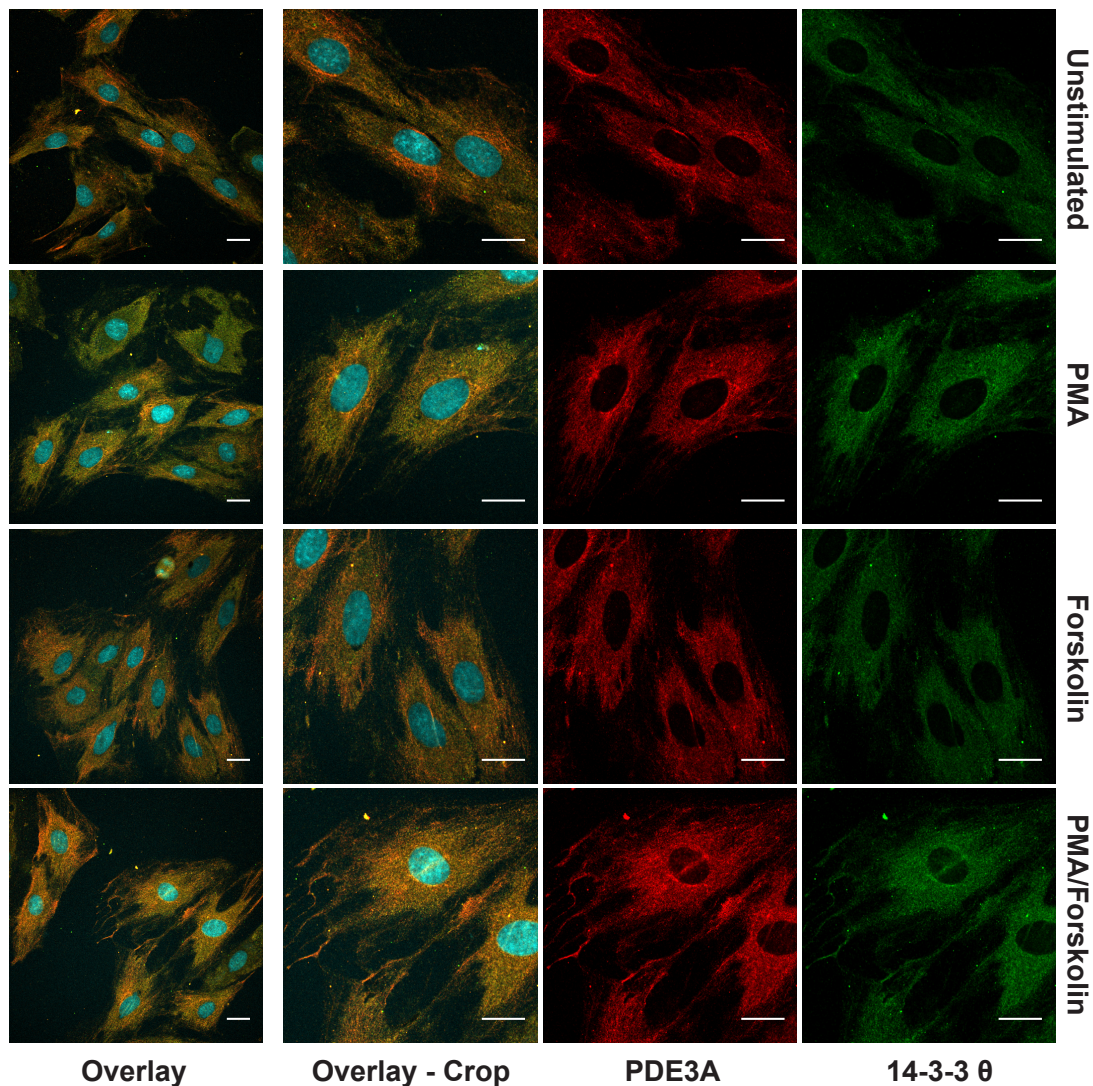


Figure 25: PDE3A and 14-3-3 θ expression in H9C2 cells. H9C2 cells were left untreated or stimulated with PMA (16 μ M, 30 min), forskolin (30 μ M, 30 min) or the combination of the two compounds. PDE3A and 14-3-3 θ were detected by immunofluorescence microscopy using specific primary antibodies (Table 7) and fluorescent dye-coupled secondary antibodies (Table 8). Nuclei were stained with DAPI. PDE3A and 14-3-3 θ are shown in the magnified views (Crop) images. Staining with the secondary antibody alone was used as a control. Scale bar: 20 μ M

5.5.2. PDE3A interacts with the catalytic subunit α of PKA in human heart and cardiomyocytes from non-affected and patient-derived induced pluripotent stem cells (IPSCs)

Another protein that appeared in the mass spectrometry results (Table 25 and Figure 22A) and was previously shown to interact with PDE3A in myocardial

Results

membranes was the catalytic subunit α of PKA (Ahmad et al. 2015b). To confirm this result, endogenous PDE3A was immunoprecipitated from human heart lysate and the catalytic subunit α of PKA was shown to co-immunoprecipitate with the enzyme (Figure 26A). Furthermore, non-affected (WT) and patient (T445N)-derived induced pluripotent stem cells (IPSCs) were differentiated into cardiomyocytes and PDE3A was successfully immunoprecipitated from these cells. The catalytic subunit α of PKA was found to co-precipitate with the enzyme (Figure 26B). Since for the T445N-derived cardiomyocytes less material was available, the amount of precipitated PDE3A was less compared to the one precipitated from the WT cells and therefore, the amount of co-precipitated PKA catalytic subunit α was also significantly less in this condition. Non-immune IgG was not used as control in these IPSC-derived cardiomyocytes due to the lack of material.

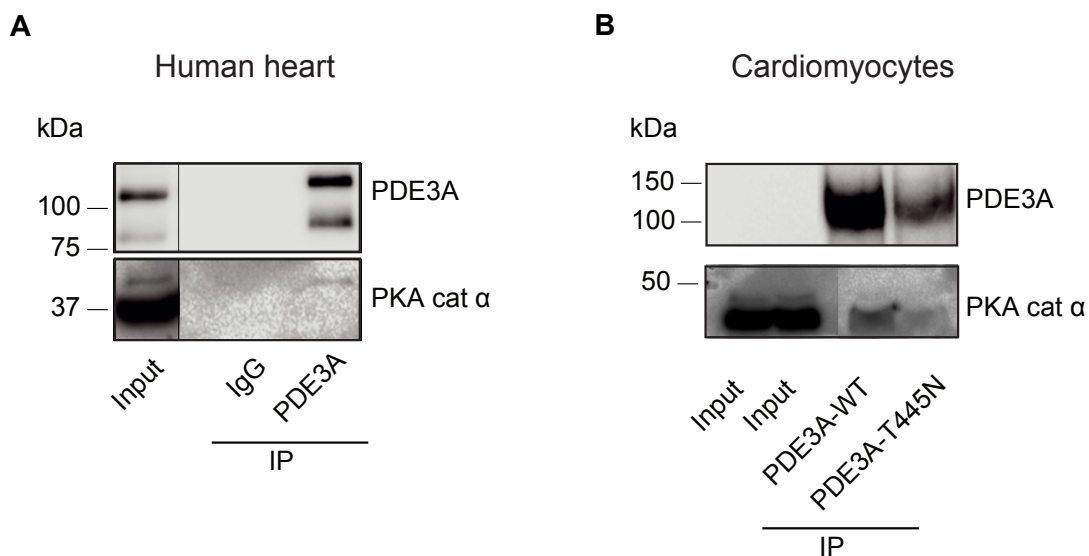


Figure 26: Endogenous PDE3A immunoprecipitations from human heart and cardiomyocytes from non-affected and patient-derived IPS cells and detection of the catalytic subunit α of PKA.

(A) PDE3A was immunoprecipitated from human heart lysate (1 mg protein, 1mL) and the catalytic subunit α of PKA was found to co-precipitate with PDE3A. Sample incubated with non-immune IgG was used as control. Input sample (30 μ g) was also loaded on the gel as positive control. **(B)** PDE3A was immunoprecipitated from non-affected and patient (T445N)-derived IPSCs differentiated into cardiomyocytes (400 μ g for WT and 200 μ g for T445N, respectively, mL) and the catalytic subunit α of PKA was found to co-precipitate with PDE3A. Input sample (20 μ g) was also loaded on the gel as positive control. Detection of PDE3A and PKA catalytic subunit α was done by Western blotting.

5.6. Hypertension-causing PDE3A mutations protect against cardiac damage

HTNB-affected individuals hardly present any signs of cardiac damage, despite suffering from life-long high blood pressure elevations. Heart rate, left ventricular mass and cardiac output values were similar in HTNB-affected and non-affected individuals (Toka et al. 2015). These data point towards a cardioprotective effect of the HTNB-causative mutations that affect the regulatory region of the *PDE3A* gene.

5.6.1. PDE3A1 and PDE3A2 expression in the heart of WT, Δ 3aa HET and functional DEL animals

Two PDE3A isoforms, PDE3A1 and PDE3A2, were detected in the left ventricles (the contractile part of the heart most commonly affected by hypertrophy) of WT and Δ 3aa HET rat hearts and were absent in the functional DEL animals. The expression level of PDE3A1 was significantly decreased in the Δ 3aa HET rats as compared to the WT animals, whereas PDE3A2 was similarly expressed in both models (Figure 27). This was not the case in the rat aorta where both PDE3A isoforms were significantly decreased in the Δ 3aa HET rats compared to the WT animals (Figure 11A).

Results

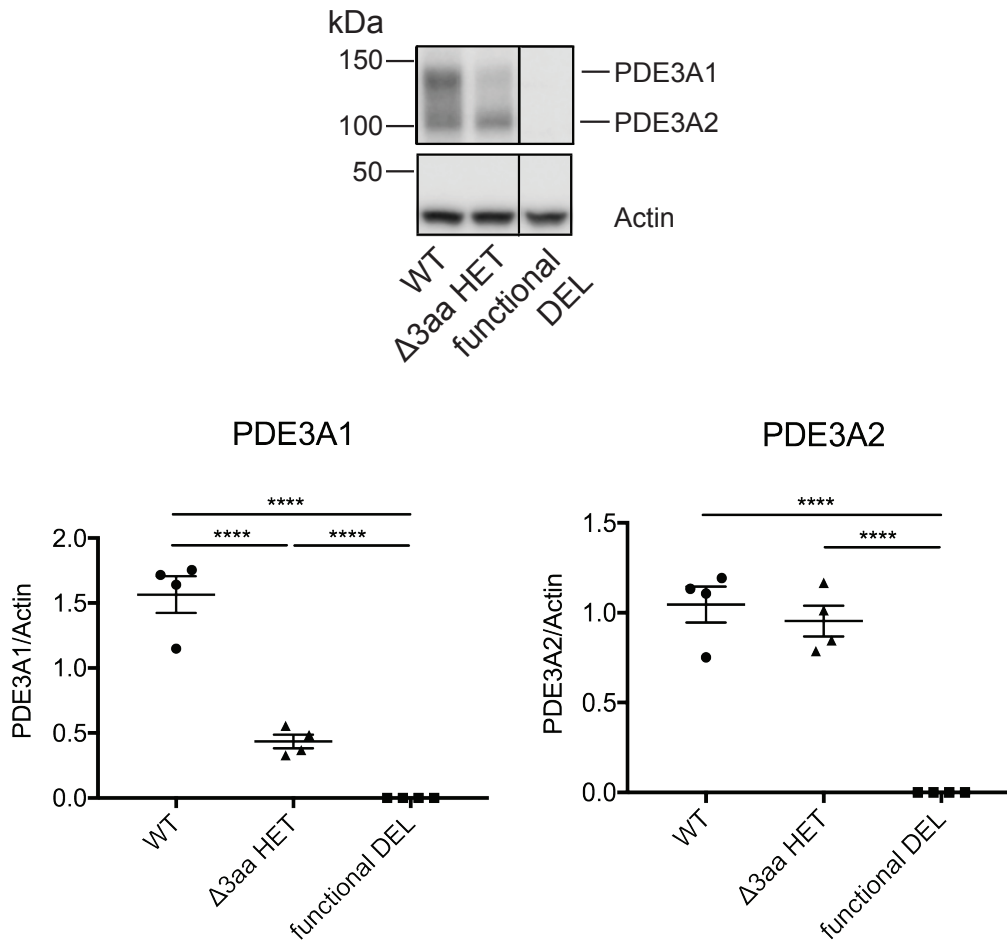


Figure 27: PDE3A1 and PDE3A2 expression in the left ventricle of WT, Δ3aa HET and functional DEL rats. Upper panel: PDE3A1 and PDE3A2 isoforms were detected by Western blotting in the left ventricle of WT, Δ3aa HET and functional DEL rats. PDE3A was not detectable in functional DEL animals. Actin was detected as loading control. Lower panel: Semi-quantitative analysis of PDE3A1 and PDE3A2 variants by densitometric analysis. Plotted are the expression levels of PDE3A1 and PDE3A2 normalized to the loading control, actin. Statistical analysis was carried out using one-way ANOVA and Bonferroni multi-comparison; n = 4 independent experiments. Mean ± SEM is plotted, ****p < 0.0001

5.6.2. Cardiac parameters of Δ3aa HET mutant rats are not significantly altered compared to those of WT animals

Similar to the HTNB patients, various cardiac parameters measured via echocardiography, including cardiac output, left ventricular mass and ejection fraction (Figure 28) (Preclinical Research Center, MDC) were not significantly altered in the Δ3aa HET and Δ3aa HOM rats compared to WT animals. These data suggest that

mutations affecting the N-terminal regulatory domain of the *PDE3A* gene, despite of causing severe hypertension, have cardioprotective effects, as observed in both patients and animal models (Ercu et al. 2020).

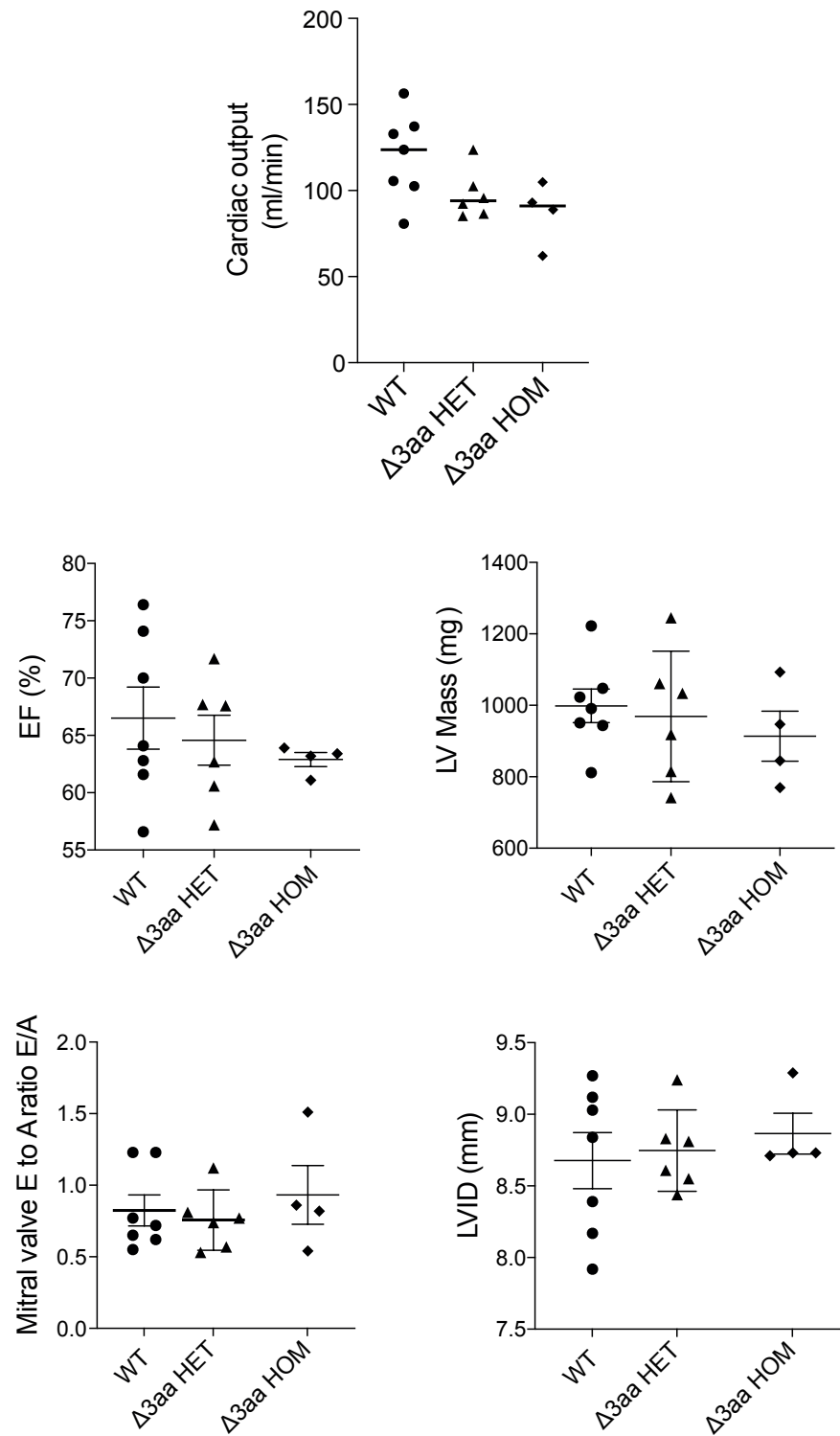


Figure 28: Cardiac parameters of $\Delta 3aa$ HET and $\Delta 3aa$ HOM rats were comparable to those of WT controls. The indicated cardiac parameters were measured by echocardiography in WT, $\Delta 3aa$

Results

HET and $\Delta 3aa$ HOM rats and no significant differences were observed. Statistical analysis was carried out using one-way ANOVA and Bonferroni multi-comparison; $n = 7$ for WT, $n = 6$ for $\Delta 3aa$ HET and $n = 4$ for $\Delta 3aa$ HOM animals. Mean \pm SEM is plotted (Ercu et al. 2020).

5.6.3. Expression of the excitation-contraction coupling components and 14-3-3 θ in rat heart of WT and mutant rats

Excitation-contraction coupling is the basis of proper functioning of the heart since it is the mechanism by which electrical activation is translated into cardiac contraction (Neef and Maier 2013). Intracellular Ca^{2+} cycling is essential for cardiac contraction and relaxation. More specifically, the L-type Ca^{2+} ($Ca_v1.2$) channels found at the T tubules open upon sarcolemma depolarization and allow Ca^{2+} to enter the cardiomyocyte. Ca^{2+} influx causes the release of more Ca^{2+} from the SR into the cytosol via the ryanodine receptors (RyR), process also known as Ca^{2+} -induced Ca^{2+} release. Cytosolic Ca^{2+} interacts with troponin T located on the thin myofibers, thus promoting contraction. Myosin-binding protein C (MyBPC) is a regulatory protein associated with myosin in the thick filament that, when phosphorylated, promotes contraction by weakening the binding of the myosin heads to the surface of the thick filament and therefore increasing their binding probability to actin on the thin filament. Relaxation occurs either *via* Ca^{2+} export outside the cardiac myocyte through the Na^+/Ca^{2+} exchangers, or *via* Ca^{2+} re-uptake into the SR, process mediated by SERCA2. Activation of SERCA2 is mediated by dissociation of PLN, a SR phosphoprotein, upon its phosphorylation. Decrease in the cytosolic Ca^{2+} during relaxation leads to its dissociation from troponin T and thus allows troponin I to re-associate to the thin filaments, thereby inhibiting actomyosin interactions. Therefore, the expression and proper function of proteins i.e. $Ca_v1.2$ channels, RyRs, SERCA2, Na^+/Ca^{2+} exchanger, MyBPC, Troponin I and PLN is detrimental for proper excitation-contraction coupling. Alterations in the expression or activity of any of these proteins results in defective excitation-contraction coupling and can lead to severe pathologies, including heart failure (Bers 2002, Layland, Solaro and Shah 2005, Kensler, Craig and Moss 2017, Zima et al. 2014).

To understand the apparent protective effect of PDE3A mutations against cardiac damage, we analyzed the expression levels of key players in the excitation-

contraction coupling process, i.e. RyR2, MyBPC, Troponin I and PLN in the left ventricles of WT, $\Delta 3aa$ HET and functional DEL rat hearts. These proteins are phosphorylated by PKA at various serine residues (i.e. Ser2808 for RyR2, Ser282 for MyBPC, Ser23/24 for Troponin I, Ser16 for PLN) and this plays a major role in cardiac contraction regulation. (Shan et al. 2010, Kensler et al. 2017, Layland et al. 2005, Simmerman and Jones 1998, Sande et al. 2002). The amount of RyR2 phosphorylated at Ser2808 was significantly increased in $\Delta 3aa$ HET rats compared to the WT animals, as it was the case for PLN phosphorylated at Ser16. The same phosphorylated proteins were expressed less in the functional DEL animals compared to the $\Delta 3aa$ HET ones, and this difference was significant for RyR2. No difference was found between WT and $\Delta 3aa$ HET rats in the expression of MyBPC phosphorylated at Ser282, but it was decreased in the functional DEL animals. Lastly, the amount of Troponin I phosphorylated at Ser23/24 was constant between the three genotypes, although it appeared to be less expressed in $\Delta 3aa$ HET animals (Figure 29).

Since we showed that the interaction between mutant PDE3A and 14-3-3 θ was increased compared to the interaction with the WT protein, we assessed the levels of the adaptor protein in our animal models. 14-3-3 θ was found to be more highly expressed in the $\Delta 3aa$ HET rats compared to the WT and functional DEL rats, whereas no difference was observed between WT and functional DEL animals (Figure 29).

Results

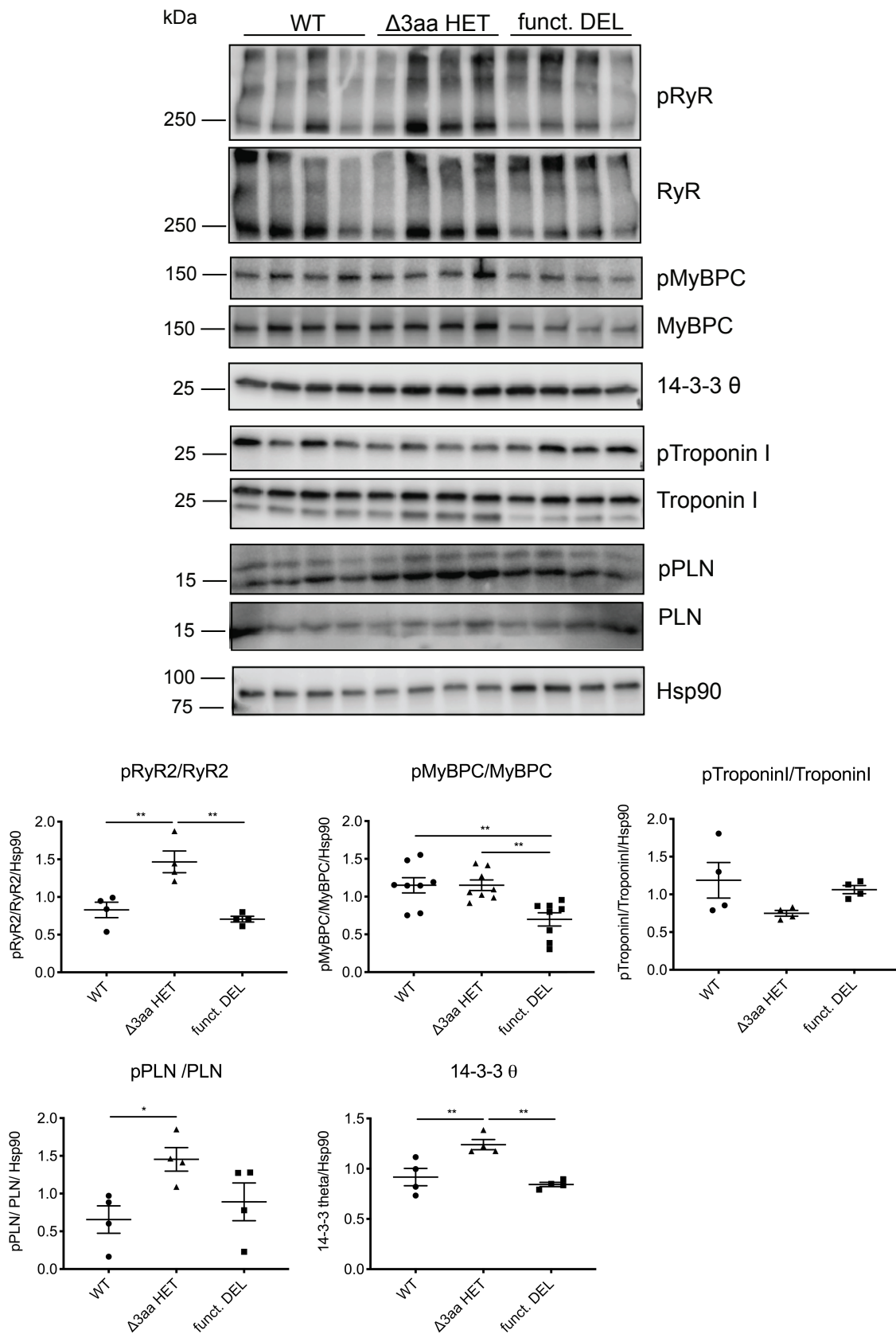


Figure 29: Expression of excitation-contraction coupling system components and 14-3-3 θ in the heart of WT and mutant animals. Upper panel: The PKA-phosphorylated and non-phosphorylated forms of RyR2, MyBPC, Troponin I and PLN as well as 14-3-3 θ were detected by

Western blotting in the left ventricle of WT, $\Delta 3aa$ HET and functional DEL rats. Hsp90 was detected as loading control. Lower panel: Semi-quantitative analysis of the above-mentioned proteins by densitometric analysis. Plotted are the expression levels of the phosphorylated proteins normalized to the expression levels of the non-phosphorylated proteins and then to the loading control. Statistical analysis was carried out using one-way ANOVA and Bonferroni multi-comparison; $n = 4$ independent experiments. Mean \pm SEM is plotted, * $p < 0.1$, ** $p < 0.01$.

5.6.4. Cardiac parameters of WT, $\Delta 3aa$ HET, functional DEL and R862C animals upon isoproterenol treatment

To further validate the cardioprotective effect of mutant PDE3A, WT, $\Delta 3aa$ HET and functional DEL animals were subjected to cardiac stress. More specifically, isoproterenol was administered for 14 days to stimulate cardiac hypertrophy and heart failure (Szabó, Csáky and Szegi 1975, Krenek et al. 2009). Sodium chloride (NaCl, physiological saline) was used as a control. Radio-telemetry measurements were performed at the beginning of the treatment and at the end of the 14 days treatment. The R862C mutant rats were also used to study the effect of the mutation affecting the region encoding the catalytic domain of PDE3A on the heart upon cardiac stress induction.

Various cardiac parameters assessing the hypertrophy of the heart, the amount of blood pumped by the heart and the volume of blood remaining in the heart at the end of contraction were measured by echocardiography (Figure 30) (Preclinical Research Center, MDC). No difference in the cardiac output or ejection fraction (EF), used to assess the volume of blood leaving the heart during systole, was observed between the four genotypes. For the $\Delta 3aa$ HET rats, increased cardiac output was observed upon stressing the heart compared to the non-stressed heart or to 14 days of NaCl treatment, suggesting that they could manifest stronger contractions after cardiac stress. The left ventricular mass (LV mass) increased in WT and functional DEL animals when stressing the heart, whereas for the $\Delta 3aa$ HET rats it did not change. Moreover, the mass of the LV was decreased in the $\Delta 3aa$ HET animals compared to the functional DEL ones upon isoproterenol treatment. The internal dimension of the left ventricle at the end of diastole (LVID) was significantly decreased in $\Delta 3aa$ HET rats compared to WT and R862C animals upon stressing the heart. The intraventricular septum diameter (IVSd) and the end-diastolic left

ventricular posterior wall thickness (LVPWd) were similar between all genotypes. These data indicate that the only animals that appeared protected against an increase in left ventricle size were the $\Delta 3aa$ HET. The heart rate was increased in the $\Delta 3aa$ HET rats upon cardiac stress induction compared to WT and $\Delta 3aa$ HET non-stressed hearts. The end-systolic volume (SV), referring to the amount of blood in a ventricle at the end of contraction was significantly decreased in the $\Delta 3aa$ HET rats compared to the WT ones after 14 days of isoproterenol treatment. This suggests that the $\Delta 3aa$ HET animals could exhibit stronger contractions. Nevertheless, more measurements are required since for the functional DEL animals, as well as for the R862C conditions, only two animals were available for each of the tested groups. The reduced number of available animals is the result of high mortality rate for animals receiving isoproterenol treatments, which was exacerbated by an early cessation of the experiment necessitated by the reduced operations of our animal facilities owing to the current coronavirus pandemic. In accordance with animal care and handling regulations, this resulted in the culling of all animals in ongoing treatments.

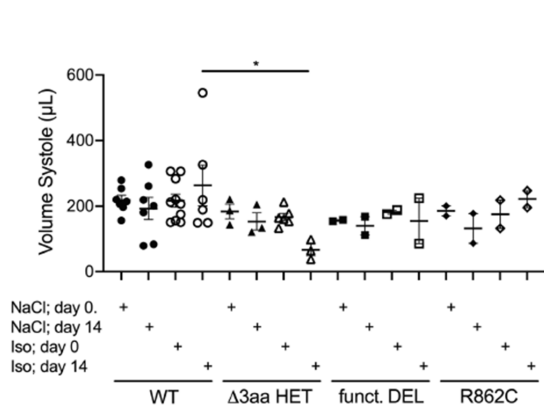
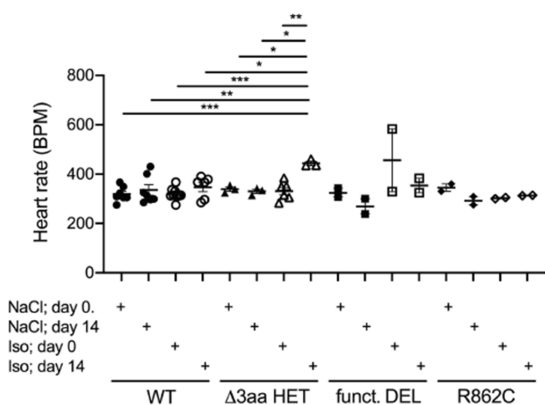
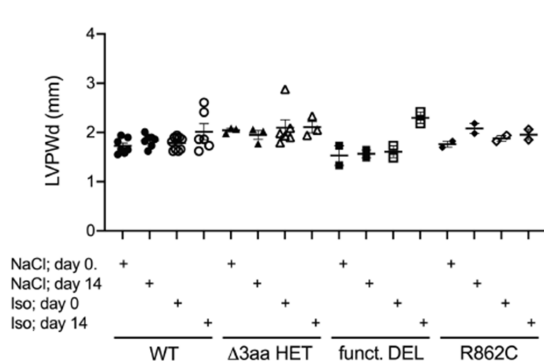
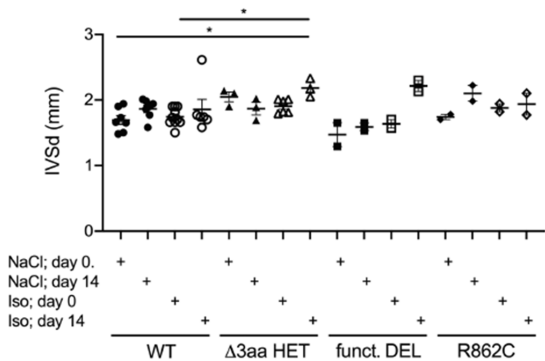
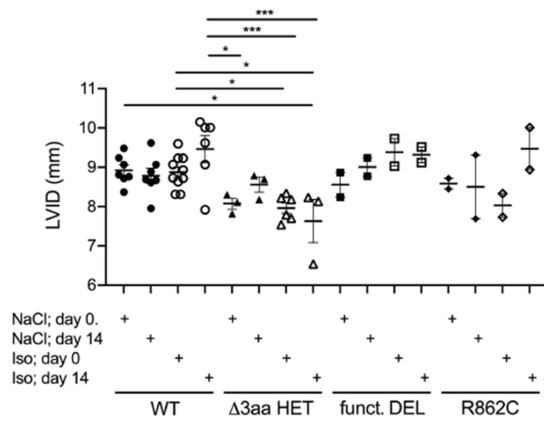
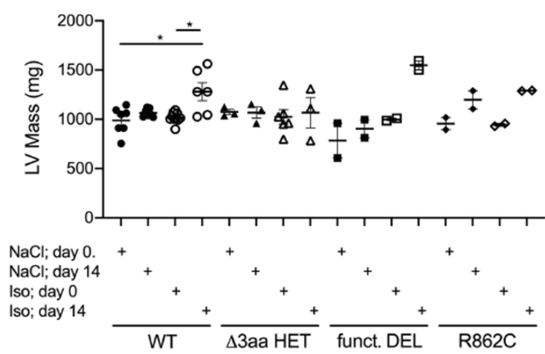
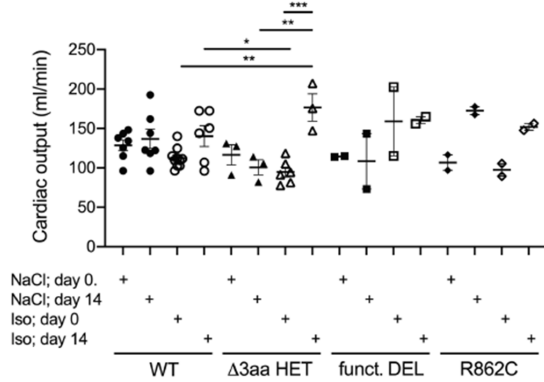
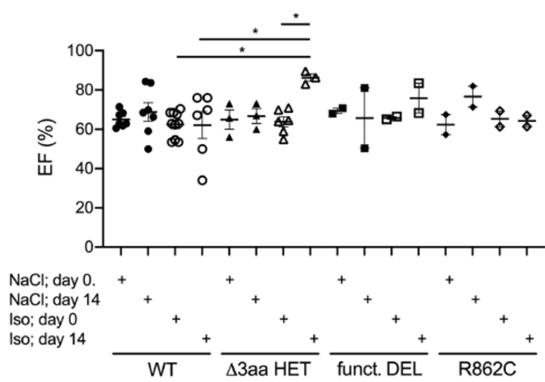


Figure 30: The cardiac response in WT, Δ 3aa HET, functional DEL and R862C rats upon stress induced by isoproterenol treatment differs between the genotypes. The indicated cardiac parameters were measured by echocardiography in WT, Δ 3aa HET, functional DEL and R862C rats after 14 days of treatment with isoproterenol or NaCl. Statistical analysis was carried out using one-way ANOVA and Bonferroni multi-comparison; WT: n = 7 (NaCl, day 0), n = 7 (NaCl, day 14), n = 10 (isoproterenol, day 0) and n = 6 (isoproterenol, day 14); Δ 3aa HET: n = 3 (NaCl, day 0), n = 3 (NaCl, day 14), n = 6 (isoproterenol, day 0) and n = 3 (isoproterenol, day 14); functional DEL: n = 2 (NaCl, day 0), n = 2 (NaCl, day 14), n = 2 (isoproterenol, day 0) and n = 2 (isoproterenol, day 14) and R862C: n = 2 (NaCl, day 0), n = 2 (NaCl, day 14), n = 2 (isoproterenol, day 0) and n = 2 (isoproterenol, day 14). Mean \pm SEM is plotted, *p < 0.1, **p < 0.01, ***p < 0.001.

5.6.5. Protein expression in rat heart from WT, Δ 3aa HET and functional DEL animals upon isoproterenol treatment

To further investigate whether mutant PDE3A is cardioprotective, initial experiments have been performed in which biochemical analysis of the rat hearts from the isoproterenol-treated WT, Δ 3aa HET and functional DEL animals was carried out (see Appendix, Supplemental Figure S1-S4). Nevertheless, these are only preliminary data and no statistical analysis could be performed since only two animals were available for each of the tested groups. This happened because the measurements had to be stopped and animals sacrificed before finishing the experiment due to the current coronavirus pandemic.

6. Discussion

Hypertension affects a billion people worldwide and the incidence is predicted to further increase to 1.5 billion by 2025 (Chockalingam 2007). The available anti-hypertensive drugs at best, slow the progression of the disease. There is a lack of effective treatment targeting the causes of essential hypertension, mainly due to insufficient understanding of the underlying mechanisms.

HTNB is a monogenic form of hypertension caused by mutations in the gene encoding for PDE3A. HTNB is characterized by age-dependent progressive hypertension induced by medial hyperplasia of peripheral vascular system, brachydactyly type E and protection from hypertension-associated end-organ damage, such as cardiac hypertrophy.

In this study, it was shown that PDE3A regulates blood pressure by controlling VSMC proliferation in the peripheral vascular system. Two new human PDE3A mutations that cause amino acid substitutions are presented, one within a five amino acid long hotspot region in the N-terminal regulatory domain of PDE3A and one in the enzymatic pocket of PDE3A. In addition, a new animal model, a hypertensive rat model that recapitulates HTNB and underscores the role of increased peripheral vascular resistance as a driving mechanism for hypertension, is introduced. Lastly, this study brings evidence that PDE3A mutations affecting the N-terminal regulatory region of the *PDE3A* gene protect the heart against cardiac remodeling, hypertrophy and heart failure.

6.1. Mutations in the regulatory region of the *PDE3A* gene are causative for HTNB, while the PDE3A enzymatic pocket is required for a normal skeletal development

A novel PDE3A mutation leading to a G449S substitution within a five amino acid long hotspot region in the N-terminal regulatory domain of PDE3A has been recently identified and shown to cause HTNB (Figure 14) (Ercu et al. 2020). To date, nine missense mutations and one single amino acid deletion clustered in the five amino acid-encoding region have been described in unrelated families affected with HTNB. Within the hotspot region, only three base pairs, encoding for amino acid 448 of PDE3A, have not yet been shown to be involved (Maass et al. 2015, Toka et al.

Discussion

2015, Ercu and Klussmann 2018, Renkema et al. 2018, Boda et al. 2016, Ercu et al. 2020). A new rat model carrying a 9 bp (three amino acids) deletion ($\Delta 3aa$ HET) in the regulatory region of the *PDE3A* gene was introduced, which corresponds to the human deletion, T445del (Ercu et al. 2020, Renkema et al. 2018). These rats apparently fully recapitulate the human HTNB phenotype. Thus, the model provides strong evidence that the mutations are causative for HTNB (Ercu et al. 2020).

The heterozygous rats carrying the three amino acid deletion in *PDE3A* had increased systolic and diastolic blood pressure, shorter fingers and presented looping of the left-side posterior inferior cerebellar artery (PICA) (Figure 10) (Ercu et al. 2020). The same was observed in the HTNB patients who suffered from severe hypertension, brachydactyly and presented PICA loops (Maass et al. 2015, Toka et al. 2015, Naraghi et al. 1997). Similar to *PDE3A* knock-out (KO) mice (Sun et al. 2007, Begum, Hockman and Manganiello 2011), the functional DEL rats displayed increased heart rate and reduced arterial blood pressure (Ercu et al. 2020), possibly due to peripheral vasodilation.

Vascular tone is one of the main determinants of peripheral vascular resistance and alterations in the vascular tone lead to severe pathologies including hypertension. Homeostasis of the vascular tone is attained by a fine-tuned balance between contraction and relaxation of VSMCs in the vascular wall (MacAllister and Vallance 1996, Brozovich et al. 2016, Tykocki, Boerman and Jackson 2017). One of the main regulators of the vascular tone is the renin-angiotensin-aldosterone system (RAAS) and angiotensin II (Ang II) is the main effector molecule of this system. Binding of Ang II to the angiotensin type I receptors (AT_1R) induces a signaling cascade that results in activation of PKC and subsequent phosphorylation of $Ca_v1.2$ channels, thereby allowing Ca^{2+} to enter the cytosol and promote contraction (Mehta and Malik 2006). The second messenger pathways cAMP and cGMP also play major roles in the regulation of the vascular tone. cAMP contributes to vascular tone regulation *via* its effector proteins, PKA, Epac and CNG ion channels (Roberts and Dart 2014). Activated PKA phosphorylates myosin light chain kinase (MLCK) and decreases its activity, which in turn leads to low levels of phosphorylated myosin light chain (MLC), resulting in vasodilation of the vasculature (Lamping 2001). Epac has also been shown to promote MLC dephosphorylation and hence VSMC relaxation and vasodilation by activation of the myosin light chain phosphatase (MLCP), *via* a Rap1-dependent reduction in RhoA activity (Roberts and Dart 2014). CNG channels

have been shown to promote Ca^{2+} influx-mediated vascular dilation and contraction (Shen et al. 2008, Leung et al. 2010). cGMP is essential for blood vessel relaxation. cGMP induces blood vessel relaxation either *via* activation of PKG and subsequent phosphorylation of target proteins or indirectly, by elevating cAMP levels (Krawutschke, Koesling and Russwurm 2015).

HTNB patients suffer from increased peripheral vascular resistance and hyperplasia of the tunica media of peripheral arteries (Schuster et al. 1996). Moreover, it was previously shown that patient-derived stem cells differentiated into VSMCs proliferated at a faster rate compared to those of unaffected family members (Maass et al. 2015, Naraghi et al. 1997). Vascular resistance is substantially influenced by small arteries (e.g. first- and second-order mesenteric arteries) (Christensen and Mulvany 1994). The $\Delta 3\text{aa}$ HET animals showed increased media-to-lumen ratio of second-order mesenteric arteries, resembling the patient situation (Figure 10C). Moreover, third-order mesenteric arteries from $\Delta 3\text{aa}$ HET rats showed weaker vasodilation in response to forskolin compared to those from WT animals. These data indicate that PDE3A hyperactivity restrains the ability of small arteries to dilate (Ercu et al. 2020).

It was previously shown that VSMCs differentiated from patient mesenchymal stem cells proliferated at a faster rate compared to those of unaffected family members (Maass et al. 2015). The proliferation rate of VSMCs from aorta of $\Delta 3\text{aa}$ HET rats was higher than that of VSMCs from WT animals (Ercu et al. 2020), reproducing the increased proliferation rate observed in the human model. However, no significant differences were observed neither in the thoracic aorta media thickness of $\Delta 3\text{aa}$ HET rats (Figure 12) (Ercu et al. 2020), nor in the expression levels of proteins essential for cellular proliferation from aorta of $\Delta 3\text{aa}$ HET animals (Figure 13). This seeming contradiction could be explained by the fact that *in vitro*, while generating the VSMCs from the aorta, the influence of the endothelium was lost, which could have changed the proliferative behavior of the cells. In the vasculature, the endothelium greatly influences the underlying VSMC layer by releasing contracting and relaxing factors, as well as paracrine factors influencing VSMC growth (Peiró et al. 1995, Milliat et al. 2006).

PDE3A1 and PDE3A2 isoforms were detected in aorta of WT and $\Delta 3\text{aa}$ HET rats, while both proteins were undetectable in the homozygous functional DEL animals. Both isoforms were expressed less in the $\Delta 3\text{aa}$ HET animals compared to

Discussion

the WT ones (Figure 11) (Ercu et al. 2020). This might be caused by altered phosphorylation of the mutant protein, as it was found in other enzymes carrying mutations in the regulatory region of the *PDE3A* gene (Maass et al. 2015), which could lead to altered protein-protein interactions (Ahmad et al. 2015b) and therefore impaired detection of the protein by the PDE3A-specific antibody. Another potential explanation could be downregulation of the expression of the mutant enzyme, or that protein degradation is increased due to the difference in the amino acid sequence.

A novel missense mutation causing an R862C substitution in the enzymatic pocket of PDE3A was discovered in a New Zealand family. Brachydactyly type E was documented in all affected members. However, hypertension was not detected in all affected individuals (Figure 15A), indicating that the hypertensive phenotype is not fully penetrant. Rat models carrying the R862C mutation were generated via CRISPR/Cas9. Analogous to the patient scenario, all of these animals had shorter digits compared to the WT controls (Figure 15B). Blood pressure measurements revealed no difference in the systolic and diastolic blood pressure compared to non-affected animals (Figure 15C), further confirming the observation that the HTNB phenotype is not fully penetrant when PDE3A mutations affect the enzymatic pocket of the enzyme. Nevertheless, it appears that PDE3A catalytic activity is required for normal skeleton development. Another rare skeletal disease involving the cAMP signaling pathway is type 2 acrodysostosis (ACRDYS2). It is a rare developmental skeletal disorder characterized by severe brachydactyly, short stature and facial dysostosis. It is caused by mutations in the *PDE4* gene. The mutations promote PKA-dependent phosphorylation and activation of PDE4D3, resulting in increased hydrolytic activity of the enzyme (Briet et al. 2017). These data further indicate that normal PDE catalytic activity is needed for proper skeletal development.

In conclusion, the fact that the full HTNB phenotype was recapitulated in the $\Delta 3aa$ HET rat model and not in the rats carrying the catalytic domain mutation confirms that mutations in the regulatory domain of the *PDE3A* gene are causative for HTNB. Furthermore, these animals emphasize the role of increased peripheral vascular resistance as a driving mechanism for hypertension.

6.2. Mutations in the regulatory domain of the *PDE3A* gene induce aberrant signaling

To gain insight into the effect the different mutations have on the location of PDE3A, WT and different mCherry-tagged PDE3A1 and PDE3A2 mutant variants were expressed in HEK293 cells and fluorescence microscopy imaging was performed (Figure 17). The mutation causing the T445N substitution was selected as representative for the mutations affecting the regulatory region of the *PDE3A* gene, while the R862C substitution, affecting the catalytic domain of PDE3A, was also investigated. PDE3A1-tagged mCherry was distributed throughout the cytosol, although PDE3A1 has been shown to exclusively localize in cardiac membranes (Hambleton et al. 2005). This could owe to the overexpression-induced high concentration of PDE3A1-mCherry and the fluorescent protein-tagging of PDE3A itself (Stadler et al. 2013). As expected, PDE3A2-mCherry variants were predominantly localized in the cytosol (Hambleton et al. 2005). No difference in PDE3A1 and PDE3A2 localization was observed between WT and the two mutant proteins. Nevertheless, one has to consider that the maximum resolution reached by conventional fluorescence microscopy is 200-300 nm in the lateral direction and 500-700 nm in the axial direction due to the diffraction of light (Huang, Bates and Zhuang 2009) and therefore subtle differences in localization would not be visible with this method. Stimulated emission depletion (STED) microscopy could be an alternative option for better visualization of cellular compartments since the lateral resolution achieved by this technique is below 50 nm and the axial resolution is about 150 nm (Hein, Willig and Hell 2008).

The effect on PDE3A activity of six of the mutations (T445N, T445A, T445S, A447T, A447V and G449V) affecting the regulatory region of the *PDE3A* gene has been investigated and was shown to increase the cAMP affinity and hydrolytic activity of the enzyme (Maass et al. 2015). It was next investigated whether the same was the case for the new PDE3A mutants, the Δ 3aa and G449S variants, as well as for the R862C construct. The activity of these PDE3A versions was measured by FRET in HEK293 cells. To validate the accuracy of the method, we also used FRET to measure the activity of the T445N variant, which was previously shown to increase cAMP hydrolysis. Taking into account that both PDE3A1 and PDE3A2 appeared to be mostly localized in the cytosol, FRET measurements were initially performed in the cytosol using the cytosolic ICUE3 sensor and the mCherry-tagged PDE3A2

Discussion

isoform, which is considered to be predominantly found in the cytosol. Under resting conditions, the WT and mutant PDE3A2 variants showed similar enzyme activities (Figure 19C). Upon forskolin-dependent stimulation of AC an increase in cAMP hydrolysis was observed for T445N, Δ 3aa and G449S compared to the WT protein (Figure 19A). This suggests that PDE3A2 variants carrying mutations in the regulatory region of the *PDE3A* gene are hyperactive, as was expected. Moreover, the R862C substitution did not cause increased cAMP hydrolysis upon forskolin treatment, reflected by comparable cAMP levels to the WT (Figure 19A). This indicates that mutations affecting the region encoding the catalytic domain of PDE3A might not be hyperactive, further confirming the fact that only mutations in the regulatory region of the *PDE3A* gene increase the hydrolytic activity of the enzyme.

Administration of PDE3 inhibitors is an established therapeutic strategy for the treatment of various cardiovascular diseases. However, severe side effects have been associated with the long-term usage of PDE3 inhibitor therapy, most likely due to the lack of selectivity for specific isoforms, which leads to activation of cAMP signaling in multiple intracellular compartments (Ahmad et al. 2015a). The two PDE3-specific inhibitors approved as drugs for the treatment of various cardiovascular diseases, milrinone and cilostazol, interact both with common and distinct residues at the active site of the enzyme (Zhang, Ke and Colman 2002). Milrinone has inotropic and vasodilatory properties, while cilostazol possesses anti-platelet, anti-proliferative and vasodilatory properties (Tariq and Aronow 2015, Rogers et al. 2015).

To better understand the changes induced by the mutations and to deduce properties of the mutant protein, the effect of various PDE inhibitors on the activity of the enzyme in HEK293 cells was investigated by FRET measurements. Milrinone partially inhibited the WT protein and all PDE3A2 variants carrying mutations in the regulatory region of the *PDE3A* gene, whereas it seemed to not affect the cAMP hydrolytic capacity of the PDE3A2-R862C version (Figure 19A). The different mutations could have different effects on the overall structure of PDE3A and subsequently on the catalytic domain of the enzyme, which would in turn affect the binding of milrinone in the active site of PDE3A. Furthermore, although the R862 residue has not been shown to directly bind to milrinone (Zhang et al. 2002, Sadeghian et al. 2009), it is still possible that the R862C substitution might affect the metal ion binding site of PDE3A, which would indirectly affect the inhibitor binding. This has been previously reported in PDE4A, where an amino acid exchange of the

metal binding residues decreased the interaction of rolipram to the enzyme (Jacobitz et al. 1996). Cilostamide, a derivative of cilostazol, was used since it is more cell-permeant than its analogue. Cilostamide appeared to be more efficient than milrinone in inhibiting both the WT protein as well as the enzymes carrying mutations in the hotspot region. The sensitivity of these proteins to cilostamide is similar to the WT enzyme (Figure 19B). This could be due to subtle conformational changes of the active site induced by the mutations that would promote cilostamide binding and therefore, would allow for better inhibition of the enzyme.

The small molecule BAY 41-8543 promotes cGMP production by stimulating sGC and therefore causes inhibition of PDE3A. Inhibition of PDE3A occurs due to the binding of cGMP in the active site of the enzyme (Zaccolo and Movsesian 2007). It was previously shown that cGMP stimulation and treatment with BAY 41-8543 in HeLa cells inhibit both WT PDE3A as well as the enzyme carrying various mutations in the hotspot region of the regulatory domain (Maass et al. 2015, Toka et al. 2015). We tested the effect of BAY 41-8543 on the activity of the WT and mutant PDE3A2 in HEK293 cells using FRET. Cyclic GMP-mediated inhibition of PDE3A was more efficient for the T445N and Δ 3aa PDE3A2 constructs as compared to the WT protein (Figure 20B), suggesting that these mutations induce changes that promote cGMP binding to the catalytic domain of PDE3A. The indirect inhibition of PDE3A achieved through cGMP binding was however not as efficient as the direct inhibition of the enzyme induced by cilostamide. On the contrary, the cGMP-mediated inhibitory effect on the mutant enzymes is comparable to the one obtained when using milrinone. Altogether, these data indicate that mutations at various sites within the *PDE3A* gene induce different protein sensitivities towards different inhibitors.

Increased cAMP signaling has been previously shown to reduce hypertension in spontaneously hypertensive rats (Berg, Degerman and Tasken 2009). Treatment with BAY 41-8543 and subsequent inhibition of PDE3A normalized the mean arterial pressure of both WT and Δ 3aa HET rats, although the effect was stronger in the mutant animals (Figure 10D) (Ercu et al. 2020). However, cGMP also leads to the activation of PKG, which has vasodilatory properties (Hofmann et al. 2009). Therefore, the observed decrease in blood pressure could also be due to cGMP-mediated PKG activation and subsequent vasodilation. These data suggest that activation of sGC could be a suitable treatment option for patients suffering from HTNB.

Discussion

To verify whether PDE3A activity differs between the cytosol and the PM, FRET measurements were performed in HEK293 cells at the PM using the membrane-bound LynICUE3 sensor and the mCherry-tagged PDE3A1 WT and T445N variants. Similar to the situation in the cytosol, the T445N mutation increased the enzymatic activity of PDE3A1 compared to the WT upon forskolin treatment, whereas under resting conditions, both the WT and mutant protein showed similar enzyme activities (Figure 21A and B).

These data show that mutations affecting the regulatory domain hotspot region of the *PDE3A* gene increase the cAMP hydrolytic activity of the enzyme both in the cytosol, as well as at the PM. Hyperactive PDE3A could prevent apoptosis and induce increased cell proliferation. It has been previously shown that PDE3A1 upregulation induces the expression of the anti-apoptotic molecule B-cell lymphoma 2 (Bcl-2) by negatively regulating the transcriptional inducible cAMP early repressor (ICER), both in vitro and in vivo (Oikawa et al. 2013). Also, PDE3A depletion was shown to induce cell cycle arrest and hence to inhibit VSMC proliferation in PDE3A-KO mice (Begum et al. 2011). Therefore, hyperactive PDE3A could prevent the apoptosis and even induce the enhanced proliferation of the VSMCs. This could potentially explain the VSMC hyperproliferation we observed in the second-order mesenteric arteries of $\Delta 3aa$ HET rats and thus the increased peripheral resistance and subsequent high blood pressure. The second-order mesenteric arteries are muscular arteries, containing more smooth muscle cells in the tunica media layer than elastic arteries, such as the aorta (Leloup et al. 2015). This could potentially explain the fact that the $\Delta 3aa$ HET rats displayed increased media thickness of second order mesenteric arteries, but not of aorta.

The enzyme carrying the R862C substitution was not hyperactive and thus might not induce increased VSMC proliferation. This could explain the fact that the blood pressure phenotype is not fully penetrant in the rats carrying the catalytic domain mutation. However, some of these animals do have increased blood pressure, suggesting that there might be additional factors other than the increased enzymatic activity of PDE3A that contribute to the observed hypertension. Altered phosphorylation and subsequent altered protein-protein interaction-driven mechanisms or aberrant oligomerization could potentially lead to increased VSMC proliferation and thus, to increased peripheral vascular resistance. In the R862C substitution, an arginine is replaced by a cysteine. This could introduce disulfide

bonds and subsequently increase the dimerization of the enzyme with a potential influence on its activity or protein-protein interactions. This possibility is supported by recent evidence showing that PDE4 activity is regulated by its dimerization (Cedervall et al. 2015).

6.3. Mutations in the regulatory region of the *PDE3A* gene lead to altered protein-protein interactions

Compartmentalization of cAMP signaling in specific locations is required to ensure the interaction of the second messenger with localized effector proteins and dysregulation in local cAMP signaling is detrimental (Zoccarato et al. 2015). To achieve a coordinated cAMP-dependent signaling response, PDEs are either tethered to specific subcellular compartments via structural motifs or are targeted to particular compartments upon engaging in protein-protein interactions (Stangherlin and Zaccolo 2012, Azevedo et al. 2014). PDEs are incorporated in a number of signaling complexes upon their interaction with AKAPs (Klussmann 2016). In the human heart, PDE3A1 is recruited in an AKAP18-based signalosome that controls the Ca²⁺ re-uptake into the SR and thereby cardiac relaxation. PDE3A1 is incorporated into the complex upon PKA-mediated phosphorylation of serine residues 292/293 (Ahmad et al. 2015b). Therefore, phosphorylation of PDE3A1 induces both a change in its localization, as well as a change in its interaction partners.

Therefore, the interactome of PDE3A in the human heart was investigated *via* mass spectrometry and verified whether the mutations might induce a change in it. Various proteins were found to potentially interact with PDE3A (Tables 25 and 26 and Figure 22). One of the identified proteins that was further investigated was the adaptor protein 14-3-3 θ (Table 25 and Figure 22A). It belongs to the 14-3-3 family of conserved regulatory proteins expressed in all eukaryotic cells. They can bind phosphorylated serine residues of a myriad of signaling proteins with diverse functionality, including kinases and phosphatases and they regulate a variety of biological processes, including signal transduction, cell cycle regulation, intracellular trafficking and apoptosis (Aitken 2002, Fu, Subramanian and Masters 2000). The 14-3-3 family consists of seven isoforms (β , γ , ε , σ , ζ , θ and η) (Fu et al. 2000) and five of them (β , γ , ε , θ and ζ) co-precipitated with PDE3A (Tables 25 and 26 and

Discussion

Supplemental Table S2), with 14-3-3 θ showing the highest intensity. Moreover, an interaction between PDE3A and 14-3-3 proteins upon PMA-induced phosphorylation of Ser428 on PDE3A was previously described in HeLa cells (Pozuelo Rubio et al. 2005, Corradini et al. 2015). In addition, 14-3-3 θ binding to PDE3B promoted by PKA phosphorylation of the enzyme prevents phosphatase-dependent inactivation (Palmer et al. 2007). Therefore, 14-3-3 θ binding to PDE3A could be involved in the regulation of local PDE3A activity.

Upon validation of the 14-3-3 θ interaction to PDE3A in the human heart (Figure 23), we tested whether PDE3A mutations that cause HTNB affect the interaction of the two proteins. We showed increased binding of 14-3-3 θ to PDE3A mutants, T445N and Δ 3aa, compared to the WT after PMA but not forskolin stimulation (Figure 24). These data confirmed that 14-3-3 θ interaction to PDE3A is dependent on phosphorylation of the enzyme at Ser428, as previously described (Pozuelo Rubio et al. 2005). Furthermore, these findings demonstrate that the HTNB phenotype is associated with mutation-induced altered phosphorylation and altered protein-protein interactions of PDE3A mutants.

Similar to the recruitment of PDE3A1 upon PKA phosphorylation into the AKAP18-based signalosome (Ahmad et al. 2015b), the increased phosphorylation-dependent interaction could induce a change in the location of the mutant proteins, which could lead to a reduction in local cAMP levels caused by the hyperactive enzymes. Therefore, it was verified whether the increased binding of 14-3-3 θ to PDE3A causes a change in the enzyme's location in the cell or with respect to 14-3-3 θ via immunofluorescence microscopy in H9C2 cells. To mimic the mutation-induced hyperphosphorylation, H9C2 cells were treated with either PMA, forskolin or both compounds in order to increase PDE3A phosphorylation. Both proteins were distributed throughout the cytosol and no difference either in PDE3A localization or with respect to 14-3-3 θ was detectable upon any of the treatments compared to the control condition (Figure 25). Once again, one limitation to this method is the relatively small resolution caused by the diffraction of light, i.e. less than 200-300 nm in the lateral direction and less than 500-700 nm in the axial direction (Huang et al. 2009). Therefore, subtle differences in PDE3A location or between 14-3-3 θ and PDE3A would not be visible under these parameters.

Another protein that co-precipitated with PDE3A is the catalytic subunit α of PKA (Table 25 and Figure 22A). An interaction between PDE3A and the catalytic

subunit α of PKA was previously described in myocardial membranes (Ahmad et al. 2015b). This result was confirmed by co-precipitating both proteins from human heart and from cardiomyocytes differentiated from WT and T445N-derived iPSCs (Figure 26). Mutation-induced alterations in PDE3A binding to the catalytic subunit α of PKA could lead to aberrant phosphorylation of substrates found in the vicinity of PDE3A and thus altering local signaling. Taking into account that PKA controls a multitude of cellular processes, including cardiomyocyte contraction and cell growth and division, some of the altered processes in the HTNB animal models, such as increased systolic and diastolic blood pressure and enhanced VSMC proliferation could be potentially explained by aberrant interaction between PDE3A and the catalytic subunit α of PKA. For instance, reduced PKA-mediated phosphorylation of vasodilator-stimulated phosphoprotein (VASP) at Ser157 has been associated with increased VSMC proliferation after angioplasty (Zhao et al. 2008, Maass et al. 2015). Therefore, a decrease in the interaction between PDE3A and the catalytic subunit α of PKA and thus subsequent decrease in VASP Ser157 phosphorylation could contribute to the observed enhanced VSMC proliferation.

The findings presented in this study are relevant not only for HTNB patients, but also to essential hypertension, as found in the general population, since understanding the molecular mechanisms that drive HTNB could provide insight into mechanisms underlying blood pressure control and essential hypertension. This conclusion is supported by a recent genome-wide linkage found in a subfamily of Chinese subjects where a locus for essential hypertension coincided with the *PDE3A* locus (Gong et al. 2003) and by further GWAS studies that underscored the importance of the *PDE3A* locus in influencing blood pressure (Ehret et al. 2016, Kato et al. 2015, Simino et al. 2013, Warren et al. 2017, Evangelou et al. 2018). Novel therapeutic approaches that target compartment-specific PDE3A-driven signaling events, and not its activity, for modulation of a disease-relevant signaling process could pave the way to new PDE3A-dependent treatments, while avoiding the deleterious side effects associated with PDE3 inhibitor therapy. Targeting unique PDE3A-dependent protein-protein interactions in a specific cellular location to generate compartment-specific effects on intracellular signaling is one example of such therapeutic approach that could be relevant not only for treating HTNB patients but also for the treatment of essential hypertension in the general population.

6.4. PDE3A mutations that cause HTNB are cardioprotective

6.4.1. HTNB rat model is protected against hypertension-associated end-organ damage

HTNB-affected individuals die of stroke by the age of 50 years if untreated however, surprisingly, they do not develop hypertension-induced target-organ damage. They show no signs of cardiac hypertrophy, heart failure or kidney damage, as would be expected after decade-long hypertension (Hattenbach et al. 1998, Toka et al. 2015). The heart responds to cardiac stress, such as increased blood pressure and myocardial infarction, by undergoing a remodeling process in the attempt to maintain normal function and satisfy the oxygen needs of the body (Towbin and Bowles 2002). At the cellular level specific genes that promote the non-mitotic growth of cardiac myocytes are upregulated and therefore they undergo compensatory hypertrophy in an attempt to maintain normal cardiac function (Frey and Olson 2003). In the long term, however, this stress-induced adaptation leads to adverse events, including cardiomyocyte death and fibrosis and ultimately to heart failure, a condition in which the heart is unable to supply the required amount of blood and oxygen throughout the body (Schirone et al. 2017). Moreover, defects in cardiac angiogenesis and vascularization further impair the oxygen supply and therefore contribute to the disease progression (Gogiraju, Bochenek and Schäfer 2019).

Similar to the absent cardiac hypertrophy, the individuals suffering from HTNB do not present any sign of impaired kidney function. Laboratory tests have been performed in which the level of electrolytes, acid-base regulation and renin-angiotensin-catecholamine values were assessed and were all found to be normal (Schuster et al. 1996, van den Born et al. 2016, Toka et al. 2015). Furthermore, no abnormalities were detected when the kidneys were visualized by echocardiography or computed tomography (Fan et al. 2020). Overall, the renal function of the HTNB-affected individuals was assessed to be normal (Toka et al. 2015, Hattenbach et al. 1998).

Analogous to the patient situation, the $\Delta 3aa$ HET and HOM rats did not display an increase in various cardiac parameters measured *via* echocardiography, suggesting that mutations affecting the hotspot region of the *PDE3A* gene have cardioprotective effects. Recently, various serum and urine parameters were also evaluated and were similar in WT and $\Delta 3aa$ HET rats. Moreover, the mutant animals

showed no signs of proteinuria or perturbed renal function. The components of the RAAS were also measured and compared. The levels of angiotensin-II, angiotensinogen, aldosterone and plasma renin were comparable between WT and $\Delta 3aa$ HET animals (Ercu et al. 2020). As already mentioned, RAAS plays an essential role in vascular tone regulation and hence, in peripheral vascular resistance (Mehta and Malik 2006). The fact that the $\Delta 3aa$ HET rats show signs of increased peripheral vascular resistance but no alterations in the components of the renin-angiotensin-aldosterone axis, further confirms that the mechanism underlying the hypertension is related to VSMC signaling and proliferation. Furthermore, the mRNA expression levels of two renal damage markers, *Lcn2* and *Havcr1*, were measured and no differences were observed between the WT and $\Delta 3aa$ HET rats (Ercu et al. 2020). In conclusion, the $\Delta 3aa$ HET rats resemble the HTNB patients and present no signs of target-organ damage, further confirming the hypothesis that HTNB-causative PDE3A mutations protect against cardiac damage and impaired renal function.

Therefore, it appears that the HTNB-causative mutations affecting the regulatory region of the *PDE3A* gene protect against hypertension-associated end-organ damage.

6.4.2. Elucidating the molecular mechanism underlying the cardioprotective effects of the PDE3A mutations

To gain insight into the molecular mechanism underlying the cardioprotective effect of PDE3A mutations, the expression of the PDE3A isoforms in the heart of WT, $\Delta 3aa$ HET and functional DEL animals was investigated. PDE3A1 but not PDE3A2 expression was downregulated in the $\Delta 3aa$ HET rats compared to the WT animals (Figure 27). PDE3A1 is the main isoform found in the heart (Hambleton et al. 2005). Since the protein carrying the $\Delta 3aa$ deletion was shown to be hyperactive, downregulation could be compensatory mechanism. Overexpression of PDE3A1 was associated with lower TGF- β levels and protected the heart against cardiac hypertrophy and fibrosis (Iwaya et al. 2014). Therefore, PDE3A1 hyperactivity observed in the $\Delta 3aa$ HET rats compared to the WT animals could, at least partly, account for the lack of hypertrophy observed in both HTNB patients and HTNB rat model.

Discussion

Alterations in the excitation-contraction coupling machinery of cardiomyocytes can cause severe pathologies, including heart failure (Bers 2002, Layland et al. 2005, Kensler et al. 2017, Zima et al. 2014). PDE3A plays a major role in cardiac contraction regulation since PKA-dependent phosphorylation is needed for the proper functioning of proteins that assure proper excitation-contraction coupling. Since PDE3A mutations appear to protect against cardiac remodeling and hence, heart failure, the expression of key players in cardiac contraction and relaxation in the left ventricle of WT, $\Delta 3aa$ HET and functional DEL rats were investigated. RyR2 are calcium channels that, when open, allow Ca^{2+} to move from the SR into the cytosol, a process known as Ca^{2+} -induced Ca^{2+} release, thus promoting contraction. PKA-dependent phosphorylation of RyR2 at Ser2808 and Ser2030, as well as Ca/Calmodulin-dependent kinase type II (CaMKII)-dependent phosphorylation at Ser2814 are considered relevant for the functionality of the channel (Zima et al. 2014). PLN, when unphosphorylated, inhibits SERCA2 activity by lowering its affinity for Ca^{2+} . PKA-dependent phosphorylation of PLN at Ser16 relieves this inhibition, thereby promoting Ca^{2+} re-uptake into the SR and relaxation (Zima et al. 2014, Kranias and Hajjar 2012). The expression levels of phosphorylated RyR2 at Ser2808 and phosphorylated PLN at Ser16 were increased in $\Delta 3aa$ HET rats compared to the WT and functional DEL animals (Figure 29), suggesting increased Ca^{2+} cycling, i.e. more Ca^{2+} available for contraction and more Ca^{2+} pumped back into the SR, facilitating relaxation, in the HTNB rat model. Taking into account that normally in response to high blood pressure the heart undergoes cardiac remodeling as an attempt to maintain normal function, the increase in Ca^{2+} cycling could explain the lack of cardiac hypertrophy despite the severe hypertension. Therefore, Ca^{2+} imaging in HTNB rat model-derived adult cardiomyocytes is required in order to investigate changes in Ca^{2+} cycling.

The loss of PDE3A in murine hearts led to increased baseline myocardial contractility associated with elevated phosphorylation of PLN at Ser16, increased RyR2 phosphorylation at Ser 2808, Ser2814 and ser2830 and reduced RyR2 expression (Beca et al. 2013). This was not the case for our functional DEL rats, where the phosphorylation levels of PLN at Ser16 and RyR2 at Ser2808 were comparable to the WT rats. A potential explanation for this difference could be the fact that in this study the protein expression in rat left ventricles was investigated, whereas Beca et al. measured the expression in whole heart lysates. Moreover, the

relative expression of *PDE* genes differs significantly by species and thus the cAMP degradation mediated by specific PDEs varies between different species. For example, in the rodent myocardium, PDE4 is responsible for up to 60 % in the rat heart and about 30 % in the mouse heart of cAMP hydrolysis (Knight and Yan 2012). Therefore, it seems that increased PDE4-mediated cAMP hydrolysis takes place in the rat heart, leading to decreased PKA-induced substrate, e.g. PLN and RyR2, phosphorylation. Furthermore, PLN is a small monomeric protein that forms oligomers, most commonly pentamers (Wittmann, Lohse and Schmitt 2015). Beca et al. investigated the phosphorylation levels of the monomer, whereas in this study the trimer PLN was analyzed, due to antibody limitations. This could also be a possible explanation for the observed difference in the PKA-mediated phosphorylation pattern of PLN.

MyBPC and Troponin I, when phosphorylated, enhance contractions and the later also accelerates relaxation (Kensler et al. 2017, Layland et al. 2005). No difference in the PKA-dependent phosphorylation of these two proteins was observed between the WT, Δ 3aa HET and functional DEL rats, with the exception of a decrease in the amount of phosphorylated MyBPC in the functional DEL animals compared to the WT ones (Figure 29). These data indicate that the cardioprotective effect is more likely given indirectly, by an increase in Ca^{2+} cycling, i.e. more Ca^{2+} being released into the cytosol from the SR thus promoting contraction and more Ca^{2+} being pumped back into the SR facilitating relaxation, rather than by directly promoting or inhibiting actomyosin interaction.

6.4.3. The HTNB animal models are protected from cardiac damage upon cardiac stress induction

To further investigate the cardioprotective effect of PDE3A mutations, various cardiac parameters were measured *via* echocardiography in WT, Δ 3aa HET, functional DEL and R862C mutant rats upon cardiac stress induction by isoproterenol treatment. Unfortunately, for the functional DEL and R862C rats, measurements have been performed for only two animals. This happened firstly due to the death of some of the animals during the procedure and secondly, the measurements had to be stopped and animals sacrificed because of the current coronavirus pandemic.

Discussion

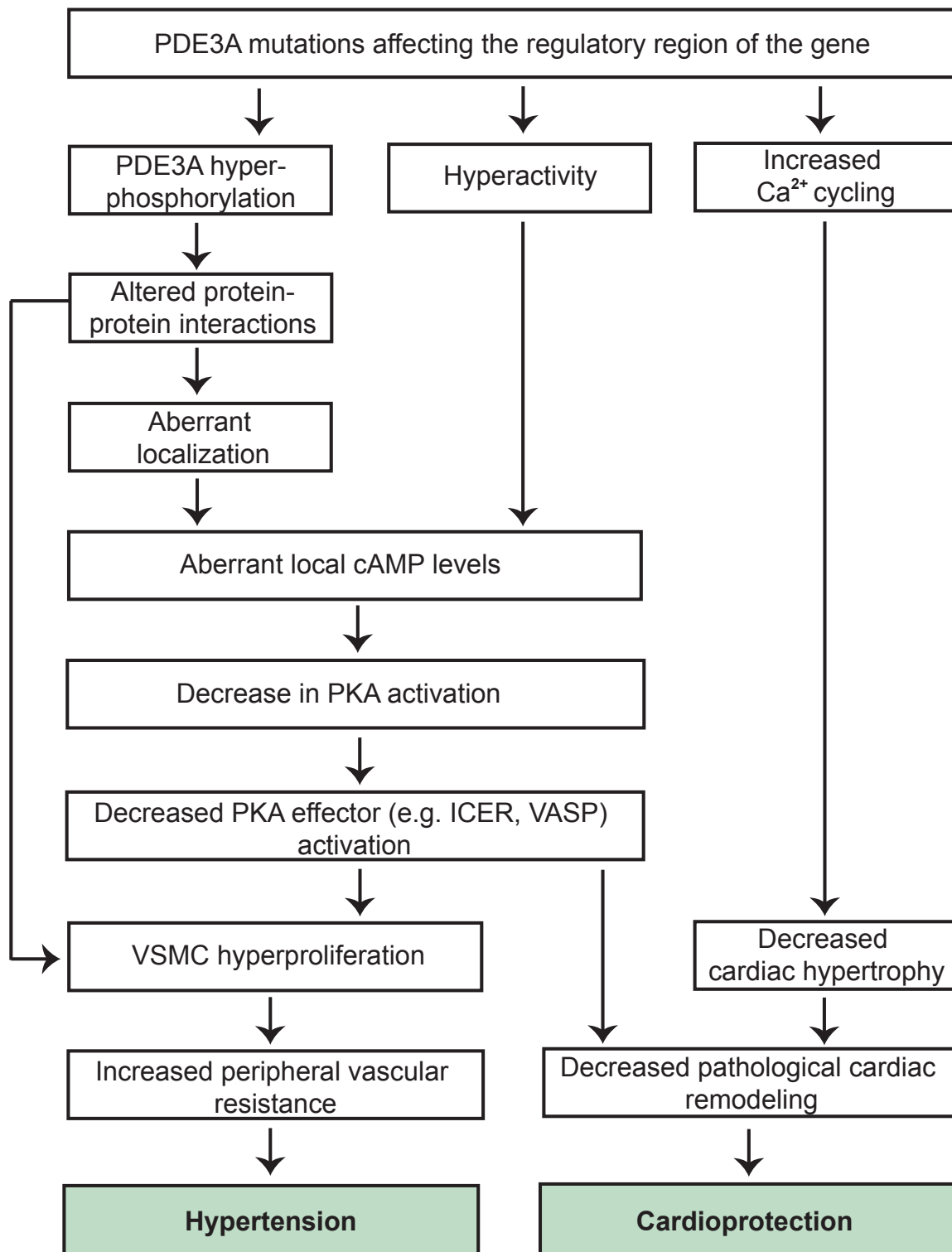
LV mass and LVID are indicative parameters for the wall thickness of the myocardium that strongly correlate with pathological cardiac remodeling (Gaasch and Zile 2011). After 14 days of isoproterenol treatment, the $\Delta 3aa$ HET rats showed unchanged or even decreased LV mass or LVID value compared to the other genotypes, suggesting that cardiac stress does not induce left ventricular hypertrophy in the $\Delta 3aa$ HET animals. These data confirm the previous observation that mutations in the regulatory region of the *PDE3A* gene protect the heart against cardiac remodeling (Toka et al. 2015).

Cardiac output and ejection fraction are two parameters used to assess the volume of blood leaving the heart during systole and when impaired, they are strong predictors of heart failure (Citation, Reddi et al., 2017). Upon cardiac stress induction, the cardiac output and ejection fraction of the $\Delta 3aa$ HET rats were higher compared to those measured in non-stressed hearts from WT rats or from $\Delta 3aa$ HET animals. Furthermore, the amount of blood in a ventricle at the end of contraction, also known as the end-systolic volume, was significantly decreased in the $\Delta 3aa$ HET rats compared to the WT after stressing the heart. Taken together, these data indicate that the $\Delta 3aa$ HET animals could manifest stronger contractions upon cardiac stress induction, which could compensate to maintain the normal function of the heart and pump the required amount of blood. This is further confirmed by the increase in the expression levels of phosphorylated RyR2 and PLN detected in the left ventricles of $\Delta 3aa$ HET rats (Figure 29), which indicate increased Ca^{2+} cycling and hence stronger contractions in these animals. Nevertheless, more measurements are needed since for the functional DEL animals, as well as for the R862C ones, only two animals were available for each of the tested groups.

6.5. PDE3A mutations can both cause and prevent disease

Collectively, the data presented here indicate that PDE3A mutations can both drive and prevent disease. In HTNB, the mutant, hyperactive PDE3A causes hypertension by driving mechanisms that increase VSMC proliferation and peripheral vascular resistance. On the contrary, PDE3A mutations affecting the regulatory region of the *PDE3A* gene protect the heart against cardiac remodeling by promoting an increase in Ca^{2+} cycling, thus inducing stronger contractions and enhancing relaxation, allowing the heart to maintain its normal function without cardiomyocyte

hypertrophy induction (Figure 31). The mutations affecting the region encoding the catalytic domain of PDE3A do not cause hyperactivity and therefore can lead to hypertension in HTNB patients via alternative mechanisms that increase VSMC proliferation and peripheral vascular resistance, such as altered protein-protein interaction-driven mechanisms or aberrant oligomerization.



Discussion

Figure 31: Schematic representation of the proposed mechanism for PDE3A mutation-induced hypertension and cardioprotection. PDE3A mutations affecting the regulatory domain have been shown to cause increased PDE3A phosphorylation, hyperactivity and appear to activate the Ca^{2+} machinery of the cardiomyocyte and induce increased Ca^{2+} cycling. The hyperphosphorylation caused by the mutations promotes altered protein-protein interactions that could change the cellular localization of the enzyme. The hyperactive enzyme decreases the cAMP levels at specific microdomains, which could potentially result in less phosphorylation and activation of PKA effector proteins (e.g. ICER, VASP) due to less active PKA. ICER has been shown to induce apoptosis and to inhibit proliferation of VSMCs (Ohtsubo et al. 2007). Therefore, a decrease in PKA-mediated ICER activation could decrease VSMC apoptosis and lead to the observed VSMC hyperproliferation and subsequent increased peripheral vascular resistance, which was shown to cause hypertension. Furthermore, reduced PKA-mediated phosphorylation of VASP has been associated with VSMC proliferation (Zhao et al. 2008). In the heart, decreased ICER activation has been shown to reduce cardiomyocyte apoptosis and to decrease the pathological cardiac remodeling (Oikawa et al. 2013), thus having a cardioprotective effect. Lastly, the increase in Ca^{2+} cycling would allow the heart to maintain its normal function and pump the required amount of blood in spite of the severe hypertension, thereby having a cardioprotective effect by decreasing the cardiac hypertrophy and subsequent cardiac remodeling.

7. Outlook

The study presented in this thesis shows that hyperactive PDE3A causes HTNB but protects against cardiac damage. The findings direct attention towards novel therapeutic approaches for lowering blood pressure and protecting against heart failure, namely by addressing PDE3A-driven signaling events and targeting its unique protein-protein interactions to achieve compartment-specific effects on intracellular signaling.

To understand the mechanisms driven by the mutated *PDE3A* gene that lead to the increased peripheral vascular resistance and decreased pathological cardiac remodeling, the expression of activated PKA effector proteins, e.g. ICER and VASP, should be measured in the heart and vessels of WT, $\Delta 3aa$ HET and functional DEL rats. Moreover, the activity of WT and mutant PDE3A could be investigated by FRET in other cellular compartments, e.g. at the mitochondria or inside the nucleus. In the mitochondria cAMP-PKA signaling is essential for various processes, including mitochondrial fission and apoptosis (Zhang et al. 2016). In the nucleus, cAMP regulates transcription *via* CREB activation mediated by PKA (Lefkimiatis and Zaccolo 2014). We already have mitochondria- and nucleus-targeted FRET biosensors for monitoring cAMP levels. Furthermore, it would be very interesting to measure PKA activity at various cellular compartments. We also have FRET biosensors for monitoring PKA activity in the cytosol, at the PM, at the mitochondria or inside the nucleus.

The consequences of the increased interaction between mutant PDE3A and 14-3-3 θ should be also further investigated to determine whether it contributes to the increased peripheral vascular resistance or to the cardioprotective effect. More specifically, it should be verified whether the increased interaction induces a change in PDE3A localization or activity. Further aberrant protein-protein interactions may contribute to both the increased peripheral vascular resistance and the cardioprotective effect of PDE3A by tethering the mutant enzyme to compartments different from those of WT PDE3A. Therefore, the interactome of mutant PDE3A in the heart of the mutant rat model should be analyzed. We expect the interactome to be different in different tissues, especially in the peripheral arteries compared to the heart. Candidate proteins, such as scaffolding proteins, will be characterized with respect to their ability to tether mutant PDE3A aberrantly to a compartment. If such

Outlook

candidate proteins are found, small molecule inhibitors of mutant PDE3A or enhancers of the WT enzyme with identified candidate protein will be searched by screening and subsequently tested for their anti-hyperproliferative or cardioprotective effects respectively.

Lastly, the mutations have been shown to induce increased PMA-dependent phosphorylation of PDE3A1 and PDE3A2 at Ser428 (Maass et al. 2015, Ercu et al. 2020), site phosphorylated by PKC (Movsesian, Ahmad and Hirsch 2018), an important modulator of cellular Ca^{2+} signaling (Lipp and Reither 2011). Therefore, Ca^{2+} imaging in adult cardiomyocytes and VSMCs from WT, $\Delta 3aa$ HET, functional DEL and R862C rats should be performed to verify whether the mutations affecting the regulatory region of the *PDE3A* gene promote an increase in Ca^{2+} cycling.

8. References

- Abi-Gerges, A., W. Richter, F. Lefebvre, P. Mateo, A. Varin, C. Heymes, J. L. Samuel, C. Lugnier, M. Conti, R. Fischmeister & G. Vandecasteele (2009) Decreased expression and activity of cAMP phosphodiesterases in cardiac hypertrophy and its impact on beta-adrenergic cAMP signals. *Circ Res*, 105, 784-92.
- Acin-Perez, R., M. Russwurm, K. Günnewig, M. Gertz, G. Zoidl, L. Ramos, J. Buck, L. R. Levin, J. Rassow, G. Manfredi & C. Steegborn (2011) A phosphodiesterase 2A isoform localized to mitochondria regulates respiration. *J Biol Chem*, 286, 30423-32.
- Ahmad, F., T. Murata, K. Shimizu, E. Degerman, D. Maurice & V. Manganiello (2015a) Cyclic nucleotide phosphodiesterases: important signaling modulators and therapeutic targets. *Oral Dis*, 21, e25-50.
- Ahmad, F., W. Shen, F. Vandeput, N. Szabo-Fresnais, J. Krall, E. Degerman, F. Goetz, E. Klussmann, M. Movsesian & V. Manganiello (2015b) Regulation of sarcoplasmic reticulum Ca²⁺ ATPase 2 (SERCA2) activity by phosphodiesterase 3A (PDE3A) in human myocardium: phosphorylation-dependent interaction of PDE3A1 with SERCA2. *J Biol Chem*, 290, 6763-76.
- Aitken, A. (2002) Functional specificity in 14-3-3 isoform interactions through dimer formation and phosphorylation. Chromosome location of mammalian isoforms and variants. *Plant Mol Biol*, 50, 993-1010.
- Anant, J. S., O. C. Ong, H. Y. Xie, S. Clarke, P. J. O'Brien & B. K. Fung (1992) In vivo differential prenylation of retinal cyclic GMP phosphodiesterase catalytic subunits. *J Biol Chem*, 267, 687-90.
- Asara, J. M., H. R. Christofk, L. M. Freemark & L. C. Cantley (2008) A label-free quantification method by MS/MS TIC compared to SILAC and spectral counting in a proteomics screen. *Proteomics*, 8, 994-9.
- Azevedo, M. F., F. R. Faucz, E. Bimpaki, A. Horvath, I. Levy, R. B. de Alexandre, F. Ahmad, V. Manganiello & C. A. Stratakis (2014) Clinical and molecular genetics of the phosphodiesterases (PDEs). *Endocr Rev*, 35, 195-233.
- Baillie, G. S., D. R. Adams, N. Bhari, T. M. Houslay, S. Vadrevu, D. Meng, X. Li, A. Dunlop, G. Milligan, G. B. Bolger, E. Klussmann & M. D. Houslay (2007) Mapping binding sites for the PDE4D5 cAMP-specific phosphodiesterase to the N- and C-domains of beta-arrestin using spot-immobilized peptide arrays. *Biochem J*, 404, 71-80.
- Baillie, G. S., E. Huston, G. Scotland, M. Hodgkin, I. Gall, A. H. Peden, C. MacKenzie, E. S. Houslay, R. Currie, T. R. Pettitt, A. R. Walmsley, M. J. Wakelam, J. Warwicker & M. D. Houslay (2002) TAPAS-1, a novel microdomain within the unique N-terminal region of the PDE4A1 cAMP-specific phosphodiesterase that allows rapid, Ca²⁺-triggered membrane association with selectivity for interaction with phosphatidic acid. *J Biol Chem*, 277, 28298-309.
- Baillie, G. S., S. J. MacKenzie, I. McPhee & M. D. Houslay (2000) Sub-family selective actions in the ability of Erk2 MAP kinase to phosphorylate and regulate the activity of PDE4 cyclic AMP-specific phosphodiesterases. *Br J Pharmacol*, 131, 811-9.
- Baillie, G. S., G. S. Tejeda & M. P. Kelly (2019) Therapeutic targeting of 3',5'-cyclic nucleotide phosphodiesterases: inhibition and beyond. *Nat Rev Drug Discov*, 18, 770-796.

References

- Beard, M. B., E. Huston, L. Campbell, I. Gall, I. McPhee, S. Yarwood, G. Scotland & M. D. Houslay (2002) In addition to the SH3 binding region, multiple regions within the N-terminal noncatalytic portion of the cAMP-specific phosphodiesterase, PDE4A5, contribute to its intracellular targeting. *Cell Signal*, 14, 453-65.
- Beavo, J. A. & L. L. Brunton (2002) Cyclic nucleotide research -- still expanding after half a century. *Nat Rev Mol Cell Biol*, 3, 710-8.
- Beca, S., F. Ahmad, W. Shen, J. Liu, S. Makary, N. Polidovitch, J. Sun, S. Hockman, Y. W. Chung, M. Movsesian, E. Murphy, V. Manganiello & P. H. Backx (2013) Phosphodiesterase type 3A regulates basal myocardial contractility through interacting with sarcoplasmic reticulum calcium ATPase type 2a signaling complexes in mouse heart. *Circ Res*, 112, 289-97.
- Begum, N., S. Hockman & V. C. Manganiello (2011) Phosphodiesterase 3A (PDE3A) deletion suppresses proliferation of cultured murine vascular smooth muscle cells (VSMCs) via inhibition of mitogen-activated protein kinase (MAPK) signaling and alterations in critical cell cycle regulatory proteins. *J Biol Chem*, 286, 26238-49.
- Berg, T., E. Degerman & K. Tasken (2009) Increased cAMP signaling can ameliorate the hypertensive condition in spontaneously hypertensive rats. *J Vasc Res*, 46, 25-35.
- Berisha, F. & V. O. Nikolaev (2017) Cyclic nucleotide imaging and cardiovascular disease. *Pharmacol Ther*, 175, 107-115.
- Bers, D. M. (2002) Cardiac excitation-contraction coupling. *Nature*, 415, 198-205.
- Bobin, P., M. Belacel-Ouari, I. Bedioune, L. Zhang, J. Leroy, V. Leblais, R. Fischmeister & G. Vandecasteele (2016) Cyclic nucleotide phosphodiesterases in heart and vessels: A therapeutic perspective. *Arch Cardiovasc Dis*, 109, 431-43.
- Boda, H., H. Uchida, N. Takaiso, Y. Ouchi, N. Fujita, A. Kuno, T. Hata, A. Nagatani, Y. Funamoto, M. Miyata, T. Yoshikawa, H. Kurahashi & H. Inagaki (2016) A PDE3A mutation in familial hypertension and brachydactyly syndrome. *J Hum Genet*, 61, 701-3.
- Bolívar, J. J. (2013) Essential hypertension: an approach to its etiology and neurogenic pathophysiology. *Int J Hypertens*, 2013, 547809.
- Brand, T. & R. Schindler (2017) New kids on the block: The Popeye domain containing (POPDC) protein family acting as a novel class of cAMP effector proteins in striated muscle. *Cell Signal*, 40, 156-165.
- Briet, C., A. Pereda, C. Le Stunff, E. Motte, J. de Dios Garcia-Diaz, G. P. de Nanclares, N. Dumaz & C. Silve (2017) Mutations causing acrodysostosis-2 facilitate activation of phosphodiesterase 4D3. *Hum Mol Genet*, 26, 3883-3894.
- Brozovich, F. V., C. J. Nicholson, C. V. Degen, Y. Z. Gao, M. Aggarwal & K. G. Morgan (2016) Mechanisms of Vascular Smooth Muscle Contraction and the Basis for Pharmacologic Treatment of Smooth Muscle Disorders. *Pharmacol Rev*, 68, 476-532.
- Brunet, A., D. Roux, P. Lenormand, S. Dowd, S. Keyse & J. Pouyssegur (1999) Nuclear translocation of p42/p44 mitogen-activated protein kinase is required for growth factor-induced gene expression and cell cycle entry. *EMBO J*, 18, 664-74.
- Bähring, S., M. Kann, Y. Neuenfeld, M. Gong, D. Chitayat, H. R. Toka, O. Toka, G. Plessis, P. Maass, A. Rauch, A. Aydin & F. C. Luft (2008) Inversion region for hypertension and brachydactyly on chromosome 12p features multiple splicing and noncoding RNA. *Hypertension*, 51, 426-31.
- Bähring, S., A. Rauch, O. Toka, C. Schroeder, C. Hesse, H. Siedler, G. Fesüs, W. E. Haefeli, A. Busjahn, A. Aydin, Y. Neuenfeld, A. Mühl, H. R. Toka, M. Gollasch, J. Jordan & F. C. Luft (2004) Autosomal-dominant hypertension with type E brachydactyly is

- caused by rearrangement on the short arm of chromosome 12. *Hypertension*, 43, 471-6.
- Cedervall, P., A. Aulabaugh, K. F. Geoghegan, T. J. McLellan & J. Pandit (2015) Engineered stabilization and structural analysis of the autoinhibited conformation of PDE4. *Proc Natl Acad Sci U S A*, 112, E1414-22.
- Chen, R. H., C. Sarnecki & J. Blenis (1992) Nuclear localization and regulation of erk- and rsk-encoded protein kinases. *Mol Cell Biol*, 12, 915-27.
- Chen, W., A. Spitzl, D. Mathes, V. O. Nikolaev, F. Werner, J. Weirather, K. Špiranec, K. Röck, J. W. Fischer, U. Kämmerer, D. Stegner, H. A. Baba, U. Hofmann, S. Frantz & M. Kuhn (2016) Endothelial Actions of ANP Enhance Myocardial Inflammatory Infiltration in the Early Phase After Acute Infarction. *Circ Res*, 119, 237-48.
- Chockalingam, A. (2007) Impact of World Hypertension Day. *Can J Cardiol*, 23, 517-9.
- Christensen, K. L. & M. J. Mulvany (1994) Perindopril changes the mesenteric pressure profile of conscious hypertensive and normotensive rats. *Hypertension*, 23, 325-8.
- Cone, J., S. Wang, N. Tandon, M. Fong, B. Sun, K. Sakurai, M. Yoshitake, J. Kambayashi & Y. Liu (1999) Comparison of the effects of cilostazol and milrinone on intracellular cAMP levels and cellular function in platelets and cardiac cells. *J Cardiovasc Pharmacol*, 34, 497-504.
- Conti, M. & J. Beavo (2007) Biochemistry and physiology of cyclic nucleotide phosphodiesterases: essential components in cyclic nucleotide signaling. *Annu Rev Biochem*, 76, 481-511.
- Cooper, D. M. (2003) Regulation and organization of adenylyl cyclases and cAMP. *Biochem J*, 375, 517-29.
- Cooper, D. M. & V. G. Tabbasum (2014) Adenylate cyclase-centred microdomains. *Biochem J*, 462, 199-213.
- Corradini, E., G. Klaasse, U. Leurs, A. J. Heck, N. I. Martin & A. Scholten (2015) Charting the interactome of PDE3A in human cells using an IBMX based chemical proteomics approach. *Mol Biosyst*, 11, 2786-97.
- Cowley, A. W. (2006) The genetic dissection of essential hypertension. *Nat Rev Genet*, 7, 829-40.
- Dell'Acqua, M. L., M. C. Faux, J. Thorburn, A. Thorburn & J. D. Scott (1998) Membrane-targeting sequences on AKAP79 bind phosphatidylinositol-4, 5-bisphosphate. *EMBO J*, 17, 2246-60.
- Dema, A., D. Faust, K. Lazarow, M. Wippich, M. Neuenschwander, K. Zühlke, A. Geelhaar, T. Pallien, E. Hallscheidt, J. Eichhorst, B. Wiesner, H. Černecká, O. Popp, P. Mertins, G. Dittmar, J. P. von Kries & E. Klussmann (2020) Cyclin-Dependent Kinase 18 Controls Trafficking of Aquaporin-2 and Its Abundance through Ubiquitin Ligase STUB1, Which Functions as an AKAP. *Cells*, 9.
- Dema, A., E. Perets, M. S. Schulz, V. A. Deák & E. Klussmann (2015) Pharmacological targeting of AKAP-directed compartmentalized cAMP signalling. *Cell Signal*, 27, 2474-87.
- Dema, A., M. F. Schröter, E. Perets, P. Skroblin, M. C. Moutty, V. A. Deák, W. Birchmeier & E. Klussmann (2016) The A-Kinase Anchoring Protein (AKAP) Glycogen Synthase Kinase 3 β Interaction Protein (GSKIP) Regulates β -Catenin through Its Interactions with Both Protein Kinase A (PKA) and GSK3 β . *J Biol Chem*, 291, 19618-30.
- Deák, V. A. & E. Klussmann (2016) Pharmacological Interference With Protein-protein Interactions of Akinase Anchoring Proteins as a Strategy for the Treatment of Disease. *Curr Drug Targets*, 17, 1147-71.

References

- Deák, V. A., P. Skroblin, C. Dittmayer, K. P. Knobloch, S. Bachmann & E. Klussmann (2016) The A-kinase Anchoring Protein GSKIP Regulates GSK3 β Activity and Controls Palatal Shelf Fusion in Mice. *J Biol Chem*, 291, 681-90.
- DiFrancesco, D. & P. Tortora (1991) Direct activation of cardiac pacemaker channels by intracellular cyclic AMP. *Nature*, 351, 145-7.
- Ding, B., J. I. Abe, H. Wei, Q. Huang, R. A. Walsh, C. A. Molina, A. Zhao, J. Sadoshima, B. C. Blaxall, B. C. Berk & C. Yan (2005) Functional role of phosphodiesterase 3 in cardiomyocyte apoptosis: implication in heart failure. *Circulation*, 111, 2469-2476.
- DiPilato, L. M. & J. Zhang (2009) The role of membrane microdomains in shaping beta2-adrenergic receptor-mediated cAMP dynamics. *Mol Biosyst*, 5, 832-7.
- Diviani, D., L. K. Langeberg, S. J. Doxsey & J. D. Scott (2000) Pericentrin anchors protein kinase A at the centrosome through a newly identified RII-binding domain. *Curr Biol*, 10, 417-20.
- Diviani, D., E. Reggi, M. Arambasic, S. Caso & D. Maric (2016) Emerging roles of A-kinase anchoring proteins in cardiovascular pathophysiology. *Biochim Biophys Acta*, 1863, 1926-36.
- Dodge-Kafka, K. L., J. Soughayer, G. C. Pare, J. J. Carlisle Michel, L. K. Langeberg, M. S. Kapiloff & J. D. Scott (2005) The protein kinase A anchoring protein mAKAP coordinates two integrated cAMP effector pathways. *Nature*, 437, 574-8.
- Dogui, A., N. Kachenoura, F. Frouin, M. Lefort, A. De Cesare, E. Mousseaux & A. Herment (2011) Consistency of aortic distensibility and pulse wave velocity estimates with respect to the Bramwell-Hill theoretical model: a cardiovascular magnetic resonance study. *J Cardiovasc Magn Reson*, 13, 11.
- Efendiev, R. & C. W. Dessauer (2011) A kinase-anchoring proteins and adenylyl cyclase in cardiovascular physiology and pathology. *J Cardiovasc Pharmacol*, 58, 339-44.
- Ehret, G. B., T. Ferreira, D. I. Chasman, A. U. Jackson, E. M. Schmidt, T. Johnson, G. Thorleifsson, J. Luan, L. A. Donnelly, S. Kanoni, A. K. Petersen, V. Pihur, R. J. Strawbridge, D. Shungin, M. F. Hughes, O. Meirelles, M. Kaakinen, N. Bouatia-Naji, K. Kristiansson, S. Shah, M. E. Kleber, X. Guo, L. P. Lyytikäinen, C. Fava, N. Eriksson, I. M. Nolte, P. K. Magnusson, E. L. Salfati, L. S. Rallidis, E. Theusch, A. J. P. Smith, L. Folkersen, K. Witkowska, T. H. Pers, R. Joehanes, S. K. Kim, L. Lataniotis, R. Jansen, A. D. Johnson, H. Warren, Y. J. Kim, W. Zhao, Y. Wu, B. O. Tayo, M. Bochud, D. Absher, L. S. Adair, N. Amin, D. E. Arking, T. Axelsson, D. Baldassarre, B. Balkau, S. Bandinelli, M. R. Barnes, I. Barroso, S. Bevan, J. C. Bis, G. Bjornsdottir, M. Boehnke, E. Boerwinkle, L. L. Bonnycastle, D. I. Boomsma, S. R. Bornstein, M. J. Brown, M. Burnier, C. P. Cabrera, J. C. Chambers, I. S. Chang, C. Y. Cheng, P. S. Chines, R. H. Chung, F. S. Collins, J. M. Connell, A. Döring, J. Dallongeville, J. Danesh, U. de Faire, G. Delgado, A. F. Dominiczak, A. S. F. Doney, F. Drenos, S. Edkins, J. D. Eicher, R. Elosua, S. Enroth, J. Erdmann, P. Eriksson, T. Esko, E. Evangelou, A. Evans, T. Fall, M. Farrall, J. F. Felix, J. Ferrières, L. Ferrucci, M. Fornage, T. Forrester, N. Franceschini, O. H. F. Duran, A. Franco-Cereceda, et al. (2016) The genetics of blood pressure regulation and its target organs from association studies in 342,415 individuals. *Nat Genet*, 48, 1171-1184.
- Ercu, M. & E. Klussmann (2018) Roles of A-Kinase Anchoring Proteins and Phosphodiesterases in the Cardiovascular System. *J Cardiovasc Dev Dis*, 5.
- Ercu, M., L. Markó, C. Schächterle, D. Tsvetkov, Y. Cui, S. Maghsodi, T. U. P. Bartolomeus, P. G. Maass, K. Zühlke, N. Gregersen, N. Hübner, R. Hodge, A. Mühl, B. Pohl, R. Molé-Illas, A. Geelhaar, S. Walter, H. Napieczynska, S. Schelenz, M. Taube, A. Heuser, Y. M. Anistan, F. Qadri, M. Todiras, R. Plehm, E. Popova, R. Langanki, J.

- Eichhorst, M. Lehmann, B. Wiesner, M. Russwurm, S. K. Forslund, I. Kamer, D. N. Müller, M. Gollasch, A. Aydin, S. Bähring, M. Bader, F. C. Luft & E. Klusmann (2020) Phosphodiesterase 3A and Arterial Hypertension. *Circulation*.
- Evangelou, E., H. R. Warren, D. Mosen-Ansorena, B. Mifsud, R. Pazoki, H. Gao, G. Ntritsos, N. Dimou, C. P. Cabrera, I. Karaman, F. L. Ng, M. Evangelou, K. Witkowska, E. Tzanis, J. N. Hellwege, A. Giri, D. R. Velez Edwards, Y. V. Sun, K. Cho, J. M. Gaziano, P. W. F. Wilson, P. S. Tsao, C. P. Kovesdy, T. Esko, R. Mägi, L. Milani, P. Almgren, T. Boutin, S. Debette, J. Ding, F. Giulianini, E. G. Holliday, A. U. Jackson, R. Li-Gao, W. Y. Lin, J. Luan, M. Mangino, C. Oldmeadow, B. P. Prins, Y. Qian, M. Sargurupremraj, N. Shah, P. Surendran, S. Thériault, N. Verweij, S. M. Willems, J. H. Zhao, P. Amouyel, J. Connell, R. de Mutsert, A. S. F. Doney, M. Farrall, C. Menni, A. D. Morris, R. Noordam, G. Paré, N. R. Poulter, D. C. Shields, A. Stanton, S. Thom, G. Abecasis, N. Amin, D. E. Arking, K. L. Ayers, C. M. Barbieri, C. Batini, J. C. Bis, T. Blake, M. Bochud, M. Boehnke, E. Boerwinkle, D. I. Boomsma, E. P. Bottinger, P. S. Braund, M. Brumat, A. Campbell, H. Campbell, A. Chakravarti, J. C. Chambers, G. Chauhan, M. Ciullo, M. Cocca, F. Collins, H. J. Cordell, G. Davies, M. H. de Borst, E. J. de Geus, I. J. Deary, J. Deelen, F. Del Greco M, C. Y. Demirkale, M. Dörr, G. B. Ehret, R. Elosua, S. Enroth, A. M. Erzurumluoglu, T. Ferreira, M. Fränberg, O. H. Franco, I. Gandin, et al. (2018) Publisher Correction: Genetic analysis of over 1 million people identifies 535 new loci associated with blood pressure traits. *Nat Genet*, 50, 1755.
- Falcão, L. M., F. Pinto, L. Ravara & P. A. van Zwieten (2004) BNP and ANP as diagnostic and predictive markers in heart failure with left ventricular systolic dysfunction. *J Renin Angiotensin Aldosterone Syst*, 5, 121-9.
- Fan, G., E. Shumay, H. Wang & C. C. Malbon (2001) The scaffold protein gravin (cAMP-dependent protein kinase-anchoring protein 250) binds the beta 2-adrenergic receptor via the receptor cytoplasmic Arg-329 to Leu-413 domain and provides a mobile scaffold during desensitization. *J Biol Chem*, 276, 24005-14.
- Fan, P., D. Zhang, K. Q. Yang, Q. Y. Zhang, F. Luo, Y. Lou, Y. X. Liu, H. M. Zhang, L. Song, J. Cai, H. Y. Wu & X. L. Zhou (2020) Hypertension and Brachydactyly Syndrome Associated With Vertebral Artery Malformation Caused by a PDE3A Missense Mutation. *Am J Hypertens*, 33, 190-197.
- Faxon, D. P., M. A. Creager, S. C. Smith, R. C. Pasternak, J. W. Olin, M. A. Bettmann, M. H. Criqui, R. V. Milani, J. Loscalzo, J. A. Kaufman, D. W. Jones, W. H. Pearce & A. H. Association (2004) Atherosclerotic Vascular Disease Conference: Executive summary: Atherosclerotic Vascular Disease Conference proceeding for healthcare professionals from a special writing group of the American Heart Association. *Circulation*, 109, 2595-604.
- Fischmeister, R., L. R. Castro, A. Abi-Gerges, F. Rochais, J. Jurevicius, J. Leroy & G. Vandecasteele (2006) Compartmentation of cyclic nucleotide signaling in the heart: the role of cyclic nucleotide phosphodiesterases. *Circ Res*, 99, 816-28.
- Francis, S. H., M. A. Blount & J. D. Corbin (2011) Mammalian cyclic nucleotide phosphodiesterases: molecular mechanisms and physiological functions. *Physiol Rev*, 91, 651-90.
- Francis, S. H., M. Conti & M. D. Houslay. 2011. *Phosphodiesterases as drug targets*. Heidelberg ; New York: Springer.
- Francis, S. H. & J. D. Corbin (1994) Structure and function of cyclic nucleotide-dependent protein kinases. *Annu Rev Physiol*, 56, 237-72.
- Fraser, I. D., S. J. Tavalin, L. B. Lester, L. K. Langeberg, A. M. Westphal, R. A. Dean, N. V. Marrion & J. D. Scott (1998) A novel lipid-anchored A-kinase Anchoring Protein facilitates cAMP-responsive membrane events. *EMBO J*, 17, 2261-72.

References

- Frey, N., H. A. Katus, E. N. Olson & J. A. Hill (2004) Hypertrophy of the heart: a new therapeutic target? *Circulation*, 109, 1580-9.
- Frey, N. & E. N. Olson (2003) Cardiac hypertrophy: the good, the bad, and the ugly. *Annu Rev Physiol*, 65, 45-79.
- Froese, A. & V. O. Nikolaev (2015) Imaging alterations of cardiomyocyte cAMP microdomains in disease. *Front Pharmacol*, 6, 172.
- Fu, H., R. R. Subramanian & S. C. Masters (2000) 14-3-3 proteins: structure, function, and regulation. *Annu Rev Pharmacol Toxicol*, 40, 617-47.
- Gaasch, W. H. & M. R. Zile (2011) Left ventricular structural remodeling in health and disease: with special emphasis on volume, mass, and geometry. *J Am Coll Cardiol*, 58, 1733-40.
- Galindo-Tovar, A., M. L. Vargas & A. J. Kaumann (2009) Phosphodiesterases PDE3 and PDE4 jointly control the inotropic effects but not chronotropic effects of (-)-CGP12177 despite PDE4-evoked sinoatrial bradycardia in rat atrium. *Naunyn Schmiedebergs Arch Pharmacol*, 379, 379-84.
- Gardner, L. A., S. J. Tavalin, A. S. Goehring, J. D. Scott & S. W. Bahouth (2006) AKAP79-mediated targeting of the cyclic AMP-dependent protein kinase to the beta1-adrenergic receptor promotes recycling and functional resensitization of the receptor. *J Biol Chem*, 281, 33537-53.
- Gillingham, A. K. & S. Munro (2000) The PACT domain, a conserved centrosomal targeting motif in the coiled-coil proteins AKAP450 and pericentrin. *EMBO Rep*, 1, 524-9.
- Gogiraju, R., M. L. Bochenek & K. Schäfer (2019) Angiogenic Endothelial Cell Signaling in Cardiac Hypertrophy and Heart Failure. *Front Cardiovasc Med*, 6, 20.
- Gold, M. G., T. Gonen & J. D. Scott (2013) Local cAMP signaling in disease at a glance. *J Cell Sci*, 126, 4537-43.
- Gong, M., H. Zhang, H. Schulz, Y. A. Lee, K. Sun, S. Bähring, F. C. Luft, P. Nürnberg, A. Reis, K. Rohde, D. Ganten, R. Hui & N. Hübner (2003) Genome-wide linkage reveals a locus for human essential (primary) hypertension on chromosome 12p. *Hum Mol Genet*, 12, 1273-7.
- Gray, P. C., B. D. Johnson, R. E. Westenbroek, L. G. Hays, J. R. Yates, T. Scheuer, W. A. Catterall & B. J. Murphy (1998) Primary structure and function of an A kinase anchoring protein associated with calcium channels. *Neuron*, 20, 1017-26.
- Greenwald, E. C., S. Mehta & J. Zhang (2018) Genetically Encoded Fluorescent Biosensors Illuminate the Spatiotemporal Regulation of Signaling Networks. *Chem Rev*, 118, 11707-11794.
- Gresele, P., S. Momi & E. Falcinelli (2011) Anti-platelet therapy: phosphodiesterase inhibitors. *Br J Clin Pharmacol*, 72, 634-46.
- Halls, M. L. & D. M. Cooper (2011) Regulation by Ca²⁺-signaling pathways of adenylyl cyclases. *Cold Spring Harb Perspect Biol*, 3, a004143.
- Hambleton, R., J. Krall, E. Tikishvili, M. Honeggar, F. Ahmad, V. C. Manganiello & M. A. Movsesian (2005) Isoforms of cyclic nucleotide phosphodiesterase PDE3 and their contribution to cAMP hydrolytic activity in subcellular fractions of human myocardium. *J Biol Chem*, 280, 39168-74.
- Han, P., P. Sonati, C. Rubin & T. Michaeli (2006) PDE7A1, a cAMP-specific phosphodiesterase, inhibits cAMP-dependent protein kinase by a direct interaction with C. *J Biol Chem*, 281, 15050-7.
- Hattenbach, L. O., H. R. Toka, O. Toka, H. Schuster & F. C. Luft (1998) Absence of hypertensive retinopathy in a Turkish kindred with autosomal dominant hypertension and brachydactyly. *Br J Ophthalmol*, 82, 1363-5.

- Hein, B., K. I. Willig & S. W. Hell (2008) Stimulated emission depletion (STED) nanoscopy of a fluorescent protein-labeled organelle inside a living cell. *Proc Natl Acad Sci U S A*, 105, 14271-6.
- Hiatt, W. R., S. R. Money & E. P. Brass (2008) Long-term safety of cilostazol in patients with peripheral artery disease: the CASTLE study (Cilostazol: A Study in Long-term Effects). *J Vasc Surg*, 47, 330-336.
- Hofmann, F., D. Bernhard, R. Lukowski & P. Weinmeister (2009) cGMP regulated protein kinases (cGK). *Handb Exp Pharmacol*, 137-62.
- Huang, B., M. Bates & X. Zhuang (2009) Super-resolution fluorescence microscopy. *Annu Rev Biochem*, 78, 993-1016.
- Huang, L. J., L. Wang, Y. Ma, K. Durick, G. Perkins, T. J. Deerinck, M. H. Ellisman & S. S. Taylor (1999) NH₂-Terminal targeting motifs direct dual specificity A-kinase-anchoring protein 1 (D-AKAP1) to either mitochondria or endoplasmic reticulum. *J Cell Biol*, 145, 951-9.
- Hudson, C., T. E. Kimura, A. Duggirala, G. B. Sala-Newby, A. C. Newby & M. Bond (2018) Dual Role of CREB in The Regulation of VSMC Proliferation: Mode of Activation Determines Pro- or Anti-Mitogenic Function. *Sci Rep*, 8, 4904.
- Hundsrucker, C., P. Skroblin, F. Christian, H. M. Zenn, V. Popara, M. Joshi, J. Eichhorst, B. Wiesner, F. W. Herberg, B. Reif, W. Rosenthal & E. Klussmann (2010) Glycogen synthase kinase 3beta interaction protein functions as an A-kinase anchoring protein. *J Biol Chem*, 285, 5507-21.
- Iwaya, S., M. Oikawa, Y. Chen & Y. Takeishi (2014) Phosphodiesterase 3A1 protects the heart against angiotensin II-induced cardiac remodeling through regulation of transforming growth factor- β expression. *Int Heart J*, 55, 165-8.
- Jacobitz, S., M. M. McLaughlin, G. P. Livi, M. Burman & T. J. Torphy (1996) Mapping the functional domains of human recombinant phosphodiesterase 4A: structural requirements for catalytic activity and rolipram binding. *Mol Pharmacol*, 50, 891-9.
- Jaiswal, B. S. & M. Conti (2003) Calcium regulation of the soluble adenylyl cyclase expressed in mammalian spermatozoa. *Proc Natl Acad Sci U S A*, 100, 10676-81.
- Jungen, C., K. Scherschel, C. Eickholt, P. Kuklik, N. Klatt, N. Bork, T. Salzbrunn, F. Alken, S. Angendohr, C. Klene, J. Mester, N. Klöcker, M. W. Veldkamp, U. Schumacher, S. Willems, V. O. Nikolaev & C. Meyer (2017) Disruption of cardiac cholinergic neurons enhances susceptibility to ventricular arrhythmias. *Nat Commun*, 8, 14155.
- Kato, N., M. Loh, F. Takeuchi, N. Verweij, X. Wang, W. Zhang, T. N. Kelly, D. Saleheen, B. Lehne, I. M. Leach, A. W. Drong, J. Abbott, S. Wahl, S. T. Tan, W. R. Scott, G. Campanella, M. Chadeau-Hyam, U. Afzal, T. S. Ahluwalia, M. J. Bonder, P. Chen, A. Dehghan, T. L. Edwards, T. Esko, M. J. Go, S. E. Harris, J. Hartiala, S. Kasela, A. Kasturiratne, C. C. Khor, M. E. Kleber, H. Li, Z. Yu Mok, M. Nakatochi, N. S. Sapari, R. Saxena, A. F. R. Stewart, L. Stolk, Y. Tabara, A. L. Teh, Y. Wu, J. Y. Wu, Y. Zhang, I. Aits, A. Da Silva Couto Alves, S. Das, R. Dorajoo, J. C. Hopewell, Y. K. Kim, R. W. Koivula, J. Luan, L. P. Lytykäinen, Q. N. Nguyen, M. A. Pereira, I. Postmus, O. T. Raitakari, M. Scannell Bryan, R. A. Scott, R. Sorice, V. Tragante, M. Traglia, J. White, K. Yamamoto, L. S. Adair, A. Ahmed, K. Akiyama, R. Asif, T. Aung, I. Barroso, A. Bjornnes, T. R. Braun, H. Cai, L. C. Chang, C. H. Chen, C. Y. Cheng, Y. S. Chong, R. Collins, R. Courtney, G. Davies, G. Delgado, L. D. Do, P. A. Doevendans, R. T. Gansevoort, Y. T. Gao, T. B. Grammer, N. Grarup, J. Grewal, D. Gu, G. S. Wander, A. L. Hartikainen, S. L. Hazen, J. He, C. K. Heng, J. E. Hixson, A. Hofman, C. Hsu, W. Huang, L. L. N. Husemoen, J. Y. Hwang, S. Ichihara, et al. (2015) Trans-ancestry

References

- genome-wide association study identifies 12 genetic loci influencing blood pressure and implicates a role for DNA methylation. *Nat Genet*, 47, 1282-1293.
- Kaupp, U. B. & R. Seifert (2002) Cyclic nucleotide-gated ion channels. *Physiol Rev*, 82, 769-824.
- Ke, H. & H. Wang (2007) Crystal structures of phosphodiesterases and implications on substrate specificity and inhibitor selectivity. *Curr Top Med Chem*, 7, 391-403.
- Kenan, Y., T. Murata, Y. Shakur, E. Degerman & V. C. Manganiello (2000) Functions of the N-terminal region of cyclic nucleotide phosphodiesterase 3 (PDE 3) isoforms. *J Biol Chem*, 275, 12331-8.
- Kensler, R. W., R. Craig & R. L. Moss (2017) Phosphorylation of cardiac myosin binding protein C releases myosin heads from the surface of cardiac thick filaments. *Proc Natl Acad Sci U S A*, 114, E1355-E1364.
- Keravis, T. & C. Lugnier (2010) Cyclic nucleotide phosphodiesterases (PDE) and peptide motifs. *Curr Pharm Des*, 16, 1114-25.
- Kim, G. E. & D. A. Kass (2017) Cardiac Phosphodiesterases and Their Modulation for Treating Heart Disease. *Handb Exp Pharmacol*, 243, 249-269.
- Klussmann, E. (2016) Protein-protein interactions of PDE4 family members - Functions, interactions and therapeutic value. *Cell Signal*, 28, 713-8.
- Knight, W. & C. Yan (2013) Therapeutic potential of PDE modulation in treating heart disease. *Future Med Chem*, 5, 1607-20.
- Knight, W. E. & C. Yan (2012) Cardiac cyclic nucleotide phosphodiesterases: function, regulation, and therapeutic prospects. *Horm Metab Res*, 44, 766-75.
- Kopperud, R., A. E. Christensen, E. Kjarland, K. Viste, H. Kleivdal & S. O. Døskeland (2002) Formation of inactive cAMP-saturated holoenzyme of cAMP-dependent protein kinase under physiological conditions. *J Biol Chem*, 277, 13443-8.
- Kovanich, D., M. A. van der Heyden, T. T. Aye, T. A. van Veen, A. J. Heck & A. Scholten (2010) Sphingosine kinase interacting protein is an A-kinase anchoring protein specific for type I cAMP-dependent protein kinase. *Chembiochem*, 11, 963-71.
- Kranias, E. G. & R. J. Hajjar (2012) Modulation of cardiac contractility by the phospholamban/SERCA2a regulatome. *Circ Res*, 110, 1646-60.
- Kraus, I., D. Besong Agbo, M. Otto, J. Wiltfang & H. Klafki (2015) Detection and Differentiation of Threonine- and Tyrosine-Monophosphorylated Forms of ERK1/2 by Capillary Isoelectric Focusing-Immunoassay. *Sci Rep*, 5, 12767.
- Krawutschke, C., D. Koesling & M. Russwurm (2015) Cyclic GMP in Vascular Relaxation: Export Is of Similar Importance as Degradation. *Arterioscler Thromb Vasc Biol*, 35, 2011-9.
- Krenek, P., J. Kmecova, D. Kucerova, Z. Bajuszova, P. Musil, A. Gazova, P. Ochodnicky, J. Klimas & J. Kyselovic (2009) Isoproterenol-induced heart failure in the rat is associated with nitric oxide-dependent functional alterations of cardiac function. *Eur J Heart Fail*, 11, 140-6.
- Kwon, H. B., Y. K. Choi, J. J. Lim, S. H. Kwon, S. Her, H. J. Kim, K. J. Lim, J. C. Ahn, Y. M. Kim, M. K. Bae, J. A. Park, C. H. Jeong, N. Mochizuki & K. W. Kim (2012) AKAP12 regulates vascular integrity in zebrafish. *Exp Mol Med*, 44, 225-35.
- Lamping, K. (2001) Interactions between NO and cAMP in the regulation of vascular tone. *Arterioscler Thromb Vasc Biol*, 21, 729-30.
- Lang, P., F. Gesbert, M. Delespine-Carmagnat, R. Stancou, M. Pouchelet & J. Bertoglio (1996) Protein kinase A phosphorylation of RhoA mediates the morphological and functional effects of cyclic AMP in cytotoxic lymphocytes. *EMBO J*, 15, 510-9.
- Langeberg, L. K. & J. D. Scott (2015) Signalling scaffolds and local organization of cellular behaviour. *Nat Rev Mol Cell Biol*, 16, 232-44.

- Layland, J., R. J. Solaro & A. M. Shah (2005) Regulation of cardiac contractile function by troponin I phosphorylation. *Cardiovasc Res*, 66, 12-21.
- Lefkimmiatis, K. & M. Zaccolo (2014) cAMP signaling in subcellular compartments. *Pharmacol Ther*, 143, 295-304.
- Leloup, A. J., C. E. Van Hove, A. Heykers, D. M. Schrijvers, G. R. De Meyer & P. Franssen (2015) Elastic and Muscular Arteries Differ in Structure, Basal NO Production and Voltage-Gated Ca(2+)-Channels. *Front Physiol*, 6, 375.
- Leung, Y. K., J. Du, Y. Huang & X. Yao (2010) Cyclic nucleotide-gated channels contribute to thromboxane A2-induced contraction of rat small mesenteric arteries. *PLoS One*, 5, e11098.
- Lezoualc'h, F., L. Fazal, M. Laudette & C. Conte (2016) Cyclic AMP Sensor EPAC Proteins and Their Role in Cardiovascular Function and Disease. *Circ Res*, 118, 881-97.
- Lifton, R. P. (2004) Genetic dissection of human blood pressure variation: common pathways from rare phenotypes. *Harvey Lect*, 100, 71-101.
- Lipp, P. & G. Reither (2011) Protein kinase C: the "masters" of calcium and lipid. *Cold Spring Harb Perspect Biol*, 3.
- Liu, D., X. Mei, L. Wang & X. Yang (2017) RhoA inhibits apoptosis and increases proliferation of cultured SPCA1 lung cancer cells. *Mol Med Rep*, 15, 3963-3968.
- Liu, Y., Y. Shakur & J. Kambayashi (2011) Phosphodiesterases as targets for intermittent claudication. *Handb Exp Pharmacol*, 211-36.
- Lohse, M. J., S. Engelhardt & T. Eschenhagen (2003) What is the role of beta-adrenergic signaling in heart failure? *Circ Res*, 93, 896-906.
- Long, F., E. Schipani, H. Asahara, H. Kronenberg & M. Montminy (2001) The CREB family of activators is required for endochondral bone development. *Development*, 128, 541-50.
- Lopez, M. J., S. K. Wong, I. Kishimoto, S. Dubois, V. Mach, J. Friesen, D. L. Garbers & A. Beuve (1995) Salt-resistant hypertension in mice lacking the guanylyl cyclase-A receptor for atrial natriuretic peptide. *Nature*, 378, 65-8.
- Lorenz, R., D. Bertinetti & F. W. Herberg (2017) cAMP-Dependent Protein Kinase and cGMP-Dependent Protein Kinase as Cyclic Nucleotide Effectors. *Handb Exp Pharmacol*, 238, 105-122.
- Luft, F. C., O. Toka, H. R. Toka, J. Jordan & S. Bähring (2003) Mendelian hypertension with brachydactyly as a molecular genetic lesson in regulatory physiology. *Am J Physiol Regul Integr Comp Physiol*, 285, R709-14.
- Lygren, B., C. R. Carlson, K. Santamaria, V. Lissandron, T. McSorley, J. Litzenberg, D. Lorenz, B. Wiesner, W. Rosenthal, M. Zaccolo, K. Taskén & E. Klussmann (2007) AKAP complex regulates Ca²⁺ re-uptake into heart sarcoplasmic reticulum. *EMBO Rep*, 8, 1061-7.
- Maass, P. G., A. Aydin, F. C. Luft, C. Schächterle, A. Weise, S. Stricker, C. Lindschau, M. Vaegler, F. Qadri, H. R. Toka, H. Schulz, P. M. Krawitz, D. Parkhomchuk, J. Hecht, I. Hollfinger, Y. Wefeld-Neuenfeld, E. Bartels-Klein, A. Mühl, M. Kann, H. Schuster, D. Chitayat, M. G. Bialer, T. F. Wienker, J. Ott, K. Rittscher, T. Liehr, J. Jordan, G. Plessis, J. Tank, K. Mai, R. Naraghi, R. Hodge, M. Hopp, L. O. Hattenbach, A. Busjahn, A. Rauch, F. Vandeput, M. Gong, F. Rüschenhoff, N. Hübner, H. Haller, S. Mundlos, N. Bilginturan, M. A. Movsesian, E. Klussmann, O. Toka & S. Bähring (2015) PDE3A mutations cause autosomal dominant hypertension with brachydactyly. *Nat Genet*, 47, 647-53.
- MacAllister, R. J. & P. Vallance (1996) Systemic vascular adaptation to increases in blood volume: the role of the blood-vessel wall. *Nephrol Dial Transplant*, 11, 231-4.

References

- Marx, S. O., J. Kurokawa, S. Reiken, H. Motoike, J. D'Armiento, A. R. Marks & R. S. Kass (2002) Requirement of a macromolecular signaling complex for beta adrenergic receptor modulation of the KCNQ1-KCNE1 potassium channel. *Science*, 295, 496-9.
- Marx, S. O., S. Reiken, Y. Hisamatsu, T. Jayaraman, D. Burkhoff, N. Roseblit & A. R. Marks (2000) PKA phosphorylation dissociates FKBP12.6 from the calcium release channel (ryanodine receptor): defective regulation in failing hearts. *Cell*, 101, 365-76.
- Maurice, D. H., H. Ke, F. Ahmad, Y. Wang, J. Chung & V. C. Manganiello (2014) Advances in targeting cyclic nucleotide phosphodiesterases. *Nat Rev Drug Discov*, 13, 290-314.
- Maurice, D. H., D. Palmer, D. G. Tilley, H. A. Dunkerley, S. J. Netherton, D. R. Raymond, H. S. Elbatarny & S. L. Jimmo (2003) Cyclic nucleotide phosphodiesterase activity, expression, and targeting in cells of the cardiovascular system. *Mol Pharmacol*, 64, 533-46.
- Mebratu, Y. & Y. Tesfaygi (2009) How ERK1/2 activation controls cell proliferation and cell death: Is subcellular localization the answer? *Cell Cycle*, 8, 1168-75.
- Mehta, D. & A. B. Malik (2006) Signaling mechanisms regulating endothelial permeability. *Physiol Rev*, 86, 279-367.
- Miller, C. L., M. Oikawa, Y. Cai, A. P. Wojtovich, D. J. Nagel, X. Xu, H. Xu, V. Florio, S. D. Rybalkin, J. A. Beavo, Y. F. Chen, J. D. Li, B. C. Blaxall, J. Abe & C. Yan (2009) Role of Ca²⁺/calmodulin-stimulated cyclic nucleotide phosphodiesterase 1 in mediating cardiomyocyte hypertrophy. *Circ Res*, 105, 956-64.
- Milliat, F., A. François, M. Isoir, E. Deutsch, R. Tamarat, G. Tarlet, A. Atfi, P. Validire, J. Bourhis, J. C. Sabourin & M. Benderitter (2006) Influence of endothelial cells on vascular smooth muscle cells phenotype after irradiation: implication in radiation-induced vascular damages. *Am J Pathol*, 169, 1484-95.
- Mons, N., L. Decorte, R. Jaffard & D. M. Cooper (1998) Ca²⁺-sensitive adenylyl cyclases, key integrators of cellular signalling. *Life Sci*, 62, 1647-52.
- Movsesian, M. (2015) New pharmacologic interventions to increase cardiac contractility: challenges and opportunities. *Curr Opin Cardiol*, 30, 285-91.
- (2016) Novel approaches to targeting PDE3 in cardiovascular disease. *Pharmacol Ther*, 163, 74-81.
- Movsesian, M., F. Ahmad & E. Hirsch (2018) Functions of PDE3 Isoforms in Cardiac Muscle. *J Cardiovasc Dev Dis*, 5.
- Musheshe, N., M. Schmidt & M. Zaccolo (2017) cAMP: From Long-Range Second Messenger to Nanodomain Signalling. *Trends Pharmacol Sci*.
- Muñoz-Gutiérrez, C., D. Cáceres-Rojas, F. Adasme-Carreño, I. Palomo, E. Fuentes & J. Caballero (2017) Docking and quantitative structure-activity relationship of bicyclic heteroaromatic pyridazinone and pyrazolone derivatives as phosphodiesterase 3A (PDE3A) inhibitors. *PLoS One*, 12, e0189213.
- Naraghi, R., H. Schuster, H. R. Toka, S. Bähring, O. Toka, O. Oztekin, N. Bilginturan, H. Knoblauch, T. F. Wienker, A. Busjahn, H. Haller, R. Fahlbusch & F. C. Luft (1997) Neurovascular compression at the ventrolateral medulla in autosomal dominant hypertension and brachydactyly. *Stroke*, 28, 1749-54.
- Navedo, M. F. & L. F. Santana (2013) CaV1.2 sparklets in heart and vascular smooth muscle. *J Mol Cell Cardiol*, 58, 67-76.
- Neef, S. & L. S. Maier (2013) Novel aspects of excitation-contraction coupling in heart failure. *Basic Res Cardiol*, 108, 360.
- Nikolaev, V. O. & M. Zaccolo. 2017. *Microdomains in the Cardiovascular System*. Springer International Publishing.

- Ohtsubo, H., T. Ichiki, R. Miyazaki, K. Inanaga, I. Imayama, Y. Hashiguchi, J. Sadoshima & K. Sunagawa (2007) Inducible cAMP early repressor inhibits growth of vascular smooth muscle cell. *Arterioscler Thromb Vasc Biol*, 27, 1549-55.
- Oikawa, M., M. Wu, S. Lim, W. E. Knight, C. L. Miller, Y. Cai, Y. Lu, B. C. Blaxall, Y. Takeishi, J. Abe & C. Yan (2013) Cyclic nucleotide phosphodiesterase 3A1 protects the heart against ischemia-reperfusion injury. *J Mol Cell Cardiol*, 64, 11-9.
- Omori, K. & J. Kotera (2007) Overview of PDEs and their regulation. *Circ Res*, 100, 309-27.
- Overgaard, C. B. & V. Dzavík (2008) Inotropes and vasopressors: review of physiology and clinical use in cardiovascular disease. *Circulation*, 118, 1047-56.
- Palmer, D., S. L. Jimmo, D. R. Raymond, L. S. Wilson, R. L. Carter & D. H. Maurice (2007) Protein kinase A phosphorylation of human phosphodiesterase 3B promotes 14-3-3 protein binding and inhibits phosphatase-catalyzed inactivation. *J Biol Chem*, 282, 9411-9.
- Pavlaki, N. & V. O. Nikolaev (2018) Imaging of PDE2- and PDE3-Mediated cGMP-to-cAMP Cross-Talk in Cardiomyocytes. *J Cardiovasc Dev Dis*, 5.
- Peiró, C., J. Redondo, M. A. Rodríguez-Martínez, J. Angulo, J. Marín & C. F. Sánchez-Ferrer (1995) Influence of endothelium on cultured vascular smooth muscle cell proliferation. *Hypertension*, 25, 748-51.
- Penmatsa, H., W. Zhang, S. Yarlagadda, C. Li, V. G. Conoley, J. Yue, S. W. Bahouth, R. K. Buddington, G. Zhang, D. J. Nelson, M. D. Sonecha, V. Manganiello, J. J. Wine & A. P. Naren (2010) Compartmentalized cyclic adenosine 3',5'-monophosphate at the plasma membrane clusters PDE3A and cystic fibrosis transmembrane conductance regulator into microdomains. *Mol Biol Cell*, 21, 1097-110.
- Perera, R. K. & V. O. Nikolaev (2013) Compartmentation of cAMP signalling in cardiomyocytes in health and disease. *Acta Physiol (Oxf)*, 207, 650-62.
- Perera, R. K., J. U. Sprenger, J. H. Steinbrecher, D. Hübscher, S. E. Lehnart, M. Abesser, K. Schuh, A. El-Armouche & V. O. Nikolaev (2015) Microdomain switch of cGMP-regulated phosphodiesterases leads to ANP-induced augmentation of β -adrenoceptor-stimulated contractility in early cardiac hypertrophy. *Circ Res*, 116, 1304-11.
- Perry, S. J., G. S. Baillie, T. A. Kohout, I. McPhee, M. M. Magiera, K. L. Ang, W. E. Miller, A. J. McLean, M. Conti, M. D. Houslay & R. J. Lefkowitz (2002) Targeting of cyclic AMP degradation to beta 2-adrenergic receptors by beta-arrestins. *Science*, 298, 834-6.
- Pidoux, G. & K. Taskén (2010) Specificity and spatial dynamics of protein kinase A signaling organized by A-kinase-anchoring proteins. *J Mol Endocrinol*, 44, 271-84.
- Pierce, K. L., R. T. Premont & R. J. Lefkowitz (2002) Seven-transmembrane receptors. *Nat Rev Mol Cell Biol*, 3, 639-50.
- Pozuelo Rubio, M., D. G. Campbell, N. A. Morrice & C. Mackintosh (2005) Phosphodiesterase 3A binds to 14-3-3 proteins in response to PMA-induced phosphorylation of Ser428. *Biochem J*, 392, 163-72.
- Puxeddu, E., M. Uhart, C. C. Li, F. Ahmad, G. Pacheco-Rodriguez, V. C. Manganiello, J. Moss & M. Vaughan (2009) Interaction of phosphodiesterase 3A with brefeldin A-inhibited guanine nucleotide-exchange proteins BIG1 and BIG2 and effect on ARF1 activity. *Proc Natl Acad Sci U S A*, 106, 6158-63.
- Rababa'h, A., S. Singh, S. V. Suryavanshi, S. E. Altarabsheh, S. V. Deo & B. K. McConnell (2014) Compartmentalization role of A-kinase anchoring proteins (AKAPs) in mediating protein kinase A (PKA) signaling and cardiomyocyte hypertrophy. *Int J Mol Sci*, 16, 218-29.

References

- Radeva, M. Y., D. Kugelmann, V. Spindler & J. Waschke (2014) PKA compartmentalization via AKAP220 and AKAP12 contributes to endothelial barrier regulation. *PLoS One*, 9, e106733.
- Redheuil, A., C. O. Wu, N. Kachenoura, Y. Ohyama, R. T. Yan, A. G. Bertoni, G. W. Hundley, D. A. Duprez, D. R. Jacobs, L. B. Daniels, C. Darwin, C. Sibley, D. A. Bluemke & J. A. C. Lima (2014) Proximal aortic distensibility is an independent predictor of all-cause mortality and incident CV events: the MESA study. *J Am Coll Cardiol*, 64, 2619-2629.
- Renkema, K. Y., J. M. Westermann, R. A. J. Nievelstein, S. M. Lo-A-Njoe, B. van der Zwaag, M. E. Manshande & M. M. van Haelst (2018) PDE3A gene screening improves diagnostics for patients with Bilginturan syndrome (hypertension and brachydactyly syndrome). *Hypertens Res*, 41, 981-988.
- Richter, W. & M. Conti (2002) Dimerization of the type 4 cAMP-specific phosphodiesterases is mediated by the upstream conserved regions (UCRs). *J Biol Chem*, 277, 40212-21.
- Roberts, O. L. & C. Dart (2014) cAMP signalling in the vasculature: the role of Epac (exchange protein directly activated by cAMP). *Biochem Soc Trans*, 42, 89-97.
- Rogers, K. C., C. S. Oliphant & S. W. Finks (2015) Clinical efficacy and safety of cilostazol: a critical review of the literature. *Drugs*, 75, 377-95.
- Rosman, G. J., T. J. Martins, W. K. Sonnenburg, J. A. Beavo, K. Ferguson & K. Loughney (1997) Isolation and characterization of human cDNAs encoding a cGMP-stimulated 3',5'-cyclic nucleotide phosphodiesterase. *Gene*, 191, 89-95.
- Ross, B. L., B. Tenner, M. L. Markwardt, A. Zviman, G. Shi, J. P. Kerr, N. E. Snell, J. J. McFarland, J. R. Mauban, C. W. Ward, M. A. Rizzo & J. Zhang (2018) Single-color, ratiometric biosensors for detecting signaling activities in live cells. *Elife*, 7.
- Russwurm, C., G. Zoidl, D. Koesling & M. Russwurm (2009) Dual acylation of PDE2A splice variant 3: targeting to synaptic membranes. *J Biol Chem*, 284, 25782-90.
- Sadeghian, H., S. M. Seyedi, M. R. Saberi, R. S. Nick, A. Hosseini, M. Bakavoli, S. M. Mansouri & H. Parsaee (2009) Design, synthesis and pharmacological evaluation of 6-hydroxy-4-methylquinolin-2(1H)-one derivatives as inotropic agents. *J Enzyme Inhib Med Chem*, 24, 918-29.
- Sande, J. B., I. Sjaastad, I. B. Hoen, J. Bøkenes, T. Tønnessen, E. Holt, P. K. Lunde & G. Christensen (2002) Reduced level of serine(16) phosphorylated phospholamban in the failing rat myocardium: a major contributor to reduced SERCA2 activity. *Cardiovasc Res*, 53, 382-91.
- Savarese, G. & L. H. Lund (2017) Global Public Health Burden of Heart Failure. *Card Fail Rev*, 3, 7-11.
- Sawada, N., H. Itoh, K. Miyashita, H. Tsujimoto, M. Sone, K. Yamahara, Z. P. Arany, F. Hofmann & K. Nakao (2009) Cyclic GMP kinase and RhoA Ser188 phosphorylation integrate pro- and antifibrotic signals in blood vessels. *Mol Cell Biol*, 29, 6018-32.
- Scapin, G., S. B. Patel, C. Chung, J. P. Varnerin, S. D. Edmondson, A. Mastracchio, E. R. Parmee, S. B. Singh, J. W. Becker, L. H. Van der Ploeg & M. R. Tota (2004) Crystal structure of human phosphodiesterase 3B: atomic basis for substrate and inhibitor specificity. *Biochemistry*, 43, 6091-100.
- Schevzov, G., A. J. Kee, B. Wang, V. B. Sequeira, J. Hook, J. D. Coombes, C. A. Lucas, J. R. Stehn, E. A. Musgrove, A. Cretu, R. Assoian, T. Fath, T. Hanoch, R. Seger, I. Pleines, B. T. Kile, E. C. Hardeman & P. W. Gunning (2015) Regulation of cell proliferation by ERK and signal-dependent nuclear translocation of ERK is dependent on Tm5NM1-containing actin filaments. *Mol Biol Cell*, 26, 2475-90.

- Schirone, L., M. Forte, S. Palmerio, D. Yee, C. Nocella, F. Angelini, F. Pagano, S. Schiavon, A. Bordin, A. Carrizzo, C. Vecchione, V. Valenti, I. Chimenti, E. De Falco, S. Sciarretta & G. Frati (2017) A Review of the Molecular Mechanisms Underlying the Development and Progression of Cardiac Remodeling. *Oxid Med Cell Longev*, 2017, 3920195.
- Schmieder, R. E. (2010) End organ damage in hypertension. *Dtsch Arztebl Int*, 107, 866-73.
- Scholten, A., M. K. Poh, T. A. van Veen, B. van Breukelen, M. A. Vos & A. J. Heck (2006) Analysis of the cGMP/cAMP interactome using a chemical proteomics approach in mammalian heart tissue validates sphingosine kinase type 1-interacting protein as a genuine and highly abundant AKAP. *J Proteome Res*, 5, 1435-47.
- Schuster, H., O. Toka, H. R. Toka, A. Busjahn, O. Oztekin, T. F. Wienker, N. Bilginturan, S. Bähring, F. Skrabal, H. Haller & F. C. Luft (1998) A cross-over medication trial for patients with autosomal-dominant hypertension with brachydactyly. *Kidney Int*, 53, 167-72.
- Schuster, H., T. E. Wienker, S. Bähring, N. Bilginturan, H. R. Toka, H. Neitzel, E. Jeschke, O. Toka, D. Gilbert, A. Lowe, J. Ott, H. Haller & F. C. Luft (1996) Severe autosomal dominant hypertension and brachydactyly in a unique Turkish kindred maps to human chromosome 12. *Nat Genet*, 13, 98-100.
- Scott, J. D., C. W. Dessauer & K. Taskén (2013) Creating order from chaos: cellular regulation by kinase anchoring. *Annu Rev Pharmacol Toxicol*, 53, 187-210.
- Senzaki, H., C. J. Smith, G. J. Juang, T. Isoda, S. P. Mayer, A. Ohler, N. Paolocci, G. F. Tomaselli, J. M. Hare & D. A. Kass (2001) Cardiac phosphodiesterase 5 (cGMP-specific) modulates beta-adrenergic signaling in vivo and is down-regulated in heart failure. *FASEB J*, 15, 1718-26.
- Shah, A. M. & P. A. MacCarthy (2000) Paracrine and autocrine effects of nitric oxide on myocardial function. *Pharmacol Ther*, 86, 49-86.
- Shakur, Y., K. Takeda, Y. Kenan, Z. X. Yu, G. Rena, D. Brandt, M. D. Houslay, E. Degerman, V. J. Ferrans & V. C. Manganiello (2000) Membrane localization of cyclic nucleotide phosphodiesterase 3 (PDE3). Two N-terminal domains are required for the efficient targeting to, and association of, PDE3 with endoplasmic reticulum. *J Biol Chem*, 275, 38749-61.
- Shan, J., A. Kushnir, M. J. Betzenhauser, S. Reiken, J. Li, S. E. Lehnart, N. Lindegger, M. Mongillo, P. J. Mohler & A. R. Marks (2010) Phosphorylation of the ryanodine receptor mediates the cardiac fight or flight response in mice. *J Clin Invest*, 120, 4388-98.
- Shen, B., K. T. Cheng, Y. K. Leung, Y. C. Kwok, H. Y. Kwan, C. O. Wong, Z. Y. Chen, Y. Huang & X. Yao (2008) Epinephrine-induced Ca²⁺ influx in vascular endothelial cells is mediated by CNGA2 channels. *J Mol Cell Cardiol*, 45, 437-45.
- Simino, J., Y. J. Sung, R. Kume, K. Schwander & D. C. Rao (2013) Gene-alcohol interactions identify several novel blood pressure loci including a promising locus near SLC16A9. *Front Genet*, 4, 277.
- Simmerman, H. K. & L. R. Jones (1998) Phospholamban: protein structure, mechanism of action, and role in cardiac function. *Physiol Rev*, 78, 921-47.
- Sin, Y. Y., H. V. Edwards, X. Li, J. P. Day, F. Christian, A. J. Dunlop, D. R. Adams, M. Zaccolo, M. D. Houslay & G. S. Baillie (2011) Disruption of the cyclic AMP phosphodiesterase-4 (PDE4)-HSP20 complex attenuates the β -agonist induced hypertrophic response in cardiac myocytes. *J Mol Cell Cardiol*, 50, 872-83.
- Skroblin, P., S. Grossmann, G. Schäfer, W. Rosenthal & E. Klussmann (2010) Mechanisms of protein kinase A anchoring. *Int Rev Cell Mol Biol*, 283, 235-330.

References

- Smith, F. D., J. L. Esseltine, P. J. Nygren, D. Veessler, D. P. Byrne, M. Vonderach, I. Strashnov, C. E. Eyers, P. A. Eyers, L. K. Langeberg & J. D. Scott (2017) Local protein kinase A action proceeds through intact holoenzymes. *Science*, 356, 1288-1293.
- Sprenger, J. U. & V. O. Nikolaev (2013) Biophysical techniques for detection of cAMP and cGMP in living cells. *Int J Mol Sci*, 14, 8025-46.
- Sprenger, J. U., R. K. Perera, J. H. Steinbrecher, S. E. Lehnart, L. S. Maier, G. Hasenfuss & V. O. Nikolaev (2015) In vivo model with targeted cAMP biosensor reveals changes in receptor-microdomain communication in cardiac disease. *Nat Commun*, 6, 6965.
- Stadler, C., E. Rexhepaj, V. R. Singan, R. F. Murphy, R. Pepperkok, M. Uhlén, J. C. Simpson & E. Lundberg (2013) Immunofluorescence and fluorescent-protein tagging show high correlation for protein localization in mammalian cells. *Nat Methods*, 10, 315-23.
- Stangherlin, A. & M. Zaccolo (2012) Phosphodiesterases and subcellular compartmentalized cAMP signaling in the cardiovascular system. *Am J Physiol Heart Circ Physiol*, 302, H379-90.
- Struthers, R. S., W. W. Vale, C. Arias, P. E. Sawchenko & M. R. Montminy (1991) Somatotroph hypoplasia and dwarfism in transgenic mice expressing a non-phosphorylatable CREB mutant. *Nature*, 350, 622-4.
- Sun, B., H. Li, Y. Shakur, J. Hensley, S. Hockman, J. Kambayashi, V. C. Manganiello & Y. Liu (2007) Role of phosphodiesterase type 3A and 3B in regulating platelet and cardiac function using subtype-selective knockout mice. *Cell Signal*, 19, 1765-71.
- Surapisitchat, J., K. I. Jeon, C. Yan & J. A. Beavo (2007) Differential regulation of endothelial cell permeability by cGMP via phosphodiesterases 2 and 3. *Circ Res*, 101, 811-8.
- Szabó, J., L. Csáky & J. Szegi (1975) Experimental cardiac hypertrophy induced by isoproterenol in the rat. *Acta Physiol Acad Sci Hung*, 46, 281-5.
- Szaszák, M., F. Christian, W. Rosenthal & E. Klussmann (2008) Compartmentalized cAMP signalling in regulated exocytic processes in non-neuronal cells. *Cell Signal*, 20, 590-601.
- Takigawa, T., Y. Matsumaru, M. Hayakawa, S. Nemoto & A. Matsumura (2010) Cilostazol reduces restenosis after carotid artery stenting. *J Vasc Surg*, 51, 51-6.
- Tariq, S. & W. S. Aronow (2015) Use of Inotropic Agents in Treatment of Systolic Heart Failure. *Int J Mol Sci*, 16, 29060-8.
- Taskén, K. & E. M. Aandahl (2004) Localized effects of cAMP mediated by distinct routes of protein kinase A. *Physiol Rev*, 84, 137-67.
- Taskén, K. A., P. Collas, W. A. Kemmner, O. Witczak, M. Conti & K. Taskén (2001) Phosphodiesterase 4D and protein kinase a type II constitute a signaling unit in the centrosomal area. *J Biol Chem*, 276, 21999-2002.
- Taylor, S. S., R. Ilouz, P. Zhang & A. P. Kornev (2012) Assembly of allosteric macromolecular switches: lessons from PKA. *Nat Rev Mol Cell Biol*, 13, 646-58.
- Thestrup, T., J. Litzlbauer, I. Bartholomäus, M. Mues, L. Russo, H. Dana, Y. Kovalchuk, Y. Liang, G. Kalamakis, Y. Laukat, S. Becker, G. Witte, A. Geiger, T. Allen, L. C. Rome, T. W. Chen, D. S. Kim, O. Garaschuk, C. Griesinger & O. Griesbeck (2014) Optimized ratiometric calcium sensors for functional in vivo imaging of neurons and T lymphocytes. *Nat Methods*, 11, 175-82.
- Toka, H. R., J. M. Koshy & A. Hariri (2013) The molecular basis of blood pressure variation. *Pediatr Nephrol*, 28, 387-99.
- Toka, O., J. Tank, C. Schächterle, A. Aydin, P. G. Maass, S. Elitok, E. Bartels-Klein, I. Hollfinger, C. Lindschau, K. Mai, M. Boschmann, G. Rahn, M. A. Movsesian, T.

- Müller, A. Doescher, S. Gnoth, A. Mühl, H. R. Toka, Y. Wefeld-Neuenfeld, W. Utz, A. Töpfer, J. Jordan, J. Schulz-Menger, E. Klussmann, S. Bähring & F. C. Luft (2015) Clinical effects of phosphodiesterase 3A mutations in inherited hypertension with brachydactyly. *Hypertension*, 66, 800-8.
- Towbin, J. A. & N. E. Bowles (2002) The failing heart. *Nature*, 415, 227-33.
- Trotter, K. W., I. D. Fraser, G. K. Scott, M. J. Stutts, J. D. Scott & S. L. Milgram (1999) Alternative splicing regulates the subcellular localization of A-kinase anchoring protein 18 isoforms. *J Cell Biol*, 147, 1481-92.
- Tykocki, N. R., E. M. Boerman & W. F. Jackson (2017) Smooth Muscle Ion Channels and Regulation of Vascular Tone in Resistance Arteries and Arterioles. *Compr Physiol*, 7, 485-581.
- van den Born, B. J., L. C. Oskam, M. Zidane, C. Schächterle, E. Klussmann, S. Bähring & F. C. Luft (2016) The Case| A handful of hypertension. *Kidney Int*, 90, 911-3.
- Walker-Gray, R., F. Stengel & M. G. Gold (2017) Mechanisms for restraining cAMP-dependent protein kinase revealed by subunit quantitation and cross-linking approaches. *Proc Natl Acad Sci U S A*, 114, 10414-10419.
- Wang, P., P. Wu, R. W. Egan & M. M. Billah (2003) Identification and characterization of a new human type 9 cGMP-specific phosphodiesterase splice variant (PDE9A5). Differential tissue distribution and subcellular localization of PDE9A variants. *Gene*, 314, 15-27.
- Warren, H. R., E. Evangelou, C. P. Cabrera, H. Gao, M. Ren, B. Mifsud, I. Ntalla, P. Surendran, C. Liu, J. P. Cook, A. T. Kraja, F. Drenos, M. Loh, N. Verweij, J. Marten, I. Karaman, M. P. Segura Lepe, P. F. O'Reilly, J. Knight, H. Snieder, N. Kato, J. He, E. S. Tai, M. A. Said, D. Porteous, M. Alver, N. Poulter, M. Farrall, R. T. Gansevoort, S. Padmanabhan, R. Mägi, A. Stanton, J. Connell, S. J. L. Bakker, A. Metspalu, D. C. Shields, S. Thom, M. Brown, P. Sever, T. Esko, C. Hayward, P. van der Harst, D. Saleheen, R. Chowdhury, J. C. Chambers, D. I. Chasman, A. Chakravarti, C. Newton-Cheh, C. M. Lindgren, D. Levy, J. S. Kooner, B. Keavney, M. Tomaszewski, N. J. Samani, J. M. M. Howson, M. D. Tobin, P. B. Munroe, G. B. Ehret, L. V. Wain, M. R. Barnes, I. Tzoulaki, M. J. Caulfield, P. Elliott, T. C. E. C. International Consortium of Blood Pressure (ICBP) 1000G Analyses, The ExomeBP Consortium, The T2D-GENES Consortium, The GoT2DGenes Consortium, The Cohorts for Heart and Ageing Research in Genome Epidemiology (CHARGE) BP Exome Consortium, The International Genomics of Blood Pressure (iGEN-BP) Consortium & U. B. C. C. B. w. group (2017) Corrigendum: Genome-wide association analysis identifies novel blood pressure loci and offers biological insights into cardiovascular risk. *Nat Genet*, 49, 1558.
- Wechsler, J., Y. H. Choi, J. Krall, F. Ahmad, V. C. Manganiello & M. A. Movsesian (2002) Isoforms of cyclic nucleotide phosphodiesterase PDE3A in cardiac myocytes. *J Biol Chem*, 277, 38072-8.
- Welch, E. J., B. W. Jones & J. D. Scott (2010) Networking with AKAPs: context-dependent regulation of anchored enzymes. *Mol Interv*, 10, 86-97.
- Wheeler-Jones, C. P. (2005) Cell signalling in the cardiovascular system: an overview. *Heart*, 91, 1366-74.
- Willoughby, D., W. Wong, J. Schaack, J. D. Scott & D. M. Cooper (2006) An anchored PKA and PDE4 complex regulates subplasmalemmal cAMP dynamics. *EMBO J*, 25, 2051-61.
- Willoughby, S., A. Holmes & J. Loscalzo (2002) Platelets and cardiovascular disease. *Eur J Cardiovasc Nurs*, 1, 273-88.

References

- Wittmann, T., M. J. Lohse & J. P. Schmitt (2015) Phospholamban pentamers attenuate PKA-dependent phosphorylation of monomers. *J Mol Cell Cardiol*, 80, 90-7.
- Wright, P. T., S. Schobesberger & J. Gorelik (2015) Studying GPCR/cAMP pharmacology from the perspective of cellular structure. *Front Pharmacol*, 6, 148.
- Xie, M., B. Blackman, C. Scheitrum, D. Mika, E. Blanchard, T. Lei, M. Conti & W. Richter (2014) The upstream conserved regions (UCRs) mediate homo- and hetero-oligomerization of type 4 cyclic nucleotide phosphodiesterases (PDE4s). *Biochem J*, 459, 539-50.
- Yan, C., C. L. Miller & J. Abe (2007) Regulation of phosphodiesterase 3 and inducible cAMP early repressor in the heart. *Circ Res*, 100, 489-501.
- Yang, S., W. H. Fletcher & D. A. Johnson (1995) Regulation of cAMP-dependent protein kinase: enzyme activation without dissociation. *Biochemistry*, 34, 6267-71.
- Zaccolo, M. (2009) cAMP signal transduction in the heart: understanding spatial control for the development of novel therapeutic strategies. *Br J Pharmacol*, 158, 50-60.
- Zaccolo, M. & M. A. Movsesian (2007) cAMP and cGMP signaling cross-talk: role of phosphodiesterases and implications for cardiac pathophysiology. *Circ Res*, 100, 1569-78.
- Zhang, F., L. Zhang, Y. Qi & H. Xu (2016) Mitochondrial cAMP signaling. *Cell Mol Life Sci*, 73, 4577-4590.
- Zhang, H., X. H. Liu, K. Zhang, C. K. Chen, J. M. Frederick, G. D. Prestwich & W. Baehr (2004) Photoreceptor cGMP phosphodiesterase delta subunit (PDEdelta) functions as a prenyl-binding protein. *J Biol Chem*, 279, 407-13.
- Zhang, W., H. Ke & R. W. Colman (2002) Identification of interaction sites of cyclic nucleotide phosphodiesterase type 3A with milrinone and cilostazol using molecular modeling and site-directed mutagenesis. *Mol Pharmacol*, 62, 514-20.
- Zhao, H., Q. Guan, C. J. Smith & J. Quilley (2008) Increased phosphodiesterase 3A/4B expression after angioplasty and the effect on VASP phosphorylation. *Eur J Pharmacol*, 590, 29-35.
- Zima, A. V., E. Bovo, S. R. Mazurek, J. A. Rochira, W. Li & D. Terentyev (2014) Ca handling during excitation-contraction coupling in heart failure. *Pflugers Arch*, 466, 1129-37.
- Zoccarato, A., N. C. Surdo, J. M. Aronsen, L. A. Fields, L. Mancuso, G. Dodoni, A. Stangherlin, C. Livie, H. Jiang, Y. Y. Sin, F. Gesellchen, A. Terrin, G. S. Baillie, S. A. Nicklin, D. Graham, N. Szabo-Fresnais, J. Krall, F. Vandeput, M. Movsesian, L. Furlan, V. Corsetti, G. Hamilton, K. Lefkimmiatis, I. Sjaastad & M. Zaccolo (2015) Cardiac Hypertrophy Is Inhibited by a Local Pool of cAMP Regulated by Phosphodiesterase 2. *Circ Res*, 117, 707-19.

9. Publications

9.1. Articles

- Ercu, M., L. Markó, C. Schächterle, D. Tsvetkov, Y. Cui, S. Maghsodi, T. U. P. Bartolomaeus, P. G. Maass, K. Zühlke, N. Gregersen, N. Hübner, R. Hodge, A. Mühl, B. Pohl, R. Molé-Illas, A. Geelhaar, S. Walter, H. Napieczynska, S. Schelenz, M. Taube, A. Heuser, Y. M. Anistan, F. Qadri, M. Todiras, R. Plehm, E. Popova, R. Langanki, J. Eichhorst, M. Lehmann, B. Wiesner, M. Russwurm, S. K. Forslund, I. Kamer, D. N. Müller, M. Gollasch, A. Aydin, S. Bähring, M. Bader, F. C. Luft & E. Klussmann (2020) Phosphodiesterase 3A and Arterial Hypertension. *Circulation*.
- Ercu, M. & E. Klussmann (2018) Roles of A-Kinase Anchoring Proteins and Phosphodiesterases in the Cardiovascular System. *J Cardiovasc Dev Dis*, 5.

9.2. Oral presentations

- PDE3A and hypertension. *Extended local cAMP signaling international group meeting*. Online meeting, June 08, 2020.
- PDE3A-caused hypertension with brachydactyly (HTNB) and new targets for the treatment of cardiovascular diseases. *16th Retreat "Schmilka"*. Seiffen/Erzgebirge, Germany, August 25-28, 2019.
- PDE3A-caused hypertension with brachydactyly (HTNB) and new targets for the treatment of cardiovascular diseases. *DZHK Partner Site Retreat*. Berlin, Germany, October, 19, 2018.
- PDE3A-caused hypertension with brachydactyly (HTNB) and new targets for the treatment of cardiovascular diseases. *Wollenberger Seminar*. Berlin, Germany, October, 08, 2018.
- PDE3A-caused hypertension with brachydactyly (HTNB) and new targets for the treatment of cardiovascular diseases. *MDC-FMP PhD Retreat*. Templin, Germany, September, 27-29, 2018.
- Elucidating PDE3A-caused hypertension and uncovering new treatment targets. *15th Retreat "Schmilka"*. Grüty/Havelland, Germany, August 26-29, 2018.

Publications

- Elucidating PDE3A-caused hypertension and uncovering new treatment targets. *AG Klussmann Group Retreat*. Dambeck, Germany, September 05-07, 2017.
- Elucidating PDE3A-caused hypertension and uncovering new treatment targets. *TransCard Graduate School PhD Retreat*. Valencia, Spain, June 29-July 02, 2017.

9.3. Poster presentations

- Ercu M., Walker-Gray R., Bader M., Heuser A., Marko L., Müller D., Aydin A., Zühlke K., Geelhaar A., Eichhorst J., Wiesner B., Lehmann M., Bähring S., Luft F.C. and Klussmann E. PDE3A-caused hypertension with brachydactyly (HTNB) and new targets for the treatment of cardiovascular diseases. *CRC 1365 Renoprotection, 1st International Retreat*. Berlin, Germany, November 14-15, 2019.
- Ercu M., Walker-Gray R., Bader M., Heuser A., Marko L., Müller D., Aydin A., Zühlke K., Geelhaar A., Eichhorst J., Wiesner B., Lehmann M., Bähring S., Luft F.C. and Klussmann E. PDE3A-caused hypertension with brachydactyly (HTNB) and new targets for the treatment of cardiovascular diseases. *Nanodomains in cyclic nucleotide signaling: from mechanisms to therapeutic approaches Conference*. London, UK, September 16-18, 2019.
- Ercu M., Schächterle C., Bähring S., Wiesner B., Eichhorst J., Friedrich C.L., Bader M. and Klussmann E. PDE3A-caused hypertension with brachydactyly (HTNB) and new targets for the treatment of cardiovascular diseases. *Workshop "Cardiovascular Research @ Bayer"*. Boston, USA, June 28-30, 2019.
- Ercu M., Schächterle C., Bader M., Aydin A., Heuser A., Eichhorst J., Wiesner B., Bähring S., Friedrich C.L. and Klussmann E. Elucidating PDE3A-caused HTNB and uncovering new treatment targets. *9th Ascona International Workshop on Cardiomyocyte Biology, CSF Conference*. Monte Verità, Ascona, Switzerland, April 22-26, 2018.
- Ercu M., Schächterle C., Friedrich C.L., Bähring S., Aydin A., Bader M., Heuser A., Wiesner B., Eichhorst J. and Klussmann E. Elucidating local PDE3A-directed cAMP signaling. *Berlin Interdisciplinary Symposium for Young GPCR Researchers*. Freie Universität Berlin, Berlin, Germany, April, 12, 2018.

10. Acknowledgements

First and foremost, I would like to thank PD Dr. Enno Klussmann for giving me the opportunity to be a member of his lab. I am really grateful for all the help, the time and support he has given me during these 3.5 years. I highly appreciate that he always took the time and had a lot of patience to discuss all the details of my project, that he made it possible for me to attend amazing conferences and workshops throughout the world and to publish my work in renowned journals. Also, I highly appreciate the time he took in helping me with and correcting this PhD thesis.

I am extremely grateful to Dr. Sylvia Bähring for her guidance and help as well as for taking the time to correct this thesis and to Prof. Dr. Friedrich Luft, without whom this project would have not existed.

I am also thankful to Prof. Dr. Helge Ewers for agreeing to be my second supervisor and for participating in my committee meetings and bringing valuable input to the project.

I would also like to thank Dr. Daniela Panakova for taking part in my committee meetings and for her valuable input to my project.

I am so very grateful to the previous and present members of AG Klussmann. I had a great time during these last 3.5 years and this is mainly due to the amazing people that have been and are part of this lab, which have created such a pleasant working environment and atmosphere. I am especially grateful to Dr. Carolin Schächterle and Dr. Maike Schultz, who helped and supported me in the beginning of my PhD, to Dr. Mohamed Elkewedi for always having something nice to say when things were not going so well, to Dr. Ryan Walker-Gray, for his constant help, the nice collaboration and for taking the time to correct this thesis and to Sandrine Baltzer, for her help and support, as well as for taking the time to translate the abstract of this thesis in german.

A special thank you to Dr. Burkhard Wiesner, Dr Martin Lehmann and Jenny Eichhorst for all the help and support with the FRET experiments and confocal microscopy.

I am extremely thankful to Andrea Geelhaar, Bärbel Pohl and Astrid Mühl for the huge support and excellent technical assistance.

Acknowledgements

I would like to thank my collaborators for working with such high dedication to this project. Therefore, a special thank you to members from AG Bader, AG Müller, AG Gollasch, AG Forslund, AG Hübner and AG Heuser

Many thanks also go to all my friends throughout the years, starting with the amazing friends that I know since almost forever, from my hometown, to the awesome people and life-long friends that I met during my university studies and to the newer ones, with whom I also share so many valuable moments, that I got the chance to know during my time in Berlin. Thank you so much to all of you for being there for me when I needed you and for the amazing time we had together!

Lastly, but not least, I would like to thank my family, especially to my parents, for their continuous love, help and support. You were there for me in my most difficult moments as well as in the happiest ones, you made sure that I don't forget who I am or what I am capable of and you constantly encouraged me to become a better version of myself. All I am today is because of you and I would have never made it that far without you. Thank you for everything!

11. Appendix

11.1. Supplemental Results

Supplemental Table S1: Statistical analysis for the SBP, DBP and heart rate measured for WT, $\Delta 3aa$ HET, $\Delta 3aa$ HOM and functional DEL rat models. Shown are the p values corresponding to the data presented in Figure 10B.

P (genotype rats, systolic) = 3.371249e-08

P (genotype rats, diastolic) = 1.127179e-17

P (genotype rats, heart rate) = 0.00034653

Systolic WT vs. functional DEL = 0.000781638481121916

Systolic WT vs. $\Delta 3aa$ HET = 1.87298941789806e-05

Systolic WT vs. $\Delta 3aa$ HOM = 0.00390622244654646

Systolic functional DEL vs. $\Delta 3aa$ HET = 6.46910576721325e-08

Systolic functional DEL vs. $\Delta 3aa$ HOM = 5.63714446462809e-06

Systolic $\Delta 3aa$ HET vs. $\Delta 3aa$ HOM = 0.664605889221758

Diastolic WT vs. functional DEL = 0.0471172223084532

Diastolic WT vs. $\Delta 3aa$ HET = 1.82252752067942e-06

Diastolic WT vs. $\Delta 3aa$ HOM = 8.257144939323e-07

Diastolic functional DEL vs. $\Delta 3aa$ HET = 1.80855674803871e-06

Diastolic functional DEL vs. $\Delta 3aa$ HOM = 3.21764541459098e-12

Diastolic $\Delta 3aa$ HET vs. $\Delta 3aa$ HOM = 0.00186857643850765

HR WT vs. functional DEL = 1.24113096775992e-05

HR WT vs. $\Delta 3aa$ HET = 0.375719381357057

HR WT vs. $\Delta 3aa$ HOM = 0.905779123838626

HR functional DEL vs. $\Delta 3aa$ HET = 2.20296081439421e-06

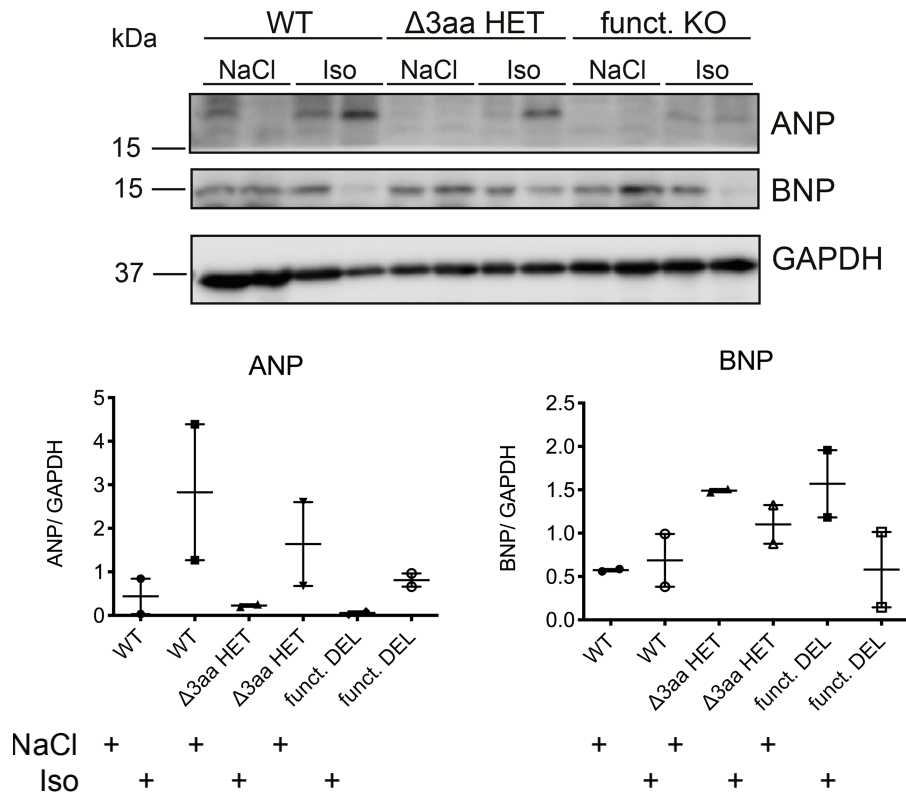
HR functional DEL vs. $\Delta 3aa$ HOM = 0.0183140364364043

HR $\Delta 3aa$ HET vs. $\Delta 3aa$ HOM = 0.793912351589182

Western blotting was performed and the expression levels of proteins essential for cardiac stress response, proliferation and excitation-contraction coupling was investigated. The expression levels of atrial natriuretic peptide (ANP) and B-type natriuretic peptide (BNP), two endogenously generated peptides whose expression is elevated in chronic heart failure (Falcão et al. 2004) were assessed in the hearts' left ventricles of WT, $\Delta 3aa$ HET and functional DEL animals. Increased expression of ANP was observed in the isoproterenol-treated rats compared to the NaCl-treated controls. The increase in ANP expression appeared to be smaller in the $\Delta 3aa$ HET

Appendix

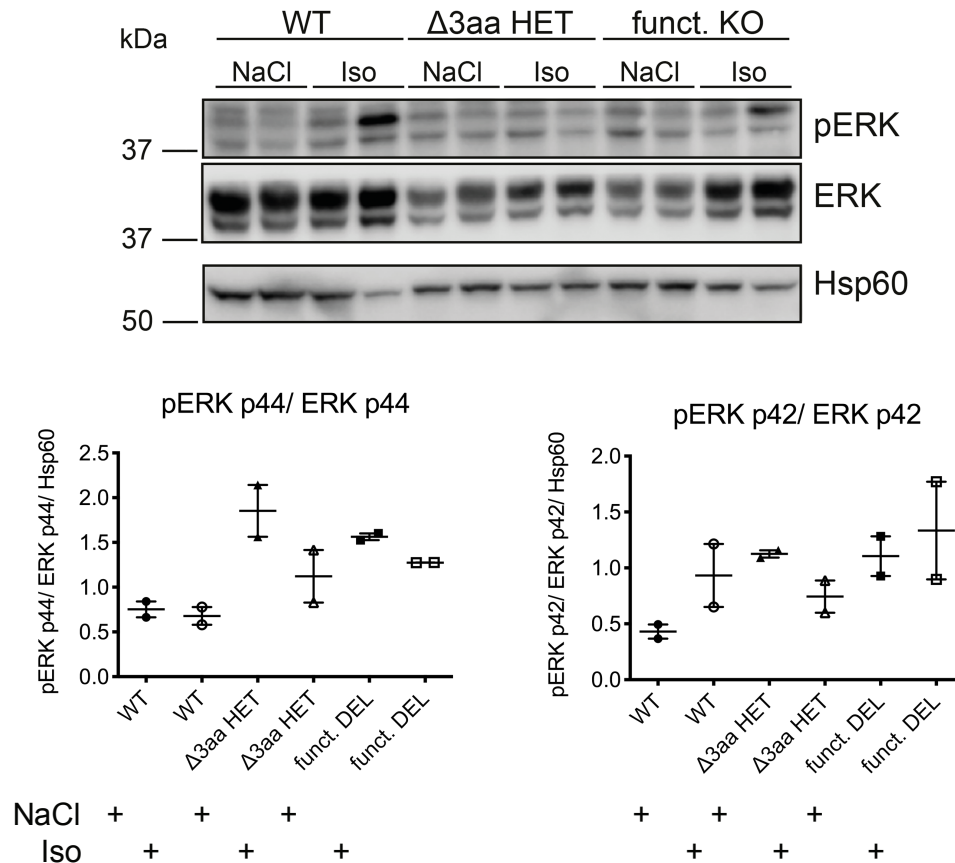
animals compared to the WT controls and even smaller in the functional DEL rats after 14 days of isoproterenol treatment. BNP abundance seemed to decrease in $\Delta 3aa$ HET and functional DEL rats upon isoproterenol treatment compared to the respective controls, whereas no decrease was observed in the WT animals (Supplemental Figure S1).



Supplemental Figure S1: Expression of hypertrophy markers, ANP and BNP, in the heart of WT and mutant animals. Upper panel: ANP and BNP were detected by Western blotting in the left ventricles of WT, $\Delta 3aa$ HET and functional DEL rats after 14 days of either NaCl or isoproterenol treatment. GAPDH was detected as loading control. Lower panel: Semi-quantitative analysis of ANP and BNP by densitometric analysis. Plotted are the expression levels of the proteins normalized to the loading control; $n = 2$ independent experiments. Mean \pm SEM is plotted.

To test whether there are differences in cell proliferation between WT and mutant animals, the expression of phosphorylated ERK1/2 (44 kDa and 42 kDa, respectively) was examined. The abundance of both ERK proteins appeared to decrease upon isoproterenol treatment in the left ventricles of $\Delta 3aa$ HET animals compared to the NaCl-treated ones. ERK2 expression seemed to increase in left

ventricles from WT animals upon cardiac stress induction compared to the control condition, whereas ERK1 appeared to remain unchanged. For the functional DEL animals, the experiments suggest that ERK1 expression was slightly decreased upon isoproterenol treatment, while ERK2 levels remained unchanged (Supplemental Figure S2).

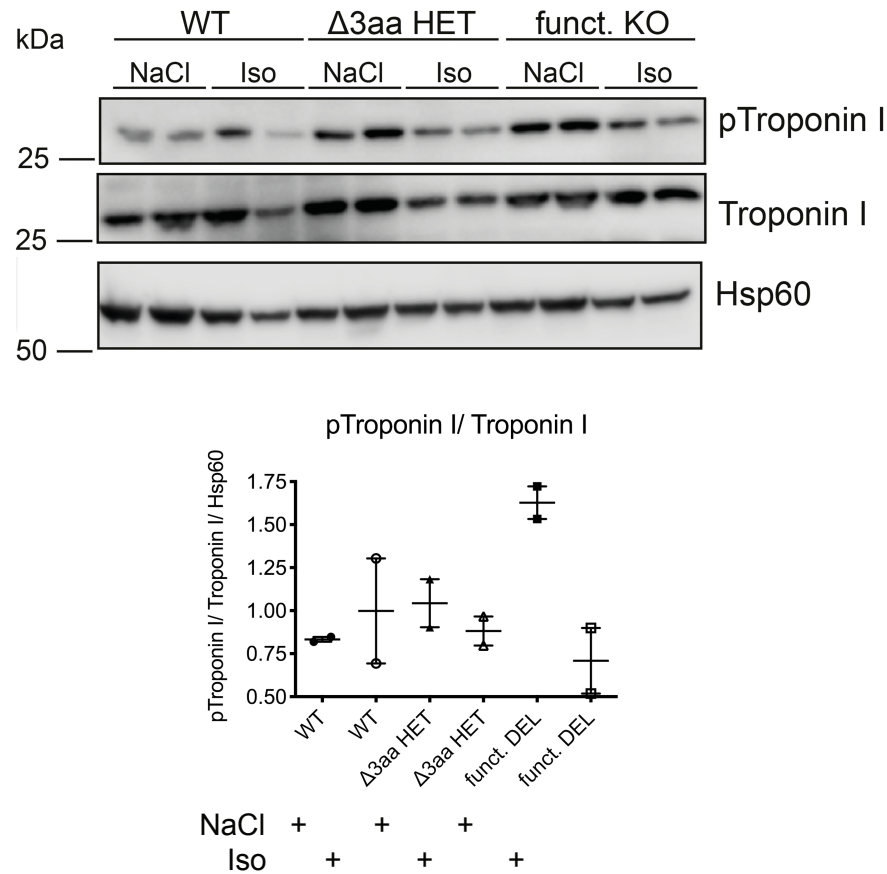


Supplemental Figure S2: Expression of cell proliferation markers in the heart of WT and mutant animals. Upper panel: The PKA-phosphorylated and non-phosphorylated forms of ERK were detected by Western blotting in the heart of WT, Δ3aa HET and functional DEL rats. Hsp60 was detected as loading control. Lower panel: Semi-quantitative analysis of the 42 kDa and 44 kDa-sized ERK and phosphorylated ERK (pERK) by densitometric analysis. Plotted are the expression levels of the phosphorylated proteins normalized to the expression levels of the non-phosphorylated proteins and then to the loading control; n = 2 independent experiments. Mean ± SEM is plotted.

To assess the effect of isoproterenol treatment on cardiac contraction and relaxation in WT, Δ3aa HET and functional DEL rats, the amount of phosphorylated Troponin I was examined. In functional DEL animals, decreased levels of phosphorylated Troponin I were observed upon 14-day isoproterenol treatment

Appendix

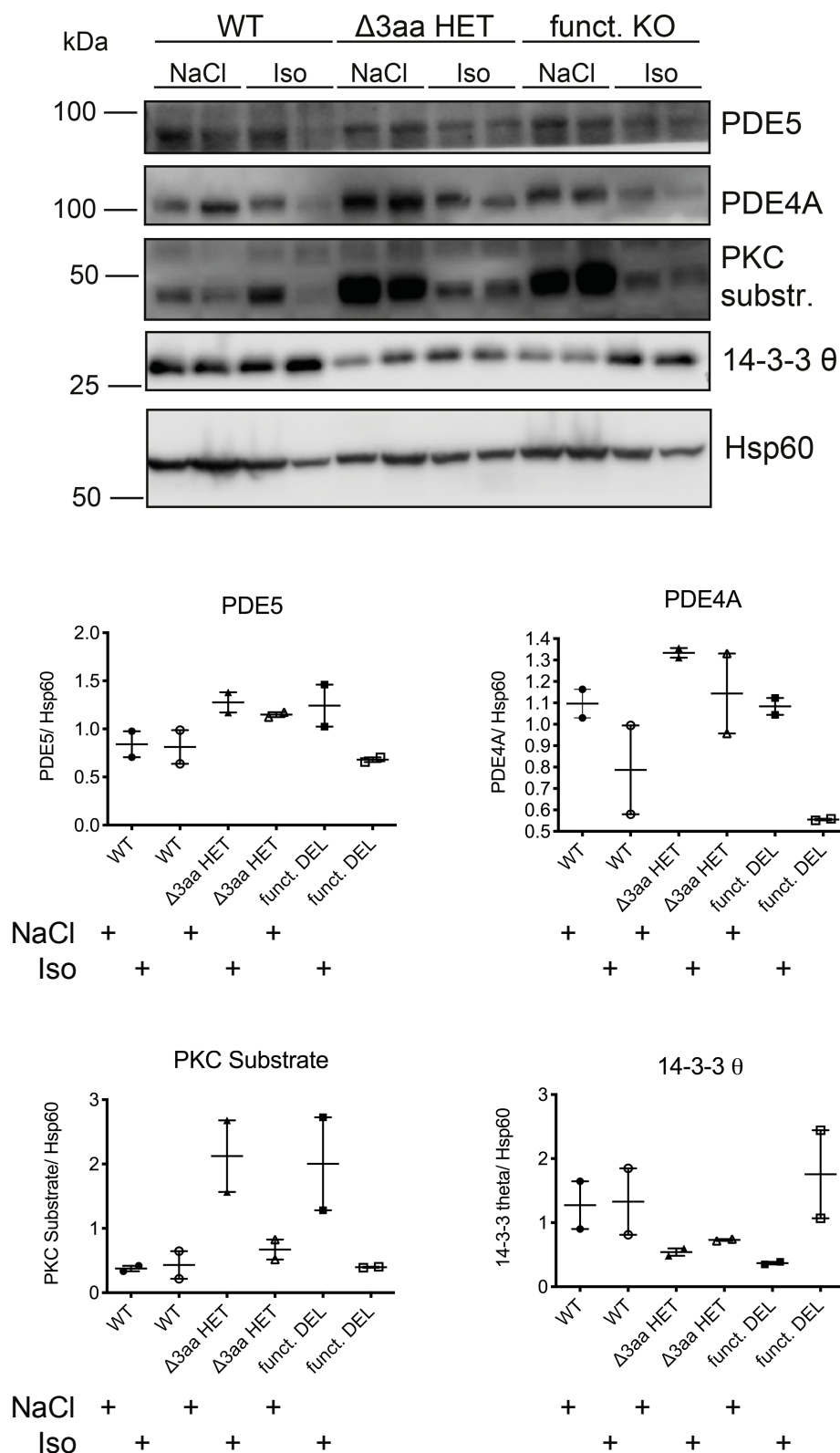
compared to the NaCl control condition. No difference was apparent in the left ventricles of WT and $\Delta 3aa$ HET rats (Supplemental Figure S3).



Supplemental Figure S3: Expression of excitation-contraction coupling system components in the heart of WT and mutant animals. Upper panel: The PKA-phosphorylated and non-phosphorylated forms of Troponin I were detected by Western blotting in the left ventricles of hearts of WT, $\Delta 3aa$ HET and functional DEL rats. Hsp60 was detected as loading control. Lower panel: Semi-quantitative analysis of the above-mentioned proteins by densitometric analysis. Plotted are the expression levels of the phosphorylated proteins normalized to the expression levels of the non-phosphorylated proteins and then to the loading control; $n = 2$ independent experiments. Mean \pm SEM is plotted.

The expression of other PDEs, which could indicate potential compensatory effect, was also assessed. PDE5 protein levels decreased in the functional DEL rat hearts after isoproterenol treatment. A decrease in the abundance of PDE4A was observed for all three genotypes upon induction of cardiac stress, the highest expression levels being detected in the $\Delta 3aa$ HET animals. Since we showed that the interaction of mutant PDE3A to 14-3-3 θ is increased compared to the WT protein,

the expression levels of the adaptor protein were also investigated in our animal models. 14-3-3 θ protein abundance was decreased in the Δ 3aa HET rats compared to the WT ones and did not seem to be affected by isoproterenol administration. For the functional DEL animals however, isoproterenol treatment led to an increase in 14-3-3 θ expression. Lastly, taking into account that PDE3A interaction to 14-3-3 θ is dependent on the PKC-mediated phosphorylation of Ser428 on PDE3A, the abundance of phosphorylated PKC substrates in the left ventricles of WT, Δ 3aa HET and functional DEL rat hearts upon isoproterenol treatment was also addressed. The abundance of phosphorylated PKC substrates was greater in the left ventricles of Δ 3aa HET and functional DEL rat hearts compared to the WT ones. Isoproterenol administration did not affect the expression levels of phosphorylated PKC substrates in the WT animals, whereas it led to a decrease in their abundance for both Δ 3aa HET and functional DEL animals (Supplemental Figure S4).



Supplemental Figure S4: Expression of other PDEs, phosphorylated PKC substrate proteins and 14-3-3 θ in the left ventricle of WT and mutant animals. Upper panel: PDE4A, PDE5, phosphorylated PKC substrates and 14-3-3 θ were detected by Western blotting in the heart of WT, Δ3aa HET and functional DEL rats. Hsp60 was detected as loading control. Lower panel: Semi-

quantitative analysis of the above-mentioned proteins by densitometric analysis. Plotted are the expression levels of the described proteins normalized to the loading control; n = 2 independent experiments. Mean \pm SEM is plotted.

11.2. Plasmid sequences of cloned constructs

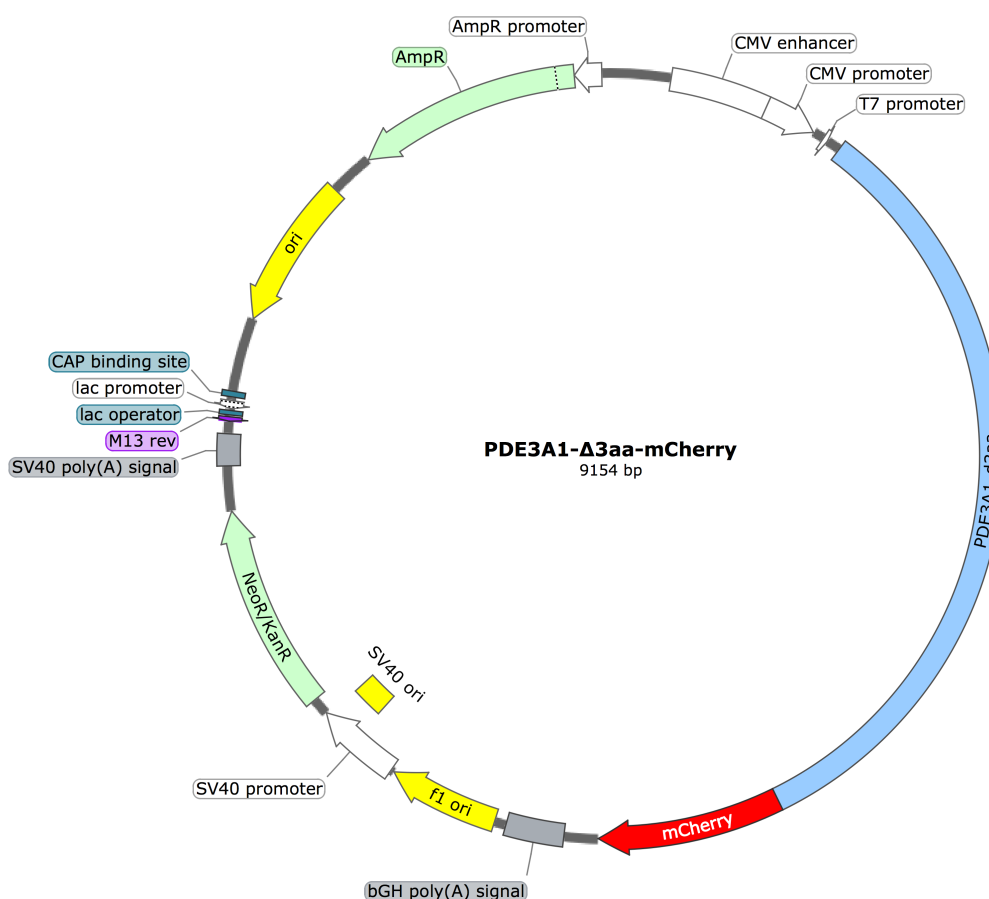
The inserted genes of interest are labeled in green and the mCherry tag is labeled in red. The corresponding mutations are shown in bold and underlined. All the following genes are cloned into the mCherry-N1 vector and therefore the whole sequence is given only one time. Subsequent sequences start from the CMV promoter (underlined sequence) and end after the stop codon (labeled in red and bold).

1. PDE3A1- Δ 3aa-mCherry

```
GACGGATCGGGAGATCTCCCGATCCCCTATGGTGCACCTCTCAGTACAATCTGCTCTGATGCCGCATAGTTAAGCC
AGTATCTGCTCCCTGCTTGTGTGTTGGAGGTTCGCTGAGTAGTGC CGGAGCAAAAATTTAAGCTACAACAAGGCAAG
GCTTGACCGACAATTGCATGAAGAATCTGCTTAGGGTTAGGCGTTTTGCGCTGCTTCGCGATGTACGGGCCAGAT
ATACGCGTTGACATTGATTATTGACTAGTTATTAATAGTAATCAATTACGGGGTCATTAGTTCATAGCCCATATA
TGGAGTTCGCGTTACATAACTTACGGTAAATGGCCCGCTGGCTGACCGCCAACGACCCCCGCCATTGACGT
CAATAATGACGTATGTTCCCATAGTAACGCCAATAGGGACTTTCCATTGACGTCAATGGGTGGAGTATTTACGGT
AAACTGCCCACTTGGCAGTACATCAAGTGTATCATATGCCAAGTACGCCCCATTGACGTCAATGACGGTAAAT
GGCCCGCTGGCATTATGCCAGTACATGACCTTATGGGACTTTCTACTTGGCAGTACATCTACGTATTAGTCA
TCGCTATTACCATGGTGTATGCGTTTTGGCAGTACATCAATGGGCGTGGATAGCGGTTGACTCACGGGGATTC
CAAGTCTCCACCCCATTTGACGTCAATGGGAGTTTTGTTTTGGCACAAAATCAACGGGACTTTCCAAAATGTCGTA
ACAACCTCCGCCCATTTGACGCAAAATGGGCGGTAGGCGTGTACGGTGGGAGGTCTATATAAGCAGAGCTCTCTGGC
TAACTAGAGAACCCTGCTTACTGGCTTATCGAAATTAATACGACTCACTATAGGGAGACCCAAGCTGGCTAGC
GTTTAAACGGGCCCTCTAGAATTGCCCTTACCGCCATGGGCTGTACCTCTGCGCGCCGGGGTFCGCGCTGCCTC
TGGCTGTGCGCTGCTGGCCGCTGCTGCGGGGGGAAGCGCTCCGTCAGATTGGGCTGGGCGTFCGGGAGGATC
ACTTACTCTCACTCCCCGCCGCGGGGGTGGTGTCTCAGCTGCTTGGCCGCCGCGACATGGCTGGTGTGAGGCTGA
GGCTGGGCGTCTCATGATCGCCTTACTAGCGCGGTGAGGACCGTGTCCCTCATTTCCCTTAGAGAGGTTCAAGG
TCGCCTGGAGACCTTACCTGGCGTACCTGGCCGGCGTGTGGGGATCCTCTTGGCCAGGTACGTGGAACAAAATCT
TGCCGCGAGTCCGCGGAGGCGGCTCCAAGGGAGCATTGGGGTCCAGCTGATTGCTGGGACCAAGGAAGATATCC
CGGTGTTTAAAGAGGAGGAGGCGGTCCAGCTCCGTCGTGTCGCGGAGATGTCGGCTGCAGCAGCAAGTCCCATC
GGAGGACCTCCCTGCCCTGTATACCGAGGGAACAGCTCATGGGCGATTGAGAAATGGGACCAAAACGAGGGCCAA
GAGGATCACAGTCTTACGGAACCAGTATTACTGTGGACATCGCCGTGATGGGCGAGGCCACGGCTCATTTACCG
ACCTCCTGGCAGACCCTTCTCTTCCACCAAACGTGTGCACATCCTTGGAGCCGTGAGCAACTTGTCTCAGCACAC
AGCTCACCTTCCAGGCCATTACAAGCCAGAGTGAATCCCGTTACTTCGCTCAGTGAAAATATACCTGTTCTG
ACTCTGAAGAGAGCTCTGAAAAGACAAGCTTGTATTCCAAAGCGCTGAGAAGGAGTTTGGCTCCTGGCTTGT
TGAGACGAGTTTCTTCCACTTGGACCACCGCCACAGGTCTACCCACCTTGGAGCCTGCACCAGTACGGAGAGACC
GCAGCACCAGCATCAAACGCAGGAAGCACCTTCAATCCAGTCTGATTCTTGAATAATCCAGTATGATGACCC
TCACCAAAGCAGATCCTTACTTTCATCCTATGCTATTTCTGCAGTAAACATGTAAAGGCTAAAAAGCAAAGTC
GACCAGGTGCCCTCGCTAAAATTTACCTCTTTCATCGCCCTGCTCCTCACCTCTCCAAGGGACTCCTGCCAGCA
GCCTGGTCAAGAAAATTTCTGCAGTGCAGTTTCCAGAATCTGCTGACACAACCTGCCAAAACAAAGCCTAGGTTCTC
ACAGGGCCTTAACTTACACTCAGAGTGCCCCAGACCTATCCCCTCAAATCCTGACTCCACCTGTTATATGTAGCA
GCTGTGGCAGACCATATTTCCAAGGGAATCCTGCTGATGAGCCCCTGGAGAGAAGTGGGGTAGCCACTCGGACAC
CAAGTAGAACAGATGACACTGCTCAAGTTACCTCTGATTATGAAACCAATAACAACAGTGCAGCAGTGCATTG
TACAGAATGAAGATGAAACAGAGTGCCTGAGAGAGCCTCTGAGGAAAGCATCGGCTTGCAGCACCATTGTCCTG
AGACCATGATGTTTTCTGGACAAACCAATTTGCTCCCGAACCTCTTGTGATGGATAACCTGGACTCAATTTATGG
AGCAGCTAAATACTTGAATTTTCCAATTTTGTATTTAGTGGAAAATATAGGAAGAAAATGTGGCCGATTTCTTA
GTCAGGTATCTTACAGACTTTTTGAAGACATGGGCTGTTTGAAGCTTTTAAAAATTTCAAATTAGGGAAATTTATGA
ATTATTTTCATGCTTTGGAGATTGGATATAGGGATATTCCTTATCATAACAGAATCCATGCCACTGATGTTTTAC
ATGCTGTTTTGGTACTTACTACACAGCCTATTCCAGGCTCTCAACTGTGATTAATGATCATGGTTCAACCAGTG
ATTTCAGATTCTGACAGTGGATTACACATGGACATGGGATATGTAATTTCAAAAACGTATAATGTGACAGATG
ATAAATACGGATGTCTGTCTGGGAATATCCCTGCCTTGGAGTTGATGGCGCTGTATGTGGCTGCAGCCATGCACG
```

ATTATGATCATCCAGGAAGGACTAATGCTTTCCTGGTTGCAACTAGTGCTCCTCAGGCGGTGCTATATAACGATC
GTTTCAGTTTTGGAGAATCATCACGCAGCTGCTGCATGGAATCTTTTTTCATGTCCCAGGCCAGAGTATAACTTCTTAA
TTAACCTTGACCATGTGGAATTTAAGCATTTCCTGTTTCCTTGTTCATTTGAAGCAATTTTGGCCACTGACCTGAAGA
AACACTTTGACTTCGTAGCCAAATTTAATGGCAAGGTAAATGATGATGTTGGAATAGATTGGACCAATGAAAATG
ATCGTCTACTGGTTTGTCAAATGTGTATAAAGTTGGCTGATATCAATGGTCCAGCTAAATGTAAAGAACTCCATC
TTCAGTGGACAGATGGTATTGTCAATGAATTTTATGAACAGGGTGATGAAGAGGCCAGCCTTGGATTACCCATAA
GCCCTTTCATGGATCGTTCTGCTCCTCAGCTGGCCAACTTCAGGAATCCTTCATCTCACATTTGTGGGGCCTC
TGTGCAACTCCTATGATTGAGCAGGACTAATGCTTGGAAAATGGGTGGAAGACAGCGATGAGTCAGGAGATACTG
ATGACCCAGAAGAAGAGGAGGAAGAAGCACCAGCACCAATGAAGAGGAAAACCTGTGAAAATAATGAATCTCCAA
AAAAGAAGACTTTCAAAGGAGAAAATCTACTGCCAAATAACTCAGCACCTCTTACAGAACCACAAGATGTGGA
AGAAAGTCATTGAAGAGGAGCAACGGTTGGCAGGCATAGAAAATCAATCCCTGGACCAGACCCCTCAGTCGCACT
CTTCAGAACAGATCCAGGCTATCAAGGAAGAAGAAGAAGAGAAAAGGAAACCAAGAGGCGAGGAGATACCAACC
AAAAGCCAGACCAGGTGAGCAAGGGCGAGGAGGATAACATGGCCATCATCAAGGAGTTTCATGCGCTTCAAGGTGC
ACATGGAGGGCTCCGTGAACGGCCACGAGTTTCAGATCGAGGGCGAGGGCGAGGGCCGCCCTACGAGGGCACCC
AGACCGCAAGCTGAAGGTGACCAAGGGTGGCCCCCTGCCCTTCGCCTGGGACATCCTGTCCCTCAGTTCATGT
ACGGCTCCAAGGCCTACGTGAAGCACCCCGCCGACATCCCCGACTACTTGAAGCTGTCTTCCCGAGGGCTTCA
AGTGGGAGCGCGTGATGAACTTCGAGGACGGCGGGCGTGGTGACCGTGACCCAGGACTCCTCCCTGCAGGACGGCG
AGTTTCATCTACAAGTGAAGCTGCGCGGCACCAACTTCCCTCCGACGGCCCCGTAATGCAGAAGAAGACCATGG
GCTGGGAGGCCCTCCTCCGAGCGGATGTACCCCGAGGACGGCGCCCTGAAGGGCGAGATCAAGCAGAGGCTGAAGC
TGAAGGACGGCGCCACTACGACGCTGAGGTCAAGACCCTTACAAGGCCAAGAAGCCCTGCAGCTGCCCGGGC
CCTACAACGTCAACATCAAGTTGGACATCACCTCCCACAACGAGGACTACACCATCGTGGAAACAGTACGAACGGC
CCGAGGGCCGCCACTCCACCGGCGGCATGGACGAGCTGTACAAGTAACTCGAGGAATTCAGGCCTCCATGGGAGC
TCGCGGCCGCCACTGTGCTGGATATCTGCAGAATTCACCACACTGGACTAGTGATCCGAGCTCGGTACCAAGC
TTAAGTTTTAAACCGCTGATCAGCCTCGACTGTGCCTTCTAGTTGCCAGCCATCTGTTGTTTGGCCCTCCCCGTG
CCTTCCCTTGACCCTGGAAGGTGCCACTCCCCTGTCTTCTTAATAAAAATGAGGAAAATGCATCGCATTTGTCTG
AGTAGGTGTATTCTATTCTGGGGGTGGGGTGGGGCAGGACAGCAAGGGGGAGGATTGGGAAGACAATAGCAGG
CATGCTGGGGATGCGGTGGGCTCTATGGCTTCTGAGGCGGAAAGAACCAGCTGGGGCTCTAGGGGGTATCCCCAC
GCGCCCTGTAGCGGCGCATTAAGCGCGGGCGGGTGTGGTGGTTACGCGCAGCGTGACCGCTACACTTGCAGCGCC
CTAGCGCCCGCTCCTTTCGCTTTCCTTCCCTTCTTCTCGCCAGCTTCGCGGGCTTTCCTCCGTCATAAT
CGGGGGCTCCTTTAGGGTTCGATTTAGTGTCTTACGGCACCTCGACCCAAAAAACTTGATTTAGGGTGTATGGT
TCACGTAGTGGCCATCGCCCTGATAGACGGTTTTTCGCCCTTTCGACGTTGGAGTCCACGTCTTTAATAGTGA
CTCTTGTTCCAAACCTGGAACAACACTCAACCCTATCTCGGTCTATTCTTTTGATTTATAAGGGATTTTGGCGATT
TCGGCCTATTGGTTAAAAAATGAGCTGATTTAAACAAAAATTTAACGCGAATTAATTTCTGTGGAATGTGTGTGCTG
TAGGGTGTGGAAGTCCCAGGCTCCCAGCAGGCAGAAGTATGCAAAGCATGCATCTCAATTAGTCAGCAACCATAG
GGTGTGGAAGTCCCAGGCTCCCAGCAGGCAGAAGTATGCAAAGCATGCATCTCAATTAGTCAGCAACCATAG
TCCCGCCCTAACTCCGCCATCCCGCCCTAACTCCGCCAGTTCCGCCATTCCTCCGCCCATGGCTGACTAA
TTTTTTTTTATTTATGCAGAGGCCGAGGCCGCTCTGCCTCTGAGCTATTCCAGAAGTAGTGAGGAGGCTTTTTTG
GAGGCTAGGCTTTTGAAGAGCTCCCGGGAGCTTGTATATCCATTTTCGGATCTGATCAAGAGACAGGATGAG
GATCGTTTTCGCATGATTGAACAAGATGGATTGCACGCAGGTTCTCCGGCCGCTTGGGTGGAGAGGCTATTCCGGCT
ATGACTGGGCACAACAGACAATCGGCTGCTCTGATGCCCGGTGTTCCGGCTGTCAGCGCAGGGGCGCCCGGTTT
TTTTTGTCAAGACCGACCTGTCCGGTGCCTGAATGAACTGCAGGACGAGGCAGCGGGCTATCGTGGCTGGCCA
CGACGGGCGTTCCTTGCAGCTGTGCTCGACGTTGTACTGAAAGCGGGAAGGGACTGGCTGCTATTGGGCGAAG
TGCCGGGCGAGGATCTCTGTCTACCTTGTCTCCGCTCCGAGAAAGTATCCATCATGGCTGATGCAATGCGGC
GGATGCAACGCTTGTATCCGGCTACCTGCCCATTTCGACCCACCAAGCAACATCGCATCGAGCGAGCAGTATC
GGATGGAAGCCGGTCTTGTGATCAGGATGATCTGGACGAAGAGCATCAGGGGCTCGCGCCAGCCGAACTTTCG
CCAGGCTCAAGGCGCGCATGCCGACGGCGAGGATCTCGTCTGACCCATGGCGATGCCTGCTTGGCGAATATCA
TGGTGGAAAATGGCCGCTTTTCTGGATTTCATCGACTGTGGCCGGCTGGGTGTGGCGGACCCTATCAGGACATAG
CGTTGGCTACCCGTGATATTGCTGAAGAGCTTGGCGGCAATGGGCTGACCGCTTCTCGTGTCTTACGGTATCG
CCGCTCCCATTTCGAGCGCATCGCCTTCTATCGCCTTCTTTCGACGAGTTCTTCTGAGCGGGACTCTGGGGTTCGA
AATGACCGACCAAGCGACGCCAACCTGCCATCACGAGATTTTCGATTCCACCAGCCGCTTCTATGAAAGGTTGGG
CTTCCGAATCGTTTTCCGGGACGCCGGCTGGATGATCCTCCAGCGCGGGGATCTCATGCTGGAGTTCTTCGCCCA
CCCCAATTGTTTTATTGCAGCTTATAATGGTTACAAAATAAAGCAATAGCATCACAAAATTTACAAAATAAAGCATT
TTTTTCACTGCATTCTAGTTGTGGTTTGTCCAAACTCATCAATGTATCTTATCATGTCTGTATACCGTFCGACCTC
TAGCTAGAGCTTGGCGTAATCATGGTCATAGCTGTTTCTGTGTGAAATTTGTATCCGCTCACAAATTCACACAA
CATACGAGCCGGAAGCAAAAGTGTAAAGCCTGGGGTGCCTAATGAGTGAGCTAACTCACATTAATTCGCTTGGC
CTCACTGCCCGCTTTCCAGTCGGGAAACCTGTCTGGCCAGCTGCATTAATGAATCGGCCAACGCGCGGGGAGG
CGTTTTGCGTATTGGGCGCTTTCGCTTCTCGCTCACTGACTCGCTCGCTCGGCTCGGCTCGGCTCGGCTCGGAGC
GGTATCAGCTCACTCAAAGGCGGTAATACGGTTATCCACAGAATCAGGGGATAACGCAGGAAAAGACATGTGAGC
AAAAGGCCAGCAAAGGCCAGGAACCGTAAAAAGGCCGCTTGTGGGCTTTTTCCATAGGCTCCGCCCCCTGA
CGAGCATCACAAAATCGACGCTCAAGTCAGAGGTGGCGAAACCCGACAGGACTATAAAGATAACAGGCGTTTCC
CCCTGGAAGCTCCCTCGTGCCTCTCCTGTTCCGACCTGCCGCTTACCGGATACCTGTCCGCTTCTCCTTTC
GGGAAGCGTGGCGCTTCTCATAGCTCACGCTGTAGGTATCTCAGTTCCGGTGTAGGTGCTTCGCTCCAAGCTGGG
CTGTGTGCACGAACCCCGTTTCAGCCCGACCGCTGCGCCTTATCCGGTAACTATCGTCTTTCGAGTCCAACCCGGT
AAGACACGACTTATCGCCACTGGCAGCAGCCACTGGTAAACAGGATTAGCAGAGCGAGGATGTAGGCGGGTGTAC

AGAGTTCTTGAAGTGGTGGCCTAACTACGGCTACACTAGAAGAACAGTATTTGGTATCTGCGCTCTGCTGAAGCC
 AGTTACCTTCGGAAAAAGAGTTGGTAGCTCTTGATCCGGCAAACAAACCACCGCTGGTAGCGGTTTTTTTTGTTT
 CAAGCAGCAGATTACGCGCAGAAAAAAGGATCTCAAGAAGATCCTTTTGATCTTTTCTACGGGGTCTGACGCTCA
 GTGGAACGAAAACCTCACGTTAAGGGATTTTGGTCATGAGATTATCAAAAAGGATCTTCACCTAGATCCTTTTAAA
 TTAATAATGAAGTTTTAAATCAATCTAAAGTATATATGAGTAAACTTGGTCTGACAGTTACCAATGCTTAATCAG
 TGAGGCACCTATCTCAGCGATCTGTCTATTTTCGTTTCATCCATAGTTGCCTGACTCCCGTCTGTGTAGATAACTAC
 GATACGGGAGGGCTTACCATCTGGCCCCAGTGCTGCAATGATACCGCGAGACCCACGCTCACCGGCTCCAGATTT
 ATCAGCAATAAACCAGCCAGCCGGAAGGGCCGAGCGCAGAAGTGGTCTGCAACTTTATCCGCCTCCATCCAGTC
 TATTAATTGTTGCCGGGAAGCTAGAGTAAGTAGTTCCGCCAGTTAATAGTTTTCGCAACGTTGTTGCCATTGCTAC
 AGGCATCGTGGTGTACGCTCGTCTGTTTGGTATGGCTTCATTCAGCTCCGGTTCCTCAACGATCAAGGCGAGTTAC
 ATGATCCCCCATGTTGTGCAAAAAGCGGTTAGCTCCTTCGGTCTCCGATCGTTGTCAGAAGTAAGTTGGCCGC
 AGTGTATCACTCATGTTATGGCAGCACTGCATAATTCTCTTACTGTTCATGCCATCCGTAAGATGCTTTTCTGT
 GACTGGTGAGTACTCAACCAAGTCATTCTGAGAATAGTGTATGCGGCGACCGAGTTGCTCTTGCCTCGGCTCAAT
 ACGGGATAATACCGCGCCACATAGCAGAAGTTTAAAAGTGCTCATCATTGGAAAACGTTCTTTCGGGGCGAAAAC
 CTAAGGATCTTACCGCTGTTGAGATCCAGTTTCGATGTAACCCACTCGTGCACCCAACTGATCTTCAGCATCTTT
 TACTTTACCAGCGTTTCTGGGTGAGCAAAAACAGGAAGGCAAAATGCCGCAAAAAGGGAAATAAGGGCGACACG
 GAAATGTTGAATACTCATACTCTTCTTTTCAATATTATTGAAGCATTATCAGGGTTATTGTCTCATGAGCGG
 ATACATATTTGAATGTATTTAGAAAAATAAACAAATAGGGGTTCCGCGCACATTTCCCGAAAAGTGCCACCTGA
 CGTC



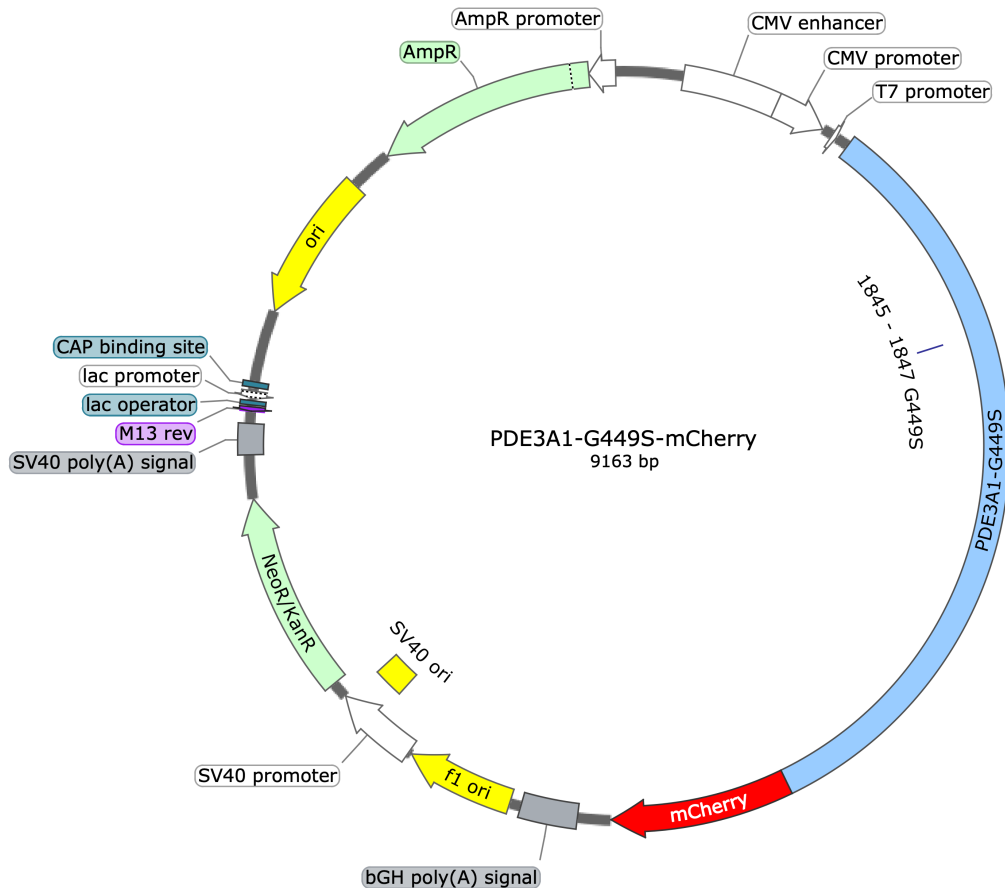
Supplemental Figure S5: Vector map of PDE3A1-Δ3aa-mCherry

2. PDE3A1-G449S-mCherry

GTGATGCGGTTTTGGCAGTACATCAATGGGCGTGGATAGCGGTTTTGACTCACGGGGATTTCCAAGTCTCCACCC
ATTGACGTCAATGGGAGTTTTGTTTTGGCACAAAATCAACGGGACTTTCCAAAATGTCGTAACAACCTCCGCCCA
TTGACGCAAAATGGGCGGTAGGCGTGTACGGTGGGAGGTCTATATAAGCAGAGCTCTCTGGCTAACTAGAGAACCC
ACTGCTTACTGGCTTATCGAAATTAATACGACTCACTATAGGGAGACCCAAGCTGGCTAGCGTTTAAACGGGCCC

Appendix

TCTAGAATTGCCCTTACCGCCATGGGCTTGTACCTCCTGCGCGCCGGGGTGCCTGCTCTGGCTGTCGCGCTG
CTGGCCGCTGCTGCGGGGGGAAGCGCTCGTCCAGATTGGGCTGGGCGTCGGGGAGGATCACTTACTCTCACTC
CCCGCCGCGGGGGTGGTGTCTCAGCTGCTTGGCCGCGCGACATGGCTGGTGTGAGGCTGAGGCTGGGCGTCCTC
ATGATCGCCTTGACTAGCGCGGTGAGGACCGTGTCCCTCATTTCTTAGAGAGGTTCAAGGTCGCTGGAGACCT
TACCTGGCGTACCTGGCCGGCGTGTGGGGATCCTCTTGGCCAGGTACGTGGAACAAAATCTTGGCCGAGTCCGCG
GAGGCGGCTCCAAGGGAGCATTGGGGTCCCAGCTGATTGCTGGGACCAAGGAAGATATCCCGGTGTTAAGAGG
AGGAGCGGTCCAAGTCCGTGCTGCTCCGCGAGATGCTCCGGCTGCAGCAGCAAGTCCCATCGGAGGACCTCCCTG
CCCTGTATAACCGAGGGAACAGCTCATGGGGCATTGAGAAATGGGACCACAAACGAGGGCCAAGAGGATCACAGTCT
TCAGGAACCAGTATTACTGTGGACATCGCCGTATGGGCGAGGCCACGGCTCATTACCAGCTCCTGGCAGAC
CCTTCTCTTCCACCAAACGTGTGCACATCCTTGAGAGCCGTGAGCAACTTGTCTCAGCACACAGCTCACCTTCCAG
GCCATTACAAGCCAGAGTGAATCCCGTACTTCGCTCAGTGAAAATATACTGTTCTGACTCTGAAGAGAGC
TCTGAAAAGACAAGCTTGTATTCCAAAGCGCTGAGAAGGAGTTTGCCTCCTGGCTTGTGAGACGAGTTTCT
TCCACTTGGACCACCACCCTCGGCCACAAGTCTACCCACCTTGGAGCCTGCACCAGTACGGAGAGACCGCAGC
ACCAGCATCAAACGAGGAAGCACCTTCATCCAGTCCCTGATTCTTGGAAATAATCCAGTGATGATGACCCCTACC
AAAAGCAGATCCTTTACTTCATCCTATGCTATTTCTGCAGCTAACCATGTAAAGGCTAAAAAGCAAAGTCGACCA
GGTGCCTCGCTAAAATTTACCTCTTTTCATCGCCCTGCTCCTCACCTCTCCAAGGGACTCCTGCCAGCAGCCTG
GTCAGCAAAAATTTCTGCAGTGCAGTTTCCAGAATCTGCTGACACAACCTGCCAAAACAAAGCCTAGGTTCTCACAGG
GCCTTAACCTTACACTCAGAGTGCACCAAGCTTCCCTCAAATCCTGACTCCACCTGTTATATGTAGCAGCTGT
GGCAGACCATATTTCCAAGGGAATCTGCTGATGAGCCCTGGAGAGAAGTGGGGTAGCCACTCGGACACCAAGT
AGAACAGATGACACTGCTCAAGTTACCTCTGATTATGAAACCAATAACAACAGTGACAGCAGTGACATTTGTACAG
AATGAAGATGAAACAGAGTGCCTGAGAGAGCCTCTGAGGAAAGCATCGGCTTGCAGCACCTATGCTCCTGAGACC
ATGATGTTTCTGGACAAAACCAATTTCTTGTCTCCGAACTCTTGTGATGGATAACCTGGACTCAATTATGGAGCAG
CTAAATACTTGAATTTTCCAATTTTGTATTTAGTGGAAAATATAGGAAGAAAATGTGGCCGTATTTCTTAGTCAG
GTATCTTACAGACTTTTTGAAGACATGGGCTGTTTGAAGCTTTTAAAATCCAATTAGGGAATTTATGAATTAI
TTTCATGCTTTGGAGATTGGATATAGGGATATTCCTTATCATAACAGAATCCATGCCACTGATGTTTTACATGCT
GTTTGGTATCTTACTACACAGCCTATTCCAGGCCTCTCAACTGTGATTAATGATCATGGTTCACCAGTGATTC
GATTCTGACAGTGGATTTACACATGGACATATGGGATATGATTTCTCAAAAACGTATAATGTGACAGATGATAAA
TACGGATGTCTGTCTGGGAATATCCCTGCCTTGGAGTTGATGGGCGTGTATGTGGCTGCAGCCATGCACGATTAT
GATCATCCAGGAAGGACTAATGCTTTCCTGGTTGCAACTAGTGCTCCTCAGGCGGTGCTATATAACGATCGTTCA
GTTTGGAGAATCATCACGAGCTGCTGCATGGAATCTTTTCATGTCCCGCCAGAGTATAACTTCTTAATTAAC
CTTCCAGCATTTGAATTTAAGCATTTCCTTGTGATTTGAAGCAATTTTGGCCACTGACCTGAAGAAACAC
TTTACTTTCGTAGCCAAATTTAATGGCAAGGTAAATGATGATGTTGGAATAGATTGGACCAATGAAAATGATCGT
CTACTGGTTTTGTCAAATGTGTATAAAGTTGGCTGATATCAATGGTCCAGCTAAATGTAAAGAACTCCATCTTCAG
TGGACAGATGGTATTGTCAATGAATTTTATGAACAGGGTATGAAGAGGCCAGCCTTGGATTACCCATAAGCCCC
TTCATGGATCGTTCTGCTCCTCAGCTGGCCAACCTTCAGGAATCCTTCATCTCTCACATTTGTGGGGCTCTGTGC
AACTCCTATGATTACAGCAGGACTAATGCCTGGAAAATGGGTGGAAGACAGCGATGAGTCAGGAGATACTGATGAC
CCAGAAGAAGAGGAGGAAGAAGCACCAGCACCAATGAAGAGGAAACCTGTGAAAATAATGAATCTCCAAAAAAG
AAGACTTTCAAAGGAGAAAAATCTACTGCCAAATAACTCAGCACCTCTTACAGAACCACAAGATGTGGAAGAAA
GTCATTGAAGAGGAGCAACGGTTGGCAGGCATAGAAAATCAATCCCTGGACCAGACCCCTCAGTCGCACTCTTCA
GAACAGATCCAGGCTATCAAGGAAGAAGAAGAAGAGAAAAGGGAAAACCAAGAGGCGAGGAGATACCAACCCAAAAG
CCAGACCAGGTGAGCAAGGGCGAGGAGGATAACATGGCCATCATCAAGGAGTTCATGCGCTTCAAGGTGCACATG
GAGGGCTCCGTGAACGGCCACGAGTTCGAGATCGAGGGCGAGGGCGAGGGCCGCCCTACGAGGGCACCAGACC
GCCAAGCTGAAGGTGACCAAGGGTGGCCCCCTGCCCTTCGCTGGGACATCCTGTCCCTCAGTTTTCATGTACGGC
TCCAAGGCTACGTGAAGCACCCCGCCGACATCCCCGACTACTTGAAGCTGTCCCTTCCCGAGGGCTTCAAGTGG
GAGCGCGTGTGAACTTCGAGGACGGCGGCGTGGTGACCTGACCCAGGACTCCTCCCTGCAGGACGGCGAGTTC
ATCTACAAGGTGAAGCTGCGCGGCACCAACTTCCCTCCGACGGCCCCGTAATGCAGAAGAAGACCATGGGCTGG
GAGGCCCTCCTCCGAGCGGATGTACCCGAGGACGGCGCCCTGAAGGGCGAGATCAAGCAGAGGCTGAAGCTGAAG
GACGGCGGCCACTACGACGCTGAGGTCAAGACCACCTACAAGGCCAAGAAGCCCGTGCAGCTGCCCGGCGCCTAC
AACGTCAACATCAAGTTGGACATCACCTCCCACAACGAGGACTACACCATCGTGGAACAGTACGAACGCGCCGAG
GGCCGCCACTCCACCGGCGGCATGGACGAGCTGTACAAGTAA



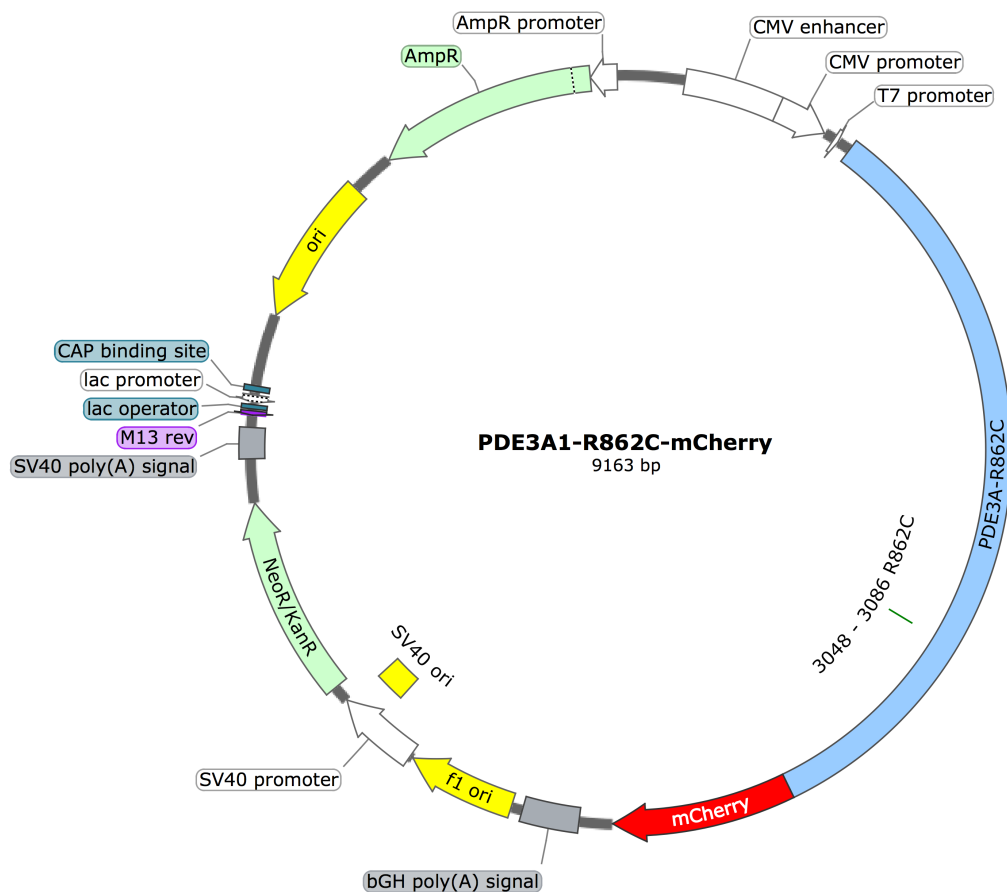
Supplemental Figure S6: Vector map of PDE3A1-G449S-mCherry

3. PDE3A1-R862C-mCherry

GTGATGCGGTTTTTGGCAGTACATCAATGGGCGTGGATAGCGGTTTGACTCACGGGGATTTCCAAGTCTCCACCCC
 ATTGACGTCAATGGGAGTTTGTTTTGGCACCAAAATCAACGGGACTTTCCAAAATGTCGTAACAACTCCGCCCA
 TTGACGCAAATGGGCGGTAGGCGGTACGGTGGGAGGTTCTATATAAGCAGAGCTCTCTGGCTAACTAGAGAACCC
 ACTGCTTACTGGCTTATCGAAATTAATACGACTCACTATAGGGAGACCCAAGCTGGCTAGCGTTTAAACGGGCC
 TCTAGAATTGCCCTTACCGCCATGGGCTTGTACCTCCTGCGCGCCGGGGTGCCTGCTGCTGCTGCTGCGCGT
 CTGGCCGCTGCTGCGGGGGGAAGCGCTCGTCCAGATTGGGCTGGGCGTTCGGGGAGGATCACTTACTCTCACTC
 CCCGCCGCGGGGGTGGTGCTCAGCTGCTTGGCCGCCGACATGGCTGGTGTGAGGCTGAGGCTGGGCGTCCCTC
 ATGATCGCCTTGACTAGCGCGGTGAGGACCGTGTCCCTCATTTCCCTTAGAGAGGTTCAAGGTCGCTGGAGACCT
 TACCTGGCGTACCTGGCCGGCGTGTGGGATCCTCTTGGCCAGGTACGTGGAACAAATCTTGCCGAGTCCGCG
 GAGGCGGCTCCAAGGAGCATTGGGGTCCCAGCTGATTGCTGGGACCAAGGAAGATATCCCGTGTTTAAGAGG
 AGGAGGCGGTCCAGCTCCGTCGTGTCCGCCGAGATGTCCGGCTGCAGCAGCAAGTCCCATCGGAGGACCTCCCTG
 CCCTGTATACCGAGGGAACAGCTCATGGGGCATTCAGAATGGGACCACAAACGAGGGCCAAGAGGATCACAGTCT
 TCAGGAACCAGTATTACTGTGGACATCGCCGTCATGGGCGAGGCCACGGCTCATTACCGACCTCCTGGCAGAC
 CCTTCTCTCCACCAACGTGTGCACATCCTTGAGAGCCGTGAGCAACTTGCTCAGCACACAGCTCACCTTCCAG
 GCCATTACAAGCCCAAGTGAATCCCGTTACTTCGCTCAGTGAAAACCTATACCTGTCTGACTCTGAAGAGAGC
 TCTGAAAAGACAAGCTTGCTATTCCAAAGCGCCTGAGAAGGAGTTTGCCTCTGGCTGTGTGAGACGAGTTTCT
 TCCACTTGGACCACCACCTCGGCCACAGGTCTACCCACCTTGGAGCCTGCACCAGTACGGAGAGACCGCAGC
 ACCAGCATCAAACGAGGAAGCACCTTCATCCAGTCTGATTTCTTGGAAATAATCCAGTGATGATGACCCCTACC
 AAAAGCAGATCCTTTACTTTCATCCTATGCTATTTCTGCAGCTAACCATGTAAGGCTAAAAAGCAAAGTCGACCA
 GGTGCCCTCGCTAAAATTTACCTCTTTTCATCGCCCTGCTCCTCACCTCTCAAGGGACTCTGCCAGCAGCCTG
 GTCAGCAAAATTTCTGCAGTGCAGTTTCCAGAATCTGCTGACACAACCTGCCAAACAAAGCCTAGGTTCTCACAGG
 GCCTTAACTTACACTCAGAGTGCCCCAGACCTATCCCTCAAATCCTGACTCCACCTGTATATGTAGCAGCTGT
 GGCAGACCATATTTCCAAGGGAATCCTGCTGATGAGCCCTGGAGAGAAAGTGGGGTAGCCACTCGGACACCAAGT
 AGAACAGATGACTGCTCAAGTTACCTCTGATTATGAAACCAATAACAACAGTGACAGCAGTGACATTTGTACAG
 AATGAAGATGAAACAGAGTGCTGAGAGAGCCTCTGAGGAAAGCATCGGCTTGCAGCACCTATGCTCCTGAGACC

Appendix

ATGATGTTTCTGGACAAACCAATTCTTGCTCCCGAACCTCTTGTCATGGATAACCTGGACTCAATTATGGAGCAG
CTAAATACTTGGAAATTTTCCAATTTTGGATTTAGTGGAAAAATATAGGAAGAAAAATGTGGCCGTATTTCTTAGTCAG
GTATCTTACAGACTTTTTGAAGACATGGGCCTGTTTGAAGCTTTTAAAAATCCAATTAGGGAATTTATGAATTTAT
TTTCATGCTTTGGAGATTGGATATAGGGATATTCCTTATCATAACAGAATCCATGCCACTGATGTTTTACATGCT
GTTTGGTATCTTACTACACAGCCTATTCCAGGCCTCTCAACTGTGATTAATGATCATGGTTCAACCAGTGATTCA
GATTCTGACAGTGGATTTACACATGGACATATGGGATATGTATTCTCAAAAACGTATAATGTGACAGATGATAAA
TACGGATGTCTGTCTGGGAATATCCCTGCCTTGGAGTTGATGGCGCTGTATGTGGCTGCAGCCATGCACGATTTAT
GATCATCCAGGAAGGACTAATGCTTTCTGGTTGCAACTAGTGCTCCTCAGGCGGTGCTATATAACGATTTGTTCA
GTTTTGGAGAATCATCACGCAGCTGCTGCATGGAATCTTTTCATGTCCCGCCAGAGTATAAATTTCTTAATTAAC
CTTGACCATGTGGAATTTAAGCATTTCCTGTTTCTTGTCAATTGAAGCAATTTTGGCCACTGACCTGAAGAAACAC
TTTGACTTCGTAGCCAAATTTAATGGCAAGGTAATGATGATGTTGGAATAGATTGGACCAATGAAAAATGATCGT
CTACTGGTTTTGTCAAATGTGTATAAAGTTGGCTGATATCAATGGTCCAGCTAAATGTAAAGAACTCCATCTTCAG
TGGACAGATGGTATTGTCAATGAATTTTATGAACAGGGTGATGAAGAGGCCAGCCTTGGATTACCCATAAGCCCC
TTCATGGATCGTTCTGCTCCTCAGCTGGCCAACCTTCAGGAATCCTTCATCTCTCACATTTGTGGGGCCTCTGTGC
AACTCCTATGATTCAGCAGGACTAATGCCTGGAAAAATGGGTGGAAGACAGCGATGAGTCAGGAGATACTGATGAC
CCAGAAGAAGAGGAGGAAGAAGCACCAGCACCAAAATGAAGAGGAAAACCTGTGAAAAATAATGAATCTCCAAAAAAG
AAGACTTTCAAAGGAGAAAAATCTACTGCCAAATAACTCAGCACCTTTACAGAACCACAAGATGTGGAAAGAAA
GTCATTGAAGAGGAGCAACGGTTGGCAGGCATAGAAAAATCAATCCCTGGACCAGACCCCTCAGTCGCACCTTTCA
GAACAGATCCAGGCTATCAAGGAAGAAGAAGAAGAGAAAGGAAACCAAGAGGCGAGGAGATACCAACCCAAAAAG
CCAGACCAGGTGAGCAAGGGCGAGGAGGATAACATGGCCATCATCAAGGAGTTTCATGCGCTTCAAGGTGCACATG
GAGGGCTCCGTGAACGGCCACGAGTTCGAGATCGAGGGCGAGGGCGAGGGCCGCCCTTACGAGGGCAGCCAGACC
GCCAAGCTGAAGGTGACCAAGGGTGGCCCCCTGCCCTTCGCTGGGACATCCTGTCCCCTCAGTTTCATGTACGGC
TCCAAGGCCTACGTGAAGCACCCCGCCGACATCCCCGACTACTTGAAGCTGTCTTCCCCGAGGGCTTCAAGTGG
GAGCGCGTGATGAACTTCGAGGACGGCGGCGTGGTGACCGTGACCCAGGACTCCTCCTGCAGGACGGCGAGTTC
ATCTACAAGGTGAAGCTGCGCGGCACCAACTTCCCCTCCGACGGCCCCGTAATGCAGAAGAAGACCATGGGCTGG
GAGGCCTCCTCCGAGCGGATGTACCCGAGGACGGCGCCCTGAAGGGCGAGATCAAGCAGAGGCTGAAGCTGAAG
GACGGCGGCCACTACGACGCTGAGGTCAAGACCACCTACAAGGCCAAGAAGCCCGTGCAGCTGCCCGGGCGCCAC
AACGTCAACATCAAGTTGGACATCACCTCCCACAACGAGGACTACACCATCGTGGAACAGTACGAACGCGCCGAG
GGCCGCCACTCCACCGGGCGCATGGACGAGCTGTACAAGTAA



Supplemental Figure S7: Vector map of PDE3A1-R862C-mCherry

4. PDE3A1-T445N-mCherry

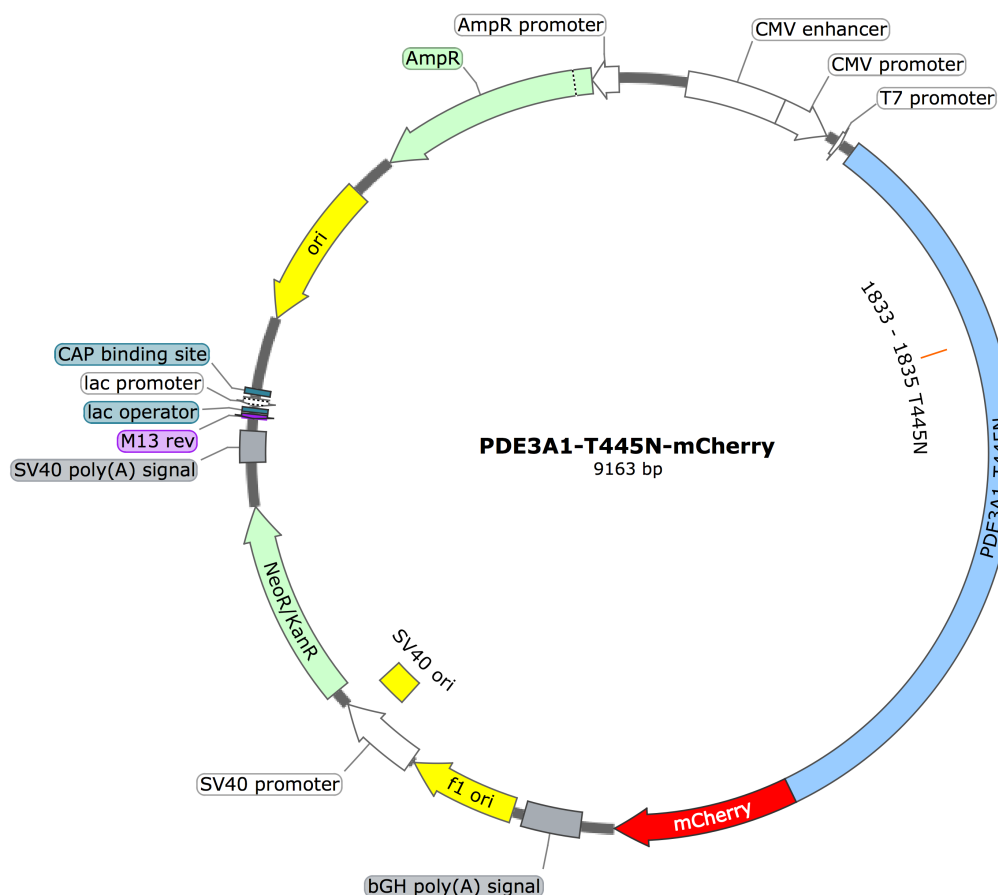
```

GTGATGCGGTTTTGGCAGTACATCAATGGGCGTGGATAGCGGTTTTGACTCACGGGGATTTCCAAGTCTCCACCC
ATTGACGTCAATGGGAGTTTTGTTTTGGCACAAAATCAACGGGACTTTCCAAAATGTCGTAACAACCTCCGCCCA
TTGACGCAAATGGGCGGTAGGCGTGTACGGTGGGAGGTCTATATAAGCAGAGCTCTCTGGCTAACTAGAGAACC
ACTGCTTACTGGCTTATCGAAATTAATACGACTCACTATAGGGAGACCCAAGCTGGCTAGCGTTTAAACGGGCC
TCTAGAATTGCCCTTACCGCCATGGGCTTGTACCTCCTGCGCGCCGGGGTGCCTTGCCTCTGGCTGTGCGGCTG
CTGGCCGCTGCTGCGGGGGGAAGCGCTCGTCCAGATTGGCTGGGCGTGGGGAGGATCACTTACTCTCACTC
CCCGCCGCGGGGTGGTGCTCAGCTGCTTGGCCGCGGACATGGCTGGTGCTGAGGCTGAGGCTGGGCGTCCCTC
ATGATCGCCTTGACTAGCGCGGTGAGGACCGTGTCCCTCATTTCCTTAGAGAGGTTCAAGGTCGCTGGAGACCT
TACCTGGCGTACCTGGCCGGCGTGTGGGGATCCTCTTGGCCAGGTACGTGGAACAAAATCTTGGCCGAGTCCGG
GAGGCGGCTCCAAGGGAGCATTGGGGTCCCAGCTGATTGCTGGGACCAAGGAAGATATCCCGGTGTTAAGAGG
AGGAGGCGGTCCAGCTCCGTCGTGTCGCGGAGATGTCCGGCTGCAGCAGCAAGTCCCATCGGAGGACCTCCCTG
CCCTGTATAACGAGGGAACAGCTCATGGGGCATTGAGAATGGGACCACAAACGAGGGCCAAGAGGATCACAGTCT
TCAGGAACCAGTATTACTGTGGACATCGCCGTATGGGCGAGGCCACGGCCTCATTACCGACCTCCTGGCAGAC
CCTTCTCTCCACCAAACGTGTGCACATCCTTGAGAGCCGTGAGCAACTTGTCTCAGCACACAGCTCACCTTCCAG
GCCATTACAAGCCAGAGTGAATCCCGTTACTTCGCTCAGTGAAAATATACCTGTTCTGACTCTGAAGAGAGC
TCTGAAAAGACAAGCTTGTATTCCAAGCGCCTGAGAAGGAGTTTGCCTCCTGGCTTGTGAGACGAGTTTCTT
TCCACTTGGACCACCACCAACTCGGCCACAGGTCTACCCACCTTGGAGCCTGCACCAGTACGGAGAGACCGCAGC
ACCAGCATCAAATCGAGGAAGCAGCTTCACTTCTGATTCCTTGGAAATAATCCAGTGTATGATGACCTCACC
AAAAGCAGATCCTTTACTTCACTTATGCTATTTCTGCTCAGTAACTGTAAGGCTAAAAGCAAAGTCCGACCA
GGTGCCTCGCTAAAATTTACCTCTTTCATCGCCCTGCTCCTCACCTCTCCAAGGGACTCCTGCCAGCAGCCTG
GTCAGCAAAAATTTCTGCAGTGCAGTTTCCAGAATCTGCTGACACAACCTGCCAAAACAAAGCCTAGGTTCTCACAG
GCCTTAACTTACACTCAGAGTGCCCCAGACCTATCCCTCAAATCCTGACTCCACCTGTTATATGTAGCAGTGT
GGCAGACCATATTTCCAAGGGAATCCTGCTGATGAGCCCTGGAGAGAAGTGGGGTAGCCACTCGGACACCAAGT
AGAACAGATGACACTGCTCAAGTTACCTCTGATTATGAAACCAATAACAACAGTGACAGCAGTGACATTGTACAG
AATGAAGATGAAACAGAGTGCCTGAGAGAGCCTCTGAGGAAAGCATCGGCTTGCAGACCTATGCTCCTGAGACC

```

Appendix

ATGATGTTTCTGGACAAACCAATTCTTGCTCCCGAACCTCTTGTCATGGATAACCTGGACTCAATTATGGAGCAG
CTAAATACTTGGAAATTTTCCAATTTTTGATTTAGTGGAAAAATATAGGAAGAAAAATGTGGCCGTATTTCTTAGTCAG
GTATCTTACAGACTTTTTGAAGACATGGGCCTGTTTGAAGCTTTTAAAAATCCAATTAGGGAATTTATGAATTTAT
TTTCATGCTTTGGAGATTGGATATAGGGATATTCCTTATCATAACAGAATCCATGCCACTGATGTTTTACATGCT
GTTTGGTATCTTACTACACAGCCTATTCCAGGCCTCTCAACTGTGATTAATGATCATGGTTCAACCAGTGATTCA
GATTCTGACAGTGGATTTACACATGGACATATGGGATATGTATTCTCAAAAACGTATAATGTGACAGATGATAAA
TACGGATGTCTGTCTGGGAATATCCCTGCCTTGGAGTTGATGGCGCTGTATGTGGCTGCAGCCATGCACGATTAT
GATCATCCAGGAAGGACTAATGCTTTCCCTGGTTGCAACTAGTGCTCCTCAGGCGGTGCTATATAACGATCGTTCA
GTTTTGGAGAATCATCACGCAGCTGCTGCATGGAATCTTTTCATGTCCCGCCAGAGTATAAATTTCTTAATTAAC
CTTGACCATGTGGAATTTAAGCATTTCCTGTTTCTTGTCAATTGAAGCAATTTTGGCCACTGACCTGAAGAAAAC
TTTACTTCGTAGCCAAATTTAATGGCAAGGTAAATGATGATGTTGGAATAGATTGGACCAATGAAAAATGATCGT
CTACTGGTTTTGTCAAATGTGTATAAAGTTGGCTGATATCAATGGTCCAGCTAAATGTAAAGAACTCCATCTTCAG
TGGACAGATGGTATTGTCAATGAATTTTATGAACAGGGTGATGAAGAGGCCAGCCTTGGATTACCCATAAGCCCC
TTCATGGATCGTTCTGCTCCTCAGCTGGCCAACCTTCAGGAATCCTTCATCTCTCACATTGTGGGGCCTCTGTGC
AACTCCTATGATTACAGCAGGACTAATGCCTGGAAAAATGGGTGGAAGACAGCGATGAGTCAGGAGATACTGATGAC
CCAGAAGAAGAGGAGGAAGAAGCACCAGCACCAAAATGAAGAGGAAAACCTGTGAAAAATAATGAATCTCCAAAAAAG
AAGACTTTCAAAGGAGAAAAATCTACTGCCAAATAACTCAGCACCTTTACAGAACCACAAGATGTGGAAAGAAA
GTCATTGAAGAGGAGCAACGGTTGGCAGGCATAGAAAAATCAATCCCTGGACCAGACCCCTCAGTCGCACCTTTCA
GAACAGATCCAGGCTATCAAGGAAGAAGAAGAAGAGAAAAGGAAACCAAGAGGCGAGGAGATACCAACCCAAAAG
CCAGACCAGGTGAGCAAGGGCGAGGAGGATAACATGGCCATCATCAAGGAGTTTCATGCGCTTCAAGGTGCACATG
GAGGGCTCCGTGAACGGCCACGAGTTCGAGATCGAGGGCGAGGGCGAGGGCCGCCCTACGAGGGCAGCCAGACC
GCCAAGCTGAAGGTGACCAAGGGTGGCCCCCTGCCCTTCGCTGGGACATCCTGTCCCCTCAGTTTCATGTACGGC
TCCAAGGCCTACGTGAAGCACCCCGCCGACATCCCCGACTACTTGAAGCTGTCTTCCCCGAGGGCTTCAAGTGG
GAGCGCGTGATGAACTTCGAGGACGGCGGCGTGGTGACCGTGACCCAGGACTCCTCCTGCAGGACGGCGAGTTC
ATCTACAAGGTGAAGCTGCGCGGCACCAACTTCCCCTCCGACGGCCCCGTAATGCAGAAGAAGACCATGGGCTGG
GAGGCCTCCTCCGAGCGGATGTACCCGAGGACGGCGCCCTGAAGGGCGAGATCAAGCAGAGGCTGAAGCTGAAG
GACGGCGGCCACTACGACGCTGAGGTCAAGACCACCTACAAGGCCAAGAAGCCCCGTGCAGCTGCCCGGGCGCCAC
AACGTCAACATCAAGTTGGACATCACCTCCCACAACGAGGACTACACCATCGTGGAACAGTACGAACGCGCCGAG
GGCCGCCACTCCACCGGCGGCATGGACGAGCTGTACAAGTAA



Supplemental Figure S8: Vector map of PDE3A1-T445N-mCherry

5. PDE3A1-WT-mCherry

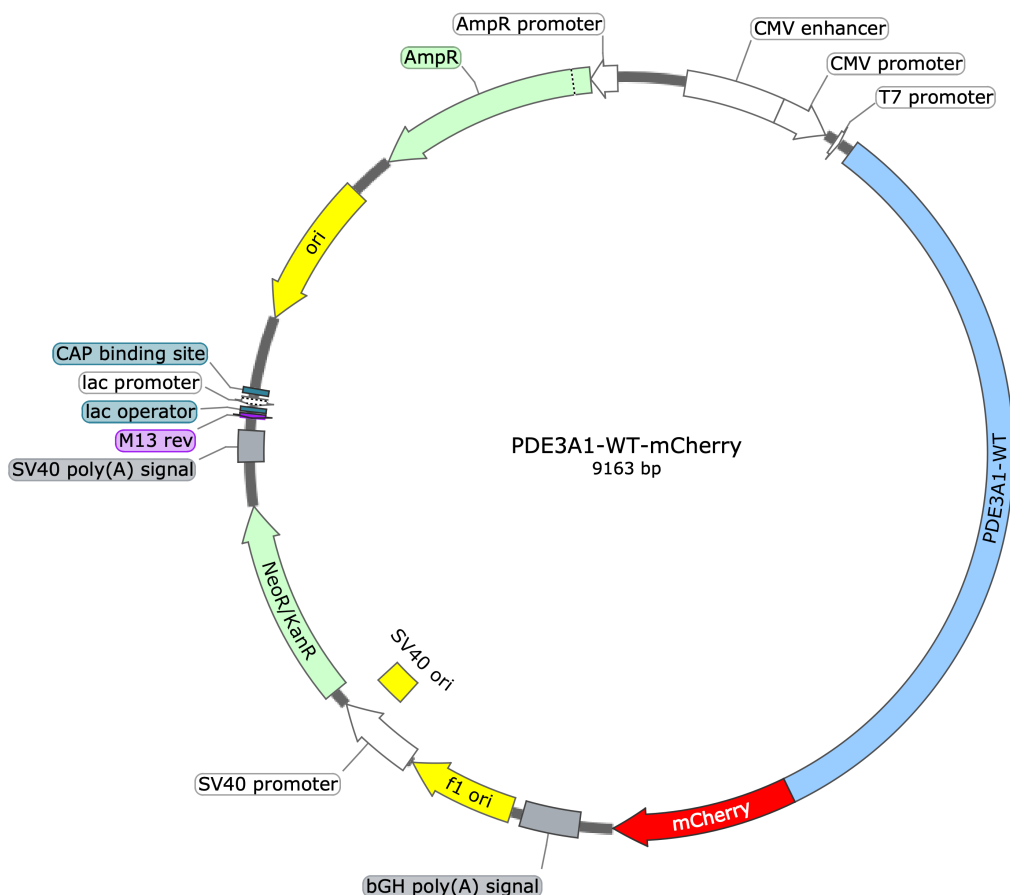
```

GTGATGCGGTTTTGGCAGTACATCAATGGGCGTGGATAGCGGTTTTGACTCACGGGGATTTC AAGTCTCCACCC
ATTGACGTCAATGGGAGTTTTGTTTTGGCACAAAATCAACGGGACTTTCCAAAATGTCGTAACAAC TCCGCCCA
TTGACGCAAATGGGCGGTAGGCGTGTACGGTGGGAGGTCTATATAAGCAGAGCTCTCTGGCTAACTAGAGA ACCC
ACTGCTTACTGGCTTATCGAAATTAATACGACTCACTATAGGGAGACCCAAGCTGGCTAGCGTTTAAACGGGCCC
TCTAGAATTGCCCTTACCGCCATGGGCTTGACCTCCTGCGCGCCGGGGTGC GCCTGCCTCTGGCTGTGCGGCTG
CTGGCCGCCTGCTGCGGGGGGAAGCGCTCGTCCAGATTGGGCTGGGCGTCGGGAGGATCACTTACTCTCACTC
CCCGCCGCGGGGGTGGTGCTCAGCTGCTTGCCCGCCGACATGGCTGGTGCTGAGGCTGAGGCTGGGCGTCCCTC
ATGATCGCCTTGACTAGCGCGGTCAGGACCGTGTCCCTCATTTCCTTAGAGAGGTTCAAGGTCGCCTGGAGACCT
TACCTGGCGTACCTGGCCGGCGTGCTGGGGATCCTCTTGGCCAGGTACGTGGAACAAAATCTTGCCGCAGTCCGCG
GAGGCGGCTCCAAGGGAGCATTGGGGTCCCAGCTGATTGCTGGGACCAAGGAAGATATCCCGGTGTTTAAGAGG
AGGAGGCGGTCCAGCTCCGTCGTGTCGCGGAGATGTCCGGCTGCAGCAGCAAGTCCCATCGGAGGACCTCCCTG
CCCTGTATAACCGAGGGAACAGCTCATGGGGCATTGAGAATGGGACCACAAACGAGGGCCAAGAGGATCACAGTCT
TCAGGAACCAGTATTACTGTGGACATCGCCGTATGGGCGAGGCCACGGCCTCATTACCGACCTCCTGGCAGAC
CCTTCTCTCCACCAAACGTGTGCACATCCTTGAGAGCCGTGAGCAACTTGCTCAGCACACAGCTCACCTTCCAG
GCCATTACAAGCCCAGAGTGAATCCCGTTACTTCGCTCAGTGAAAACATACCTGTCTGACTCTGAAGAGAGC
TCTGAAAAAGACAAGCTTGCTATTCCAAAGCGCCTGAGAAGGAGTTTGCTCCTGGCTTGTGAGACGAGTTTCT
TCCACTTGACCACCACCTCGGCCACAGGTCTACCCACCTTGAGGCTGCACCAGTACGGAGAGACCGCAGC
ACCAGCATCAAATGCAGGAAGCAGCTTCATATCTGCTGATTCCTTGAATAATCCAGTGATGATGACCTCACC
AAAAGCAGATCCTTTACTTACCTATCTATGCTATTTCTGACGTAACCATGTAAGGCTAAAAAGCAAAGTCGACCA
GGTGCCTCGCTAAAATTTACCTCTTTTCATCGCCCTGCTCCTCACCTCTCCAAGGGACTCCTGCCAGCAGCCTG
GTCAGCAAAAATTTCTGCAGTGCAGTTTCCAGAATCTGCTGACACAACCTGCCAAAACAAAGCCTAGGTTCTCACAGG
GCCTTAACTTACACTCAGAGTGCCCCAGACCTATCCCTCAAATCCTGACTCCACCTGTTATATGTAGCAGCTGT
GGCAGACCATATTTCCAAGGGAATCCTGCTGATGAGCCCTGGAGAGAAGTGGGGTAGCCACTCGGACACCAAGT
AGAACAGATGACACTGCTCAAGTTACCTCTGATTATGAAACCAATAACAACAGTGACAGCAGTGACATTGTACAG
AATGAAGATGAAACAGAGTGCTGAGAGAGCCTCTGAGGAAAGCATCGGCTTGCAGCACCTATGCTCCTGAGACC

```

Appendix

ATGATGTTTCTGGACAAACCAATTCTTGCTCCCGAACCTCTTGTCATGGATAACCTGGACTCAATTATGGAGCAG
CTAAATACTTGGAAATTTTCCAATTTTGGATTTAGTGGAAAAATATAGGAAGAAAAATGTGGCCGTATTTCTTAGTCAG
GTATCTTACAGACTTTTTGAAGACATGGGCCTGTTTGAAGCTTTTAAAAATCCAATTAGGGAATTTATGAATTTAT
TTTCATGCTTTGGAGATTGGATATAGGGATATTCCTTATCATAACAGAATCCATGCCACTGATGTTTTACATGCT
GTTTGGTATCTTACTACACAGCCTATTCCAGGCCTCTCAACTGTGATTAATGATCATGGTTCAACCAGTGATTCA
GATTCTGACAGTGGATTTACACATGGACATATGGGATATGTATTCTCAAAAACGTATAATGTGACAGATGATAAA
TACGGATGTCTGTCTGGGAATATCCCTGCCTTGGAGTTGATGGCGCTGTATGTGGCTGCAGCCATGCACGATTAT
GATCATCCAGGAAGGACTAATGCTTTCCCTGGTTGCAACTAGTGCTCCTCAGGCGGTGCTATATAACGATCGTTCA
GTTTTGGAGAATCATCACGCAGCTGCTGCATGGAATCTTTTCATGTCCCGCCAGAGTATAAATTTCTTAATTAAC
CTTGACCATGTGGAATTTAAGCATTTCCTGTTTCTTGTCAATTGAAGCAATTTTGGCCACTGACCTGAAGAAAAC
TTTGACTTCGTAGCCAAATTTAATGGCAAGGTAATGATGATGTTGGAATAGATTGGACCAATGAAAATGATCGT
CTACTGGTTTTGTCAAATGTGTATAAAGTTGGCTGATATCAATGGTCCAGCTAAATGTAAAGAACTCCATCTTCAG
TGGACAGATGGTATTGTCAATGAATTTTATGAACAGGGTGATGAAGAGGCCAGCCTTGGATTACCCATAAGCCCC
TTCATGGATCGTTCTGCTCCTCAGCTGGCCAACCTTCAGGAATCCTTCATCTCTCACATTGTGGGGCCTCTGTGC
AACTCCTATGATTACAGCAGGACTAATGCCTGGAAAATGGGTGGAAGACAGCGATGAGTCAGGAGATACTGATGAC
CCAGAAGAAGAGGAGGAAGAAGCACCAGCACCAAAATGAAGAGGAAAACCTGTGAAAAATAATGAATCTCCAAAAAAG
AAGACTTTCAAAGGAGAAAAATCTACTGCCAAATAACTCAGCACCTTTACAGAACCACAAGATGTGGAAAGAAA
GTCATTGAAGAGGAGCAACGGTTGGCAGGCATAGAAAATCAATCCCTGGACCAGACCCCTCAGTCGCACCTTTCA
GAACAGATCCAGGCTATCAAGGAAGAAGAAGAAGAGAAAAGGAAACCAAGAGGCGAGGAGATACCAACCCAAAAG
CCAGACCAGGTGAGCAAGGGCGAGGAGGATAACATGGCCATCATCAAGGAGTTTCATGCGCTTCAAGGTGCACATG
GAGGGCTCCGTGAACGGCCACGAGTTCGAGATCGAGGGCGAGGGCGAGGGCCGCCCTACGAGGGCAGCCAGACC
GCCAAGCTGAAGGTGACCAAGGGTGGCCCCCTGCCCTTCGCTGGGACATCCTGTCCCCTCAGTTTCATGTACGGC
TCCAAGGCCTACGTGAAGCACCCCGCCGACATCCCCGACTACTTGAAGCTGTCTTCCCCGAGGGCTTCAAGTGG
GAGCGCGTGATGAACTTCGAGGACGGCGGCGTGGTGACCGTGACCCAGGACTCCTCCTGCAGGACGGCGAGTTC
ATCTACAAGGTGAAGCTGCGCGGCACCAACTTCCCCTCCGACGGCCCCGTAATGCAGAAGAAGACCATGGGCTGG
GAGGCCTCCTCCGAGCGGATGTACCCGAGGACGGCGCCCTGAAGGGCGAGATCAAGCAGAGGCTGAAGCTGAAG
GACGGCGGCCACTACGACGCTGAGGTCAAGACCACCTACAAGGCCAAGAAGCCCCGTGCAGCTGCCCGGCGCCCTAC
AACGTCAACATCAAGTTGGACATCACCTCCCACAACGAGGACTACACCATCGTGGAACAGTACGAACGCGCCGAG
GGCCGCCACTCCACCGGCGGCATGGACGAGCTGTACAAGTAA



Supplemental Figure S9: Vector map of PDE3A1-WT-mCherry

6. PDE3A2- Δ 3aa-mCherry

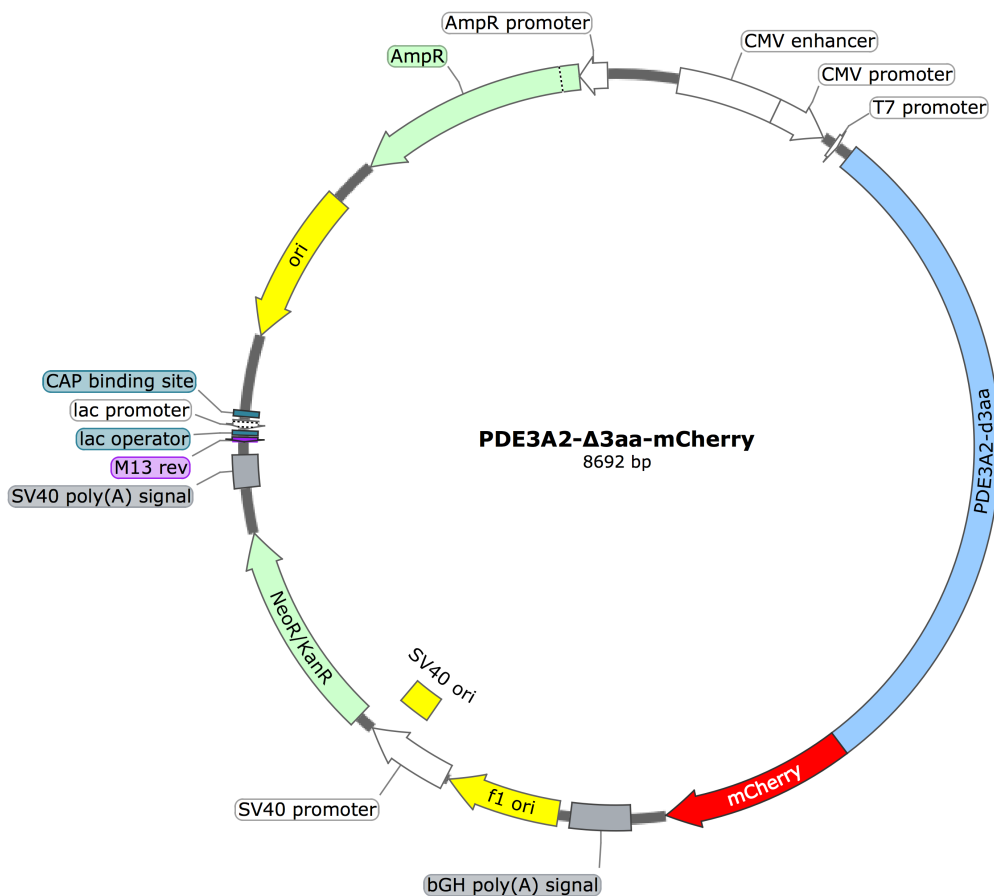
```

GTGATGCGGTTTTGGCAGTACATCAATGGGCGTGGATAGCGGTTTGACTCACGGGGATTTCCAAGTCTCCACCCC
ATTGACGTCAATGGGAGTTTTGTTTTGGCACCAAAATCAACGGGACTTTCCAAAATGTCGTAACAACCTCGCCCCA
TTGACGCAAATGGGCGGTAGGCGTGTACGGTGGGAGGTCTATATAAGCAGAGCTCTCTGGCTAACTAGAGAACC
ACTGCTTACTGGCTTATCGAAATTAATACGACTCACTATAGGGAGACCCAAAGCTGGCTAGCGTTTAAACGGGCC
TCTAGAATTGCCCTTACCGCCATGTCCGGCTGCAGCAGCAAGTCCCATCGGAGGACCTCCCTGCCCTGTATAACC
AGGGAACAGCTCATGGGGCATTGAGAATGGGACCACAAACGAGGGCCAAGAGGATCACAGTCTTCAGGAACCAGT
ATTACTGTGGACATCGCCGTGATGGGCGAGGCCACGGCCTCATTACCGACCTCCTGGCAGACCCTTCTCTTCCA
CCAAACGTGTGCACATCCTTGAGAGCCGTGAGCAACTTGCTCAGCACACAGCTCACCTTCCAGGCCATTCACAAG
CCCAGAGTGAATCCCGTTACTTCGCTCAGTGAAAACATAACCTGTTCTGACTCTGAAGAGAGCTCTGAAAAAGAC
AAGCTTGCTATTCCAAAGCGCCTGAGAAGGAGTTTGCTCCTGGCTTGTGAGACGAGTTTCTTCCACTTGGACC
ACCGCCACAGGTCTACCCACCTTGGAGCCTGCACCAGTACGGAGAGACCCGAGCACCAGCATCAAACCTGCAGGAA
GCACCTTCATCCAGTCTGATTCTTGGAAATAATCCAGTGATGATGACCCCTCACAAAAGCAGATCCTTTACTTCA
TCTTATGCTATTTCTGCAGCTAACCATGTAAGGCTAAAAAGCAAAGTCGACCAGGTGCCCTCGTAAAAATTTCA
CCTCTTTTCATCGCCCTGCTCCTCACCTCTCCAAGGGACTCCTGCCAGCAGCCTGGTCAGCAAAAATTTCTGCAGT
CAGTTTTCCAGAATCTGCTGACACAACCTGCCAAACAAAGCCTAGGTTCTCACAGGGCCTTAACTTACACTCAGAGT
GCCCCAGACCTATCCCCTCAAATCCTGACTCCACCTGTTATATGTAGCAGCTGTGGCAGACCATATTTCCAAAGG
AATCCTGCTGATGAGCCCCTGGAGAGAAGTGGGGTAGCCACTCGGACACCAAGTAGAACAGATGACACTGCTCAA
GTTACCTCTGATTATGAAACCAATAACAACAGTGACAGCAGTGACATTGTACAGAATGAAGATGAAACAGAGTGC
CTGAGAGAGCCTCTGAGGAAAGCATCGGCTTGACAGCCTATGCTCCTGAGACCATGATGTTTCTGGACAAACCA
ATTCTTGCTCCCGAACCTCTGTGATGGATAACCTGGACTCAATTATGGAGCAGCTAAATACTTGGAAATTTTCCA
ATTTTTGATTTAGTGGAAAATATAGGAAGAAAATGTGGCCGATTTCTTAGTCAGGTATCTTACAGACTTTTTGAA
GACATGGGCCTGTTTGAAGCTTTTAAATTTCCAATTAGGGAATTTATGAATTTATTTTCATGCTTTGGAGATTGGA
TATAGGGATATTCCTTATCATAACAGAATCCATGCCACTGATGTTTTACATGCTGTTTGGTATCTTACTACACAG
CCTATTCAGGCCTCTCAACTGTGATTAATGATCATGGTTCAACCAGTGATTCAGATTCCTGCAGTGGATTTACA
CATGGACATATGGGATATGTATTCTCAAAAACGTATAATGTGACAGATGATAAATACGGATGTCTGTCTGGGAAT
ATCCCTGCCTTGGAGTTGATGGCGCTGTATGTGGCTGCAGCCATGCACGATTATGATCATCCAGGAAGGACTAAT

```

```

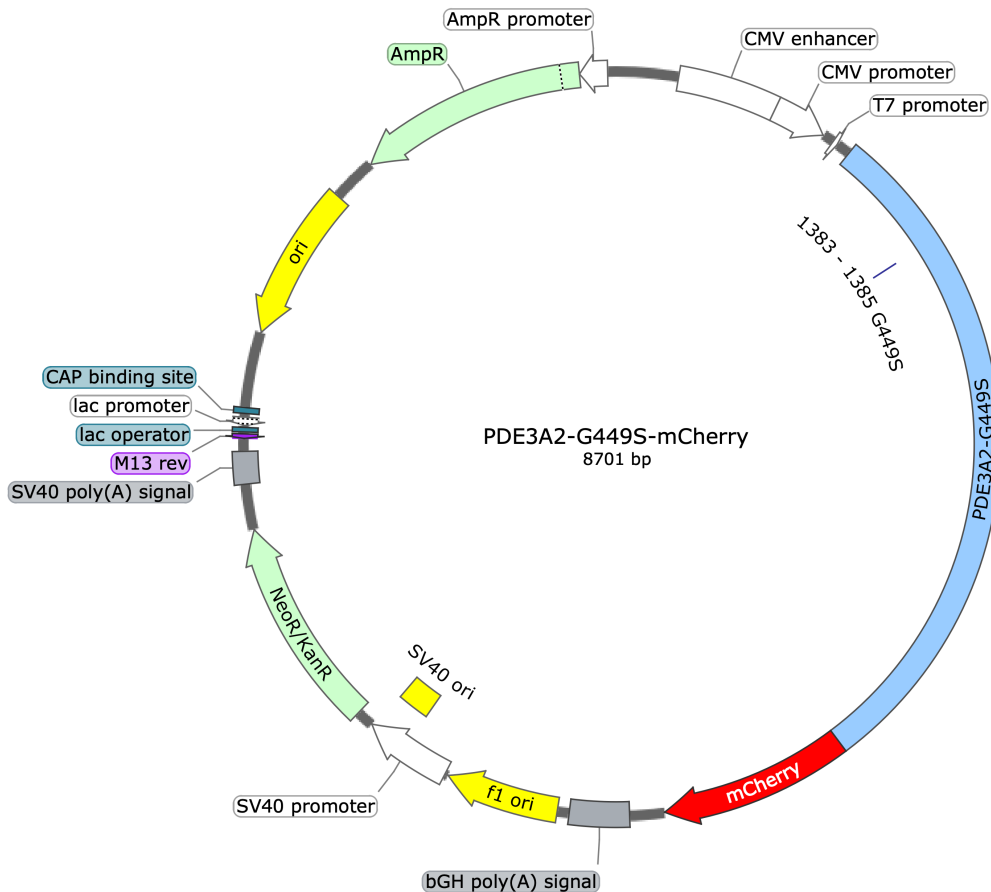
GCTTTCCTGGTTGCAACTAGTGCTCCTCAGGCGGTGCTATATAACGATCGTTCAGTTTTGGAGAATCATCACGCA
GCTGCTGCATGGAATCTTTTCATGTCCCAGGCCAGAGTATAACTTCTTAATTAACCTTGACCATGTGGAATTTAAG
CATTTCCTGTTTCTTGTTCATTGAAGCAATTTTGGCCACTGACCTGAAGAAACACTTTGACTTCGTAGCCAAATTT
AATGGCAAGGTAAATGATGATGTTGGAATAGATTGGACCAATGAAAATGATCGTCTACTGGTTTTGTCAAATGTGT
ATAAAGTTGGCTGATATCAATGGTCCAGCTAAATGTAAAGAACTCCATCTTCAGTGGACAGATGGTATTGTCAAT
GAATTTTATGAACAGGGTGATGAAGAGGCCAGCCTTGGATTACCCATAAGCCCCTTCATGGATCGTTCTGCTCCT
CAGCTGGCCAACCTTCAGGAATCCTTCATCTCTCACATTGTGGGGCCTCTGTGCAACTCCTATGATTCAGCAGGA
CTAATGCCTGGAAAATGGGTGGAAGACAGCGATGAGTCAGGAGATACTGATGACCCAGAAGAAGAGGAGGAAGAA
GCACCAGCACCAATGAAGAGGAAACCTGTGAAAATAATGAATCTCCAAAAAAGAAGACTTTCAAAAAGGAGAAAA
ATCTACTGCCAAATAACTCAGCACCTTTACAGAACCACAAGATGTGGAAGAAAAGTCATTGAAGAGGAGCAACGG
TTGGCAGGCATAGAAAATCAATCCCTGGACCAGACCCCTCAGTCGACTCTTCAGAACAGATCCAGGCTATCAAG
GAAGAAGAAGAAGAGAAAAGGAAACCAAGAGGGCAGGAGATACCAACCCAAAAGCCAGACCAGGTGAGCAAGGGC
GAGGAGGATAACATGGCCATCATCAAGGAGTTCATGCGCTTCAAGGTGCACATGGAGGGCTCCGTGAACGGCCAC
GAGTTCGAGATCGAGGGCGAGGGCGAGGGCCGCCCTACGAGGGCACCCAGACCCCAAGCTGAAGGTGACCAG
GGTGGCCCCCTGCCCTTCGCCTGGGACATCCTGTCCCCCTCAGTTCATGTACGGCTCCAAGGCCTACGTGAAGCAC
CCCGCCGACATCCCCGACTACTTGAAGCTGTCTTCCCCGAGGGCTTCAAGTGGGAGCGCGTGATGAACTTCGAG
GACGGCGGGCGTGGTGACCGTGACCCAGGACTCCTCCCTGCAGGACGGCGAGTTCATCTACAAGGTGAAGCTGCGC
GGCACCAACTTCCCCCTCCGACGGCCCCGTAATGCAGAAGAAGACCATGGGCTGGGAGGCCTCCTCCGAGCGGATG
TACCCCGAGGACGGCGCCCTGAAGGGCGAGATCAAGCAGAGGCTGAAGCTGAAGGACGGCGGCCACTACGACGCT
GAGGTCAAGACCCTACAAGGCCAAGAAGCCCGTGACGCTGCCCGGCCCTACAACGTCAACATCAAGTTGGAC
ATCACCTCCACAACGAGGACTACACCATCGTGGAACAGTACGAACCGCCGAGGGCCGCCACTCCACCGGCGGC
ATGGACGAGCTGTACAAGTAA
    
```



Supplemental Figure S10: Vector map of PDE3A2-Δ3aa-mCherry

7. PDE3A2-G449S-mCherry

GTGATGCGGTTTTGGCAGTACATCAATGGGCGTGGATAGCGGTTTGACTCACGGGGATTTCCAAGTCTCCACCCC
 ATTGACGTCAATGGGAGTTTGTTTTGGCACAAAATCAACGGGACTTTCCAAAATGTCGTAACTCCGCCCA
 TTGACGCAAATGGGCGGTAGGCGGTACGGTGGGAGGTCTATATAAGCAGAGCTCTCTGGCTAACTAGAGAACC
 ACTGCTTACTGGCTTATCGAAATTAATACGACTCACTATAGGGAGACCCAAGCTGGCTAGCGTTTAAACGGGCC
 TCTAGAATTGCCCTTACCGCCATGTCCGGCTGCAGCAGCAAGTCCCATCGGAGGACCTCCCTGCCCTGTATACCC
 AGGGAACAGCTCATGGGGCATTGAGAATGGGACCACAAACGAGGGCCAAGAGGATCACAGTCTTCAGGAACCAGT
 ATTACTGTGGACATCGCCGTATGGGCGAGGCCACGGCTCATTACCGACCTCCTGGCAGACCCTTCTCTTCCA
 CCAAACGTGTGCACATCCTTGAGAGCCGTGAGCAACTTGCTCAGCACACAGCTCACCTTCCAGGCCATTACAAG
 CCCAGAGTGAATCCCGTTACTTCGCTCAGTGAAAACCTATACCTGTTCTGACTCTGAAGAGAGCTCTGAAAAAGAC
 AAGCTTGCTATTCCAAGCGCCTGAGAAGGAGTTTGCTCCTGGCTTGTTGAGACGAGTTTCTTCCACTTGGACC
 ACCACCACCTCGGCCACAAGTCTACCCACCTTGGAGCCTGCACCAGTACGGAGAGACCCGAGCACCAGCATCAA
 CTGCAGGAAGCACCTTCATCCAGTCTGATTCTTGGAAATAATCCAGTGATGATGACCTCACCAAAAGCAGATCC
 TTTACTTCATCCTATGCTATTTCTGCAGCTAACCATGTAAAGGCTAAAAAGCAAAGTCGACCAGGTGCCCTCGCT
 AAAATTTACCTCTTTTCATCGCCCTGCTCCTCACCTCTCCAAGGGACTCCTGCCAGCAGCCTGGTCAGCAAAAT
 TCTGCAGTGCAGTTCCAGAATCTGCTGACACAACCTGCCAAACAAAGCCTAGGTTCTCACAGGGCCTTAACCTTAC
 ACTCAGAGTGCCTCCAGCACTATCCCTCAAATCCTGACTCCACTGTTATATGTAGCAGTGTGGCAGACCATAT
 TCCCAAGGGAATCCTGCTGATGAGCCCTGGAGAGAAGTGGGGTAGCCACTCGGACACCAAGTAGAACAGATGAC
 ACTGCTCAAGTTACCTCTGATTATGAAACCAATAACAACAGTGACAGCAGTGACATTTGTACAGAATGAAGATGAA
 ACAGAGTGCCTGAGAGAGCCTCTGAGGAAAGCATCGGCTTGACAGCACCTATGCTCCTGAGACCATGATGTTTCTG
 GACAAACCAATTTCTTGCTCCCGAACCTCTTGTCATGGATAACCTGGACTCAATTATGGAGCAGTAAATACTTGG
 AATTTTCCAATTTTTGATTTAGTGGAAAATATAGGAAGAAAATGTGGCCGATTCTTAGTCAGGTATCTTACAGA
 CTTTTTGAAGACATGGGCCTGTTTGAAGCTTTTAAAATCCAATTAGGGAATTTATGAATTAATTTTCATGCTTTG
 GAGATTGGATATAGGGATATTCCTTATCATAACAGAATCCATGCCACTGATGTTTACATGCTGTTTGGTATCTT
 ACTACACAGCCTATTCCAGGCCTCTCAACTGTGATTAATGATCATGGTTCAACCAGTGATTCAGATTCTGACAGT
 GGATTTACACATGGACATATGGGATATGATTCTCAAAAACGTATAATGTGACAGATGATAAATACGGATGTCTG
 TCTGGGAATATCCCTGCCTTGGAGTTGATGGCGCTGTATGTGGCTGCAGCCATGCACGATTAATGATCATCCAGGA
 AGGACTAATGCTTCTCGTTGCAACTAGTGTCTCAGGCGGTGCTATATAACGATCGTTTCAAGTTTGGAGAAAT
 CATCACGCTGCTTCCATGGAATCTTTTCATGCTCCCGCCAGAGTAACTTCTTAATTAACCTTGACCATTGTG
 GAATTTAAGCATTTCGGTTTCTTGTCAATTGAAGCAATTTTGGCCACTGACCTGAAGAAAACACTTTGACTTCGTA
 GCCAAATTTAATGGCAAGGTAATGATGATGTTGGAATAGATTTGGACCAATGAAAATGATCGTCTACTGGTTTGT
 CAAATGTGTATAAAGTTGGCTGATATCAATGGTCCAGCTAAATGTAAAAGAACTCCATCTTCAGTGGACAGATGGT
 ATTGTCAATGAATTTTATGAACAGGGTGATGAAGAGGCCAGCCTTGGATTACCATAAGCCCTTCATGGATCGT
 TCTGCTCCTCAGCTGGCCAACCTTCAGGAATCCTTCATCTCTCACATTGTGGGGCCTCTGTGCAACTCCTATGAT
 TCAGCAGGACTAATGCCTGGAAAATGGGTGGAAGACAGCGATGAGTCAGGAGATACTGATGACCAGAAGAAGAG
 GAGGAAGAAGCACCAGCACCAATGAAGAGGAAACCTGTGAAAATAATGAATCTCCAAAAAAGAAGACTTTCAA
 AGGAGAAAATCTACTGCCAAATAACTCAGCACCTTTACAGAACCACAAGATGTGGAAGAAAAGTCATTGAAGAG
 GAGCAACGGTTGGCAGGCATAGAAAATCAATCCCTGGACCAGACCCCTCAGTCGCACTCTTCAGAACAGATCCAG
 GCTATCAAGGAAGAAGAAGAAGAGAAAAGGAAACCAAGAGGCGAGGAGATACCAACCAAAAAGCCAGACCAGGTG
 AGCAAGGGCGAGGAGGATAACATGGCCATCATCAAGGAGTTCATGCGCTTCAAGGTGCACATGGAGGGCTCCGTG
 AACGGCCACGAGTTCGAGATCGAGGGCGAGGGCGAGGGCCGCCCTACGAGGGCACCCAGACCCGCAAGCTGAAG
 GTGACCAAGGGTGGCCCCCTGCCCTTCGCTGGGACATCCTGTCCCTCAGTTTTCATGTACGGCTCCAAGGCCATC
 GTGAAGCACCCCGCCGACATCCCCGACTACTTGAAGCTGTCTTCCCCGAGGGCTTCAAGTGGGAGCGCGTGATG
 AACTTCGAGGACGGCGGCGTGGTGACCGTGACCCAGGACTCCTCCCTGCAGGACGGCGAGTTCATCTACAAGGTG
 AAGCTGCGCGGCACCAACTTCCCTCCGACGGCCCCGTAATGCAGAAGAAGACCATGGGCTGGGAGGCCTCCTCC
 GAGCGGATGTACCCCGAGGACGGCGCCCTGAAGGGCGAGATCAAGCAGAGGCTGAAGCTGAAGGACGGCGGCCAC
 TACGACGCTGAGGTCAAGACCACCTACAAGGCCAAGAAGCCCGTGCAGCTGCCCGGCGCTACAACGTCAACATC
 AAGTTGGACATCACCTCCACAACGAGGACTACACCATCGTGAACAGTACGAACCGCGCCGAGGGCCGCCACTCC
 ACCGGCGGCATGGACGAGCTGTACAAGTAA



Supplemental Figure S11: Vector map of PDE3A2-G449S-mCherry

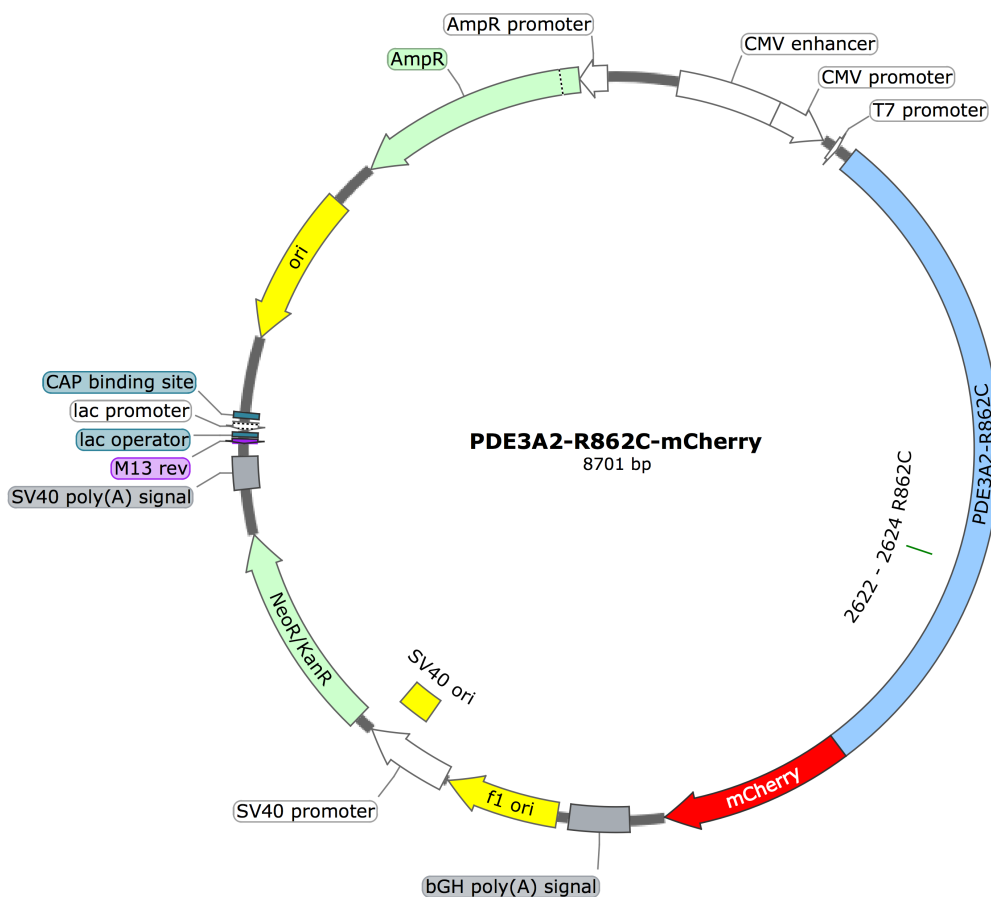
8. PDE3A2-R862C-mCherry

GTGATGCGGTTTTTGGCAGTACATCAATGGGCGTGGATAGCGGTTTGACTCACGGGGATTTCCAAGTCTCCACCCC
ATTGACGTCAATGGGAGTTTTGTTTTGGCACCAAAATCAACGGGACTTTCCAAAATGTCGTAACTCCGCCCA
TTGACGCAAATGGGCGGTAGGCGGTACGGTGGGAGGCTATATAAGCAGAGCTCTCTGGCTAACTAGAGAACCC
ACTGCTTACTGGCTTATCGAAATTAATACGACTCACTATAGGGAGACCCAAGCTGGCTAGCGTTTAAACGGGCC
TCTAGAATTGCCCTTACCGCCATGTCGGCTGCAGCAGCAAGTCCCATCGGAGGACCTCCCTGCCCCGTATACCC
AGGGAACAGCTCATGGGGCATTGAGAATGGGACCACAAACGAGGGCCAAGAGGATCACAGTCTTCAGGAACCAGT
ATTACTGTGGACATCGCCGTCATGGGCGAGGCCACGGCCTCATTACCGACCTCCTGGCAGACCCCTTCTCTTCCA
CCAAACGTGTGCACATCCTTGAGAGCCGTGAGCAACTTGCTCAGCACACAGCTCACCTTCCAGGCCATTCACAAG
CCCAGAGTGAATCCCGTTACTTCGCTCAGTGAAGTATACTGTTCTGACTCTGAAGAGAGCTCTGAAAAAGAC
AAGCTTGCTATTCCAAAGCGCTGAGAAGGAGTTTGCTCCTGGCTTGTTGAGACGAGTTTCTTCCACTTGGACC
ACCACCACCTCGGCCACAGGTCTACCCACCTTGGAGCCTGCACCAGTACGGAGAGACCCGAGCACCAGCATCAA
CTGCAGGAAGCACCTTCATCCAGTCTGATTCTTGGAAATAATCCAGTGATGATGACCCTCACCAAAAGCAGATCC
TTTACTTCATCCTATGCTATTTCTGCAGCTAACCATGTAAAGGCTAAAAAGCAAAGTCGACCAGGTGCCCTCGCT
AAAATTTACCTCTTTTCATCGCCCTGCTCCTCACCTCTCCAAGGGACTCCTGCCAGCAGCCTGGTCAGCAAAAT
TCTGACTGCAGTTCCAGAATCTGCTGACACAACCTGCCAAACAAAGCCTAGGTCTCACAGGGCCTTAACTTAC
ACTCAGAGTGCCCAACCTATCCCCTCAAATCCTGACTCCACTGTTTATATGTAGCAGCTGTGGCAGACCATAT
TCCCAAGGGAATCCTGCTGATGAGCCCTGGAGAGAAAGTGGGCTAGCCACTCGGACACCAAGTAGAACAGATGAC
ACTGCTCAAGTTACCTCTGATTATGAAACCAATAACAACAGTGACAGCAGTGACATTGTACAGAATGAAGATGAA
ACAGAGTGCCTGAGAGAGCCTCTGAGGAAAGCATCGGCTTGCAGCACCTATGCTCCTGAGACCATGATGTTTCTG
GACAAACCAATCTTGCTCCCGAACCTCTTGTCATGGATAACCTGGACTCAATTATGGAGCAGCTAAATACTTGG
AATTTTCCAATTTTTGATTTAGTGAAAATATAGGAAGAAAATGTGGCCGTAATCTTAGTCAGGTATCTTACAGA
CTTTTTGAAGACATGGGCCTGTTTGAAGCTTTTAAAATCCAATTAGGGAATTTATGAATTAATTTTCATGCTTTG
GAGATTGGATATAGGGATATTCCTTATCATAACAGAATCCATGCCACTGATGTTTTACATGCTGTTTGGTATCTT
ACTACACAGCCTATTCCAGGCCTCTCAACTGTGATTAATGATCATGGTTCAACCAGTGATTCAGATTCTGACAGT
GGATTTACACATGGACATATGGGATATGATTCTCAAAAACGTATAATGTGACAGATGATAAATACGGATGCTCTG

```

TCTGGGAATATCCCTGCCTTGGAGTTGATGGCGCTGTATGTGGCTGCAGCCATGCACGATTATGATCATCCAGGA
AGGACTAATGCTTTTCTGGTTGCAACTAGTGCTCCTCAGGCGGTGCTATATAACGATTTGTTTCAGTTTTGGGAGAA
CATCACGCAGCTGCTGCATGGAATCTTTTCATGTCCCGGCCAGAGTATAAATCTTTAATTAACCTTGACCATGTG
GAATTTAAGCATTTCGGTTTCTTGTTCATTGAAGCAATTTTGGCCACTGACCTGAAGAAAACACTTTGACTTCGTA
GCCAAATTTAATGGCAAGGTAATGATGATGTTGGAATAGATTGGACCAATGAAAATGATCGTCTACTGGTTTGT
CAAATGTGTATAAAGTTGGCTGATATCAATGGTCCAGCTAAATGTAAAGAATCCATCTTCAGTGGACAGATGGT
ATTGTCAATGAATTTTATGAACAGGGTGATGAAGAGGCCAGCCTTGGATTACCCATAAGCCCCCTCATGGATCGT
TCTGCTCCTCAGCTGGCCAACCTTCAGGAATCCTTTCATCTCTCACATTGTGGGGCCTCTGTGCAACTCCTATGAT
TCAGCAGGACTAATGCCTGGAAAATGGGTGGAAGACAGCGATGAGTCAGGAGATACTGATGACCCAGAAGAAGAG
GAGGAAGAAGCACCAGCACCAATGAAGAGGAAAACCTGTGAAAATAATGAATCTCCAAAAAAGAAGACTTTCAA
AGGAGAAAAATCTACTGCCAAATAACTCAGCACCTTTACAGAACCACAAGATGTGGAAGAAAGTCATTGAAGAG
GAGCAACGGTTGGCAGGCATAGAAAATCAATCCCTGGACCAGACCCCTCAGTCGCACTCTTCAGAACAGATCCAG
GCTATCAAGGAAGAAGAAGAAGAGAAAAGGGAAACCAAGAGGCGAGGAGATACCAACCCAAAAGCCAGACCAGGTG
AGCAAGGGCGAGGAGGATAACATGGCCATCATCAAGGAGTTCATGCGCTTCAAGGTGCACATGGAGGGCTCCGTG
AACGGCCACGAGTTCGAGATCGAGGGCGAGGGCGAGGGCCGCCCTACGAGGGCACCAGACCAGCCAAAGCTGAAG
GTGACCAAGGGTGGCCCCCTGCCCTTCGCCTGGGACATCCTGTCCCCTCAGTTCATGTACGGCTCCAAGGCCAC
GTGAAGCACCCCGCCGACATCCCCGACTACTTGAAGCTGTCTTCCCCGAGGGCTTCAAGTGGGAGCGCGTGATG
AACTTCGAGGACGGCGGCGTGGTGACCGTGACCCAGGACTCCTCCCTGCAGGACGGCGAGTTCATCTACAAGGTG
AAGCTGCGCGGCACCAACTTCCCCTCCGACGGCCCCGTAATGCAGAAGAAGACCATGGGCTGGGAGGCCTCCTCC
GAGCGGATGTACCCGAGGACGGCGCCCTGAAGGGCGAGATCAAGCAGAGGCTGAAGCTGAAGGACGGCGGCCAC
TACGACGCTGAGGTCAAGACCACCTACAAGGCCAAGAAGCCCGTGCAGCTGCCCGGCGCCTACAACGTCAACATC
AAGTTGGACATCACCTCCACAACGAGGACTACACCATCGTGAACAGTACGAACGCGCCGAGGGCCGCCACTCC
ACCGGCGGCATGGACGAGCTGTACAAGTAA

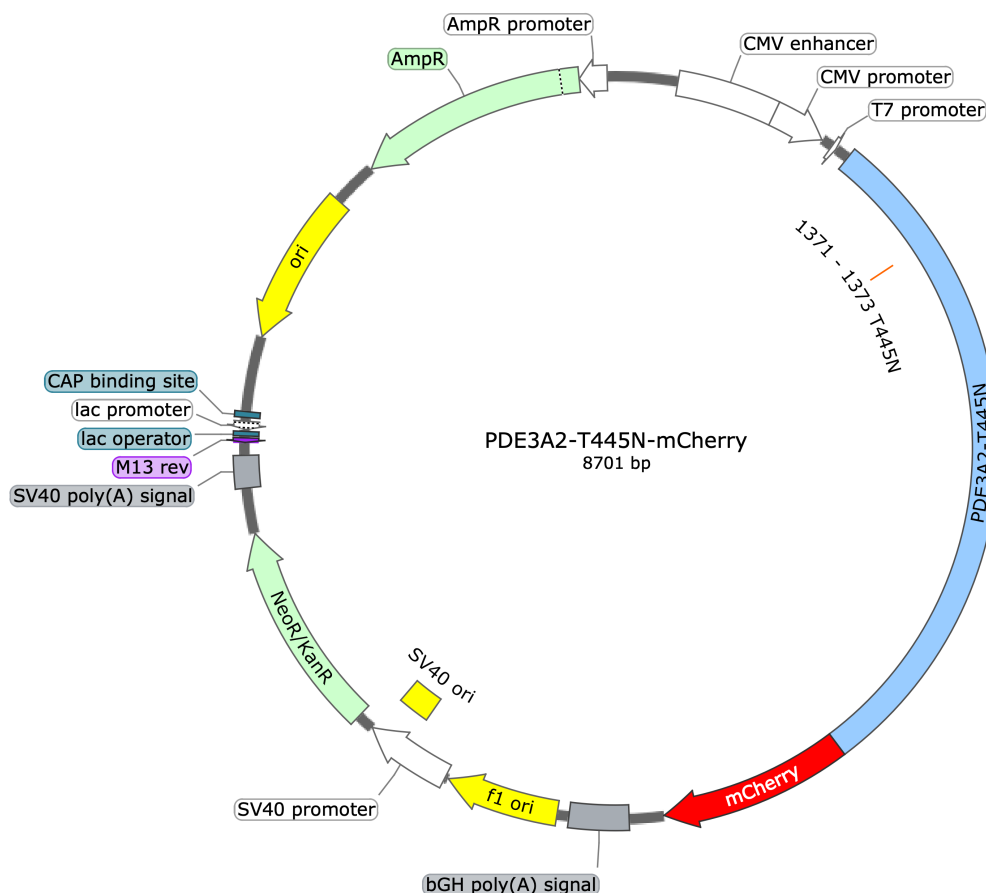
```



Supplemental Figure S12: Vector map of PDE3A2-R862C-mCherry

9. PDE3A2-T445N-mCherry

GTGATGCGGTTTTTGGCAGTACATCAATGGGCGTGGATAGCGGTTTGACTCACGGGGATTTCCAAGTCTCCACCCC
ATTGACGTCAATGGGAGTTTGTTTTGGCACCAAAATCAACGGGACTTTCCAAAATGTCGTAACTCCGCCCA
TTGACGCAAATGGGCGGTAGGCCGTGTACGGTGGGAGGTCTATATAAGCAGAGCTCTCTGGCTAAGAGAACCC
ACTGCTTACTGGCTTATCGAAATTAATACGACTCACTATAGGGAGACCCAAGCTGGCTAGCGTTTAAACGGGCC
TCTAGAATTGCCCTTACCGCCATGTCCGGCTGCAGCAGCAAGTCCCATCGGAGGACCTCCCTGCCCTGTATACCG
AGGGAACAGCTCATGGGGCATTGAGAATGGGACCACAAACGAGGGCCAAGAGGATCACAGTCTTCAGGAACCAGT
ATTACTGTGGACATCGCCGTATGGGCGAGGCCACGGCTCATTACCGACCTCCTGGCAGACCCTTCTCTTCCA
CCAAACGTGTGCACATCCTTGAGAGCCGTGAGCAACTTGCTCAGCACACAGCTCACCTTCCAGGCCATTCACAAG
CCCAGAGTGAATCCCGTTACTTCGCTCAGTGAAAACCTATACCTGTTCTGACTCTGAAGAGAGCTCTGAAAAAGAC
AAGCTTGCTATTCCAAAGCGCTGAGAAGGAGTTTGCTCCTGGCTTGTTGAGACGAGTTTCTTCCACTTGGACC
ACCACCAACTCGGCCACAGGTCTACCCACCTTGGAGCCTGCACCAGTACGGAGAGACCCGAGCACCAGCATCAA
CTGCAGGAAGCACCTTCATCCAGTCTGATTCTTGGAAATTAATCCAGTGATGATGACCTCACCAAAAGCAGATCC
TTTACTTCATCCTATGCTATTTCTGCAGCTAACCATGTAAAGGCTAAAAAGCAAAGTCGACCAGGTGCCCTCGCT
AAAATTTACCTCTTTTCATCGCCCTGCTCCTCACCTCTCCAAGGGACTCCTGCCAGCAGCCTGGTCAGCAAAAT
TCTGCAGTGCAGTTCCAGAATCTGCTGACACAACCTGCCAAACAAAGCCTAGGTTCTCACAGGGCCTTAACTTAC
ACTCAGAGTGCCTCCAGCCTATCCCCTCAAATCCTGACTCCACTGTTATATGTAGCAGTGTGGCAGACCATAT
TCCCAAGGGAATCCTGCTGATGAGCCCTGGAGAGAAGTGGGGTAGCCACTCGGACACCAAGTAGAACAGATGAC
ACTGCTCAAGTTACCTCTGATTATGAAACCAATAACAACAGTGACAGCAGTGACATTTGTACAGAATGAAGATGAA
ACAGAGTGCCTGAGAGAGCCTCTGAGGAAAGCATCGGCTTGCAGCACCTATGCTCCTGAGACCATGATGTTTCTG
GACAAACCAATTTCTTGCTCCCGAACCTCTTGTATGGATAACCTGGACTCAATTATGGAGCAGTAAATACTTGG
AATTTTCCAATTTTTGATTTAGTGGAAAATATAGGAAGAAAATGTGGCCGATTCTTAGTCAGGTATCTTACAGA
CTTTTTGAAGACATGGGCCTGTTTGAAGCTTTTAAAATCCAATTAGGGAATTTATGAATTAATTTTCATGCTTTG
GAGATTGGATATAGGGATATTCCTTATCATAACAGAATCCATGCCACTGATGTTTACATGCTGTTTGGTATCTT
ACTACACAGCCTATTCCAGGCCTCTCAACTGTGATTAATGATCATGGTTCAACCAGTGATTCAGATTCTGACAGT
GGATTTACACATGGACATATGGGATATGATTCTCAAAAACGTATAATGTGACAGATGATAAATACGGATGTCTG
TCTGGGAATATCCCTGCCTTGGAGTTGATGGCGCTGTATGTGGCTGCAGCCATGCACGATTAATGATCATCCAGGA
AGGACTAATGCTTCTCTGGTTGCAACTAGTGTCTCCTCAGGCGGTGTATATAACGATCGTTTCAAGTTTGGAGAAT
CATCACGAGCTTCTCAGTGAATCTTTTCATGCTCCCGCCAGAGTATAACTTCTTAATTAACCTTGACCATTGTG
GAATTTAAGCATTTCGGTTTCTTGTCAATTGAAGCAATTTTGGCCACTGACCTGAAGAAAACACTTTGACTTCGTA
GCCAAATTTAATGGCAAGGTAATGATGATGTTGGAATAGATTTGGACCAATGAAAATGATCGTCTACTGGTTTGT
CAAATGTGTATAAAGTTGGCTGATATCAATGGTCCAGCTAAATGTAAAAGAACTCCATCTTCAGTGGACAGATGGT
ATTGTCAATGAATTTTATGAACAGGGTGATGAAGAGGCCAGCCTTGGATTACCATAAGCCCTTCATGGATCGT
TCTGCTCCTCAGCTGGCCAACCTTCAGGAATCCTTCATCTCTCACATTGTGGGGCCTCTGTGCAACTCCTATGAT
TCAGCAGGACTAATGCCTGGAAAATGGGTGGAAGACAGCGATGAGTCAGGAGATACTGATGACCAGAAGAAGAG
GAGGAAGAAGCACCAGCACCAATGAAGAGGAAAACCTGTGAAAATAATGAATCTCCAAAAAAGAAGACTTTCAA
AGGAGAAAATCTACTGCCAAATAACTCAGCACCTCTTACAGAACCACAAGATGTGGAAGAAAAGTCATTGAAGAG
GAGCAACGGTTGGCAGGCATAGAAAATCAATCCCTGGACCAGACCCCTCAGTCGCACTCTTCAGAACAGATCCAG
GCTATCAAGGAAGAAGAAGAAGAGAAAAGGAAACCAAGAGGCGAGGAGATACCAACCCAAAAGCCAGACCAGGTG
AGCAAGGGCGAGGAGGATAACATGGCCATCATCAAGGAGTTCATGCGCTTCAAGGTGCACATGGAGGGCTCCGTG
AACGGCCACGAGTTCGAGATCGAGGGCGAGGGCGAGGGCCGCCCTACGAGGGCACCCAGACCCGCAAGCTGAAG
GTGACCAAGGGTGGCCCCCTGCCCTTCGCTGGGACATCCTGTCCCTCAGTTTTCATGTACGGCTCCAAGGCCATC
GTGAAGCACCCCGCCGACATCCCCGACTACTTGAAGCTGTCTTCCCCGAGGGCTTCAAGTGGGAGCGCGTGATG
AACTTCGAGGACGGCGGCGTGGTGACCGTGACCCAGGACTCCTCCCTGCAGGACGGCGAGTTCATCTACAAGGTG
AAGCTGCGCGGCACCAACTTCCCCTCCGACGGCCCCGTAATGCAGAAGAAGACCATGGGCTGGGAGGCCTCCTCC
GAGCGGATGTACCCCGAGGACGGCGCCCTGAAGGGCGAGATCAAGCAGAGGCTGAAGCTGAAGGACGGCGGCCAC
TACGACGCTGAGGTCAAGACCACCTACAAGGCCAAGAAGCCCGTGCAGCTGCCCGGCGCTACAACGTCAACATC
AAGTTGGACATCACCTCCACAACGAGGACTACACCATCGTGAACAGTACGAACCGCGCCGAGGGCCGCCACTCC
ACCGGCGGCATGGACGAGCTGTACAAGTAA



Supplemental Figure S13: Vector map of PDE3A2-T445N-mCherry

10. PDE3A2-WT-mCherry

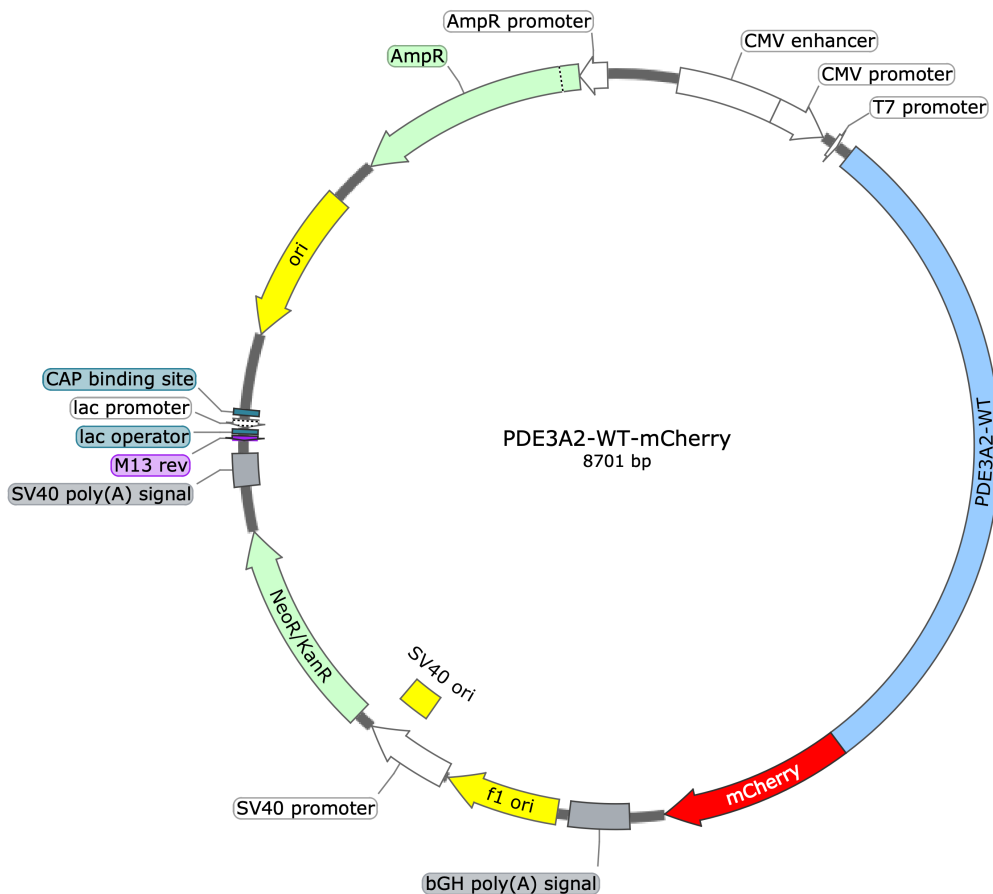
```

GTGATGCGGTTTTGGCAGTACATCAATGGGCGTGGATAGCGGTTTGACTCACGGGGATTTCCAAGTCTCCACCCC
ATTGACGTCAATGGGAGTTTGTGGCACCACAAAATCAACGGGACTTTCCAAAATGTCGTAACTCCGCCCA
TTGACGCAAATGGGCGGTAGGCGGTACGGTGGGAGGCTATATAAGCAGAGCTCTCTGGCTAACTAGAGAACCC
ACTGCTTACTGGCTTATCGAAATTAATACGACTCACTATAGGGAGACCCAAGCTGGCTAGCGTTTAAACGGGCC
TCTAGAATTGCCCTTACCGCCATGTCGGCTGCAGCAGCAAGTCCCATCGGAGGACCTCCCTGCCCTGTATACCC
AGGGAACAGCTCATGGGGCATTGAGAATGGGACCACAAACGAGGGCCAAGAGGATCACAGTCTTCAGGAACCAGT
ATTACTGTGGACATCGCCGTCATGGGCGAGGCCACGGCCTCATTACCGACCTCCTGGCAGACCCTTCTCTTCCA
CCAAACGTGTGCACATCCTTGAGAGCCGTGAGCAACTTGCTCAGCACACAGCTCACCTTCCAGGCCATTCACAAG
CCCAGAGTGAATCCCGTTACTTCGCTCAGTGAAGTATACTGTTCTGACTCTGAAGAGAGCTCTGAAAAAGAC
AAGCTTGCTATTCCAAGCGCCTGAGAAGGAGTTGCTCCTGGCTTGTTGAGACGAGTTTCTTCCACTTGGACC
ACCACCCTCGGCCACAGGTCTACCCACCTTGGAGCCTGCACCAGTACGGAGAGACCGCAGCACCAGCATCAA
CTGCAGGAAGCACCTTCATCCAGTCTGATTTCTTGAATAATCCAGTGATGATGACCCTCACCAAAAGCAGATCC
TTTACTTCATCCTATGCTATTTCTGCAGCTAACCATGTAAAGGCTAAAAAGCAAAGTCGACCAGGTGCCCTCGCT
AAAATTTACCTCTTTTATCGCCCTGCTCCTCACCTCTCCAAGGGACTCCTGCCAGCAGCCTGGTCAGCAAAAT
TCTGCAGTGCAGTTTCCAGAATCTGCTGACACAACCTGCCAAACAAAGCCTAGGTTCTCAGAGGCTTAACTTAC
ACTCAGAGTGCCCAACCTATCCCCTCAAATCCTGACTCACCTGTTATATATGTAGCAGCTGTGGCAGACCATAT
TCCCAAGGGAATCCTGCTGATGAGCCCTGGAGAGAAGTGGGGTAGCCACTCGGACACCAAGTAGAACAGATGAC
ACTGCTCAAGTTACCTCTGATTATGAAACCAATAACAACAGTGACAGCAGTGACATTTGTACAGAATGAAGATGAA
ACAGAGTGCCTGAGAGAGCCTCTGAGGAAAGCATCGGCTTGCAGCACCTATGCTCCTGAGACCATGATGTTTCTG
GACAAACCAATTTCTTGCTCCCGAACCTCTTGTTCATGGATAACCTGGACTCAATTATGGAGCAGCTAAATACTTG
AATTTTCCAATTTTTGATTTAGTGGAATAATAGGAAGAAAATGTGGCCGTAATCTTAGTCAGGTATCTTACAGA
CTTTTTGAAGACATGGGCTGTTTGAAGCTTTTAAAATCCAATTAGGGAATTTATGAATTAATTTTCATGCTTTG
GAGATTGGATATAGGGATATTCCTTATCATAACAGAATCCATGCCACTGATGTTTACATGCTGTTTGGTATCTT
ACTACACAGCCTATTCCAGGCTCTCAACTGTGATTAATGATCATGGTTCAACCAGTGATTCAGATTTCTGACAGT
GGATTTACACATGGACATATGGGATATGATTTCTCAAAAACGTATAATGTGACAGATGATAAATACGGATGCTCTG

```

```

TCTGGGAATATCCCTGCCTTGGAGTTGATGGCGCTGTATGTGGCTGCAGCCATGCACGATTATGATCATCCAGGA
AGGACTAATGCTTTCCTGGTTGCAACTAGTGCTCCTCAGGCGGTGCTATATAACGATCGTTCAGTTCCTGGAGAA
CATCACGCAGCTGCTGCATGGAATCTTTTCATGTCCCGGCCAGAGTATAAATCTTAAATTAACCTTGACCATGTG
GAATTTAAGCATTTCGGTTTCCTTGTCAATTGAAGCAATTTTGGCCACTGACCTGAAGAAAACACTTTGACTTCGTA
GCCAAATTTAATGGCAAGGTAATGATGATGTTGGAATAGATTGGACCAATGAAAATGATCGTCTACTGGTTTGT
CAAATGTGTATAAAGTTGGCTGATATCAATGGTCCAGCTAAATGTAAAGAATCCATCTTCAGTGGACAGATGGT
ATTGTCAATGAATTTATGAACAGGGTGATGAAGAGGCCAGCCTTGGATTACCCATAAGCCCCCTCATGGATCGT
TCTGCTCCTCAGCTGGCCAACCTTCAGGAATCCTTCATCTCTCACATTGTGGGGCCTCTGTGCAACTCCTATGAT
TCAGCAGGACTAATGCCTGGAAAATGGGTGGAAGACAGCGATGAGTCAGGAGATACTGATGACCCAGAAGAAGAG
GAGGAAGAAGCACCAGCACCAATGAAGAGGAAAACCTGTGAAAATAATGAATCTCCAAAAAAGAAGACTTTCAAA
AGGAGAAAAATCTACTGCCAAATAACTCAGCACCTTTACAGAACCACAAGATGTGGAAGAAAGTCATTGAAGAG
GAGCAACGGTTGGCAGGCATAGAAAATCAATCCCTGGACCAGACCCCTCAGTCGCACTCTTCAGAACAGATCCAG
GCTATCAAGGAAGAAGAAGAAGAGAAAAGGGAAACCAAGAGGCGAGGAGATACCAACCCAAAAGCCAGACCAGGTG
AGCAAGGGCGAGGAGGATAACATGGCCATCATCAAGGAGTTCATGCGCTTCAAGGTGCACATGGAGGGCTCCGTG
AACGGCCACGAGTTCGAGATCGAGGGCGAGGGCGAGGGCCGCCCTACGAGGGCACCAGACCAGCCAAAGCTGAAG
GTGACCAAGGGTGGCCCCCTGCCCTTCGCCTGGGACATCCTGTCCCCTCAGTTCATGTACGGCTCCAAGGCCAC
GTGAAGCACCCCGCCGACATCCCGGACTACTTGAAGCTGTCTTCCCGGAGGGCTTCAAGTGGGAGCGCGTGATG
AACTTCGAGGACGGCGGGCTGGTGACCGTGACCCAGGACTCCTCCCTGCAGGACGGCGAGTTCATCTACAAGGTG
AAGTGCAGCGGCCCAACTTCCCCTCCGACGGCCCCGTAATGCAGAAGAAGACCATGGGCTGGGAGGCCTCCTCC
GAGCGGATGTACCCGAGGACGGCGCCCTGAAGGGCGAGATCAAGCAGAGGCTGAAGCTGAAGGACGGCGGCCAC
TACGACGCTGAGGTCAAGACCACCTACAAGGCCAAGAAGCCCGTGCAGCTGCCCGGCGCCTACAACGTCAACATC
AAGTTGGACATCACCTCCACAACGAGGACTACACCATCGTGGAACAGTACGAACGCGCCGAGGGCCGCCACTCC
ACCGGCGGCATGGACGAGCTGTACAAGTAA
    
```



Supplemental Figure S14: Vector map of PDE3A2-WT-mCherry

11.3. Mass spectrometry results

Supplemental Table S2: All proteins identified to co-precipitate with PDE3A in the human heart via mass spectrometry

Protein names	Gene names	Intensity IgG IP	Intensity PDE3A IP	LFQ intensity IgG IP	LFQ intensity PDE3A IP	Intensity PDE3A IP/ IgG IP	LFQ intensity PDE3A IP/ IgG IP
cGMP-inhibited 3,5-cyclic phosphodiesterase A	PDE3A	1571400	1248500000	0	2226900000	794,5144457	#DIV/0!
	IGKV2D-29	3110200000	3125900000	0	749820000	1,005047907	#DIV/0!
	IGHV3-74	1937700000	1916900000	0	676490000	0,989265624	#DIV/0!
Ig lambda chain V-I region WAH		882020000	900510000	0	300300000	1,020963243	#DIV/0!
Ig kappa chain V-III region NG9		1533000000	1194700000	0	293100000	0,779321592	#DIV/0!
Ig kappa chain V-I region Wes		404320000	518080000	0	90126000	1,281361298	#DIV/0!
Protein S100-A7	S100A7	10578000	99446000	0	84095000	9,401210059	#DIV/0!
	IGHV5-51	271910000	204050000	0	61998000	0,750432128	#DIV/0!
UHRF1-binding protein 1	UHRF1BP1	371780	57215000	0	57388000	153,8947765	#DIV/0!
Complement C4-A; Complement C4 beta chain; Complement C4-A alpha chain; C4a anaphylatoxin; C4b-A; C4d-A; Complement C4 gamma chain	C4A	26982000	46261000	0	55839000	1,714513379	#DIV/0!
Superoxide dismutase; Superoxide dismutase [Mn], mitochondrial	SOD2	40637000	55950000	0	47663000	1,376824077	#DIV/0!
Protein S100-A8; Protein S100-A8, N-terminally processed	S100A8	7889700	57470000	0	36332000	7,284180641	#DIV/0!
	IGKV3D-15; IGKV3-15	104430000	146890000	0	34779000	1,406588145	#DIV/0!
Actin, alpha skeletal muscle	ACTA1	11438000	54556000	0	30449000	4,769714985	#DIV/0!
Four and a half LIM domains protein 1	FHL1	63170000	67418000	0	29490000	1,067247111	#DIV/0!
Tubulin beta-4B chain	TUBB4B	63720000	82553000	0	24796000	1,295558694	#DIV/0!
ATP synthase subunit delta, mitochondrial	ATP5D	15023000	11684000	0	23180000	0,777740797	#DIV/0!
14-3-3 protein theta	YWHAQ	2718300	61927000	0	22603000	22,78151786	#DIV/0!
14-3-3 protein sigma	SFN	6497700	17798000	0	19528000	2,739123074	#DIV/0!
Basement membrane-specific heparan sulfate proteoglycan core protein; Endorepellin; LG3 peptide	HSPG2	164610000	56334000	0	15905000	0,342227082	#DIV/0!

Appendix

Sarcalumenin	SRL	33340000	22208000	0	14611000	0,666106779	#DIV/0!
Ig lambda chain V-I region NEW; Ig lambda chain V-I region BL2		4094000	11862000	0	14503000	2,897410845	#DIV/0!
Glycogen phosphorylase, brain form	PYGB	8514800	9459400	0	13140000	1,110936252	#DIV/0!
FYN-binding protein	FYB	905780	18605000	0	12138000	20,5403078	#DIV/0!
40S ribosomal protein S10; Putative 40S ribosomal protein S10-like	RPS10; RPS10P5	798800	2076500	0	11559000	2,599524286	#DIV/0!
Involucrin	IVL	2657200	16636000	0	10686000	6,260725576	#DIV/0!
Eukaryotic initiation factor 4A-I	EIF4A1	19600000	13891000	0	10521000	0,70872449	#DIV/0!
Staphylococcal nuclease domain-containing protein 1	SND1	2955200	2805300	0	10205000	0,949275853	#DIV/0!
Up-regulated during skeletal muscle growth protein 5	USMG5	3986400	5593200	0	10068000	1,403070439	#DIV/0!
Ig kappa chain V-I region Mev		350940000	28772000	0	9904400	0,081985525	#DIV/0!
Myomesin-2	MYOM2	1269600	6548900	0	9774200	5,158238815	#DIV/0!
[Protein ADP-ribosylarginine] hydrolase-like protein 1	ADPRHL1	2690600	14322000	0	9199500	5,322976288	#DIV/0!
Short/branched chain specific acyl-CoA dehydrogenase, mitochondrial	ACADSB	5523600	12710000	0	8164200	2,301035557	#DIV/0!
HIG1 domain family member 1A, mitochondrial	HIGD1A	3067300	4382600	0	7889000	1,428813615	#DIV/0!
Transaldolase	TALDO1	2655100	10010000	0	7592800	3,770102821	#DIV/0!
Integrin beta-1	ITGB1	3404400	3008000	0	7253300	0,883562449	#DIV/0!
Heterogeneous nuclear ribonucleoprotein K	HNRNPK	2609400	3255500	0	7186400	1,247604813	#DIV/0!
Caveolin; Caveolin-1	CAV1	756430	3159900	0	7040200	4,177385878	#DIV/0!
Annexin A3; Annexin	ANXA3	2095800	9884400	0	6320300	4,716289722	#DIV/0!
Collagen alpha-1(VI) chain	COL6A1	3319700	3364100	0	6039400	1,013374703	#DIV/0!
Starch-binding domain-containing protein 1	STBD1	3846200	10387000	0	6014000	2,700587593	#DIV/0!
Clathrin heavy chain; Clathrin heavy chain 1	CLTC	1048000	2037600	0	5729900	1,944274809	#DIV/0!
Voltage-dependent anion-selective channel protein 3	VDAC3	15858000	19646000	0	5632100	1,238869971	#DIV/0!
Leucine-rich repeat-containing protein 47	LRRC47	1587700	6868300	0	5514000	4,325943188	#DIV/0!
Protein kinase C and casein kinase substrate in neurons protein 3	PACSIN3	11662000	17745000	0	5372300	1,521608643	#DIV/0!
Zyxin	ZYX	2635700	5569100	0	5339200	2,112949122	#DIV/0!
3-hydroxyisobutyrate dehydrogenase, mitochondrial	HIBADH	2548100	6902100	0	5177300	2,708724147	#DIV/0!
Proteasome-associated protein ECM29 homolog	KIAA0368; ECM29	448400	846270	0	5162000	1,887310437	#DIV/0!
WD repeat-containing protein 47	WDR47	143430	2868500	0	5115000	19,9993028	#DIV/0!
60S acidic ribosomal protein P0; 60S acidic ribosomal protein P0-like	RPLP0; RPLP0P6	1009200	4474600	0	5089300	4,433808958	#DIV/0!

Poly(rC)-binding protein 1	PCBP1	6918600	6731200	0	4856200	0,972913595	#DIV/0!
NADH-cytochrome b5 reductase 3; NADH-cytochrome b5 reductase 3 membrane-bound form; NADH-cytochrome b5 reductase 3 soluble form	CYB5R3	4956100	8219100	0	4789000	1,658380582	#DIV/0!
Tubulin beta-6 chain	TUBB6	9946900	22061000	0	4437600	2,217876926	#DIV/0!
Alpha-1-antichymotrypsin; Alpha-1-antichymotrypsin His-Pro-less	SERPINA3	5478200	12494000	0	4414700	2,280676134	#DIV/0!
6-phosphogluconate dehydrogenase, decarboxylating	PGD	1843100	5348400	0	4271000	2,901850144	#DIV/0!
Elongation factor 1-gamma	EEF1G	4254800	4171200	0	4144400	0,980351603	#DIV/0!
Fructose-bisphosphate aldolase; Fructose-bisphosphate aldolase C	ALDOC	3197800	7123400	0	3974200	2,227593971	#DIV/0!
Alpha-aminoacidic semialdehyde dehydrogenase	ALDH7A1	1723800	14288000	0	3888800	8,288664578	#DIV/0!
Ribonuclease UK114	HRSP12	1794100	2062700	0	3712900	1,149712948	#DIV/0!
High affinity immunoglobulin gamma Fc receptor I; Putative high affinity immunoglobulin gamma Fc receptor IC	FCGR1A; FCGR1C	3770500	5012000	0	3354900	1,329266676	#DIV/0!
Myozenin-2	MYOZ2	238430	7044200	0	3269400	29,54410099	#DIV/0!
Heterogeneous nuclear ribonucleoproteins A2/B1	HNRNPA2B1	8044500	2992200	0	3242100	0,371955995	#DIV/0!
Ceruloplasmin	CP	2145700	1790800	0	3214900	0,834599431	#DIV/0!
T-complex protein 1 subunit alpha	TCP1	3554300	5407700	0	3206700	1,521452888	#DIV/0!
Delta-sarcoglycan	SGCD	1652400	4745100	0	3047900	2,871641249	#DIV/0!
	IGLV3-9	6860300	15376000	0	2990200	2,241301401	#DIV/0!
Actin-related protein 2	ACTR2	917980	3832300	0	2672500	4,174709689	#DIV/0!
Adenosylhomocysteinase	AHCY	1064400	1406400	0	2608200	1,321307779	#DIV/0!
Glutaryl-CoA dehydrogenase, mitochondrial	GCDH	4089300	7112600	0	2577700	1,739319688	#DIV/0!
Titin	TTN	6793600	6285100	0	2522900	0,925150141	#DIV/0!
Eukaryotic translation initiation factor 3 subunit I	EIF3I	603090	1877700	0	2502900	3,113465652	#DIV/0!
cAMP-dependent protein kinase catalytic subunit alpha; cAMP-dependent protein kinase catalytic subunit beta	KIN27; PRKACA; PRKACB	270020	3879600	0	2492000	14,36782461	#DIV/0!
Calcium/calmodulin-dependent protein kinase type II subunit beta	CAMK2B	1208600	2988600	0	2480300	2,472778421	#DIV/0!
CDGSH iron-sulfur domain-containing protein 1	CISD1	3508200	1358100	0	2444600	0,387121601	#DIV/0!
Glutamine synthetase	GLUL	282980	3729200	0	2395300	13,17831649	#DIV/0!
40S ribosomal protein S4, X isoform;40S ribosomal protein S4, Y isoform 1	RPS4X; RPS4Y1	4554900	7059900	0	2348900	1,549957189	#DIV/0!
F-actin-capping protein subunit alpha-1	CAPZA1	992730	3547100	0	2198200	3,573076264	#DIV/0!

Appendix

F-actin-capping protein subunit beta	CAPZB	404930	3620800	0	2190100	8,941792409	#DIV/0!
Cytochrome b-c1 complex subunit Rieske, mitochondrial; Cytochrome b-c1 complex subunit 11; Putative cytochrome b-c1 complex subunit Rieske-like protein 1	UQCRFS1; UQCRFS1P1	7653900	11153000	0	2093700	1,457165628	#DIV/0!
Plasminogen activator inhibitor 1 RNA-binding protein	SERBP1	229330	1865100	0	1756000	8,132821698	#DIV/0!
28S ribosomal protein S28, mitochondrial	MRPS28	237300	783040	0	1744600	3,299789296	#DIV/0!
Sorting nexin-9	SNX9	1115500	2081600	0	1727600	1,866069027	#DIV/0!
Guanine nucleotide-binding protein subunit beta-4; Guanine nucleotide-binding protein G(I)/G(S)/G(T) subunit beta-2; Guanine nucleotide-binding protein G(I)/G(S)/G(T) subunit beta-1	GNB4; GNB2; GNB1	1154200	2699500	0	1722300	2,33884942	#DIV/0!
Calreticulin	CALR	3268300	3452900	0	1626600	1,056481963	#DIV/0!
Quinone oxidoreductase	CRYZ	1319700	2459500	0	1579800	1,86368114	#DIV/0!
NADH dehydrogenase [ubiquinone] 1 alpha subcomplex subunit 5	NDUFA5	831270	730200	0	1314400	0,878414955	#DIV/0!
Pyruvate dehydrogenase protein X component, mitochondrial	PDHX	8888600	4826600	0	1232800	0,543010148	#DIV/0!
Tubulin alpha-8 chain	TUBA8	4918500	4804500	0	1227200	0,976822202	#DIV/0!
UTP--glucose-1-phosphate uridylyltransferase	UGP2	2125800	4175500	0	1200100	1,964201712	#DIV/0!
Acetyl-coenzyme A synthetase 2-like, mitochondrial	ACSS1	2481000	1440400	0	1195400	0,58057235	#DIV/0!
Methylmalonyl-CoA mutase, mitochondrial	MUT	1196800	1371700	0	1138400	1,146139706	#DIV/0!
Envoplakin	EVPL	1575100	1725000	0	1108000	1,095168561	#DIV/0!
L-xylulose reductase	DCXR	8023300	5177300	0	971940	0,645283113	#DIV/0!
Prothrombin; Activation peptide fragment 1; Activation peptide fragment 2; Thrombin light chain; Thrombin heavy chain	F2	1782200	1147500	0	952360	0,643867131	#DIV/0!
Methylcrotonoyl-CoA carboxylase beta chain, mitochondrial	MCCC2	1872400	3696400	0	944160	1,974150822	#DIV/0!
NADH dehydrogenase [ubiquinone] flavoprotein 2, mitochondrial	NDUFV2	5730800	4677400	0	878090	0,816186222	#DIV/0!
Ras-related protein R-Ras2; Ras-related protein R-Ras	RRAS2; RRAS	3971100	3240000	0	608240	0,81589484	#DIV/0!
Protein phosphatase 1 regulatory subunit 12B	sm-M20; PPP1R12B	3493800	3152800	0	591880	0,902398535	#DIV/0!
DNA-dependent protein kinase catalytic subunit	PRKDC	4211600	19493000	0	0	4,628407256	#DIV/0!
Translational activator GCN1	GCN1L1	1017200	646420	0	0	0,635489579	#DIV/0!
Fatty acid synthase; [Acyl-carrier-protein] S-acetyltransferase;[Acyl-carrier-protein] S-	FASN	4560500	5649400	0	0	1,238767679	#DIV/0!

malonyltransferase;3-oxoacyl-[acyl-carrier-protein] synthase;3-oxoacyl-[acyl-carrier-protein] reductase;3-hydroxyacyl-[acyl-carrier-protein] dehydratase; Enoyl-[acyl-carrier-protein] reductase; Oleoyl-[acyl-carrier-protein] hydrolase								
Keratin, type I cytoskeletal 18	KRT18	62711000	422150	0	0	0,006731674	#DIV/0!	
Polyadenylate-binding protein; Polyadenylate-binding protein 1	PABPC1	3823600	945510	0	0	0,247282666	#DIV/0!	
ATP-dependent RNA helicase DDX3X; ATP-dependent RNA helicase DDX3Y	DDX3X; DDX3Y	211530	314330	0	0	1,485983076	#DIV/0!	
Protein disulfide-isomerase A4	PDIA4	177550	17140000	0	0	96,53618699	#DIV/0!	
T-complex protein 1 subunit zeta	CCT6A	2456100	5516100	0	0	2,245877611	#DIV/0!	
T-complex protein 1 subunit delta	CCT4	178390	1698100	0	0	9,519031336	#DIV/0!	
Nucleolin	NCL	1891500	944720	0	0	0,499455459	#DIV/0!	
Neutral alpha-glucosidase AB	GANAB	1312200	970870	0	0	0,739879592	#DIV/0!	
RuvB-like 2	RUVBL2	1127100	69455	0	0	0,061622749	#DIV/0!	
ATP-dependent RNA helicase A	DHX9	897930	4443400	0	0	4,948492644	#DIV/0!	
Proliferation-associated protein 2G4	PA2G4	2880800	2814900	0	0	0,97712441	#DIV/0!	
Exportin-2	CSE1L	1284900	474020	0	0	0,368915869	#DIV/0!	
Lysine--tRNA ligase	KARS	266240	1257600	0	0	4,723557692	#DIV/0!	
Matrin-3	MATR3	304740	70187	0	0	0,230317648	#DIV/0!	
Heat shock protein 75 kDa, mitochondrial	TRAP1	5039800	1472900	0	0	0,292253661	#DIV/0!	
T-complex protein 1 subunit epsilon	CCT5	878800	2679500	0	0	3,049044151	#DIV/0!	
Emerin	EMD	385340	554400	0	0	1,438729434	#DIV/0!	
X-ray repair cross-complementing protein 6	XRCC6	1080600	366890	0	0	0,339524338	#DIV/0!	
Tropomyosin alpha-4 chain	TPM4	229150	5068900	0	0	22,12044512	#DIV/0!	
Structural maintenance of chromosomes protein 2	SMC2	9723800	7530300	0	0	0,774419466	#DIV/0!	
Carbonyl reductase [NADPH] 1	CBR1	1798600	758010	0	0	0,421444457	#DIV/0!	
Phosphoglycerate mutase 1; Probable phosphoglycerate mutase 4	PGAM1; PGAM4	658880	14684000	0	0	22,28630403	#DIV/0!	
Ras-related protein Rab-14	RAB14	3051400	2192900	0	0	0,718653733	#DIV/0!	
Proteasome subunit beta type-5	PSMB5	647510	289220	0	0	0,446664916	#DIV/0!	
Microtubule-associated protein; Microtubule-associated protein 4	MAP4	1105300	2674000	0	0	2,419252692	#DIV/0!	
S-adenosylmethionine synthase isoform type-2	MAT2A	234890	299520	0	0	1,27515007	#DIV/0!	
Glucose-6-phosphate 1-dehydrogenase	G6PD	1190500	344090	0	0	0,289029819	#DIV/0!	

Appendix

Ras-related protein Rab-1A	RAB1A	2550400	1546300	0	0	0,606297051	#DIV/0!
Proteasome subunit alpha type-3	PSMA3	3745600	6481500	0	0	1,730430372	#DIV/0!
Tubulin-specific chaperone A	TBCA	666030	221660	0	0	0,332807831	#DIV/0!
Peptidyl-prolyl cis-trans isomerase B	PPIB	1788600	1694100	0	0	0,947165381	#DIV/0!
Transgelin-2	TAGLN2	5180900	886390	0	0	0,171088035	#DIV/0!
Rab GDP dissociation inhibitor beta	GDI2	1226700	1344400	0	0	1,09594848	#DIV/0!
RuvB-like 1	RUVBL1	18306000	12022000	0	0	0,656724571	#DIV/0!
Stathmin	STMN1	17770	309780	0	0	17,43275183	#DIV/0!
Sodium/potassium-transporting ATPase subunit alpha-1; Sodium/potassium-transporting ATPase subunit alpha-3	ATP1A1; ATP1A3	1714800	1700400	0	0	0,991602519	#DIV/0!
Guanine nucleotide-binding protein subunit beta-2-like 1; Guanine nucleotide-binding protein subunit beta-2-like 1, N-terminally processed	GNB2L1	2492600	1343200	0	0	0,53887507	#DIV/0!
Proteasome subunit alpha type-5	PSMA5	2321700	2389800	0	0	1,029331955	#DIV/0!
40S ribosomal protein S8	RPS8	3490500	2606000	0	0	0,746597909	#DIV/0!
Ras-related protein Rab-11A; Ras-related protein Rab-11B	RAB11A; RAB11B	1371500	2176400	0	0	1,586875684	#DIV/0!
Enoyl-CoA hydratase, mitochondrial	ECHS1	9381200	9392400	0	0	1,001193877	#DIV/0!
Replication factor C subunit 4	RFC4	555870	836670	0	0	1,505154083	#DIV/0!
Adenylyl cyclase-associated protein 1; Adenylyl cyclase-associated protein	CAP1	162340	7763800	0	0	47,82431933	#DIV/0!
Basigin	BSG	2136100	2131400	0	0	0,997799728	#DIV/0!
Protein phosphatase inhibitor 2; Protein phosphatase inhibitor 2-like protein 3	PPP1R2; PPP1R2P3	7416700	9241900	0	0	1,246093276	#DIV/0!
Lysosome-associated membrane glycoprotein 1	LAMP1	1425700	533260	0	0	0,374033808	#DIV/0!
Protein disulfide-isomerase A6	PDIA6	1477700	4066800	0	0	2,752114773	#DIV/0!
Myosin regulatory light chain 12A; Myosin regulatory light chain 12B; Myosin regulatory light polypeptide 9	MYL12A; MYL12B; MYL9	1080600	521500	0	0	0,482602258	#DIV/0!
Protein SET; Protein SETSIP	SET; SETSIP	607840	741860	0	0	1,220485654	#DIV/0!
Sterol O-acyltransferase 1	SOAT1	6452400	13645000	0	0	2,114717005	#DIV/0!
Proteasome subunit alpha type-1; Proteasome subunit alpha type	PSMA1	11149000	2130100	0	0	0,191057494	#DIV/0!
Protein S100-A11; Protein S100-A11, N-terminally processed	S100A11	4275700	3609900	0	0	0,844282807	#DIV/0!
Thioredoxin	TXN	12698000	11138000	0	0	0,877146007	#DIV/0!

Proteasome subunit alpha type-7; Proteasome subunit alpha type-7-like	PSMA7; PSMA8	3316500	3829400	0	0	1,154650987	#DIV/0!
Calumenin	CALU	2552300	1400600	0	0	0,548759942	#DIV/0!
Adenylate kinase 2, mitochondrial; Adenylate kinase 2, mitochondrial; Adenylate kinase 2, mitochondrial, N-terminally processed	AK2	553760	2995900	0	0	5,410105461	#DIV/0!
DnaJ homolog subfamily B member 11	DNAJB11	1054700	1924800	0	0	1,824973926	#DIV/0!
Glutathione S-transferase Mu 3	GSTM3	1231200	1588600	0	0	1,2902859	#DIV/0!
Heterogeneous nuclear ribonucleoprotein F; Heterogeneous nuclear ribonucleoprotein F, N-terminally processed	HNRNPF	25842000	30210000	0	0	1,169027165	#DIV/0!
Proteasome subunit beta type-6; Proteasome subunit beta type	PSMB6	3874400	448840	0	0	0,115847615	#DIV/0!
Radixin	RDX	101850	142760	0	0	1,401669121	#DIV/0!
Polyadenylate-binding protein; Polyadenylate-binding protein 4	PABPC4	870820	87475	0	0	0,100451299	#DIV/0!
60S acidic ribosomal protein P2	RPLP2	7052700	1373300	0	0	0,194719753	#DIV/0!
Glucosidase 2 subunit beta	PRKCSH	2234400	527980	0	0	0,236296097	#DIV/0!
Transcription elongation factor B polypeptide 2	TCEB2	558690	415680	0	0	0,744026204	#DIV/0!
60S ribosomal protein L7	RPL7	7217300	967760	0	0	0,134088925	#DIV/0!
Glutathione synthetase	GSS	705560	8505400	0	0	12,0548217	#DIV/0!
Calmodulin	CALM2; CALM1; CALM3	3410100	7351200	0	0	2,155713909	#DIV/0!
40S ribosomal protein S14	RPS14	2282100	2937000	0	0	1,286972525	#DIV/0!
40S ribosomal protein S25	RPS25	5836000	1853400	0	0	0,317580535	#DIV/0!
Receptor expression-enhancing protein 5; Receptor expression-enhancing protein	REEP5	1186900	563080	0	0	0,474412335	#DIV/0!
Gamma-glutamylcyclotransferase	GGCT	4900300	3380000	0	0	0,689753689	#DIV/0!
ADP-ribosylation factor 1; ADP-ribosylation factor 3	ARF1; ARF3	3404900	1135000	0	0	0,333343123	#DIV/0!
Phosphoglucomutase-1	PGM1	3080100	2530800	0	0	0,821661634	#DIV/0!
ATP-dependent DNA helicase Q1	RECQL	14698000	9493500	0	0	0,645904205	#DIV/0!
Serpin B5	SERPINB5	8759200	4977900	0	0	0,568305325	#DIV/0!
Plakophilin-2	PKP2	671730	1938600	0	0	2,885980974	#DIV/0!
Galectin-3; Galectin	LGALS3	1261600	3882200	0	0	3,077203551	#DIV/0!
RNA-binding protein EWS	EWSR1	1203100	1078300	0	0	0,896267974	#DIV/0!
Proteasome subunit beta type-2	PSMB2	613650	809300	0	0	1,318829952	#DIV/0!

Appendix

Histone H2A type 1-J; Histone H2A type 1-H; Histone H2A.J; Histone H2A type 2-C; Histone H2A type 2-A; Histone H2A type 1-D; Histone H2A type 1; Histone H2A	HIST1H2AJ; HIST1H2AH; H2AFJ; HIST2H2AC; HIST2H2AA3; HIST1H2AD; HIST1H2AG	120250000	22643000	0	0	0,188299376	#DIV/0!
Proteasome subunit beta type-7	PSMB7	353850	563780	0	0	1,593273986	#DIV/0!
Glutathione S-transferase kappa 1	GSTK1	6134100	2396300	0	0	0,390652255	#DIV/0!
60S ribosomal protein L15; Ribosomal protein L15	RPL15	12328000	158890	0	0	0,012888546	#DIV/0!
Lipoma-preferred partner	LPP	350240	311300	0	0	0,888819095	#DIV/0!
60S ribosomal protein L22	RPL22	6862400	5923000	0	0	0,863109116	#DIV/0!
F-actin-capping protein subunit alpha-2	CAPZA2	320170	2049000	0	0	6,399725146	#DIV/0!
Dihydropyrimidinase-related protein 2; Dihydropyrimidinase-related protein 1	DPYSL2; CRMP1	2262400	6464800	0	0	2,857496464	#DIV/0!
Mitochondrial import inner membrane translocase subunit TIM50	TIMM50	678890	1393400	0	0	2,052467999	#DIV/0!
Phenylalanine--tRNA ligase alpha subunit	FARSA	1075800	1449000	0	0	1,346904629	#DIV/0!
Proteasome subunit alpha type; Proteasome subunit alpha type-4	PSMA4	1041100	2186700	0	0	2,100374604	#DIV/0!
Nucleolar and coiled-body phosphoprotein 1	NOLC1	394050	250390	0	0	0,635426976	#DIV/0!
Superoxide dismutase [Cu-Zn]	SOD1	2257000	7125400	0	0	3,157022596	#DIV/0!
Proteasome activator complex subunit 3	PSME3	1905800	335620	0	0	0,176104523	#DIV/0!
40S ribosomal protein S20	RPS20	2386100	2189000	0	0	0,917396589	#DIV/0!
Mitotic checkpoint protein BUB3	BUB3	3783100	3575200	0	0	0,945045069	#DIV/0!
Parathymosin	PTMS	939230	806340	0	0	0,85851176	#DIV/0!
Lon protease homolog, mitochondrial	LONP1	1273600	706780	0	0	0,554946608	#DIV/0!
Prostaglandin E synthase 2; Prostaglandin E synthase 2 truncated form	PTGES2	5768900	4394800	0	0	0,76180901	#DIV/0!
ADP/ATP translocase 3; ADP/ATP translocase 3, N-terminally processed	SLC25A6	3813800	2772900	0	0	0,727070114	#DIV/0!
Calpain small subunit 1	CAPNS1	498140	610780	0	0	1,226121171	#DIV/0!
Beta-2-microglobulin; Beta-2-microglobulin form pl 5.3	B2M	231340	242950	0	0	1,050185874	#DIV/0!
Coiled-coil-helix-coiled-coil-helix domain-containing protein 2; Putative coiled-coil-helix-coiled-coil-helix domain-containing protein CHCHD2P9, mitochondrial	CHCHD2; CHCHD2P9	614780	975790	0	0	1,587218192	#DIV/0!
Alpha-centractin; Beta-centractin	ACTR1A; ACTR1B	1041400	724400	0	0	0,695602074	#DIV/0!

Protein NipSnap homolog 1	NIPSNAP1	301520	327730	0	0	1,08692624	#DIV/0!
Casein kinase II subunit beta	CSNK2B; CSNK2B- LY6G5B- 1181;CSNK2B -LY6G5B--991	529400	1117300	0	0	2,110502456	#DIV/0!
Transmembrane protein 109	TMEM109	1177300	1377700	0	0	1,170219995	#DIV/0!
Transcription factor A, mitochondrial	TFAM	8005900	17399000	0	0	2,173272212	#DIV/0!
Target of rapamycin complex subunit LST8	MLST8	816610	2062100	0	0	2,525195626	#DIV/0!
Serine/threonine-protein phosphatase 2A 65 kDa regulatory subunit A alpha isoform	PPP2R1A	691080	793330	0	0	1,147956821	#DIV/0!
Bifunctional methylenetetrahydrofolate dehydrogenase/cyclohydrolase, mitochondrial;NAD-dependent methylenetetrahydrofolate dehydrogenase;Methenyltetrahydrofolate cyclohydrolase	MTHFD2	2941600	3912300	0	0	1,329990481	#DIV/0!
Copine-3; Copine-8; Copine-5; Copine-2; Copine-9; Copine-4; Copine-6; Copine-7	CPNE3; CPNE8; CPNE5; CPNE2; CPNE9; CPNE4; CPNE6; CPNE7	777730	535170	0	0	0,688117984	#DIV/0!
40S ribosomal protein S2	RPS2	3726200	742550	0	0	0,199278085	#DIV/0!
Exportin-7	XPO7	234000	80395	0	0	0,343568376	#DIV/0!
Guanine nucleotide-binding protein G(k) subunit alpha; Guanine nucleotide-binding protein G(t) subunit alpha-1; Guanine nucleotide-binding protein G(i) subunit alpha-1; Guanine nucleotide-binding protein G(t) subunit alpha-2; Guanine nucleotide-binding protein G(o) subunit alpha; Guanine nucleotide-binding protein G(t) subunit alpha-3; Guanine nucleotide-binding protein G(i) subunit alpha-2; Guanine nucleotide-binding protein G(s) subunit alpha isoforms short; Guanine nucleotide-binding protein G(olf) subunit alpha; Guanine nucleotide-binding protein G(s) subunit alpha isoforms XLas	GNAI3; GNAO1; GNAS; GNAT2; GNAT1; GNAI1; GNAT3; GNAI2; GNAL	893410	1420800	0	0	1,590311279	#DIV/0!
Inositol monophosphatase 1	IMPA1	2433800	2120500	0	0	0,871271263	#DIV/0!
Annexin A7	ANXA7	336600	995770	0	0	2,958318479	#DIV/0!

Appendix

40S ribosomal protein S13	RPS13	545420	1490800	0	0	2,733306443	#DIV/0!
Calnexin	CANX	2415500	4195700	0	0	1,736990271	#DIV/0!
Single-stranded DNA-binding protein, mitochondrial	SSBP1	1282900	645040	0	0	0,502798347	#DIV/0!
Galectin-7	LGALS7	17552000	41013000	0	0	2,336656791	#DIV/0!
Eukaryotic translation elongation factor 1 epsilon-1	EEF1E1; EEF1E1- BLOC1S5	643300	608780	0	0	0,946339189	#DIV/0!
Glutathione reductase, mitochondrial	GSR	2000500	2093000	0	0	1,04623844	#DIV/0!
Cytoplasmic dynein 1 heavy chain 1	DYNC1H1	2424900	1193400	0	0	0,492144006	#DIV/0!
MARCKS-related protein	MARCKSL1	495780	387200	0	0	0,780991569	#DIV/0!
26S proteasome non-ATPase regulatory subunit 4	PSMD4	10537000	9549200	0	0	0,906254152	#DIV/0!
Sorcin	SRI	441310	227820	0	0	0,516235753	#DIV/0!
Ubiquitin-conjugating enzyme E2 variant 1	UBE2V1; UBE2V2; TMEM189- UBE2V1	13936000	1263400	0	0	0,09065729	#DIV/0!
Septin-2	37500	561020	1076000	0	0	1,917935189	#DIV/0!
Keratin, type II cytoskeletal 6B	KRT6B	11664000	4269000	0	0	0,365997942	#DIV/0!
Uridine-cytidine kinase 2	UCK2	3066700	2560900	0	0	0,83506701	#DIV/0!
Heat shock-related 70 kDa protein 2	HSPA2	1046500	1011300	0	0	0,966364071	#DIV/0!
Macrophage migration inhibitory factor	MIF	2671800	2929500	0	0	1,09645183	#DIV/0!
ADP-ribosylation factor 4	ARF4	1598400	607590	0	0	0,380123874	#DIV/0!
Hsp90 co-chaperone Cdc37; Hsp90 co-chaperone Cdc37, N-terminally processed	CDC37	410810	361640	0	0	0,880309632	#DIV/0!
Glycogen debranching enzyme;4-alpha-glucanotransferase; Amylo-alpha-1,6-glucosidase	AGL	1393700	1542900	0	0	1,107053168	#DIV/0!
Myoferlin	MYOF	957540	6546200	0	0	6,836476805	#DIV/0!
Protein POF1B	POF1B	1172800	3202900	0	0	2,730985675	#DIV/0!
Serine hydroxymethyltransferase, cytosolic	SHMT1	6610200	341620	0	0	0,051680736	#DIV/0!
BTB/POZ domain-containing protein KCTD3; SH3KBP1-binding protein 1	KCTD3; SHKBP1	1234400	993310	0	0	0,804690538	#DIV/0!
Titin	TTN	5168400	70197000	4936000	100400000	13,5819596	20,34035656
Serpin B3	SERPINB3	14037000	152360000	9954100	120750000	10,85417112	12,13067982
Alpha-actinin-2	ACTN2	3822500	60922000	8277400	96312000	15,93773708	11,63553773
Desmin	DES	19940000	82937000	3185700	22132000	4,159327984	6,947295728
Myosin-7; Myosin-6	MYH7; MYH6	264870000	1125600000	315320000	1806700000	4,249631895	5,729734873

Creatine kinase S-type, mitochondrial	CKMT2	177670000	257050000	49983000	212250000	1,446783362	4,246443791
Creatine kinase M-type; Creatine kinase M-type, N-terminally processed	CKM	245490000	288380000	78308000	331010000	1,174711801	4,227026613
Fatty acid-binding protein, epidermal	FABP5	37191000	57468000	25586000	107340000	1,545212551	4,195263034
Annexin A5; Annexin	ANXA5	8530700	25738000	3838800	15809000	3,017102934	4,118214025
2,4-dienoyl-CoA reductase, mitochondrial	DECR1	79213000	198610000	23647000	95929000	2,50729047	4,056709096
Troponin T, cardiac muscle	HNTN1; TNNT2	7996600	75380000	10831000	41371000	9,426506265	3,81968424
Poly [ADP-ribose] polymerase 1	PARP1	7597600	14016000	6607800	23006000	1,844793093	3,481642907
Myosin light chain 3	MYL3	77500000	249890000	18223000	61347000	3,224387097	3,366459968
Myosin-9	MYH9	1435800	8278500	1752700	5683400	5,765775178	3,242654191
Medium-chain specific acyl-CoA dehydrogenase, mitochondrial	ACADM	65959000	117510000	26796000	85867000	1,781561273	3,204470817
		75646000	119650000	22605000	72094000	1,581709542	3,189294404
Glycogenin-1	GYG1	12186000	17331000	8747900	26402000	1,42220581	3,018095772
Ig kappa chain C region	IGKC	1701700000	13795000000	2242800000	6738100000	0,810659928	3,004324951
Cytochrome c oxidase subunit 5A, mitochondrial	COX5A	17976000	16833000	12548000	36418000	0,93641522	2,902295186
14-3-3 protein gamma; 14-3-3 protein gamma, N-terminally processed	YWHAG	16057000	43966000	3526100	9838100	2,738120446	2,790079691
Leukocyte elastase inhibitor	SERPINB1	3261700	7429600	1860000	5152400	2,277830579	2,770107527
Prohibitin-2	PHB2	6232200	22917000	4043300	10721000	3,677192645	2,651547004
Voltage-dependent anion-selective channel protein 2	VDAC2	19326000	28448000	7236100	18849000	1,472006623	2,604856207
Decorin	DCN	2552300	3611500	2644900	6654100	1,414998237	2,515822904
14-3-3 protein beta/alpha; 14-3-3 protein beta/alpha, N-terminally processed	YWHAB	3880200	9326400	2482600	6038800	2,403587444	2,432449851
Calmodulin-like protein 3	CALML3	6054200	21102000	5950400	14169000	3,485514188	2,381184458
Myosin-binding protein C, cardiac-type	MYBPC3	25619000	81882000	51445000	122420000	3,196143487	2,37962873
Ryanodine receptor 2	RYR2	4998500	5669500	3594200	8538100	1,134240272	2,375521674
14-3-3 protein epsilon	YWHAE	51446000	158990000	10161000	23206000	3,090424912	2,283830332
Collagen alpha-2(VI) chain	COL6A2	4325200	5887600	4745900	10595000	1,361231851	2,232453275
L-lactate dehydrogenase A chain	LDHA	4937500	15821000	5754400	12526000	3,204253165	2,176769081
Galectin-3-binding protein	LGALS3BP	4777400	14340000	4549700	9780900	3,001632687	2,149790096
Isocitrate dehydrogenase [NAD] subunit, mitochondrial; Isocitrate dehydrogenase [NAD] subunit beta, mitochondrial	IDH3B	8707300	21985000	6549700	13892000	2,524892906	2,121013176

Appendix

Troponin I, cardiac muscle	TNNI3	46561000	96985000	17954000	37812000	2,082966431	2,106048791
Pyruvate dehydrogenase E1 component subunit beta, mitochondrial	PDHB	43305000	70694000	25160000	52309000	1,632467383	2,079054054
Hexokinase-1	HK1	17440000	37806000	29123000	60502000	2,167775229	2,077464547
Cadherin-13	CDH13	11485000	12187000	10391000	21155000	1,061123204	2,035896449
Malate dehydrogenase, mitochondrial; Malate dehydrogenase	MDH2	166480000	289600000	100860000	204390000	1,739548294	2,026472338
Aspartate aminotransferase, cytoplasmic	GOT1	31137000	39308000	15428000	31221000	1,262420914	2,023658284
Sarcoplasmic/endoplasmic reticulum calcium ATPase 2; Sarcoplasmic/endoplasmic reticulum calcium ATPase 1	ATP2A2; ATP2A1	71085000	78944000	65700000	129140000	1,110557783	1,965601218
Polymerase I and transcript release factor	PTRF	25416000	40327000	9938800	18903000	1,586677683	1,901939872
Vinculin	VCL	26986000	28921000	29520000	55668000	1,071703846	1,885772358
Electron transfer flavoprotein subunit alpha, mitochondrial	ETFFA	20731000	46787000	12491000	23323000	2,256861705	1,867184373
Hemoglobin subunit alpha	HBA1; HBA2	170220000	188950000	156520000	290270000	1,110034074	1,854523384
	IGLV6-57	26715000	52566000	10177000	18816000	1,967658619	1,848874914
Malate dehydrogenase, cytoplasmic; Malate dehydrogenase	MDH1	40607000	89468000	36947000	67882000	2,203265447	1,837280429
Alpha-actinin-4	ACTN4	7551300	17036000	11415000	20838000	2,256035385	1,825492773
Trifunctional enzyme subunit beta, mitochondrial;3-ketoacyl-CoA thiolase	HADHB	235730000	319860000	69205000	125940000	1,356891359	1,819810707
Dermcidin; Survival-promoting peptide;DCD-1	DCD	180440000	190310000	178070000	323990000	1,054699623	1,819453024
Immunoglobulin lambda-like polypeptide 5; Ig lambda-1 chain C regions	IGLL5; IGLC1	1950400000	1027000000	293790000	522480000	0,526558655	1,778413152
	IGHV3-49	244860000	117390000	39648000	68633000	0,47941681	1,731058313
Isocitrate dehydrogenase [NAD] subunit alpha, mitochondrial	IDH3A	12221000	26386000	9908100	17126000	2,159070452	1,728484775
DNA damage-binding protein 1	DDB1	6932000	8855900	10682000	18448000	1,27753895	1,727017412
Delta (3,5)-Delta (2,4)-dienoyl-CoA isomerase, mitochondrial	ECH1	35658000	79402000	11575000	19862000	2,226765382	1,715939525
Glyceraldehyde-3-phosphate dehydrogenase	GAPDH	76243000	122280000	45119000	77312000	1,603819367	1,713513154
Ig gamma-1 chain C region	IGHG1	3759500000 0	39700000000	15472000000	2595300000 0	1,055991488	1,67741727
L-lactate dehydrogenase B chain; L-lactate dehydrogenase	LDHB	100520000	149020000	68843000	109830000	1,482491047	1,595369173
Tropomyosin alpha-1 chain	TPM1	56280000	282880000	73196000	116640000	5,026297086	1,593529701
ES1 protein homolog, mitochondrial	C21orf33	21423000	32912000	4101200	6535100	1,536292769	1,593460451

Tubulin alpha-4A chain	TUBA4A	116440000	154730000	49317000	78528000	1,328838887	1,592310968
Protein disulfide-isomerase	P4HB	10459000	22871000	4779800	7610900	2,186729133	1,592305117
Ig gamma-2 chain C region	IGHG2	1175100000	2303400000	576470000	893000000	1,960173602	1,549083213
Electron transfer flavoprotein subunit beta	ETFB	46042000	67650000	11157000	17263000	1,469310629	1,547279735
Bifunctional glutamate/proline--tRNA ligase; Glutamate--tRNA ligase; Proline--tRNA ligase	EPRS	834840	2474300	3135800	4844700	2,963801447	1,544964602
Cysteine and glycine-rich protein 3	CSRP3	101550000	108640000	58776000	89510000	1,069817824	1,522900504
Voltage-dependent anion-selective channel protein 1	VDAC1	25982000	77519000	22482000	34101000	2,983565545	1,516813451
Endoplasmic reticulum chaperone protein	HSP90B1	10593000	10675000	11562000	17466000	1,007740961	1,510638298
Cystatin-A; Cystatin-A, N-terminally processed	CSTA	68978000	94958000	56091000	84444000	1,376641828	1,505482163
3-ketoacyl-CoA thiolase, mitochondrial	ACAA2	28625000	23475000	18730000	28059000	0,820087336	1,49807795
Triosephosphate isomerase	TPI1	62434000	70160000	16558000	24800000	1,123746676	1,497765431
Importin-5	IPO5	3964200	1784500	4855300	7220300	0,450153877	1,487096575
Heat shock 70 kDa protein 1B; Heat shock 70 kDa protein 1A	HSPA1B; HSPA1A	135830000	179060000	107070000	158580000	1,318265479	1,481087139
ATP synthase subunit O, mitochondrial	ATP5O	68701000	101660000	19658000	28615000	1,479745564	1,455641469
Creatine kinase B-type	CKB	19925000	26729000	12295000	17876000	1,341480552	1,453924359
Heat shock 70 kDa protein 4	HSPA4	2570000	2591200	5665300	8211500	1,008249027	1,449437806
Neuroblast differentiation-associated protein AHNAK	AHNAK	21771000	16467000	10624000	15012000	0,756373157	1,413027108
Heat shock cognate 71 kDa protein	HSPA8	247720000	260810000	197940000	278410000	1,052841918	1,406537335
Myoglobin	MB	320570000	409600000	404980000	564700000	1,277724054	1,394389846
AFG3-like protein 2	AFG3L2	14137000	20146000	11265000	15649000	1,425054821	1,389169996
Fructose-bisphosphate aldolase; Fructose- bisphosphate aldolase A	ALDOA	81401000	110630000	61645000	84442000	1,359074213	1,369811015
Exportin-1	XPO1	3702600	2387700	5653800	7691500	0,644871172	1,360412466
Annexin A2; Annexin; Putative annexin A2-like protein	ANXA2; ANXA2P2	97594000	119360000	74565000	101320000	1,223026006	1,358814457
Pyruvate dehydrogenase E1 component subunit alpha, somatic form, mitochondrial	PDHA1	26910000	30359000	19300000	25922000	1,128167967	1,343108808
14-3-3 protein zeta/delta	YWHAZ	27454000	55655000	14511000	19414000	2,02720915	1,337881607
Aspartate aminotransferase, mitochondrial	GOT2	149700000	171080000	126880000	168940000	1,142818971	1,331494325
Calmodulin-like protein 5	CALML5	24389000	62241000	37537000	49887000	2,552011153	1,329008711
Lan C-like protein 1	LANCL1	3279000	5146700	2109700	2766000	1,569594389	1,311086884
Phosphoglycerate kinase 1	PGK1	19059000	27977000	17888000	23214000	1,467915421	1,297741503
	IGKV1-8; IGKV1-9;	49482000	374900000	48379000	62669000	7,576492462	1,295376093

Appendix

	IGKV1-27						
Alpha-1-antitrypsin; Short peptide from AAT	SERPINA1	141700000	178990000	62306000	80627000	1,263161609	1,294048727
Annexin A6; Annexin	ANXA6	15805000	17729000	11433000	14728000	1,121733629	1,288200822
Puromycin-sensitive aminopeptidase; Puromycin-sensitive aminopeptidase-like protein	NPEPPS; NPEPPSL1	8560900	7699500	12230000	15561000	0,899379738	1,272363042
Filamin-C	FLNC	1004900000	1539500000	2500800000	3173700000	1,531993233	1,269073896
Serpin B12	SERPINB12	19465000	25121000	19909000	25179000	1,290572823	1,264704405
Cathepsin D; Cathepsin D light chain; Cathepsin D heavy chain	CTSD	15740000	21270000	9032700	11417000	1,35133418	1,263963156
Cytochrome b-c1 complex subunit 2, mitochondrial	UQCRC2	28932000	47655000	11092000	13881000	1,647138117	1,251442481
Enoyl-CoA delta isomerase 1, mitochondrial	ECI1; DCI	16638000	15590000	3356700	4187600	0,93701166	1,247534781
Transitional endoplasmic reticulum ATPase	VCP	32193000	18683000	23894000	29591000	0,580343553	1,238428057
Protein-glutamine gamma-glutamyltransferase 2	TGM2	42703000	50342000	35897000	44232000	1,178886729	1,232192105
Putative elongation factor 1-alpha-like 3; Elongation factor 1-alpha 1; Elongation factor 1-alpha	EEF1A1P5; EEF1A1	109620000	93550000	50103000	61697000	0,853402664	1,231403309
Fatty acid-binding protein, heart	FABP3	163340000	127360000	175760000	216190000	0,779723277	1,230029586
Alpha-enolase; Enolase	ENO1	50516000	60129000	22335000	27191000	1,190296144	1,217416611
Ig gamma-3 chain C region	IGHG3	1404700000	67879000	212870000	259070000	0,048322774	1,21703387
Peptidyl-prolyl cis-trans isomerase A; Peptidyl-prolyl cis-trans isomerase A, N-terminally processed; Peptidyl-prolyl cis-trans isomerase	PPIA	9418000	8609300	12863000	15461000	0,914132512	1,201974656
Lumican	LUM	6557600	7153800	5091700	6086000	1,090917409	1,195278591
Eukaryotic translation initiation factor 2 subunit 1	EIF2S1	4662600	10994000	5691000	6774500	2,357911895	1,190388332
Fibronectin; Anastellin; Ugl-Y1; Ugl-Y2; Ugl-Y3	FN1	167300000	238630000	240110000	281410000	1,426359833	1,172004498
Ig lambda-2 chain C regions; Ig lambda-3 chain C regions; Ig lambda-6 chain C region	IGLC3; IGLC2; IGLC6	1964200000	2990200000	826640000	967530000	1,522350066	1,17043695
Aldehyde dehydrogenase, mitochondrial	ALDH2	16635000	14265000	9204800	10748000	0,857529306	1,16765166
ATP-dependent 6-phosphofructokinase, muscle type	PFKM	62328000	66028000	46640000	54104000	1,059363368	1,160034305
Actin, alpha cardiac muscle 1; Actin, aortic smooth muscle; Actin, gamma-enteric smooth muscle	ACTC1; ACTA2; ACTG2	1084000000	1678400000	841100000	970780000	1,548339483	1,154179051
Acetyl-CoA acetyltransferase, mitochondrial	ACAT1	188370000	290920000	157350000	180690000	1,544407284	1,148331745
60 kDa heat shock protein, mitochondrial	HSPD1	56348000	95378000	28018000	32027000	1,692659899	1,143086587
Filamin-A	FLNA	97748000	112440000	342490000	388010000	1,150304866	1,13290899
Hemoglobin subunit beta; LVV-hemorphin-7; Spinorphin	HBB	394460000	325570000	375500000	423850000	0,825356183	1,128761651
PDZ and LIM domain protein 1	PDLIM1	4179700	4408400	2750700	3093600	1,054716846	1,124659178

Caspase-14; Caspase-14 subunit p17, mature form; Caspase-14 subunit p10, mature form; Caspase-14 subunit p20, intermediate form; Caspase-14 subunit p8, intermediate form	CASP14	32817000	31635000	29026000	32557000	0,963982082	1,121649556
Moesin	MSN	14178000	15433000	12192000	13664000	1,088517421	1,120734908
NADH dehydrogenase [ubiquinone] iron-sulfur protein 3, mitochondrial	NDUFS3	12533000	15939000	2647900	2952200	1,271762547	1,114921258
Beta-enolase; Enolase	ENO3	42043000	40093000	12586000	14021000	0,953618914	1,114015573
Very long-chain specific acyl-CoA dehydrogenase, mitochondrial	ACADVL	122010000	120590000	77740000	86594000	0,98836161	1,113892462
Protein NipSnap homolog 2	GBAS	29778000	33488000	9822200	10888000	1,124588622	1,108509295
2-oxoglutarate dehydrogenase, mitochondrial	OGDH	36000000	28054000	44165000	48682000	0,779277778	1,102275558
Heat shock protein HSP 90-alpha	HSP90AA1	14678000	17220000	18158000	20011000	1,173184358	1,102048684
Dynamin-like 120 kDa protein, mitochondrial; Dynamin-like 120 kDa protein, form S1	OPA1	5304800	4107700	3610600	3956900	0,77433645	1,095912037
Glycogen [starch] synthase, muscle	GYS1	159480000	12834000	414490000	444340000	0,008047404	1,072016213
Cytochrome c	CYCS	24411000	25036000	29938000	31778000	1,025603212	1,061460351
Serotransferrin	TF	64290000	64868000	54088000	57098000	1,008990512	1,055650052
Keratin, type II cytoskeletal 2 epidermal	KRT2	1028100000	928900000	770500000	8042900000	0,903511332	1,043854640
Calsequestrin-2	CASQ2	87201000	119970000	30765000	32088000	1,375786975	1,043003413
NAD(P) transhydrogenase, mitochondrial	NNT	49786000	35197000	62065000	64495000	0,706965814	1,039152501
Fibrinogen alpha chain; Fibrinopeptide A; Fibrinogen alpha chain	FGA	25037000	22830000	17390000	18013000	0,911850461	1,035825187
	IGLV3-10	369740000	404800000	103340000	106330000	1,094823389	1,028933617
Lipocalin-1	LCN1	71344000	30475000	54514000	55484000	0,427155752	1,017793594
Prohibitin	PHB	14492000	12785000	4429000	4492000	0,882210875	1,01422443
Elongation factor 2	EEF2	12393000	8154500	8073500	8187800	0,657992415	1,014157429
78 kDa glucose-regulated protein	HSPA5	388190000	331120000	227020000	229650000	0,852984363	1,011584882
Glucose-6-phosphate isomerase	GPI	38989000	33931000	12753000	12898000	0,870271102	1,011369874
40S ribosomal protein S3	RPS3	22748000	33600000	15350000	15477000	1,477052928	1,008273616
Protein-L-isoaspartate O-methyltransferase; Protein-L-isoaspartate (D-aspartate) O-methyltransferase	PCMT1	67289000	91638000	23385000	23523000	1,361857064	1,005901219
Hydroxysteroid dehydrogenase-like protein 2	HSDL2	31161000	35457000	9167700	9098200	1,137864638	0,992419036
ATP synthase subunit beta, mitochondrial; ATP synthase subunit beta	ATP5B	1214300000	1272100000	378310000	374460000	1,04759944	0,989823161
Leucine-rich PPR motif-containing protein,	LRPPRC	58695000	32202000	74158000	72847000	0,548632763	0,98232153

Appendix

mitochondrial							
Desmocollin-1	DSC1	29606000	20298000	17029000	16724000	0,685604269	0,982089377
Complement C3; Complement C3 beta chain; C3-beta-c; Complement C3 alpha chain; C3a anaphylatoxin; Acylation stimulating protein; Complement C3b alpha chain; Complement C3c alpha chain fragment 1; Complement C3dg fragment; Complement C3g fragment; Complement C3d fragment; Complement C3f fragment; Complement C3c alpha chain fragment 2	C3	40282000	34288000	41668000	40806000	0,851199047	0,979312662
Fumarate hydratase, mitochondrial	FH	53461000	47935000	22644000	22034000	0,89663493	0,973061297
Ketimine reductase mu-crystallin	CRYM	9683300	13630000	8003000	7780600	1,407577995	0,972210421
Isocitrate dehydrogenase [NADP], mitochondrial	IDH2	203430000	205700000	135490000	131520000	1,01115863	0,970698945
Succinyl-CoA:3-ketoacid coenzyme A transferase 1, mitochondrial	OXCT1	86580000	72318000	30458000	29543000	0,835273735	0,969958632
Atypical kinase ADCK3, mitochondrial	ADCK3	9422500	6898800	4653600	4503000	0,732162377	0,967637958
Heat shock protein HSP 90-beta	HSP90AB1	98553000	95407000	97164000	93924000	0,96807809	0,966654316
Short-chain specific acyl-CoA dehydrogenase, mitochondrial	ACADS	3070400	4899400	2739700	2636000	1,595687858	0,96214914
Cofilin-1	CFL1	21561000	15348000	34043000	32694000	0,711840824	0,960373645
Heat shock protein beta-1	HSPB1	242480000	439320000	75097000	72095000	1,811778291	0,960025034
Trifunctional enzyme subunit alpha, mitochondrial; Long-chain enoyl-CoA hydratase; Long chain 3-hydroxyacyl-CoA dehydrogenase	HADHA	422060000	397310000	351900000	335280000	0,941359048	0,952770673
Apolipoprotein A-I; Proapolipoprotein A-I; Truncated apolipoprotein A-I	APOA1	13375000	11411000	3475500	3274900	0,853158879	0,942281686
Suprabasin	SBSN	7635800	5851600	5297400	4948600	0,766337515	0,934156379
Collagen alpha-3(VI) chain	COL6A3	5282000	8561600	12649000	11805000	1,620901174	0,933275358
Pyruvate kinase PKM; Pyruvate kinase	PKM	63240000	78779000	48796000	45479000	1,245714738	0,932023117
Dihydrolipoyl dehydrogenase; Dihydrolipoyl dehydrogenase, mitochondrial	DLD	142940000	101870000	46880000	43325000	0,712676648	0,924168089
40S ribosomal protein S19	RPS19	3402100	4332800	11910000	10966000	1,273566327	0,920738875
Protein deglycase DJ-1	PARK7	19471000	11173000	5864800	5373500	0,573827744	0,916229027
Prelamin-A/C; Lamin-A/C	LMNA	36186000	45889000	37251000	34108000	1,268142376	0,915626426
ATP-dependent 6-phosphofructokinase, platelet type	PFKP	6065100	5164800	5793600	5303700	0,851560568	0,915441176
ATP synthase subunit alpha, mitochondrial	ATP5A1	1173800000	972240000	443030000	402750000	0,828284205	0,909080649
NADH-ubiquinone oxidoreductase 75 kDa subunit, mitochondrial	NDUFS1	32279000	17238000	15553000	14080000	0,534031414	0,905291584

Serpin B6	SERPINB6	6033000	15940000	7457800	6688000	2,642134925	0,896779211
60S ribosomal protein L11	RPL11	2664800	3266400	8136700	7291000	1,225758031	0,896063515
Peroxisomal multifunctional enzyme type 2;(3R)-hydroxyacyl-CoA dehydrogenase; Enoyl-CoA hydratase 2	HSD17B4	1185600000	1040200000	925360000	828880000	0,877361673	0,895737875
Laminin subunit gamma-1	LAMC1	2867900	4968900	7264100	6491300	1,732591792	0,893613799
Profilin-1	PFN1	9960400	5838000	8712400	7777100	0,586121039	0,892647261
LIM domain-binding protein 3	LDB3	103270000	73913000	86871000	77403000	0,715725767	0,891010809
Elongation factor 1-delta	EEF1D	7139900	6946900	6583100	5848600	0,972968809	0,888426425
Stress-70 protein, mitochondrial	HSPA9	650390000	537370000	507010000	444140000	0,826227341	0,875998501
Aconitate hydratase, mitochondrial	ACO2	225230000	206430000	255370000	218880000	0,91652977	0,857109292
	IGHV3-72	3662200000	2828700000	1304700000	1116700000	0,772404566	0,855905572
Ig lambda chain V-III region LOI		1793300000	1711700000	568980000	486460000	0,954497295	0,85496854
Long-chain-fatty-acid--CoA ligase 1	ACSL1	29291000	16768000	23719000	20216000	0,572462531	0,852312492
Ezrin	EZR	8286500	9465000	7668100	6475000	1,142219272	0,84440735
ADP/ATP translocase 2; ADP/ATP translocase 2, N-terminally processed	SLC25A5	32877000	23284000	7375500	6218100	0,70821547	0,843075046
Peroxiredoxin-2	PRDX2	75202000	87310000	33334000	27890000	1,161006356	0,836683266
Desmoglein-1	DSG1	106880000	78979000	97139000	80527000	0,738950225	0,828987327
Ig alpha-1 chain C region	IGHA1	591910000	888530000	449910000	370090000	1,501123482	0,82258674
Carnitine O-palmitoyltransferase 1, muscle isoform	CPT1B	19426000	12953000	15500000	12728000	0,666786781	0,82116129
Keratin, type II cytoskeletal 1	KRT1	4353400000	3492900000	3730700000	3026000000	0,802338402	0,811107835
Alpha-2-macroglobulin	A2M	12760000	16639000	29369000	23816000	1,303996865	0,810923082
Annexin A11	ANXA11	6886600	8593100	2457300	1985900	1,247800076	0,808163431
Histone H1.4; Histone H1.3	HIST1H1E; HIST1H1D	22276000	11333000	15378000	12414000	0,508753816	0,807257121
Ubiquitin-60S ribosomal protein L40; Ubiquitin;60S ribosomal protein L40; Ubiquitin-40S ribosomal protein S27a; Ubiquitin; 40S ribosomal protein S27a; Polyubiquitin-B; Ubiquitin; Polyubiquitin-C; Ubiquitin	UBB; RPS27A; UBC; UBA52	110510000	88540000	110450000	89132000	0,801194462	0,806989588
Succinate dehydrogenase [ubiquinone] flavoprotein subunit, mitochondrial	SDHA	26852000	20815000	19470000	15689000	0,775175034	0,805803801
Ig kappa chain V-I region Gal		118660000	93587000	24526000	19762000	0,788698803	0,805757156
Bleomycin hydrolase	BLMH	11239000	2683900	6314200	5078100	0,238802385	0,804234899
Citrate synthase; Citrate synthase, mitochondrial	CS	50179000	52447000	32785000	26241000	1,04519819	0,800396523

Appendix

40S ribosomal protein S18	RPS18	10462000	5084900	11920000	9537100	0,486035175	0,800092282
Zinc-alpha-2-glycoprotein	AZGP1	23883000	24894000	24677000	19527000	1,042331365	0,791303643
Protein S100-A9	S100A9	143530000	175870000	139220000	109700000	1,225318749	0,7879615
Desmoplakin	DSP	327150000	282630000	287830000	225670000	0,863915635	0,78403919
T-complex protein 1 subunit beta	CCT2	60912000	6533600	3058900	2395600	0,107262937	0,783157344
Histone H4	HIST1H4A	139770000	63030000	86971000	67860000	0,450955141	0,780260087
T-complex protein 1 subunit gamma	CCT3	3487000	2021400	5046400	3936800	0,579696014	0,780120482
Ig mu chain C region	IGHM	1358200000	1075400000	896460000	693830000	0,791783243	0,77396649
Thioredoxin-dependent peroxide reductase, mitochondrial	PRDX3	52737000	54870000	13989000	10822000	1,040445987	0,773607835
	IGHV3-15	232220000	167030000	80643000	61971000	0,719274826	0,768460995
Lactotransferrin; Lactoferricin-H; Kaliocin-1; Lactoferroxin-A; Lactoferroxin-B; Lactoferroxin-C	LTF	17289000	18209000	13121000	9981700	1,053213026	0,760742321
Tubulin beta chain	TUBB	215240000	155740000	83811000	63656000	0,723564393	0,75951844
Peroxioredoxin-1	PRDX1	28408000	27035000	11424000	8630400	0,951668544	0,755462185
3-hydroxyacyl-CoA dehydrogenase type-2	HSD17B10	11937000	6417700	2247900	1694400	0,537630896	0,753770186
Arginase-1	ARG1	50977000	43053000	48961000	36890000	0,844557349	0,753456833
Ig heavy chain V-III region JON; Ig heavy chain V-III region WEA; Ig heavy chain V-III region TRO	IGHV3-21	2023000000	1779500000	701140000	523840000	0,879634207	0,747126109
ADP/ATP translocase 1	SLC25A4	485640000	393330000	141790000	105040000	0,809920929	0,74081388
Succinyl-CoA ligase [GDP-forming] subunit beta, mitochondrial	SUCLG2	11229000	23319000	12723000	9380000	2,076676463	0,737247505
Hydroxyacyl-coenzyme A dehydrogenase, mitochondrial	HADH	24689000	34468000	22062000	16164000	1,396087326	0,732662497
Cofilin-2	CFL2	6641400	3527100	11922000	8513000	0,531077785	0,714058044
Acetyltransferase component of pyruvate dehydrogenase complex; Dihydrolipoyllysine-residue acetyltransferase component of pyruvate dehydrogenase complex, mitochondrial	DLAT	22651000	23789000	24429000	16727000	1,050240607	0,684718982
Myosin regulatory light chain 2, ventricular/cardiac muscle isoform	MYL2	61360000	51343000	50770000	33322000	0,836750326	0,65633248
Serum deprivation-response protein	SDPR	4263100	3154600	3338700	2183200	0,73997795	0,653907209
Elongation factor Tu, mitochondrial	TUFM	69527000	59788000	28994000	18914000	0,859924921	0,652341864
Dihydrolipoyllysine-residue succinyltransferase component of 2-oxoglutarate dehydrogenase complex, mitochondrial	DLST	62238000	32893000	18318000	11893000	0,528503487	0,649252102
Apoptosis-inducing factor 1, mitochondrial	AIFM1	32136000	18500000	24963000	15653000	0,575678367	0,627048031

Calcium-binding mitochondrial carrier protein Aralar1	SLC25A12	52818000	28160000	40277000	24498000	0,533151577	0,608237952
Peroxioredoxin-6	PRDX6	21617000	14879000	7887100	4792000	0,688300874	0,607574394
Heat shock protein beta-6	HSPB6	35534000	17749000	61565000	37310000	0,499493443	0,606026151
Annexin A1; Annexin	ANXA1	153550000	188190000	205800000	123860000	1,225594269	0,601846453
Junction plakoglobin	JUP	187970000	117630000	149520000	88391000	0,62579135	0,591165062
Alpha-crystallin B chain	CRYAB	328900000	201540000	119560000	69155000	0,612769839	0,578412513
Protein-glutamine gamma-glutamyltransferase K	TGM1	15616000	11731000	12849000	7354400	0,751216701	0,572371391
Adenylate kinase isoenzyme 1	AK1	23906000	22025000	5173100	2938600	0,921316824	0,568053972
40S ribosomal protein SA	RPSA	17217000	5485300	13410000	7128600	0,318597897	0,531588367
Cytochrome c oxidase subunit 4 isoform 1, mitochondrial	COX4I1	10433000	3119800	13325000	7014400	0,299031918	0,526409006
E3 ubiquitin-protein ligase TRIM21	TRIM21	89627000	29928000	19513000	9709000	0,333917235	0,497565725
Succinyl-CoA ligase [ADP-forming] subunit beta, mitochondrial	SUCLA2	31723000	22338000	25282000	12410000	0,704157867	0,490863065
Prolactin-inducible protein	PIP	38518000	13824000	39844000	17147000	0,358897139	0,430353378
Lipoamide acyltransferase component of branched-chain alpha-keto acid dehydrogenase complex, mitochondrial	DBT	9178300	3985800	2700100	1141400	0,434263426	0,422725084
Mitochondrial 2-oxoglutarate/malate carrier protein	SLC25A11	46038000	25036000	16305000	5502000	0,543811634	0,337442502
Vimentin	VIM	172610000	40166000	39591000	12744000	0,23269799	0,321891339
Transketolase	TKT	3463800	828930	6086400	1849300	0,239312316	0,303841351
MICOS complex subunit MIC60	IMMT	102230000	56780000	92521000	28027000	0,555414262	0,302925822
Plakophilin-1	PKP1	69903000	11540000	39850000	10313000	0,165085905	0,258795483
PDZ and LIM domain protein 5	PDLIM5	28604000	24800000	27881000	6959700	0,867011607	0,249621606
Four and a half LIM domains protein 2	FHL2	433730000	236500000	115620000	25796000	0,545270099	0,223110189
Protein-glutamine gamma-glutamyltransferase E; Protein-glutamine gamma-glutamyltransferase E 50 kDa catalytic chain; Protein-glutamine gamma-glutamyltransferase E 27 kDa non-catalytic chain	TGM3	35996000	7413100	32420000	5521100	0,205942327	0,170299198
Ig kappa chain V-IV region	IGKV4-1	312710000	135570000	82514000	12138000	0,433532666	0,14710231
Plectin	PLEC	3522800	1359300	6430600	0	0,38585784	0
General transcription factor II-I	GTF2I	1478300	1010300	11736000	0	0,683420145	0
T-complex protein 1 subunit theta	CCT8	5647300	5563400	2820800	0	0,985143343	0
Protein disulfide-isomerase A3	PDIA3	2408700	2866600	4093500	0	1,190102545	0
C-1-tetrahydrofolate synthase, cytoplasmic; Methylenetetrahydrofolate dehydrogenase;	MTHFD1	1518500	1644200	4815800	0	1,082779058	0

Appendix

Methenyltetrahydrofolate cyclohydrolase; Formyltetrahydrofolate synthetase; C-1- tetrahydrofolate synthase, cytoplasmic, N-terminally processed							
Ubiquitin-like modifier-activating enzyme 1	UBA1	4606100	1022800	9116000	0	0,222053364	0
Nucleophosmin	NPM1	1381100	1915900	4361800	0	1,387227572	0
Importin-7	IPO7	4011300	2423400	6789300	0	0,604143295	0
Transportin-1	TNPO1	4368800	2185300	5433000	0	0,500206006	0
Serine/threonine-protein kinase mTOR	MTOR	3545200	2721700	8749800	0	0,767714092	0
Myosin light polypeptide 6	MYL6	4385300	3811500	5902200	0	0,869153764	0
Glutamate dehydrogenase 1, mitochondrial; Glutamate dehydrogenase 2, mitochondrial	GLUD1; GLUD2	14308000	8016300	2830500	0	0,560266984	0
Cornulin	CRNN	17594000	831590	12473000	0	0,047265545	0
MICOS complex subunit MIC19	CHCHD3	26233000	12684000	4327000	0	0,483513132	0
Catalase	CAT	15809000	9858700	8636200	0	0,623613132	0
10 kDa heat shock protein, mitochondrial	HSPE1	7283100	9663000	8646800	0	1,326770194	0
Periplakin	PPL	6497100	5354000	7167000	0	0,824059965	0
Proteasome subunit alpha type; Proteasome subunit alpha type-6	PSMA6	4971600	5683100	3265800	0	1,143112881	0
Phosphatidylethanolamine-binding protein 1; Hippocampal cholinergic neurostimulating peptide	PEBP1	24928000	23743000	9036200	0	0,952463094	0
Peroxiredoxin-5, mitochondrial	PRDX5	8937600	5813200	12131000	0	0,650420695	0
ATP synthase subunit f, mitochondrial	ATP5J2- PTCD1; ATP5J2	2552000	116840	3000300	0	0,045783699	0
Acyl-coenzyme A thioesterase 9, mitochondrial	ACOT9	5114400	1180000	1215300	0	0,230721101	0
Small proline-rich protein 3	SPRR3	14140000	1797300	14955000	0	0,127107496	0
ATP-dependent RNA helicase DDX1	DDX1	2170000	1002300	1701000	0	0,461889401	0
Cystatin-B	CSTB	39029000	16396000	37309000	0	0,420097876	0
Phosphate carrier protein, mitochondrial	SLC25A3	93406000	72991000	48373000	0	0,781438023	0
Apolipoprotein D	APOD	17728000	5155200	14595000	0	0,290794224	0
Dual specificity protein phosphatase 3	DUSP3	2410300	1289200	4608200	0	0,534871178	0
F-box only protein 50	NCCRP1	10396000	10368000	13816000	0	0,997306656	0
Ferritin heavy chain; Ferritin heavy chain, N-terminally processed; Ferritin	FTH1	1773500	1168000	3406700	0	0,658584719	0
Mitochondrial import inner membrane translocase subunit TIM14	DNAJC19	1481800	1146900	1690900	0	0,773991092	0

Cytochrome c oxidase subunit 2	MT-CO2	6347100	1268300	12020000	0	0,199823541	0
EH domain-containing protein 2	EHD2	2876600	1706400	2254900	0	0,593200306	0
Zymogen granule protein 16 homolog B	ZG16B	68009000	857950	74574000	0	0,012615242	0
Lysozyme C; Lysozyme	LYZ	109030000	35508000	113710000	0	0,325671833	0
ATP synthase F (0) complex subunit B1, mitochondrial	ATP5F1	17145000	16915000	5441600	0	0,98658501	0
Cytochrome b-c1 complex subunit 1, mitochondrial	UQCRC1	8781100	5734000	4960600	0	0,652993361	0
Ig kappa chain V-III region VG	IGKV3D-11	1676300000	1526800000	409810000	0	0,910815486	0
Fibrinogen gamma chain	FGG	14577000	4549200	4212300	0	0,312080675	0
Propionyl-CoA carboxylase alpha chain, mitochondrial	PCCA	4645500	2725900	3641600	0	0,586782908	0
Sarcoplasmic reticulum histidine-rich calcium-binding protein	HRC	11332000	8500300	15619000	0	0,750114719	0
Haptoglobin; Haptoglobin alpha chain; Haptoglobin beta chain; Haptoglobin-related protein	HP; HPR	4211800	3042100	5337900	0	0,72228026	0
Glutathione S-transferase P	GSTP1	11817000	18395000	6537800	0	1,556655666	0
Troponin C, slow skeletal and cardiac muscles	TNNC1	2355000	2123200	4459600	0	0,901571125	0
Methylcrotonoyl-CoA carboxylase subunit alpha, mitochondrial	MCCC1	5655600	2037100	4433400	0	0,360191668	0
TPR and ankyrin repeat-containing protein 1	TRANK1	1893500	968080	3887000	0	0,511264853	0
Alpha-amylase 1; Alpha-amylase; Alpha-amylase 2B; Pancreatic alpha-amylase	AMY1A; AMY1B; AMY2B; AMY2A	24557000	1085700	27089000	0	0,044211426	0
Delta-1-pyrroline-5-carboxylate dehydrogenase, mitochondrial	ALDH4A1	6086500	5527900	8375400	0	0,908223117	0